STUDIES OF THE EQUATORIAL THERMOSPHERE-IONOSPHERE SYSTEM

A Thesis
Submitted for the Degree of
Doctor of Philosophy in the Faculty of Science
BANGALORE UNIVERSITY

By

H. N. RANGANATH RAO

INDIAN INSTITUTE OF ASTROPHYSICS
BANGALORE - 560034
INDIA

DECEMBER 1994

DECLARATION

I hereby declare that the matter contained in this thesis is the result of the investigations carried out by me in the Indian Institute of Astrophysics, Bangalore under the supervision of Prof. J. Hanumath Sastri. This work has not been submitted for the award of any degree, Diploma, Associateship, Fellowship, etc., of any university or institute.

H. N. RANGANATH RAO

Candidate

Prof. J. Hanumath Sastri

Research Supervisor

Bangalore - 560034

Date :

ACKNOWLEDGEMENTS

The author expresses his profound sense of gratitude to Prof. J. Hanumath Sastri for his inspiring guidance, encouragement and help which made the thesis possible.

The author is grateful to Indian Space Research Organisation (ISRO) for financial support under RESPOND programme. The author is also grateful to Indian Institute of Astrophysics (IIA) for financial support during the final phase of this work.

The author is extremely grateful to Prof. Ramanath Cowsik, Director, IIA for his encouragement and providing necessary facilities in the institute to bring this work to the present form.

The author is thankful to Dr. R. Srinivasan, Dean, Faculty of sciences, Prof. Ram Sagar, Chairman, Students affairs committee and members of the Students affairs committee, IIA for their keen interest in the progress of this work and encouragement.

The author thankfully acknowledges the keen interest shown by Prof. C. Raghavendra Rao, Chairman, Prof. B.C. Chandrasekhara and Prof. M. N. Anandaram, Department of Physics, Bangalore University, during the progress of this work.

The author is grateful to Prof. R. Sridharan, Mr. R. Narayanan, Mr. S. Gurubaran and Dr. R. Sekar of PRL for help with data reduction software and for useful discussions.

The author is grateful to Mr. K. B. Ramesh for his help during the preparation of the thesis and useful discussions.

The author thankfully acknowledges the hearty cooperation and help extended by the staff members of Mechanical and Electronics sections of IIA at Bangalore and at Kavalur, in particular Messrs. K. Sagayanathan, F. Gabrial, B. Nagaraja

Naidu during the development phase of FPI.

The author expresses his special thanks to Messrs. K. B. Raghavendra Rao (RRI) and K. Sagayanathan for producing some elegant diagrams using PC based software. The author also thanks Messrs. S. Muthukrishnan, P. U. Kamath and V. K. Subramani for their neat line drawings.

The author thankfully acknowledges the help rendered by Mrs. A. Vagiswari, Ms. Christina Louis and other staff members of library.

The author thankfully acknowledges the cheerful company provided by his fellow research scholars and friends : Gangadhar, Mayya, Bhaskaran, Harish, Eswar Reddy, Annapurni, Uma, Benerjee, Prabhu, Sujan, Pandey, Arun, Dilip, Swara, Sivarani, Krishna, Sankar, Atish, Sanjoy, Rajesh, Pavan, Murali Sankar, Ebey and others at IIA.

Finally, the author is extremely grateful to the members of his family for their encouragement and patience during the course of this work.

PREFACE

The thesis focuses on studies in the field of solar terrestrial physics. The characteristics of the earth's atmosphere are dependent and respond to the activity in the Sun on various time scales. The first chapter, the introductory one begins with a description of geophysical environment, geomagnetic storms and physical principles underlying the existence and variability of the structure of ionosphere and thermosphere which are within the earth's upper atmosphere. The description of the geophysical phenomena in this chapter leads to a discussion on response of equatorial ionosphere to geomagnetic storms and substorms. The chapter also presents and describes some of the current problems on equatorial thermosphere-ionosphere system and concludes with a note on the approach to address them. The note indicates the need for simultaneous measurements of neutral and plasma parameters of the Earth's upper atmosphere.

The second chapter starts with a discussion on various experimental techniques available to measure neutral parameters of the earth's atmosphere. The details of the Fabry-Perot interferometer(FPI) which is chosen and developed to measure neutral parameters, method of use of the FPI, data acquisition and data reduction are the contents of chapter 2. The author has actively involved in the development of the FPI and its regular operation at Kavalur.

Chapter 3 deals with the results based on nighttime neutral thermospheric temperature measurements and simultaneous neutral and plasma measurements in the Indian equatorial region. Identification of midnight temperature maximum (MTM) at Kavalur (78.5°E, 12.5°N) in the Indian sector, its characteristics and its effects on ionospheric F region plasma are the major findings.

Chapter 4 presents a discussion on interplanetary magnetic clouds and their relation to geomagnetic storms. The results from a case study of the

response of the equatorial ionosphere to the geomagnetic storm which is caused by the transit of interplanetary magnetic cloud at Earth on 13-14 January, 1967, form the essence of chapter 4.

Chapter 5 presents results based on a case study of the global nature of substorm related transient composite electric field disturbances at equatorial latitudes.

The thesis concludes with chapter 6 which summarises the results presented in the thesis and discusses the scope for further work.

The thesis is the outcome of the project "Studies on equatorial thermosphere using high resolution spectroscopy of 630 nm night airglow emissions" carried out at IIA (PI : Prof. J. Hanumath Sastri) with funding from Indian Space Research Organization (ISRO), under RESPOND programme.

PUBLICATIONS

1. J.H. Sastri, **H.N. Ranganath Rao** and K.B. Ramesh. Response of equatorial ionosphere to the transit of interplanetary magnetic cloud of Jan 13-15, 1967. Transient disturbance in F-region. **Planetary and Space Science, Vol. 40, p 519, 1992.**

2. J.H. Sastri, K.B. Ramesh and **H.N. Ranganath Rao.** Transient Composite electric field disturbances near dip equator associated with auroral substorms. **Geophysical Research Letters, Vol. 19, p 1451, 1992.**

3. J.H. Sastri and **H.N. Ranganath Rao.** Optical interferometer measurements of thermospheric temperature at Kavalur (12.5°N, 78.5°E), India. **Journal of Atmospheric and Terrestrial Physics, Vol. 56, p 775, 1994.**

4. J.H. Sastri, **H.N. Ranganath Rao**, V.V. Somayajulu and H.Chandra. Thermospheric meridional neutral winds associated with equatorial midnight temperature maximum (MTM). **Geophysical Research Letters, Vol. 21, p 825, 1994.**

5. **H.N. Ranganath Rao** and J.H. Sastri. Characteristics of the equatorial midnight temperature maximum in the Indian sector. **Annales of Geophysicae, Vol. 12, p 276, 1994.**

CONTENTS

Chapter 1

Introduction

1.1 Solar terrestrial system

The sun, the interplanetary medium and the geophysical environment are the basic domains of solar-terrestrial system. The study of the relationships (or coupling processes) between these domains and within the individual domain is the primary objective of this thesis. An example of such a coupling process is *geomagnetic storm* (see 1.1.2). The geomagnetic storm is a disturbance in geophysical environment which is due to disturbance in magnetosphere which is described below. The origin of disturbance in magnetosphere is traced to the energy and momemtum transfer to the magnetosphere from solar wind through interplanetary medium (see Carovillano and Forbes, 1983).

1.1.1 Magnetosphere

The solar wind, composed of protons, electrons and a smaller number of heavier ionized particles, blows away from the sun in all directions with speeds of several hundred kilometers per second. As solar wind approaches Earth it distorts the geomagnetic field and creates a cavity with a long tail extending hundreds of Earth radii in the antisolar direction (see plate-I). The cavity, called the *magnetosphere* is very responsive to changing solar wind conditions. Physical processes occurring therein modulate the energy flow carried by the solar wind to the Earth. Plate-I is a schematic portraying of the terrestrial magnetosphere. The solar wind, flowing from the left, is deflected and heated by the bow shock. The shocked flow flows around the magnetosphere in the region called the *magnetosheath*. A small fraction of the solar wind plasma enter the magnetosphere through the polar cusp. Some of this plasma forms a boundary layer called the *plasma mantle* and some drifts down to the region of the neutral point where it forms the plasma sheet. The ionized part of the Earth's atmosphere is *Ionosphere*

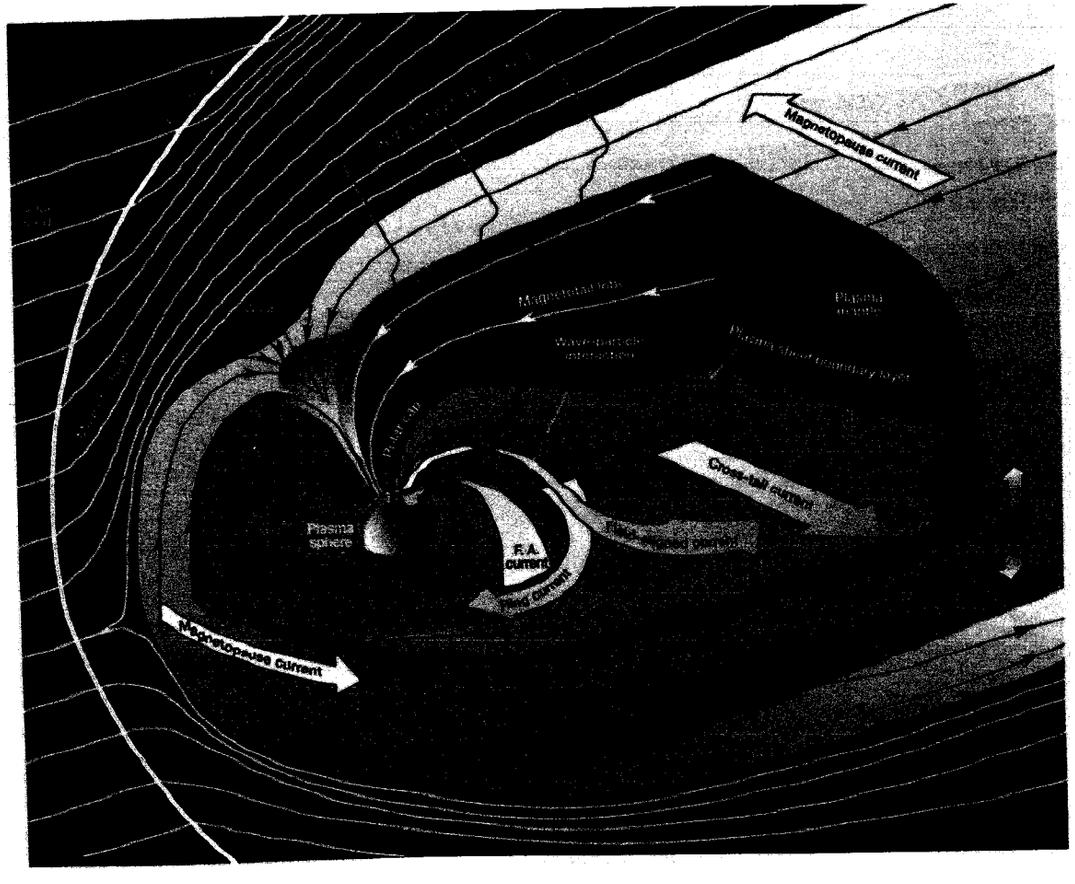

A SCHEMATIC PORTRAYING OF A GENERALLY ACCEPTED GLOBAL REPRESENTATION OF THE EARTH'S MAGNETOSPHERE [AFTER WILLIAMS ET AL., 1992]

PLATE-I

(see 1.3). There is no sharp boundary between the magnetosphere and ionosphere, but between the magnetosphere and the solar wind is a boundary, the *magnetopause* which is very significant. At this boundary energy is coupled into the magnetosphere from the solar wind. The magnetosphere may be divided into two parts i.e the outer magnetosphere and the inner magnetosphere. The outer magnetosphere is connected to polar upper atmosphere by geomagnetic field lines. The inner magnetosphere corotates with earth and the outer magnetosphere circulates under the influence of the solar wind. Some of the accelerated particles (whose exact origin is not yet clear) near the boundary of inner and outer magnetosphere penetrate deep into the polar upper atmosphere, being guided by the geomagnetic field lines which lie near the boundary and interact with atoms and molecules there. The interaction manifests itself in various phenomena such as the *aurora*.

The above brief description of magnetosphere and its connection to polar upper atmosphere is the basic frame of reference for the description of various magnetospheric phenomena and associated geophysical phenomena in the next section.

1.1.2 Geomagnetic storms

The Earth's upper atmosphere is prone to disturbances which by analogy with conventional weather, are called *storms*. In general terms, a storm is a severe departure from normal behaviour lasting usually from one to several days (see Hargreaves, 1992).

When the sun is active, the solar wind is variable and causes magnetospheric disturbances. When the disturbance is intense enough, it may be called a *magnetospheric storm*. For example a solar plasma cloud ejected during intense solar flares generates a shock wave in interplanetary plasma. The magnetospheric storm begins when both the shock wave and the plasma cloud interact with the magnetosphere. Typically, the onset of the magnetospheric storm is marked by the sudden compression of the magnetosphere, owing to the passage of the interplanetary shock wave and of the region of high pressure behind the shock. The compression is often followed by successive occurrence of explosive processes within the magnetosphere. The life-time of the individual

Akasofu, 1968).

As mentioned earlier, the magnetospheric substorm is associated with an increase of the population of protons of energies 1-50 keV in the trapping region. Their adiabatic motions induce electric currents and reduce the intensity of the geomagnetic field in low latitudes. If magnetospheric substorms occur frequently enough, these protons tend to accumulate in the trapping region and form an intense ring current or the storm-time radiation belt in the magnetosphere (see plate-I). More specifically, if substorms occur with a time interval of, say, 12 hours or so, many of the protons produced during one substorm will disappear from the trapping region before the next substorm occurs by the charge-exchange process or some other process. However, if the time interval between substorms is less than a few hours, successive substorms tend to accumulate protons in the trapping region, forming an intense radiation belt (or the ring current belt) (see Feldstein and Starkov, 1968) and causing a significant decrease in the intensity of the geomagnetic field in low latitude regions over the entire longitude range. This gives rise to the main phase of a *geomagnetic storm*. The magnetospheric storm is thus manifested as the geomagnetic storm which consists of (a) Initial phase : An increase of magnetic field lasting a few hours only. (b) Main phase : A large decrease in the H (horizontal) component of geomagnetic field building up to a maximum in about a day. (c) Recovery phase : A slow recovery to normal over a few days. The first part, the *initial phase*, is caused by the compression of the magnetosphere on the arrival of a burst of solar plasma. The second part, the *main phase*, is due to the ring current as explained above(see Hargreaves, 1992).

A substorm which is defined earlier can occur in isolation or can be present in a cluster of substorms generally associated with the main phase of a geomagnetic storm.

1.2 Earth's Atmosphere and its Nomenclature

The Earth's atmosphere is composed of mainly molecular nitrogen, oxygen and various trace gases such as carbondioxide, water vapour ... etc. Near the ground the atmosphere is dense and its density decreases with increase in altitude. The atmospheric

pressure also falls with increase in altitude. At 50 km the density and pressure are only about $10^{-3}(0.1\%)$ of their values at ground level. In to these rarified upper levels penetration of Ultra-Violet and X-ray emissions (XUV) emanating from the Sun takes place. The absorption of solar XUV radiation by the atmospheric constituents leads to heating, photodissociation as well as photoionization. Figure 1.1 is a schematic of energy-absorption processes in the Earth's atmosphere. The heating creates a hot upper region (above ~85km) in the atmosphere known as *thermosphere*. The ionized part of the atmosphere is known as *Ionosphere*.

Nomenclature :

The regions of the neutral atmosphere are named according to various schemes based on the variations with height of the temperature, the composition and the state of mixing. Fig 1.2 illustrates the most commonly used terms. The primary classification is according to the temperature gradient. On this basis the regions are called *spheres* and the boundaries are called *pauses*. Thus the *troposphere*, in which the temperature falls off at 10K/km or less is bounded by *tropopause* at a height of 10-12 km. The *stratosphere* is the region between 12 and 50 km. In stratosphere the temperature increases with height due to heating by Ultra-Violet absorption of ozone and a temperature maximum appears at about 50 km and it is known as *stratopause*. The temperature again decreases with height in the *mesosphere* and a minimum appears at about 80-85 km and is known as *mesopause*. The mesopause is the coldest region of the atmosphere and its temperature reaches as low as 180K. This is because of absence of any strong heating mechanism there. Above the mesopause due to the absorption of UV radiation by O_2 the temperature again increases and the temperature gradient remains positive, and it is known as *thermosphere*. The thermospheric temperature eventually becomes almost constant at a value that varies with time but is generally over 1000K.

On the basis of state of mixing, the lower part of the atmosphere which is well mixed is termed as *homosphere* or *turbosphere*. The upper region where mixing is inhibited and the composition varies with height, is named as *heterosphere*. The boundary between homosphere and heterosphere is known as *turbopause* at ~110 km. Within the hetero

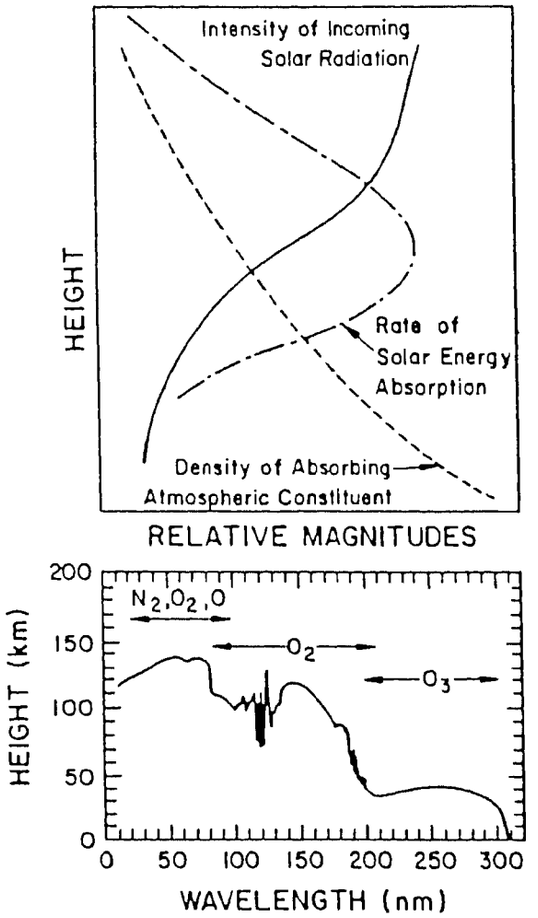

Fig 1.1 : Schematic of energy absorption processes in the earth's atmosphere. The atmospheric density decreases nearly exponentially with altitude and the solar radiation is attenuated by absorption as it penetrates deeper in to the atmosphere. The energy absorption thus has a peak altitude that depends on the cross section of the absorption species. The absorption of solar UV radiation in the atmosphere is wavelength dependent. The height at which the solar radiation intensity decreases to 37%(or 1/e) of its value above the atmosphere is plotted as a function of wavelength. Ozone absorbs most of the solar radiation from 200 to 300 nm and shorter wavelengths are absorbed in the thermosphere at heights greater than 80 Km by N_2, O_2 and O. Wavelengths greater than 400 nm penetrate the atmosphere and reach the ground.

(After Roble, 1987)

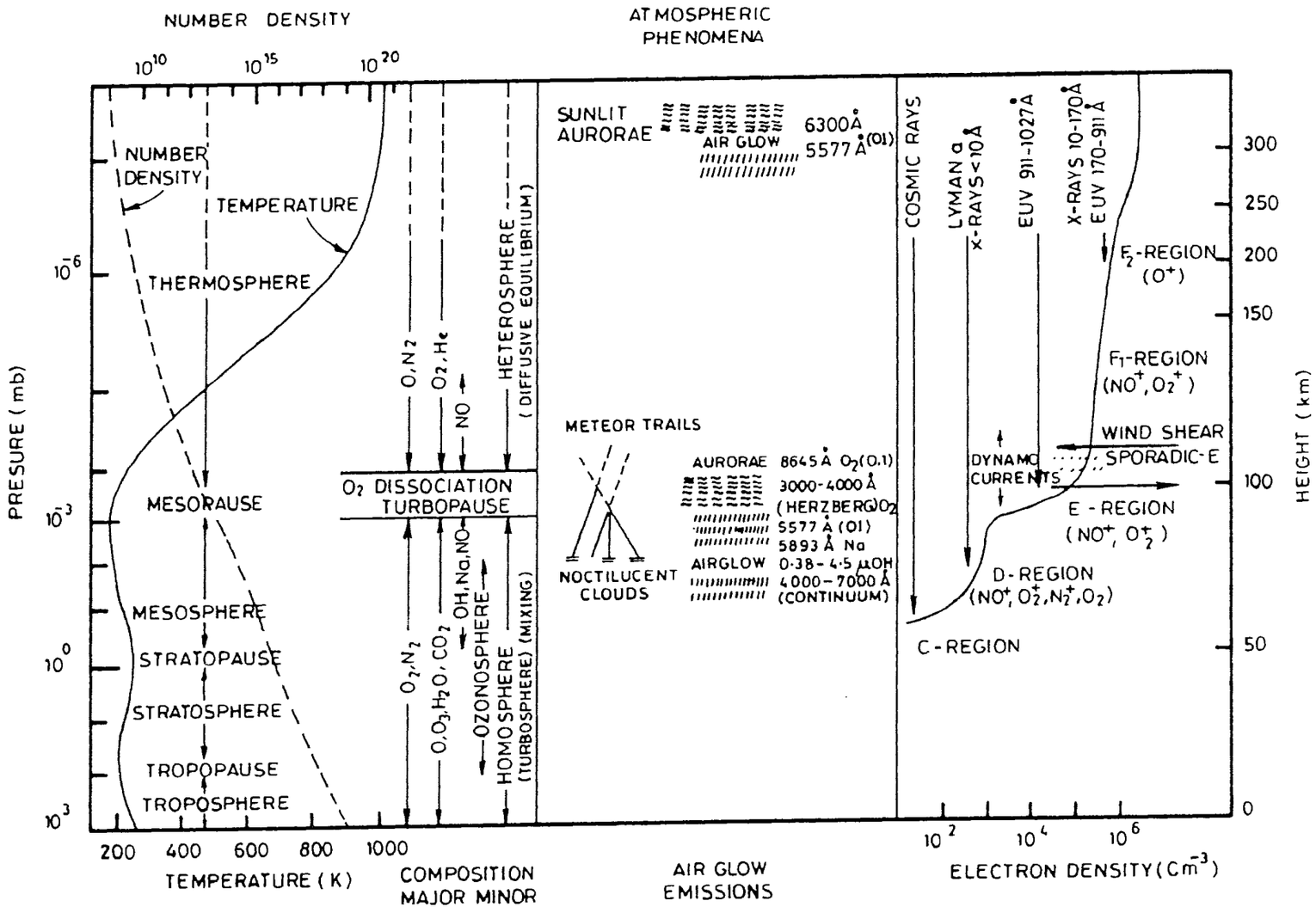

Fig 1.2 : EARTH'S UPPER ATMOSPHERE

-sphere provision is made for regions where the dominant gas is helium or hydrogen, and they are the *heliosphere* and the *protonosphere* respectively (not shown in the figure). From the higher levels, about 600 km, individual atoms can escape from the Earth's gravitation and this region is called the *exosphere.*

1.3 Ionosphere

As mentioned earlier the absorption of solar XUV radiation by atmospheric constituents leads to ionization. Ionized part of the atmosphere is the *Ionosphere.* Ionosphere contains significant numbers of free electrons and positive ions. The ionospheric medium as a whole is neutral, consisting of equal numbers of positive and negative charges within a given volume. Although the charged particles may be only a minority [about 1%] amongst the neutral ones, they exert a great influence on the medium's electrical properties. Vertical structure of the ionosphere with different regions, named, D, E, F_1 and F_2, is shown in Fig 1.2. The approximate heights of the regions and their daytime electron densities are as given below :

D region, 60 - 90 km : $10^2 - 10^4$ electrons/cm^3

E region, 90-140 km : Several 10^5 electrons/cm^3

F_1 region, 140-180 km : Several $10^5 - 10^6$ electrons/cm^3

F_2 region, maximum variable around 300 km : Upto several 10^6 electrons/cm^3.

The formation of D-region is due to ionization of (a) NO by Liman-α line of the solar spectrum at 121.5nm, (b) excited oxygen in the state $O_2(^1\Delta g)$ by EUV radiation of wavelength band 102.7-111.8 nm, (c) O_2 and N_2 by EUV radiation of wavelength band 80-102.7 nm, (d) all constituents by hard X-rays of 0.2-0.8 nm, and (e) D-region constituents by galactic cosmic rays. Apart from the sources of ionization mentioned above there are other important sources such as energetic particles from the sun or auroral origin that can ionize the D-region constituents at high latitudes. The primary ions produced by the above processes in the D region are NO^+, O_2^+, N_2^+ but N_2^+ is converted in to N_2 and O_2^+ by charge exchange reaction leaving NO^+ and O_2^+ as the

major ions in D region.

The E-region is formed due to the ionization of O_2, N_2, O, etc. by the less strongly absorbed and therefore more penetrating EUV radiation in the wavelength range 80-102.7 nm. Ionization of all the atmospheric constituents by X-rays of 1-10 nm also contributes to the formation of E-region. The primary ions of E region are N_2^+ and O_2^+ and O^+ but the subsequent chemical reactions leave NO^+ and O_2^+ as the most abundant. Metallic ions of meteoric origin such as Fe^+, Mg^+, Ca^+ and Si^+ are also present in E region. The formation of F_1 region is attributed to the most heavily absorbed part of the solar spectrum between about 20 and 90 nm. F_2 region is the upward extension of F_1 region . In the F region the primary ion is O^+ which is first converted in to a molecular ion by a charge exchange reaction as shown below.

$$0^+ + 0_2 \rightarrow 0_2^+ + 0$$

$$0^+ + N_2 \rightarrow N0^+ + N$$

The D and F_1 regions vanish at night, and the E region becomes weaker. The F_2 region, however, tends to persists but at reduced electron density.

Ionospheric electric currents :

The presence of free electrons and ions makes the ionosphere a good conductor of electricity. The basic mechanism for generating electric fields and currents in the ionosphere is the dynamo action (see Rishbeth and Garriott, 1969) of the horizontal neutral wind system due to tidal forces. The molecules of the neutral air collide with electrons and ions, forcing them initially in the direction of the wind, but their motion depends also on the geomagnetic field. In the dynamo region [i. e. E-region] the gyrofrequency is smaller than the collision frequency for ions but larger for electrons. Consequently the ions are carried along with the wind and the electrons move at right angles (and more slowly). The relative movement constitutes an electric current and the separation of charges produces an electric field which in turn affects the current.

In general, the ion current $\mathbf{J}$, the electric field $\mathbf{E}$, the ion velocity $\mathbf{v}$, and the magnetic flux density $\mathbf{B}$ are related by $\mathbf{J} = \sigma\ (\mathbf{v} \times \mathbf{B} + \mathbf{E})$ where σ is the tensor

conductivity (see Hargreaves, 1992). In this equation if some of the parameters are known it is possible to solve for others (see Kato, 1980). Comprehensive data on **J** exist from magnetometers and distribution of **J** may be used for computing winds. Alternatively a computed wind pattern may be used to evaluate a pattern of currents and winds and the evaluated currents are then varified against the measured current system. The electric field '**E**' is directed eastward during day and westward during night and this is because of tidal winds which are directed eastward during day and westward during night. This electric field in combination with the north-south component of geomagnetic field result in many geophysical phenomena such as equatorial electrojet and the equatorial ionization anomaly at equatorial latitudes.

S_q current system:

The current system generated by the tidal motion is called S_q, which means the variation related to the solar day under quiet geomagnetic conditions. Stewart (1883) suggested that the S_q currents are the cause of the small daily variations of magnetic field at the earth's surface. He further said that the electromotive force necessary to drive the current would be a motion of electrically conductive upper atmosphere across the geomagnetic field. This idea of the atmosphere dynamo was conceived a few decades before the discovery of the ionosphere by Appleton in 1924. Schieldge et al (1973) simulated global S_q current system using conductivity, geomagnetic field and a wind system which consists of four modes of the atmosphere tide, the (1, -2), (2, 2), (2, 3) and (2, 4) modes. They tried to simulate the equatorial electrojet as well as the global S_q current system by the four modes, varying the amplitudes and phases from day to day to explain the observed S_q variation. The semi diurnal tide was found important to explain the behavior during a solar minimum period. The result obtained by them is illustrated in Figure 1.3. Some observed S_q variations are shown in Figure 1.4(a). .Winds and electric field variations can be deduced from S_q observations (from equation : $\mathbf{J} = \sigma\ (\mathbf{v} \times \mathbf{B} + \mathbf{E})$. Wind and electric field variations deduced from S_q observations are shown in 1.4(b). The winds amount to tens of metres per second and the electric fields to a few millivolts per metre.

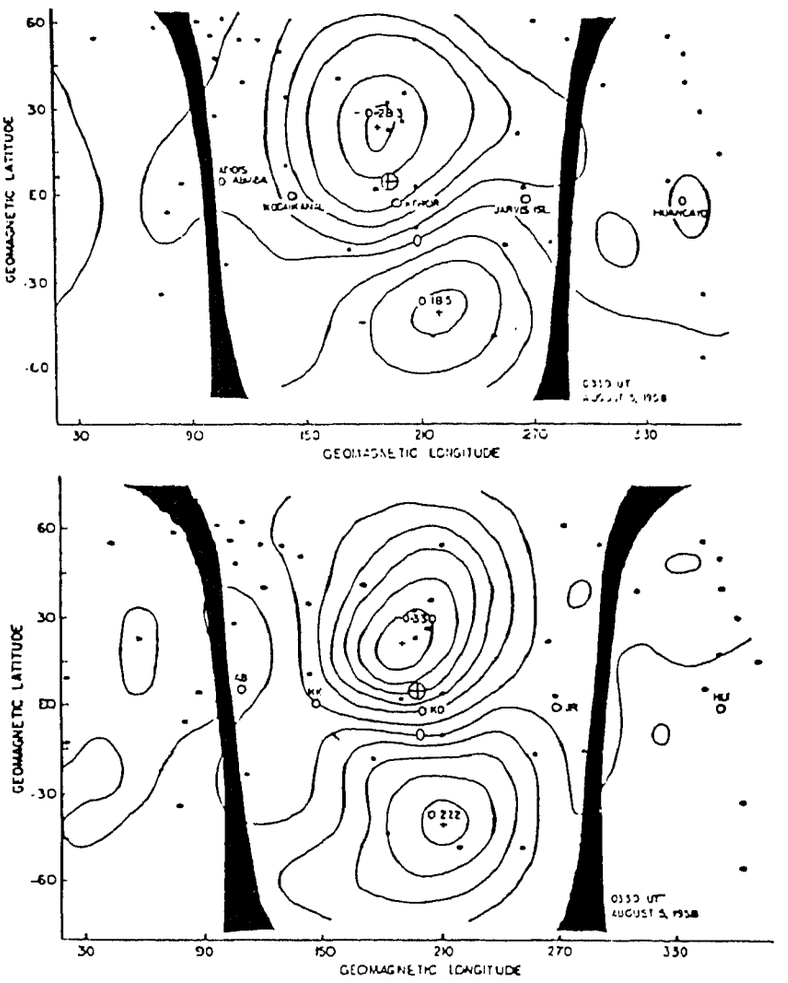

Fig 1.3 : Geomagnetic S_q variation observed (top) as magnetic potential at the ground and that calculated (bottom). The subsolar point $\oplus$ and the terminator (thick bands) are shown. The potential lines are given with spacing $5\times10^{-2} weber m^{-1}$ corresponding to 5×10^{4} A

(After Schieldge et al., 1973)

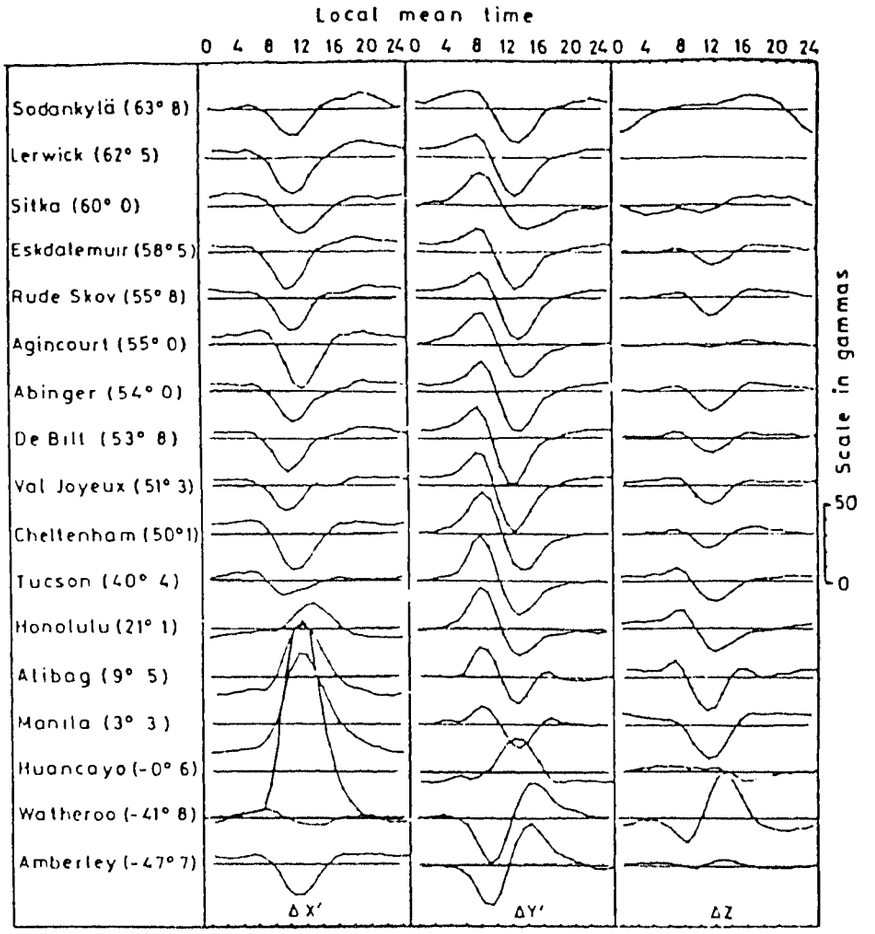

Fig 1.4(a) : S_q magnetic variations at several geomagnetic latitudes under equinoctial conditions. $\Delta X'$, $\Delta Y'$, ΔZ, are three normal components of the magnetograms, respectively geomagnetic north, geomagnetic east and vertical (down ward). Note the large excursion of $\Delta X'$, at the geomagnetic equator which is due to the equatorial electrojet.

(After E. H. Vestine in Physics of the Upper Atmosphere)

(edi: Ratcliffe, Academic press , 1960)

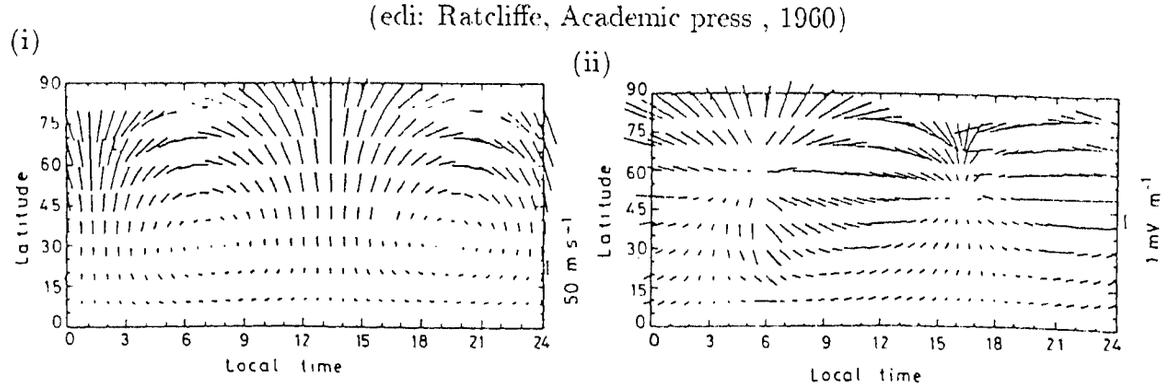

Fig 1.4(b) : Vectors of (i) wind and (ii) electric field, deduced from S_q variations.

(After Matsushita, 1969)

Disturbance Dynamo Electric fields :

Disturbance dynamo theory (BR theory) is given by Blanc and Richmond (1980). According to this theory the observed disturbances in quiet time electric fields are linked to the response of the global thermospheric circulation to storm-time heating at high latitudes. The heating results from the Joule dissipation of intensified sub-auroral currents and particle precipitation and the response consists of generation of a meridional circulation extending from the latitude of the heat source to the equator and with equatorward winds at F-region altitudes. The Coriolis force acting on the equatorward flow generates westward zonal winds. These westward winds drive equatorward Pedersen currents in the ionosphere at altitudes near 150 km where the ionospheric Pedersen conductivity is high. Such Pedersen currents will tend to accumulate positive electric charges at the equator. The equatorial buildup of charge establishes a poleward electric field which opposes and eventually stops the Pedersen current flow. In turn, this poleward electric field which is perpendicular to the vertical component of earth's magnetic field drives eastward Hall currents (and westward plasma drifts). These eastward currents (and westward drifts) are expected to reach maximum intensity in middle latitudes. The currents are interrupted at the dawn and dusk terminators where the ionospheric conductivities have large longitudinal gradients. The interrupted currents set up polarization charges at the terminators and give rise to an electric field directed from dusk to dawn. Furthermore, the currents are deflected to higher and lower latitudes where they achieve closure through two separate vortices, a polar vortex and an equatorial vortex. It is of importance to note that the equatorial disturbance current vortex has an opposite sense of flow to that of the quiet-time 'S_q' current system. In otherwords the disturbance dynamo electric fields are normally directed opposite in direction to the quiet-time fields at all local times, i.e. the electric fields are directed westward during the day and eastward at night (e.g. Matsushita and Balsley, 1972; Fejer et al., 1983; Reddy et al., 1990, 1991). The disturbance dynamo electric field related perturbations manifest with time delays of 4 to 8 hours with reference to the causative geomagnetic disturbances. According to BR theory the time delays are related to the set-up time

of the thermospheric circulation in response to high latitude heating. See Fig. 1.5 for understanding BR theory explained in this paragraph. Experimental evidences of the disturbance dynamo electric fields are presented in the next paragraph.

Fejer et al (1983) showed that at Jicamarca the disturbance dynamo related electric field perturbations manifest with delays of 16-24 hours with reference to the causative geomagnetic disturbances. Sastri (1988b) using groundbased magnetometer and ionosonde data demonstrated the presence of disturbance dynamo electric field effects with time delays of 13-22 hours with reference to the causative geomagnetic disturbances. Mazaudier and Venkateswaran (1990) made an attempt to interpret the nature of the global ionospheric and thermospheric perturbations that persisted on March 23, 1979 with a time delay of several hours after the magnetospheric substorm events of March 22, in terms of disturbance dynamo theory. In spite of these evidences the importance of the disturbance dynamo process on the low latitude zonal electric field is still not clear to some extent and the reasons are as follows : (a) at Arecibo significant disturbance dynamo effects are evident on the average F region east- west drifts but not on the upward northward drifts (Ganguly et al., 1987), (b) the average vertical drifts over Jicamarca show indications of disturbance effects only near dusk during equinox where the pre-reversal enhancement of the upward drifts decreases with magnetic activity (Fejer et al., 1989; 1990c), (c) the work of Sastri (1988b) shows that delayed electric field disturbances do not always follow enhanced magnetic activity even in the presence of ionospheric storm effects at mid latitudes, and (d) it is difficult to compare the measured disturbance dynamo electic fields with theory since the amount of high latitude heating can not be easily estimated (Mazaudier and Venkateswaran, 1990).

F-region ionospheric storm :

The *F-region ionospheric storm* resembles the magnetic storm superficially though its mechanisms are not same. Its characteristics have been established from ionosonde data as variations of the maximum electron density (N_mF_2), and height of the maximum (h_mF_2), and from the variations of ionospheric electron content (I). As in the magnetic storm there is an initial *positive phase* lasting a few hours, when the electron density

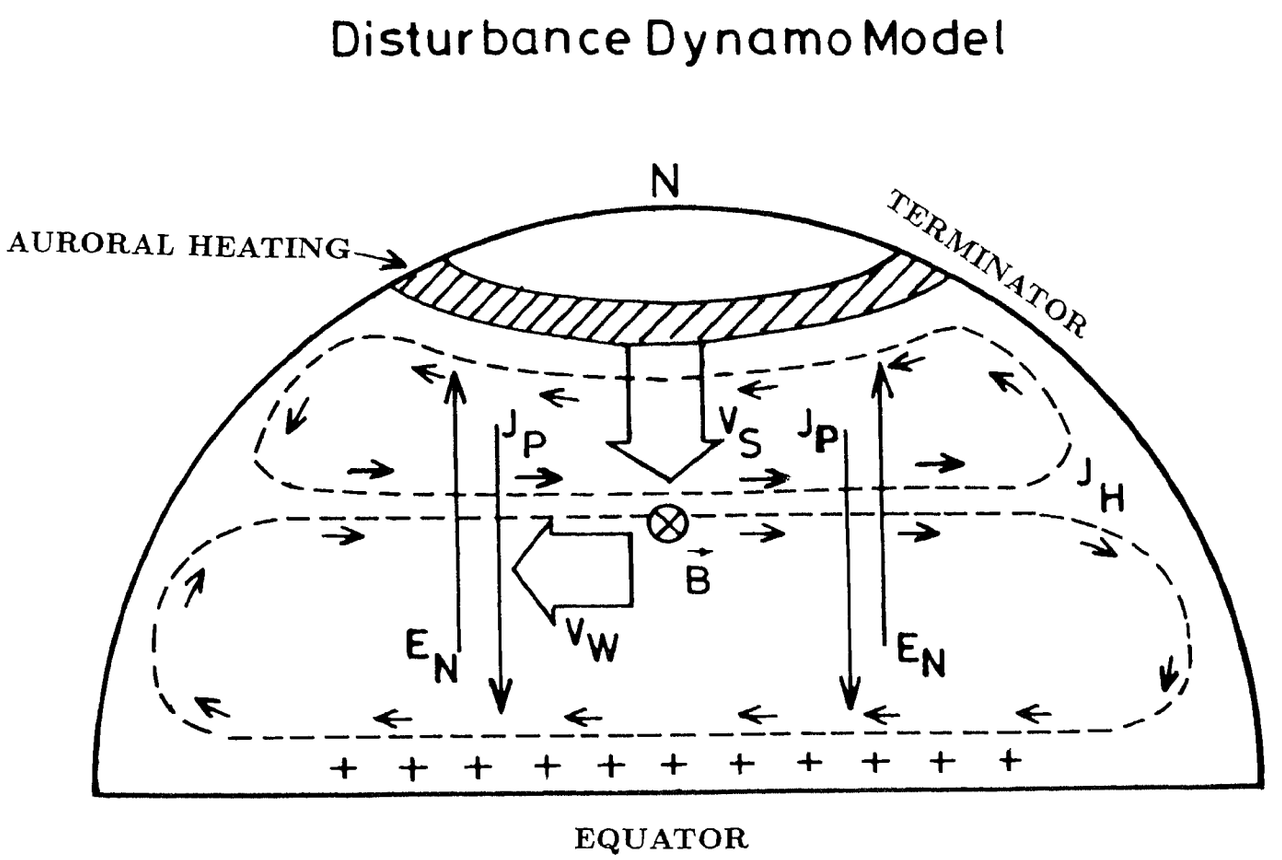

Fig 1.5 : Schematic of the variables in the Blanc-Richmond (1980) theory.The joule heating from the storm is assumed to extend uniformly around a high-latitude zone. The southward meridional winds at F region heights arising from this heating is shown as the arrow V_s. Due to the action of the Coriolis force, the southward meridional wind produce westward zonal motion (shown as the arrow V_w). The zonal motion of the ions in combination with the downward component of the magnetic field (shown as $\otimes\mathbf{B}$) produces an equatorward Pedersen current (Shown as J_p). The Pedersen current builds up positive charges at the equator until an electric field is established in the poleward direction opposing the flow of the Pedersen current. This poleward electric field is shown as E_N. This electric field which is perpendicular to the downward component of **B** gives rise to eastward Hall current with maximum intensity in middle latitudes. This Hall current is marked as J_H. The Hall current is interrupted at the terminators and gives rise to two current vortices as shown. The lower latitude disturbance current vortex is opposite in direction, to the normal Sq current vortex.

[After Mazaudier and Venkateswaran, 1990]

and electron content are greater than normal, and then a *main* or *negative phase* when these quantities are reduced below normal values. The ionosphere gradually returns to normal over a period of one to several days in the *recovery phase*(see Hargreaves, 1992). The F-region storm is a complex phenomenon and its causes are not yet clearly understood. This storm can not be accurately forecast like the geomagnetic storms. The resemblance to the magnetic storm is striking but the physical connection is not so evident.

Mathematical modelling (Roble et al., 1982 and references therein) of the thermosphere wind system has shown that the global circulation is modified by the heating of the auroral zone, which increases during storms due to intensified auroral electrojets and the precipitation of energetic particles. These sources are relatively strong, and the daytime meridional circulation of air, normally poleward, can be reversed to become an equatorward flow up to 500 m/s. The dynamic effect of an equatorward wind is to lift the F region, reducing the chemical loss rate and thus increasing the electron density at subauroral latitude.

A change of neutral composition is almost certainly one important factor in the negative phase of the ionospheric storm. Satellite observations (e.g., Hoffman, 1988; Brace et al., 1982; Carignan et al., 1982) show that the N_2 concentrations changing by a factor of 10 to 20 during a storm, and such a change is consistent with the upward expansion of the atmosphere due to heating. The ratio q/β (Production/Loss) would then be reduced and the ion density with it. The molecularly enriched air could then be advected from high to middle latitude in the equatorward flow.

Over the years a number of mechanisms, each logically sound, have been put forward to account for the F-region ionospheric storm. The task of finding the relevant mechanisms has been largely a process of elimination as more observations and more realistic modelling came along. Present thinking favors a combination of effects, notably the precipitation of ring current ions to heat the ionosphere and changes in the thermospheric wind to raise or depress the layer and alter the composition (Prolss et al., 1991 and references therein). But there remains more work to be done on this important

aspect of the ionospheric behaviour.

1.3.1 Equatorial Ionosphere

The global ionosphere has been classified in to equatorial, mid-latitude, auroral and polar ionospheres because of its different structure and dynamics in these regions. Each region responds differently to magnetospheric disturbances. Our studies are primarily concerned with the equatorial ionosphere.

The equatorial ionosphere is unique in many ways. It is precisely here that vertical diffusive equilibrium of plasma is not possible unless a horizontal east-west electric field is available to propel the plasma across the geomagnetic field lines. Such an electric field is however generated by the global E-region dynamo (Unteidt, 1967; Suguira and Poras, 1969) as mentioned earlier and the F-region plasma experiences the $E \times B$ vertical drift. At F-region altitudes, the ion gyrofrequency is much greater than the ion-neutral collision frequency and therefore the plasma once created can be moved easily along the magnetic field lines by forces due to gravity, pressure gradients and neutral winds. Plasma transport processes thus more or less govern the structure of equatorial ionosphere, and a poignant indicator of this physical situation, besides many others, is the well-known *Appleton or equatorial ionization anomaly*, EIA (Appleton, 1946). The details of EIA are presented in 1.3.4.

1.3.2 Equatorial electrojet

Egedal (1947) explained the enhanced variations of earth's magnetic field in the vicinity of the dip equator in terms of enhanced east-west current flow in a narrow latitudional belt of $\pm 3^{\circ}$ around the dip equator. This east-west current flow over the equator was later named as *Equatorial Electrojet* by Chapman (1951). The electrojet current is widely understood to result from an enhanced polarisation electric field set up at and around the dip equator by the east west electric field of global wind dynamo action due to the inhibition of Hall current flow (see Forbes, 1981 and references therein). The electric fields which drive the equatorial electrojet current consists of three components

electric fields which drive the equatorial electrojet current consists of three components with different origins : (1) An electric field originating in the dynamo action of the global scale wind system in the lower thermosphere is the predominant driving electric field on quiet days, (2) An electric field originating in the magnetosphere-polar ionosphere interaction processes seems to be the more important field on magnetically disturbed days, (3) An electric field originating in the local interaction of the height-varying neutral winds with the ionospheric plasma within the electrojet. The details of these three types of electric fields which drive electrojet current are discussed by Reddy (1981).

1.3.3 Response of equatorial electric fields to the Interplanetary magnetic field (IMF) polarity

It is known that IMF has a significant influence on geomagnetic and ionospheric phenomena of the equatorial region[e.g. Nishida, 1968; 1971; Nishida and Kokuban, 1971; Rastogi and Patel, 1975; Matsushita, 1977; Patel, 1978; Blanc, 1978; Gonzales et al., 1979; Sastri, 1989]. Rastogi and Patel (1975) and Patel (1978) found a close relation between the reversals in equatorial electric fields and south-to-north reversals of the vertical B_z component of IMF. These equatorial electric field perturbations usually occur at the onset of substorm in the auroral zone or at the onset of a substorm recovery phase [e.g. Rastogi and Patel, 1975; Patel, 1978; Gonzales et al., 1979; Fejer et al., 1990a; Sastri et al.,1992). The first case is associated with periods of southward IMF (corresponds increase in high latitude convection/increase in polar cap potential) while the second case usually associated with large northward IMF (corresponds to decrease in high latitude convection/polar cap potential) recoveries following periods of an hour or more of southward B_z.

An aspect of equatorial electric field disturbances that has not received due attention so far is the observation that they tend to appear either with an increase in high latitude convection around the onset of substorms or with a decrease in convection during its recovery phase but not both (e.g. Fejer et al., 1979). This is rather disconcerting because, typically, increase in convection around the onset of a substorm will

be followed by a decrease in its recovery phase and the effects of both have to prevail, at least in principle. Studies of composite electric field disturbances are necessary in view of their implications to the understanding of physical processes that govern the generation of disturbances in high latitude electric fields and their penetration to low latitudes at times of substorm activity. Keeping in view of this aspect and the recent work of Sastri et al (1992) on composite electric field effects, a case study of 20^{th} August 1979 event, is presented in the fifth chapter of this thesis.

1.3.4 Equatorial ionization anomaly

The formation of equatorial ionization anomaly (EIA) is established to occur through the fountain mechanism (Martyn, 1947) whereby ionization lifted vertically upwards by the eastward electric field of dynamo origin around the dip equator diffuses downwards along the field lines under the influence of gravity and pressure gradient forces, leading to crests of ionization north and south of dip equator and a trough at the dip equator (Anderson, 1973a, b; 1981)(see Fig. 1.6).

The intensity of the EIA (crest to trough density ratio), and also the crests north-south asymmetry, are controlled significantly by the meridional thermospheric wind (review of Moffett, 1979 and references therein). The persistence of EIA well in to the night, depending upon the season and solar activity phase, is known to be produced by the evening enhancement in the eastward electric field generated by the F-region dynamo (Rishbeth, 1981 and references therein) action. The quiet time EIA has many features typical of the season of the year, longitude and solar activity phase that have been the subject of numerous investigations, both observationaly and theoreticaly (e. g. Rastogi, 1959; Hanson and Moffett, 1966; Walker and Ma, 1972; Anderson, 1973a, b; Raghava Rao et al., 1978; Moffett, 1979; Sastri, 1982; Abdu et al., 1990) but the features are yet to be understood in their different details. The knowledge on the EIA response to magnetospheric disturbance seems less than satisfactory. This is because the existing investigations focusing on the subject have been rather sparse, and a coherent picture on the pattern of EIA response under disturbed conditions has yet to emerge. One of

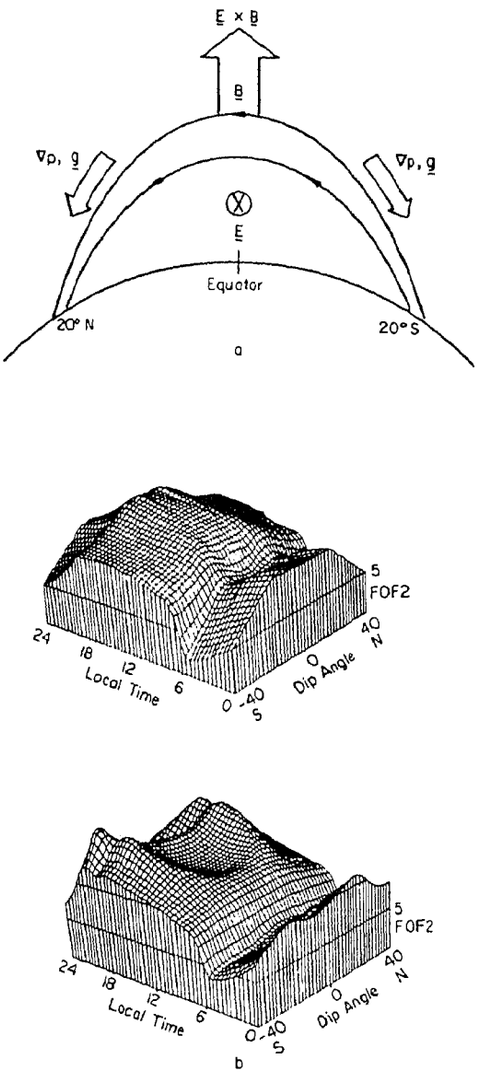

Fig 1.6 (a) Schematic diagram of how plasma uplift via electric fields transports plasma from equatorial to tropical zones, (b) contour plots of foF_2 in MHz for zero zonal electric fields (upper plot) and for a typical diurnal variation of the zonal electric field. (Ref: Kelley, 1989)

the reasons for this unsatisfactory situation is obviously the inadequate understanding on the disturbance-time behaviour of electric fields, and the thermospheric dynamics that control the EIA (Sastri, 1990; Abdu et al., 1993).

EIA response to disturbance (transient) electric fields :

Since the development and sustenance of EIA depends on equatorial electric fields, EIA shows response to the disturbed equatorial electric fields (Abdu et al., 1993 and references therein). The equatorial electric fields (eastward during daytime and westward during night time) are disturbed by the penetration of magnetospheric convection electric fields to equatorial latitudes. These penetration of magnetospheric electric fields takes place during growth or decay of the substorm (Kelley et al., 1979; Rastogi and Patel, 1975; Fejer, 1986; Gonzales et al., 1979). Observations show that perturbations in equatorial electric field occur more often in association with the decay phase of substorm rather than with the growth phase of substorms (Fejer, 1986).

Transient electric fields are known to prevail at equatorial latitudes in association with and /or immediately following storm sudden commencement (SSC or SC) (e.g Kikuchi, 1986; Somayajulu et al., 1987; Sastri et al., 1993). Takahashi et al (1987) using Hinotori satellite data, have studied several cases such as : (a) anomalous EIA development on the nightside, (b) anomalous EIA inhibition on day side, and (c) day time enhancement of EIA development. The daytime EIA enhancement in the studies of Takahashi et al.(1987) and the daytime anomalous increase in the F-region ion drift and height, measured with the Jicamarca radar by Woodman et al. (1972) seem to represent good examples of daytime eastward electric field penetration to equatorial latitudes, associated with substorm activity. Studies by Forbes (1989) and Forbes et al (1988) based on data from a latitudinal chain of ionosonde stations and storm-time K_p variations showed, for latitudes near the EIA crest and immediately following the initial large increase of K_p values, daytime foF_2 enhancements. They attributed these to possible disturbance electric field penetration to low latitudes.

EIA response to disturbance in global thermospheric circulation :

Perturbation in the global thermospheric circulation takes place due to storm-time heating at high latitudes. The heating at high latitudes is due to the Joule dissipation of intensified auroral currents and particle precipitation during geomagnetic storms. The recent simulation study on the neutral atmosphere and dynamics using the NCAR Thermospheric General Circulation Model (TGCM) by Fesen et al.(1989) showed that enhanced high latitude energy and momentum deposition associated with geomagnetic storms cause large scale wave-like perturbations in the neutral atmosphere that propagate to equatorial latitudes and modify significantly the electron density and height of the layer peak there. Their predictions were in agreement with the ionosonde observations for the 22 March 1979 magnetic storm. This showed that the disturbance neutral wind could indeed be a major source of EIA modification. Other associated sources of EIA modification (relating to storm circulation) are : (a) disturbance dynamo electric fields and (b) composition changes associated with increased molecular to atomic ratios (e.g. Mayr and Volland, 1972; Hedin, 1988; Prolss, 1982; Prolss et al., 1991 and references therein). The effects on EIA due to all these sources involve propagation times of several hours with respect to the onset of geomagnetic storm/substorm events and hence, in principle, the resulting EIA responses could be identified from those related to direct electric field penetration events which are prompt.

EIA response to disturbance in thermospheric Composition :

Mid latitude F-region compositions are affected by the transportation of molecular atmospheric species from high latitudes by the disturbed thermospheric circulation which results because of storm time heating at high latitudes. (e.g. Rishbeth, 1975; Prolss and Von Zahn 1977; Prolss, 1982; 1993). Depending upon the intensity of the storm the disturbance in the composition can modify the equatorial thermosphere (Titheridge and Buonsanto, 1988) and hence EIA.

Against this background we have studied the response of EIA to the geomagnetic storm which resulted due to the transit of an interplanetary magnetic cloud at Earth

during january 13-14, 1967. The interesting and novel results obtained from the case study are presented in the fourth chapter.

1.3.5 Interplanetary magnetic clouds

Sudden expulsions of dense clouds of plasma from the outer atmosphere of the Sun are termed as 'Coronal mass ejections' (CMEs). These CMEs are hurled into interplanetary space usually (but not exclusively) in association with the various known forms of solar activity (Wilson and Hildner 1986). Since the CME associated plasma is never observed to return to the Sun, signatures of CMEs are to be present in the interplanetary space. One such signature is the recently discovered interplanetary *magnetic cloud*(see Chapter 4. for details) or *bubble* which is a solar wind structure with a typical duration of ~1 day at Earth, and with a magnetic field strength higher than the ambient and whose direction changes smoothly by means of a rotation nearly parallel to a plane across the structure (Klein and Burlaga, 1982; Wilson and Hildner 1984; 1986; Zhang and Burlaga 1988). The transit of magnetic clouds at Earth can be expected and infact, very recently found to lead geomagnetic storms (Wilson, 1987; Zhang and Burlaga, 1988). As mentioned in earlier sections, that it is of common knowledge now that during geomagnetic storms the behaviour of the earth's ionosphere departs from the normal, with the pattern of departure depending upon parameters such as local time, season and latitude. Keeping in view of this we have investigated the response of the equatorial ionosphere [precisely the response of equatorial electric fields and EIA] to the geomagnetic storm which resulted due to the transit of interplanetary magnetic cloud of Jan 13-15, 1967. The studies and the results are presented in chapter four.

1.4 Thermosphere

As detailed earlier the thermosphere lies above mesopause and is characterised by a positive temperature gradient. Thermosphere is a multiconstituent medium with the major species being O, O_2 and N_2. These neutral species interact with a weakly ionized plasma of the ionosphere where the major ions are O^+ and NO^+. The thermosphere and

ionosphere form a dynamic system that responds to a variety of forces or momemtum sources. Diurnal and latitudinal variability in solar heating of the neutral atmosphere gas cause global pressure gradients. These pressure gradients together with the coriolis effect cause zonal and meridional winds. Ions are driven by electric fields and hence ions convect from one region of the ionosphere to another, constrained by the earth's magnetic field. Ions and neutrals undergo collisions and this results in coupled motion so that ion drag (see 1.5 for details of ion drag) participates in establishing the pattern of the winds. The resulting velocity vectors are asymmetric over the globe because the electric field configuration is dependent on magnetic field, whose poles are displaced from geographic poles, while the coriolis effect depends on the rotational symmetry of the Earth. Vertical motion is governed by gravitational acceleration and pressure gradients. Molecular diffusion causes the density of individual neutral constituents to vary independently with altitude. The effect becomes important above about 120 km, resulting in a rapid decrease in the densities of heavier molecular species with altitude compared with the lighter atomic species.

1.4.1 Energy sources of the Thermosphere

The basic sources of energy for the thermosphere are : (i) solar radiation in UV and EUV range, (ii) solar wind through its interaction with the magnetosphere, (iii) energetic particle precipitation and electric fields from the magnetosphere (Cole, 1971, 1975; Banks, 1977), (iv) lower atmosphere through the atmospheric waves, tides, acoustic gravity waves etc.. (Hines, 1965), (v) hydromagnetic waves generated at the Earth's bow shock, (vi) meteorites and (vii) neutral-plasma interactions within the system. The dynamical forcings (ii), (iii) and (v) are confined to high latitudes but their effects under severe disturbances could propagate to mid and low latitudes. A brief account of all these energy sources is given below. Figure 1.7 shows sources of energy to the thermosphere as a function of altitude.

Solar UV and EUV irradiation is the most important source of energy to thermosphere (Roble and Dickinson, 1973; Hinteregger, 1976). This source is mainly

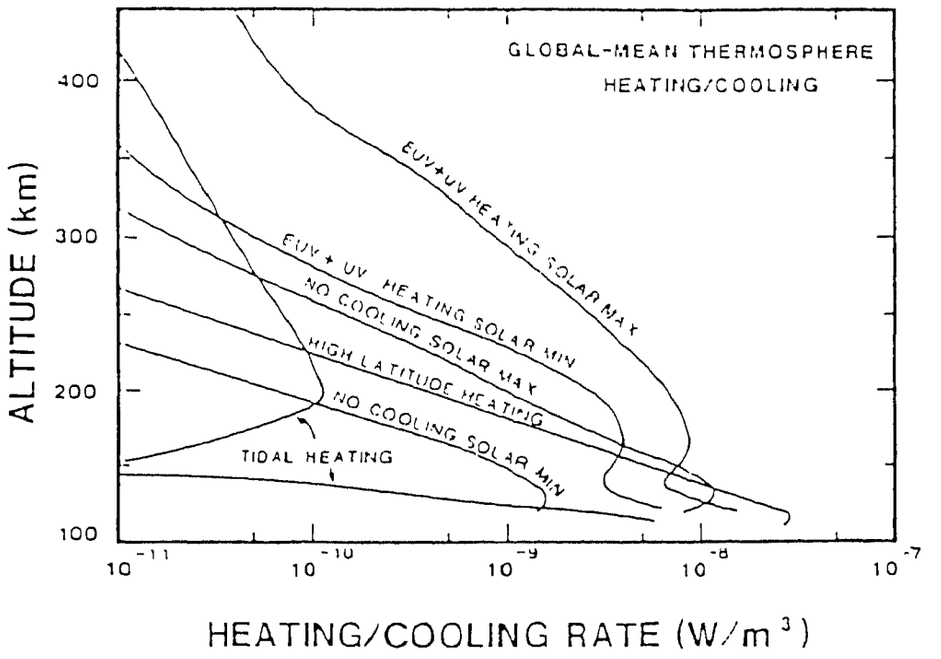

Fig 1.7 : Altitude variation of the global mean contribution of the various sources of energy to the thermosphere.
[After Killeen, 1987]

responsible for maintaining the high thermospheric temperatures and for producing the presssure gradient forces that drive the basic day-to-night thermospheric circulation. Absorption of solar EUV radiation ($\lambda < 102.7$nm) in the middle and upper thermosphere produces ionization, creating an ejected primary photoelectron that undergoes subsequent coulomb collisions with electrons and ions and inelastic collisions with neutrals. The slowing down process for the photoelectrons produces a relatively hot electron gas and contributes to the heating of the neutral gas (with $\sim$ 5% efficiency). Most of the photoelectron energy, however, is lost to space through airglow emissions (see 1.6 for airglow) from atomic and molecular states excited through inelastic collisional processes. The paths of release of energy stored in the ions produced by the photoionization process is more complicated than those for the photoelectrons. But the various paths have one common feature that every ionization ultimately results in the dissociation of an O_2 molecule in to two 'O' atoms which then diffuse downwards and release their energy of dissociation in the three-body recombination process at altitudes below the EUV-dominated region in the lower thermosphere and upper mesosphere (see review by Killen, 1987). Thus while much of the potential energy carried by the ions goes in to direct heating of the local thermosphere, part of it is lost to lower altitudes. In the lower thermosphere itself, between $\sim$90 and 150km, absorption of solar radiation in the Schumann-Runge continuum region ($\sim$ 130 to 175nm) is the dominant heat source.

The TIROS/NOVA satellite measurements (Spiro et al, 1982; Hardy et al., 1985; Evan, 1987) have revealed that energetic protons of solar wind origin deposit energy $\sim$ 0.3mW m^{-1} in to the thermosphere.

The high latitude heat sources of thermosphere are (a) Joule heating due to differential ion and neutral motion and (b) particle heating due to the collisional slowing-down processes for energetic particles precipitating from the magnetosphere. Perrault and Akasofu (1978) suggested that the AE (auroral electrojet) index could be used as a measure of the global Joule heat production. But there is a limitation in using AE index (Akasofu et al., 1983; Kamide and Akasofu, 1983). Simulation studies using TGCMs (Roble et al, 1983; Rees et al 1985; Killeen and Roble, 1986) have provided estimates

of the global Joule heating rate in the range of $\sim$ 0.3-1.5$\times 10^{11}$ watts. Estimates of the total global thermospheric heating due to particle precipitation, based on satellite measurements of the average precipitating particle fluxes (see Killen, 1987 and references therein) are typically lower than those for Joule heating, being in the approximate range 0.05-0.6$\times 10^{11}$ watts.

Energy is also transfered to the thermosphere from lower atmosphere via the upward propagation of tides and gravity waves generated at lower altitudes. Atmospheric tides can be defined as global scale oscillations of the atmospheric parameters such as winds and temperatures with periods which are integral multiples of the forcing (Fesen et al, 1986). Generally the forcing is lunar or solar in origin arising from gravitational attraction or heating respectively. Solar tide is driven by diurnally varying insolation absorption in particular by water vapour in the troposphere (Forbes, 1982) and lower stratosphere, by ozone in the stratosphere and mesosphere and by all atmospheric constituents in the thermosphere. The tide which is generated in the lower atmosphere may propagate to upper atmosphere as wave like disturbances. The oscillations of wind and temperature fields in thermosphere have diurnal (24 hrs) and semidiurnal (12 hrs) periodicities. The semidiurnal component predominates at altitudes of about 100-150 km. The diurnal component becomes important at higher altitudes. Groves and Forbes (1985) found that the tidal heating was less than radiational heating at all altitudes, except below 90 km where it maximises and the solar UV is already extinguished. The global integral tidal heating from 150-400 km was 6$\times$ 10^9 watts, which represented $\sim$7% of the EUV energy deposition rate assumed in their analysis. In this height range, the calculated tidal heating maximized at high latitudes. In the lower thermosphere, 90-150 km, the heating had a low latitude distribution and the global average tidal heat rate was $\sim$ 7.6$\times$ 10^{10} watts, or $\sim$7% of the UV heating in the same region. Below 90 km, the energy input due to tidal dissipation was comparable with that due to solar UV absorption at higher altitudes. These results suggest that tidal heating plays a secondary, but significant role in the energy budget of the thermosphere.

1.4.2 Winds and Energy balance

Winds play vital role as the carriers of thermal energy in the energy balance of the atmospheric system. The wind system of the atmosphere mainly consists of prevailing winds, super rotation of thermosphere and midnight pressure bulge. As the earth rotates about its axis, the thermosphere is subjected to a daily variation in the absorption of solar energy. The heating of thermosphere on dayside causes it to expand and at the same time the heat loss on the nightside causes it to contract. Also this heating pattern creates pressure differences which drive global thermospheric circulation and which results in transportation of heat from the warm dayside to the cool nightside.

The summer to winter hemispheric prevailing wind form a part of the meridional circulation cell which has an upward (heat absorbing), a downward (heat releasing) and a return flow at lower altitude completing the cell. Figure 1.8 shows prevailing winds for equinox and solstice for different levels of auroral activity (see Roble, 1987).

The upper atmosphere at 200-300 km altitude rotates from west to east at a velocity of $\sim 150 \mathrm{ms}^{-1}$ at mid latitude. This rotation is faster than the rotation of the earth and is known as super rotation and its effects on the energy balance of the thermosphere are known as super rotation effects (see Roble, 1987).

The midnight pressure bulge and its effects on the thermospheric energy budget are given in section 1.5.

1.4.3 Effects of winds on the F region ionization and vice versa

Meridional winds have significant control over the F region ionization. In turn the F region plasma alters the wind system thereby establishing a coupling process between the neutral and the ionized constituents of the upper atmosphere. For example, the horizontal north-south wind U produces a vertical plasma drift of $W = U\ \mathrm{Sin}(I)\ \mathrm{Cos}\ (I)$ where I is the dip angle. W will be upward or downward depending upon the direction of U. Whenever there is a downward drift, the maximum density of the F

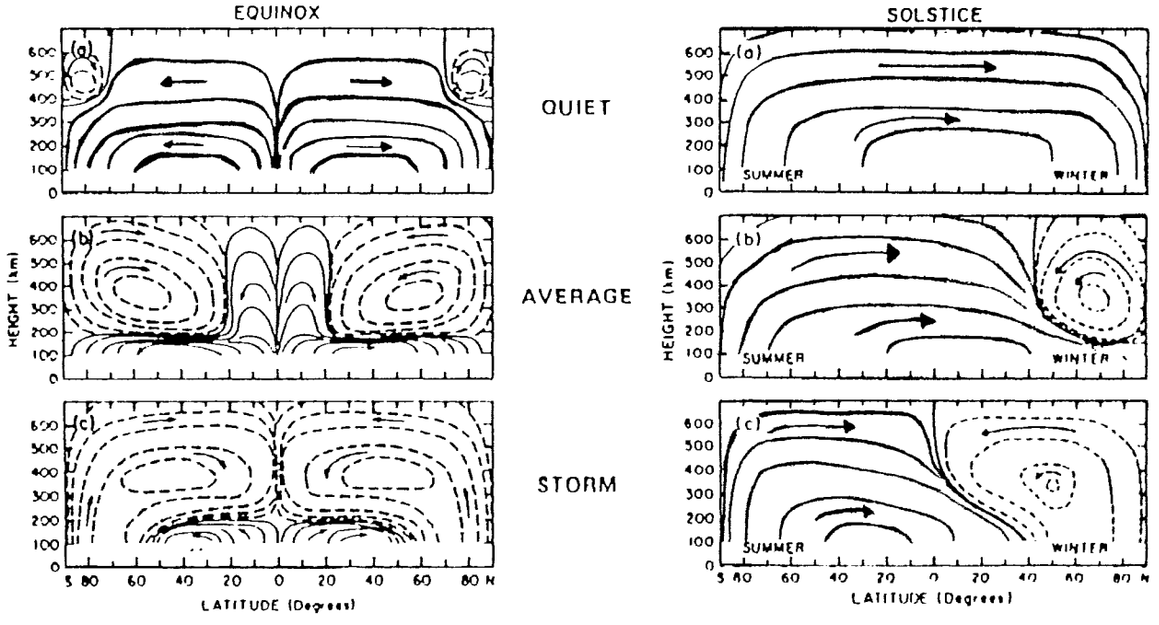

Fig 1.8: Schematic diagram of the zonal mean meridional circulation in the earth's thermosphere during equinox and solstice for various levels of auroral activity. (a) quiet auroral activity where circulation is primarily driven by solar UV heating, (b) average auroral activity where heating is 10^{11} watts and (c) during geomagnetic storms where the heating is about 10^{12} watts. The contours schematically illustrate the mass flow and the arrows indicate the direction of the motion.

(After Roble, 1987)

-region, $N_m F_2$ gets reduced as the effective recombination coefficient of the F region β increases with decrease in altitude. Thus winds can modulate $N_m F_2$. Wind effects at low latitudes are discussed in section 1.5.

1.4.4 Thermosphere models

Historically, the atmospheric regions such as troposphere, stratosphere, ionosphere, etc.. have been studied as separate entities and couplings among them are by and large ignored. This is partly because of their different dynamics and chemistry and also different experimental techniques are needed to probe the different regions. During the last one decade several studies have been made to address the coupling of the thermosphere with mesosphere below and the ionosphere within. In the same period many advances in understanding lower thermosphere also took place. The upper thermosphere is qualitatively understood. It is been realized that many outstanding problems of the thermosphere can be resolved by deploying simultaneous diagnostics on a global scale for simultaneous measurements of key neutral and plasma parameters. Significant progress has been made in understanding the thermospheric response to magnetic activity. There has been a lot of growth in development of thermospheric models which can be run on computers. The models provide a frame work within which to view experimental data and to test physical understanding.

Many models of the thermosphere are in existence today. The models range from simple empirical models to highly complex three dimensional theoretical models.

Empirical models :

The Mass-Spectrometer-Incoherent-Scatter (MSIS)-83 model (Hedin, 1983) provided predictions of neutral temperature and N_2, O_2, O, He, Ar and H densities. This model is intended to describe the long term behavior of the thermosphere. (In other words model can not predict thermospheric behavior to rapid and strong changes in geomagnetic activity especialy at sudden commencements.) This model is now superseded by MSIS-86 (Hedin, 1987), in which neutral temperature and composition data from

the Dynamics Explorer (DE-2) satellite were included to improve the representation of polar region morphology. The MSIS models are readily available for use with personal computers and are reasonably user-friendly. However these models either *overestimate* (Burnside et al., 1988; Hagan and Salah, 1988; Crowley et al., 1989) *or under estimate* (Sipler et al., 1983; Biondi and Meriwether, 1985; Murty and Kim, 1988a, b; Biondi et al., 1990a, b) the temperatures, when compared to temperatures measured by ground based incoherent scatter radar and optical (Fabry-Perot Interferometer) techniques respectively. We too found such under estimation of daily nightly average temperatures by MSIS model when we compared our optical measurements at the equatorial station, Kavalur (12.5°N, 78.5°E) with model predictions and the details are presented in chapter 3. This discrepancy is yet to be resolved.

Empirical global models of thermospheric winds are also available (Hedin et al., 1988). It is known as HWM 87 (horizontal wind model) and is analogous to the MSIS models, but is based only on wind data obtained from the AE-E and DE-2 satellites. Neither altitude nor solar cycle variations are included in the model due to the lack of data coverage, and it is only valid above about 220 km where the data coverage is best. Unlike MSIS 86 model, the HWM 87 predictions are in good agreement with ground based (Miller et al., 1990, Biondi et al., 1990b, Oliver et al., 1990) and satellite based (Burrage et al., 1990) wind measurements. HWM-87 was superseded by HWM-90 (Hedin et al , 1991) and solar activity variations were included in this model. HWM-90 is apllicable to altitudes above 100 km. Low and midlatitude wind data generally agree with HWM-90 predictions (Hedin et al, 1991).

Thermospheric general circulation models (TGCM) :

TGCMs have been developed to study global circulation, temperature and compositional structure of the thermosphere. Unlike MSIS models (which are empirical) TGCMs are computer based theoretical models. TGCMs have been useful in examining the solar-driven thermospheric circulation, response to auroral particle precipitation and to model substorms. The TGCMs such as National Center for Atmospheric Research (NCAR) models require phenomenal computing resources and difficult to use.

The main inputs to TGCM are solar EUV/UV fluxes, high latitude forcing and upward propagating tides. The accuracy of these models is being constantly improved by more realistic definition of the input parameters. For example parameterization of the particle precipitation in the auroral oval, the polar cusp and polar rain by Roble and Ridley (1987) represented an important step in TGCM development. Fesen et al.(1986) incorporated data on upward propagating semi-diurnal tides into the NCAR-TGCM model.

Changes in the thermosphere are known to affect the ionosphere and vice-versa but such interactions were not modelled in TGCMs until recently. Roble et al.(1987b) developed a global average (1-D) model of the coupled thermosphere and ionosphere, which formed the basis for a new (Roble et al., 1988b) 3-D thermosphere-ionosphere general circulation model (TIGCM). The TIGCM calculates the global ionosphere distribution of O^+, NO^+, O_2^+, N_2^+, N^+, electron density and ion temperature as well as the usual fields of neutral wind, temperature and major constituents.

A new simulation model of the upper atmospheric dynamics is presented by Richmond et al (1992). The model is an extension of TIGCM and is known as the National Center for Atmospheric Research Thermosphere-Ionosphere-Electrodynamic General Circulation Model (NCAR/TIE-GCM). TIE-GCM calculates the dynamo effects of thermospheric winds and uses the resultant electric fields and currents in calculating the neutral and plasma dynamics. The TIE-GCM also calculates global distributions of the gas temperature, winds and the number densities of the major constituents O_2, N_2, O and minor neutral constituents N, NO, He and Ar.

TGCM validation :

The temperature distribution predicted by TGCM and MSIS model were comparable (Roble et al., 1987a) but the TGCM contained much more small scale structure. Killen et al(1988) examined the relationship between F region neutral winds and the aurora. They compared DE-2 satellite wind measurements with TGCM winds and found a good agreement between them although the observed ion drag was much more

structured than the model could reproduce. Roble et al. (1988a) used time dependent auroral and convection parameterization to simulate the November 21-22, 1981 interval, which was a period of relatively steady geomagnetic forcing. The input parameterizations generally agreed with DE-2 satellite measurements of the inputs for the period. The TGCM winds also agreed well with the DE-2 measurements for a number of orbits. But TGCM overestimated temperatures and it was attributed to the method of calculating perturbation temperature and to an inadequate aeronomical scheme. This is corrected in the new coupled TIGCM. A comprehensive validation of TGCM was performed by Crowely et al.(1989a, b) using data from the equinox transition study (ETS)of 18-19 September 1984.

1.4.5 Experimental results on upper thermosphere

As explained earlier the global thermospheric structure is mainly determined by solar EUV and UV heating. Under magnetically disturbed conditions the high latitude forcing also becomes an important parameter and even dominate the global thermospheric morphology for many hours. The following is the gist of the winds and temperature measurements so far made at various locations in the world.

Winds :

Comparison of the Ariquipa (16.5°S, 71.5°W, 3.2°S dip) and Arecibo (18.6°N, 66.8°W, 30°N dip) optically measured winds for 1983 and 1988 revealed that the meriodional flows are in opposite direction while the zonal flows are in the same direction, which is an expected feature of the thermospheric circulation set up by solar heating (Biondi et al., 1990b). Wind measurements revealed that zonal velocity at Arecibo is small. The F- region peak is at lower altitudes at Arecibo, which for comparable ion densities leads to greater ion drag and hence smaller zonal velocities. This result confirms the theoretical study of Forbes and Roble (1990).

Herrero et al.(1988) examined the low latitude meridional neutral winds measured *in-situ* by the AE-E satellite between altitudes of 250-450km. Significant seasonal vari-

ations were found and which are consistent with the seasonal variation of the equatorial midnight temperature maximum(MTM) [see section 1.5.3 for MTM] and confirmed previous ground based observations. Strong diurnal and seasonal variations were found in neutral wind observations from the Arecibo Fabry-Perot interferometer(FPI) by Burnside and Tepley(1989). They were unable to detect any significant solar cycle influence on either the meridional or zonal components of the Arecibo wind velocity. This result is similar to that of Sipler et al.(1982) for Laurel Ridge, but contrasts with Hernandez and Roble (1984a) who found significant variation in the zonal winds and the meriodional gradient at Boulder and in the theoretical work of Hedin and Mayr (1987b).

Miller et al(1993) derived meridional neutral winds and peak electron densities from ionosonde measurements. They observed equatorward strengthening of the meridional wind and accompanying changes in peak electron densities during magnetically disturbed periods at mid latitudes.

Temperature :

Burnside et al.(1988) using Incoherrent Scatter Radar(ISR) data of Arecibo estimated exospheric temperatures and compared them with MSIS-86 model predictions. They found that the estimated temperatures were consistently 50K lower than the model predictions but observed diurnal variation of temperatures could be produced by MSIS-86 model.

The first summertime latitudional-temporal map of exospheric temperatures from the ISR chain at 70°W was obtained by Oliver and Salah (1988). Daytime summer temperatures were higher by 200K than winter temperatures at all latitudes. The observed temperatures were relatively low at high latitudes but MSIS-83 model showed higher temperatures at high latitudes. The observed temperatures and their gradients were well reproduced by the NCAR-TGCM. Winter quiet time exospheric temperatures from the radar chain show an unexpected low latitude suppression of exospheric temperature (Oliver and Salah, 1988; Hagan and Salah, 1988). Both MSIS and NCAR-TGCM models failed to predict the Winter time latitudional temperature gradient. The MSIS

temperatures were too high at low latitudes, while the TGCM temperatures were too small at mid-latitudes. Exospheric temperature enhancements of 350K were observed during the ETS 19 september 1984 storm (Croweley et al., 1989).

1.4.6 Studies of Lower thermosphere

Lower thermosphere plays an important role in coupling the middle atmosphere with the upper atmosphere and ionosphere. The properties of the upper thermosphere are influnced by the winds, electric fields, temperatures and composition of the lower thermosphere at an altitude of 80-150km. For example Burns et al (1989b) showed that the rapid compositional recovery of the high latitude upper thermosphere following magnetic activity is because of the downward vertical advection driven by radiational cooling of NO in the lower thermosphere.

Lower thermosphere is too low for satellite probing and too high for balloon measurements. Studies of the lower thermosphere are therefore still exploratory in nature and the data base is sparse. However the introduction of radar technology for lower thermosphereic studies has improved our understanding of dynamical processes of lower thermosphere by means of wind measurements (Avery, 1990 and references therein).

Chandra et al (1990) presented a monthly mean climatology of zonal mean temperature, zonal wind and geopotential heights with nearly pole-to-pole coverage (80°S - 80°N) for 0-120 km which can be used as a function of altitude and pressure. This climatology reproduces most of the characteristic features of the atmosphere such as the lowering and cooling of the mesopause and the lowering and warming of the stratosphere during the summer months at high latitudes.

Due to the difficulty in experimental probing of the lower thermosphere, the theoretical modelling studies are extremely important in lower thermosphere. Detailed simulations of lower thermospheric dynamics have recently been presented by Roble et al.(1987a), Clark et al.(1988), Crowely et al.(1989a, b) and Rees and Fuller-Rowell(1990b).

Tides and Waves :

Reviews by Forbes (1987), Vial (1989) and Vial and Forbes (1989) give details of main physical processes affecting the propagation of tides from the lower to the middle and upper atmosphere. Mayr et al(1990a) examined the dynamo action of the diurnal tide and its effect on thermospheric circulation. They investigated the relative importance of the E- and F- region dynamos and concluded that contrary to common perception, the main dynamo electric fields are generated primarily in the F-region and not in the E-region. Recently Buonsanto(1994) showed the evidence for polarization electric field in the daytime F-region above Millstone Hill (43° N, 289° E). The semidiurnal wind amplitude is particularly strong (50 m/s) in the E-region (Johnson et al., 1987; Rottger and Meyer, 1987).

Nitric Oxide (NO) :

NO is an important trace constituent in the thermosphere. NO is more abundant near 120 km. Since NO is chemically and radiatively more active, it plays a vital role in determining the composition and structure of the atmosphere above 100km. During solar maximum, the dominant cooling mechanism between 125-160km is radiative cooling from NO (Roble et al., 1987b, Dickinson et al., 1987). At solar minimum, NO cooling is important but not as large as molecular thermal conduction. This difference is due to the enhanced NO abundance and higher thermospheric temperatures during solar maximum. Gerard and Roble (1988) presented the importance of NO cooling in controlling the dynamic structure of the thermosphere.

Gravity Waves :

The existence of atmospheric gravity waves (AGW) in the earth's upper atmosphere was originally inferred from ground based observations of travelling ionospheric disturbances (TID) (see review by Crowley, 1991 and references therein). Gravity waves and their effects seem to be present in the thermosphere at all times and in all geographic locations. The propagation and attenuation of these waves have important consequences, for example on the energy budget of the lower thermosphere. A complete understanding

of these waves is therefore very important. The source mechanisms of AGWs and their modes of propagation are yet to be understood clearly. In the last few years, many researchers have studied the morphology of TID. Hedin and Mayr (1987a) presented statistics on wavelike fluctuations in neutral composition measured by the DE-2 satellite. There appear to be many sources which contribute to the gravity wave spectrum in the thermosphere. Most of the medium scale TIDs observed at midlatitudes originate in the troposphere with in 1500km from the point of observation(Waldock and Jones, 1987). Gravity waves are often generated by high latitude thermospheric forcing. A clear cause and effect relationship between an auroral disturbance and a large scale TID was presented by Rice et al.(1988).

Gravity Waves modelling :

The wave dispersion equation given by Hines (1960) is useful for understanding wave observations. However, in order to describe waves in relations to their sources, the global source geometry needs to be taken in to account. This requires numerical models such as those of Richmond and Matsushita (1975). However there is no detailed information about the source, and hence theoretical models serve as tools to test hypotheses and to gain an understanding of observed wave characteristics. One such model developed by Mayr et al (1984a, b; 1987) is the linear transfer function model (TFM). The development of the TFM was reviewed by Mayr et al.(1990c). Mayr et al,(1987) extended the TFM to include the electric field momemtum source. Mayr et al. (1990c) discussed the properties of realistic source geometries using the TFM and compared the response characteristics for Joule heating and momemtum coupling separately. Hedin and Mayr (1987a) used the TFM with a Joule heat source to model wave like fluctuations in neutral composition measured by the DE-2 satellite.

1.5 Equatorial thermosphere-ionosphere system

As explined earlier in section 1.4, the thermosphere and the ionosphere are coupled closely by mutual interactions. The structure of the thermosphere - ionosphere system at equatorial latitudes is significantly influenced by the dynamics of the neutral

atmosphere. Due to the dominance of ion-drag effects (Rishbeth, 1979), the interaction between the plasma and the neutral atmosphere is a normal feature at F-region altitudes.

Ion-drag :

Neutral particles of thermosphere and charged particles of ionosphere interact with each other through collisions. Motion of one influences the motion of the other. There will be a drag force if there is a relative motion. The effect of ions on neutral particles is called *ion drag*, and the ion drag force per unit volume is

$$F_{ni} = n_n m \nu_{ni} (V_i - U)$$

where V_i and U are ion and neutral air velocities. Concentration and mass of the particles are denoted by 'n' and 'm' respectively. The subscripts 'n' and 'i' represent neutrals and ions. ν_{ni} represent collision frequency of n with i. The converse effect of neutral particles on ions is called *air drag*, and the drag force per unit volume is

$$F_{in} = n_i m \nu_{in} (U - V_i)$$

where ν_{in} represent collision frequency of i with n.

Below E region the neutral air density and ν_{in} are both large and hence ions are carried along with the wind. In the F region the air drag force is smaller because of less number of neutrals. Therefore the neutral wind effectively blows the ionization along the geomagnetic field and it alters the height of the F-layer plasma by some tens of kilometres. The tidal wind in the thermospehre is larger by night than by day because the ion density and therefore the ion drag, is smaller at night.

The significance of the plasma-neutral coupling will be illustrated in the following through a discussion of a few prominent phenomena of the equatorial thermosphere-ionosphere system.

1.5.1 North-South asymmetry in the EIA crests

The first observation of neutral wind effects on the structure of the equatorial ionosphere was provided by the significant north-south asymmetry in the electron densities of EIA crests particularly during solstice months (e.g. Lyon and Thomas, 1963). According to numerical modelling studies (e.g. Anderson and Roble, 1981), such asymmetry can be accounted if the effects of trans-equatorial (north-south) neutral winds are taken into consideration.

1.5.2 Post-sunset enhancement of EIA

Post-sunset enhancement in the strength of EIA is a feature of the diurnal variation of EIA particularly during high sunspot activity (Rishbeth, 1977). This enhancement is due to the renewal of the *fountain* mechanism (Martyn, 1947) which is due to the enhancement of the eastward electric field due to the F-region dynamo (Rishbeth, 1971a). Studies based on groundbased ionosondes and TEC measurements support this view (e.g. Somayajulu, 1964; Sastri, 1982; Anderson and Klobuchar, 1983). This increase in eastward electric field in the post sunset period raises the F-region to high altitudes (about 350 to 500 km), and as the layer is raised the neutral gas accelerates because of reduced ion drag. Subsequent reversal of electric field pushes the layer down and the gas decelerates because of increased ion drag. Heelis et al (1974) successfully predicted the post sunset effect in their model, which included horizontal conductivity gradients near sunset in the F region dynamo mechanism. Farley et al (1986) introduced F region wind in their simulation study. The schematic of the model of the F region prereversal enhancement driven by a uniform F region wind U is shown in Figure 1.9. They have assumed in their calculation that the F region wind is is the only driving force blowing from west to east with a velocity of 200 ms^{-1} at all latitudes and longitudes, i.e independent of ion drag and h_{max} was kept at 350 km, an altitude which maps down along the magnetic field lines to the E region at about 10° latitude. Some of the equatorial drift velocities which are equivalent to electric fields are plotted in 1.10. The top panel (a) is the eastward ion drift near the peak of the F region. The middle panel (b) is the

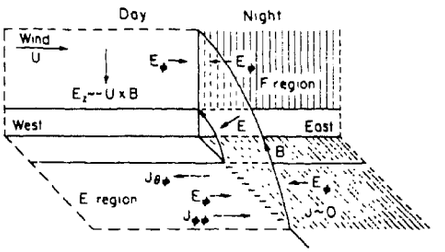

Fig : 1.9

Oversimplified model of the F region prereversal enhancement driven by a uniform F region wind U. Near the sunset terminator the F region dynamo E_z is no longer shorted out and approaches $-\mathbf{U} \times \mathbf{B}$. This field maps to an equatorward E_θ (not shown explicitly) in the E layer and drives a westward Hall current. But if no current flows in the nightside E region, a negative polarization charge must develop at the terminator, with E_ϕ as is shown and $J_{\phi\phi}$ cancelling $J_{\phi\theta}$, and this E_ϕ maps back to the F region and causes first an upward, then a downward, $\mathbf{E} \times \mathbf{B}$ plasma drift.

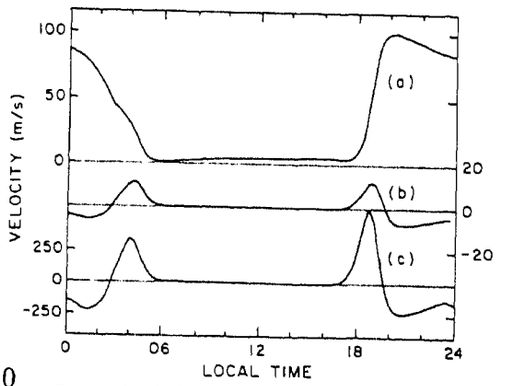

Fig : 1.10

Equatorial drift velocities driven by a uniform 200 m/s eastward F region dynamo wind only: (*a*) the eastward F region ion velocity at 350 km; (*b*) the upward F region ion velocity; and (*c*) the westward E region electron velocity. The E region drift velocity corresponds to an altitude of about 105 km and to a ratio of Hall to Pedersen electric field of 25. The sunset prereversal enhancements are clearly shown in Figures 4*b* and 4*c*. The model is not realistic near sunrise.

(After Farley et al., 1986)

vertical F region ion drift and bottom panel (c) shows the westward E region electron drift velocity. Panel (b) and (c) show exactly the prereversal enhancement effects in the E and F region. Very recently, Crain et al (1993) simulated vertical drift velocities by including the F region dynamo winds in their self consistent model and the results are shown in Figure 1.11. The E region open-circuit model (curve 1) assumes that the F region plays no role in the current generation or closure processes. The E region closed circuit model (curve 2) assumes that the F region wind is zero but includes the contribution of the F region to the flux tube integrated conductivity. Inclusion of the F region winds in the current generation process produces the vertical ion drifts shown by curve 3. These curves are compared with the model of Richmond et al (1976) which is analogous to the open circuit model mentioned above. Only curve 3 which is the result of including the F region dynamo winds matches with the observed vertical drift data of Jicamarca especially during post sunset hours i.e. reproducing the post sunset enhancement in the vertical drift.

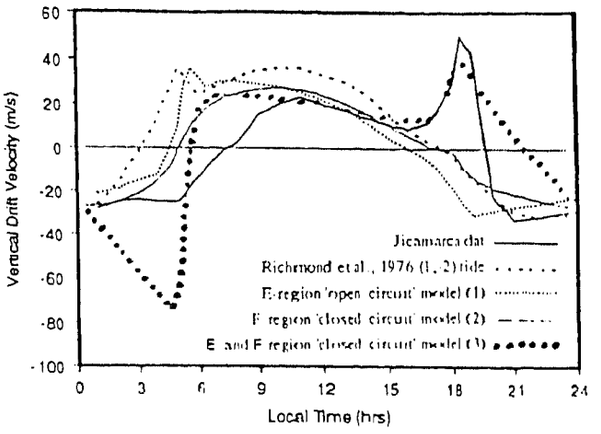

Fig 1.11 : local time variation of vertical ion drifts resulting from different model assumptions compared with empirical models and observations.

(After Crain et al., 1993)

1.5.3 Equatorial midnight temperature maximum (MTM)

The thermospheric temperature in the equatorial region does not always undergo a monotonic decrease throughout the night but experiences a pronounced enhancement typically around midnight, sometimes reaching or exceeding the daytime values (Spencer et al., 1979). This recurrent feature is referred to as the *midnight temperature maximum* (MTM) and it is an energetically significant feature of the equatorial thermosphere.

Perhaps the first manifestation of the MTM was in the airglow observations of Greenspan (1966) which were carried out aboard the ship U.S.N.S. Croatan as it travelled from North to South America. Greenspan found an enhancement of the atomic oxygen 630 nm airglow emission at an altitude of 300 km. But at that time the reason for the enhancement was not clear. Wright (1971) found a descent of the F-region around midnight at Chile (35°S) and attributed it to a variation in the neutral wind. Nelson and Cogger (1971) came out with a logical conclusion that the enhancement in 630 nm airglow emission which they observed around midnight at Arecibo(18°N), is due to the descent of the F-region. They also found that the descent occurred at later local times with increasing geomagnetic latitude. Behnke and Harper (1973) found out a reason for the descent of F-region in terms of variation of meridional wind. They also observed abatement of equatorward wind before midnight and reversing frequently to poleward after midnight. The abatement and reversal of meridional wind could be understood in terms of MTM. The first *in-situ* observation of MTM came from the data of the neutral wind and temperature experiment (NATE) of aboard AE-E satellite (Spencer et al.,1979, 1981). Figure 1.12 shows an example of MTM.

Mayr (1979) gave a theoretical explanation for the equatorial MTM. Ion-neutral momentum coupling associated with the diurnal variation in ion density is the single most important process for generating the midnight temeprature maximum. This process is illustrated in Fig. 1.13. Thermospheric motions are damped by ion drag; a decrease or increase in ion density leads to an increase or decrease in wind velocities respectively. Dynamical properties of the thermosphere can be described approximately

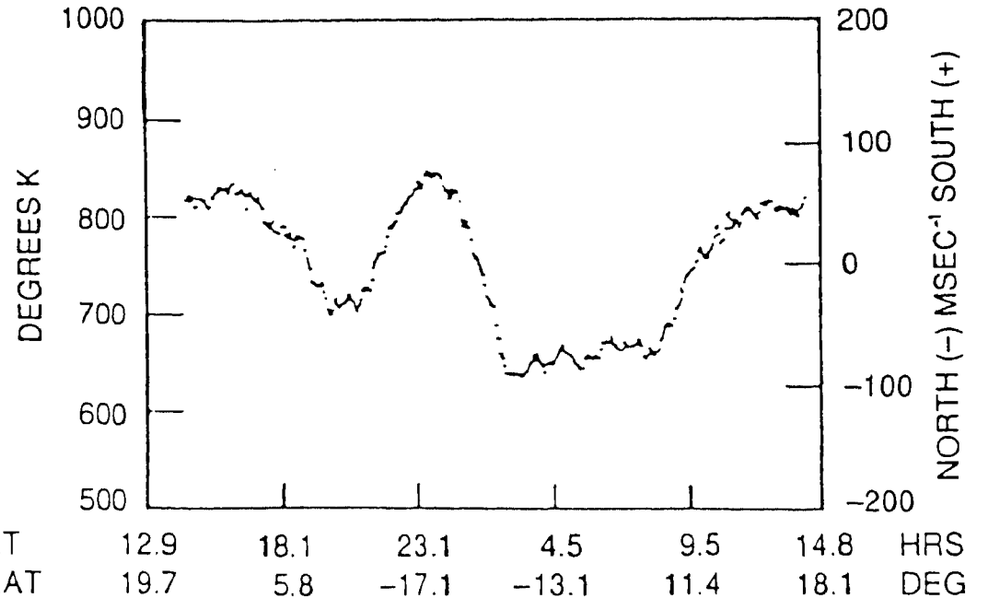

Fig 1.12 : Example of the largest midnight temperature maximum observed with the NATE instrument on the AE-E satellite. The temperature near midnight (around 24.0 LT) rises about $200^{\circ}K$ above the declining temperature background.

(After Spencer et al., 1979)

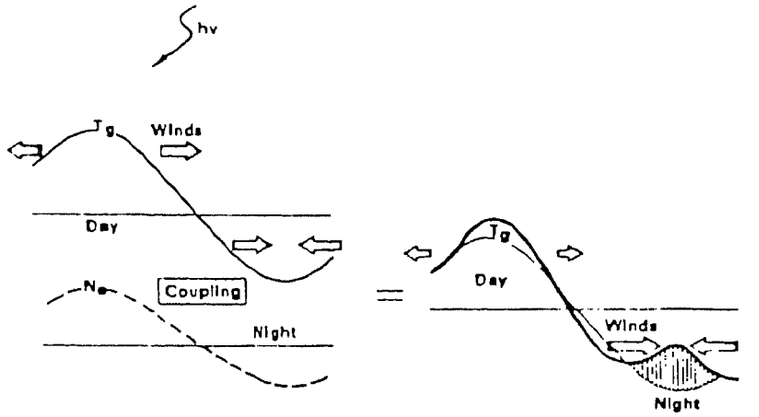

(a) (b)

Fig 1.13 : Schematic illustration of the interaction between diurnal variations in ion drag and wind fields which can lead to a nighttime temperature maximum. A constant electron density gives a day and night winds of approximately equal amplitude. The diurnal variation in electron density yields smaller daytime winds thus less expansive reduction in temperature and large nighttime winds with more heating by compression.

(After Mayr et al., 1979)

in terms of a linear tidal theory for the globally uniform component of the ion distribution. The wind system of a particular tide (e.g. fundamental diurnal component with wave number m=1) affects only the temperature variations of that same tide. Energy is transported from the dayside toward the night side thus lowering the day to night temperature contrast (see Fig. 1.13). Since the diurnal variation in the ion density is large, the wind velocities are smaller during day than those expected for the diurnal averaged ion density. As a result less energy is carried away from the dayside, relative to the diurnal average, producing a higher equilibrium temperature (compare heavy and light solid lines in the right half of Fig. 1.13b). During the night the ion density is smaller than the diurnal average, thus more energy is carried toward the night side and a localized maximum can develop. In the context of tidal theory this change in temperature structure signifies a transfer of energy from one mode to another. The diurnal variations (m=1) of the ion density combine to produce a momentum source for the semidiurnal tide (m=2). Interaction between the diurnal and semidiurnal variations in the wind fields and ion drag, in turn, excite terdiurnal tides and so forth.

Figure. 1.14 is a block diagram which illustrates the processes that contribute to the midnight temperature maximum. The fundamental diurnal tide (m=1) is primarily excited *in situ* by absorption of EUV radiation and by the global (average) ion distribution, both of which are presumably stable for time periods of several days. On the other hand, the semidiurnal tide of the upper thermosphere is much more complex. It has three major contributions of which only the EUV source is stable and its contribution is very small in the upper thermosphere. The other two are (a) tidal waves originating in the lower atmosphere and (b) momemtum coupling associated with the diurnal (m=1) variations in the wind field and ion density. These two components are of comparable magnitude but they are out of phase. Since (a) and (b) are variables the resultant semidiurnal tide is also variable. This variability significantly contributes to the variability of the MTM (Mayr et al. 1979). The contributions from EUV heating and lower atmospehric tidal waves are small for the terdiurnal component (m=3). Momentum coupling associated with diurnal variations in ion drag is the dominant excitation

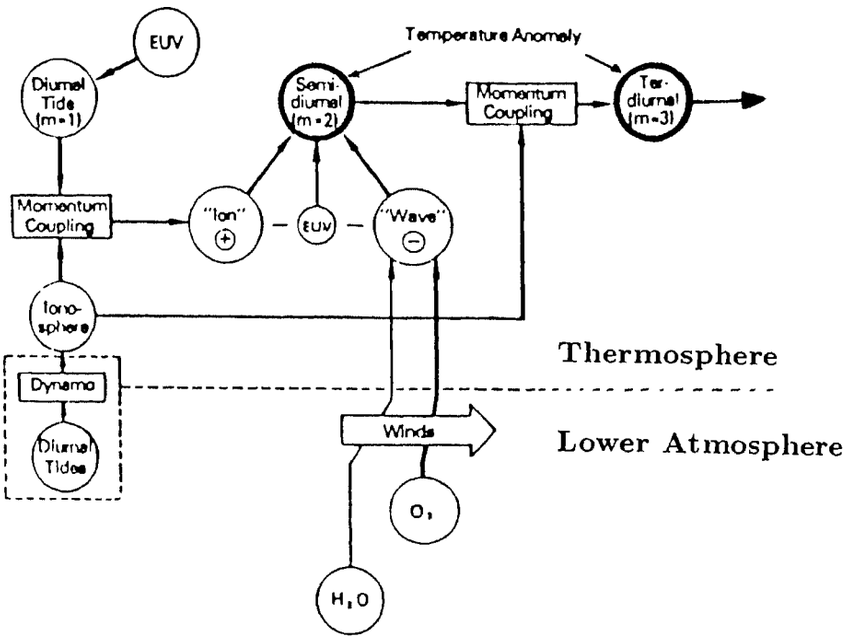

Fig 1.14 : Block diagram illustrating the processes that contribute to the midnight temperature anomaly.
(After Mayr et al., 1979)

process. This involves the semidiurnal wind field and the large diurnal component in ion density. The variability of both contributes again to the variability of the MTM.

Figure 1.15a shows the four most important sources of to the semidiunal temperature and N_2 density variations. Plus and minus signs are shown to indicate phases near 00LT (or 1200 LT) and 600 LT (or 1800 LT) respectively. The main results of the theoretical studies of Mayr et al. (1979) are as follows. The ion drag component produces a temperature enhancement (plus) (see Fig. 1.15a) near midnight (0200 LT). The wave from below has a dominant effect in the temperature and N_2 density below 200 km and 300 km, respectively, and it shifts the semidiurnal phases to later local times ($\sim$ 0800 LT). It is noted that the ion drag component contributes more to temperature than to density.

The terdiurnal tide of the temperature is illustrated in Fig. 1.15b. Except for the contribution labeled 'EUV' which comes from the terdiurnal component of the radiative heat input, all other contributions are the result of coupling between the diurnal variations in ion drag and the semidiurnal variations of the wind field. The latter in turn is driven by the semidiurnal components due to EUV, H_2O, O_3 and ion drag whose effects on temperature and density are shown in Fig. 1.15a. While the O_3 component is of secondary importance for the semidiurnal tide it is dominant in the terdiurnal tide. Both O_3 and ion drag components are nearly in phase and tend to produce a temperature maximum (plus) near midnight. A synthesis of the theoretical results for tides up to order m=4 is shown in Fig. 1.16 [after Mayr et al. 1979]. The results resemble the observed MTM. The maximum occurs almost two hours after midnight which is within the range of the observations. The temperature variations are similar at 200 and 410 km and consistent with observations. A synthesis of the diiurnal variations in the meridional wind velocity is shown in Fig. 1.17 for 10° and 20° latitudes. The computed zonal wind field (not shown in fig) exhibits a surge of the eastward velocities before midnight which is followed by a change in direction near 0200 LT. Both zonal and meridional wind components form a pronounced convergence zone near midnight which is the cause of the temperature anomaly.

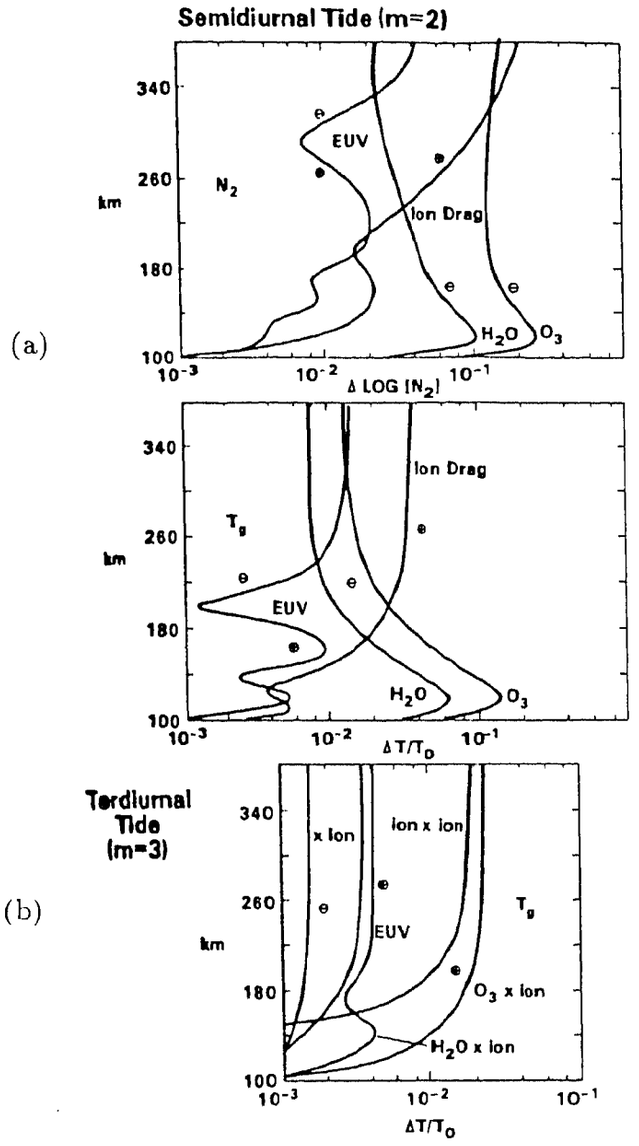

Fig 1.15 : (a) Semidiurnal tides for T_g and N_2 density associated with various excitation mechanisms. Plus and minus signs indicate phases in quadrants near 00(12) and 06(18) local times respectively. (b) The terdiurnal component for the temperature. Plus and minus signs indicat phases in quadrants near 00(8) and 04(12) local times respectively. Except for the EUV contribution the terdiurnal components are the result of nonlinear interactions between semidiurnal wind field (due to EUV, ion drag, O_3 and H_2O) and diurnal variations in the ion density.

(After Mayr et al., 1979)

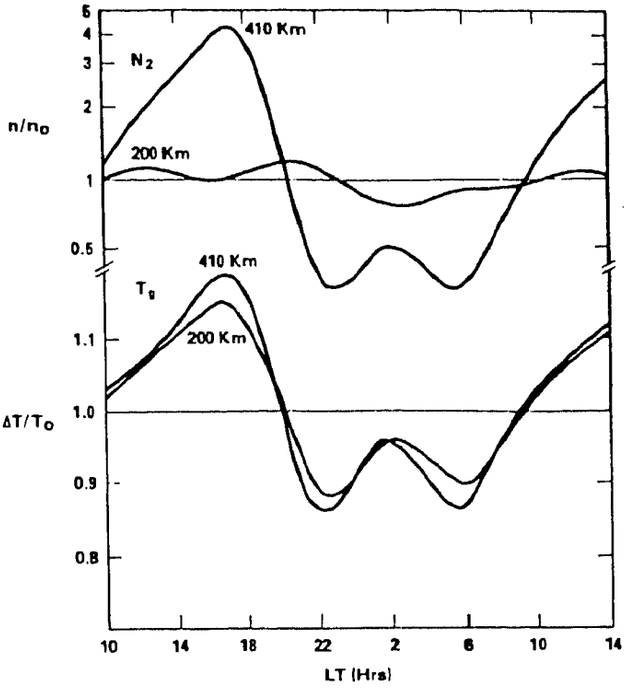

Fig 1.16 : Theoretical diurnal variations of temperature and N_2 density. Note that at 200 km N_2 does not yet show the signature of a nighttime temperature maximum. (After Mayr et al., 1979)

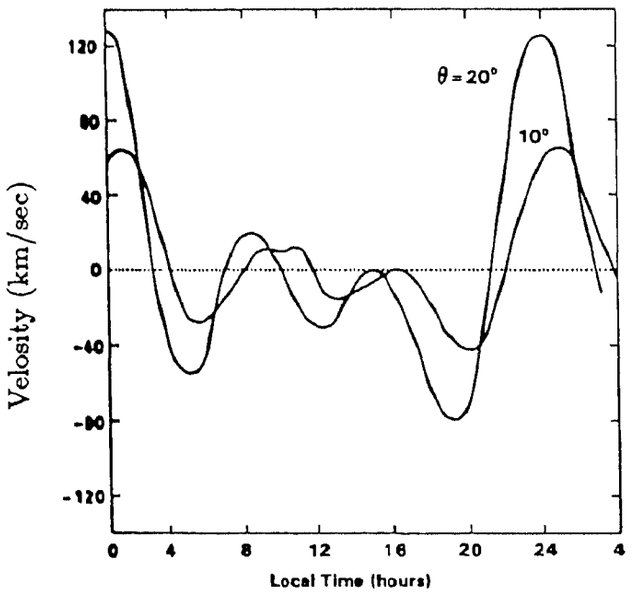

Fig 1.17 :Meridional winds computed from the theoretical model for conditions of hemispherical symmetry (equinox). Positive winds are directed toward the equator. (After Mayr et al., 1979)

It is clear from the above synopsies (i.e from 1.5.1 to 1.5.3)of the important phenomena of equatorial thermosphere-ionosphere system, that simultaneous measurements of neutral parameters like temperatures and winds and plasma parameters like electron density as a function of height are needed to understand the structure and dynamics of the thermosphere-ionosphere system.

1.5.4 Neutral Anomaly (NA) and Equatorial Temperature and Wind Anomaly (ETWA)

The latitudinal distribution of the neutral densities (N_2 and O) (see Fig. 1.18) at 450 km altitude in the dip equatorial region indicates the importance of ion-drag effects for the structure of the neutral atmosphere. The spatial distribution is characterized by two crests on either side of the dip equator and a trough on the dip equator. This structure which manifests prominently in the evening hours is referred to as *neutral anomaly,* NA as its features are similar to those of *equatorial ionization anomaly*, EIA (Hedin and Mayr, 1973).

The existence of NA has been explained in terms of ion-drag force in the zonal direction, which depends on ion density and the difference in velocity between ions and neutrals acting on the neutrals. The neutrals move westward in the forenoon and eastward in the afternoon while the ion motions are westward throughout day time. As such the ion-drag force becomes significant around noon when the speed of neutrals becomes a minimum. At this time the well developed EIA imposes a similar variation in the neutral flow retaining more heat energy of the neutrals at the EIA crests, leading to higher temperatures and densities at crests than those over the trough. Two phenomenon are closely related to this physical situation. One is the formation of small 'cusps' [an apex or peak] or 'ledges' [a narrow horizontal surface projecting out] of ionization in the topside ionosphere (Lockwood and Nelms, 1964). The 'ledge' formation is understood to be primarily due to the inhibition of plasma flow along the field lines by the field aligned enhancements of neutral densities characterizing the NA

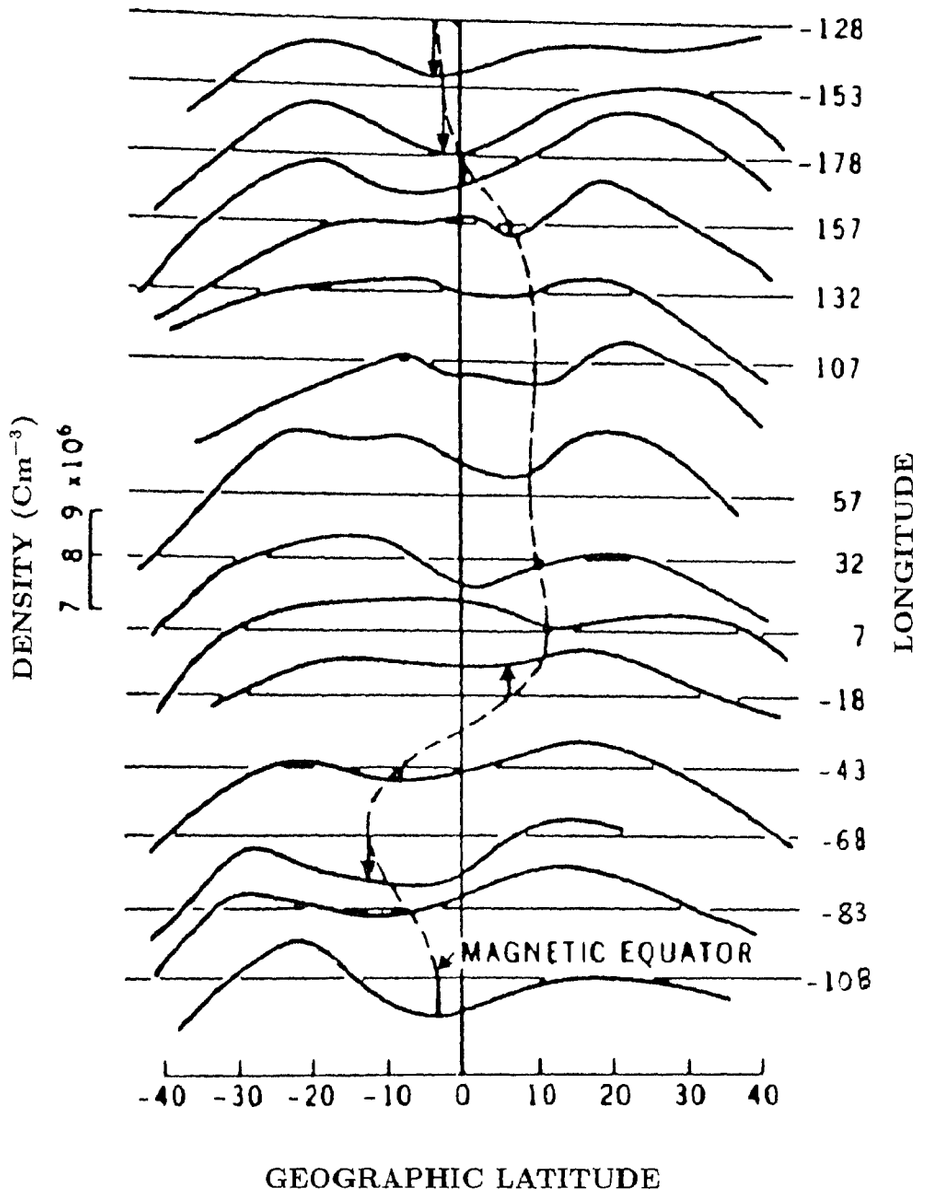

Fig 1.18 : Field aligned enhancement of neutral densities indicating the formation of the neutral anomaly.
(After Hedin and Mayr, 1973)

(Raghava Rao and Sivaraman, 1975). The other phenomenon is the recently discovered *equatorial temperature and wind anomaly*, ETWA (Raghava Rao et al., 1991). ETWA refers to the anomalous latitudinal variations in the zonal neutral winds and neutral temperature, with the zonal winds exhibiting a broad maximum centered around the dip equator flanked by minima on either side(see Fig. 1.19). The temperature, on the otherhand, shows a pronounced bowl-shaped minimum at the dip equator with maxima on either side. The two minima (maxima) in the zonal winds (temperature) are colocated with the crests of the equatorial anomaly, EIA. ETWA which is found (so far) to manifest during daytime and postsunset periods of high solar activity epochs can be understood in terms of the effect of EIA-associated ion-drag on the zonal winds and the energy balance of the thermosphere as originally proposed by Hedin and Mayr (1973). The neutral motion is impeded to a larger extent at the EIA crests due to increased ion drag than at the EIA trough. With the result the zonal wind flow is modulated to have minima at crests and maximum around trough. The modulation in zonal flow in turn affects the thermal energy balance and hence the temperature. Around the crests where the zonal flow is reduced the energy transport from the dayside to the nightside is reduced leading to an increase in the diurnal amplitude of the temperature. The reverse situation prevails in the trough region where the flow velocity is larger. It is thus clear that the structure and dynamics of the plasma and neutral constituents of the equatorial upper atmosphere are intricately coupled. The dynamo electric field produces the EIA which, in turn, affects the neutral atmosphere dynamics leading to NA and ETWA. The NA and ETWA in turn modify the EIA by forming the ledge in the topside ionosphere.

The above summary illustrations indicates the fairly complex and interactive nature of the physical processes operative in the equatorial thermosphere-ionosphere system under essentially quiet geomagnetic conditions. The complexity increases at the times of geomagnetic storms and substorms due to, among other things, the dynamic/electrodynamic coupling of the high latitude-low latitude ionospheres. During magnetic storms enhancements in the electron density of the bottomside ionosphere usually prevail at

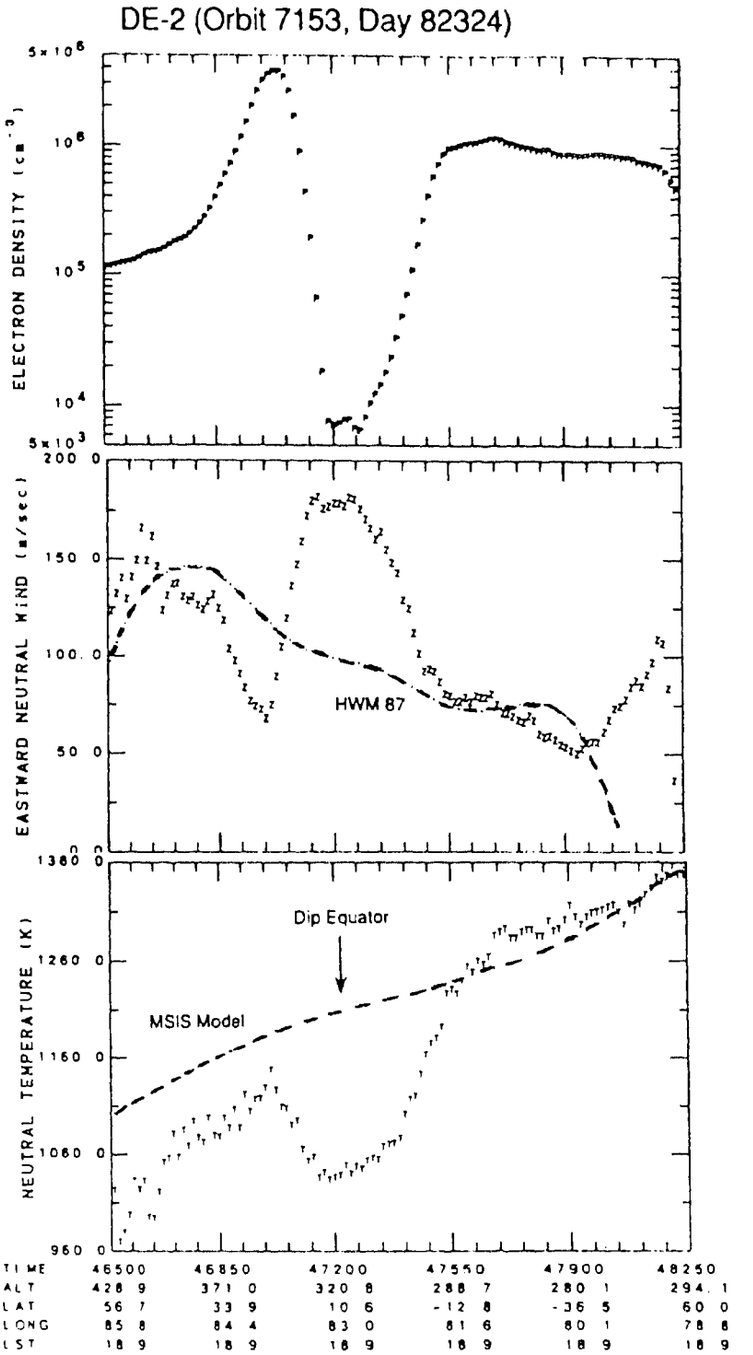

Fig 1.19 : DE-2 data of electron density (upper panel) zonal winds (middle panel) and temperature (lower panel) at low latitudes on November 20, 1982.
(After Raghava Rao et al., 1991)

equatorial latitudes, and this is thought to be due to the reduction of the electrojet strength and hence the effectiveness of the 'fountain' mechanism (e.g. Rajaram, 1977). The origin of the storm-time weakening of the electrojet is still unclear. In the topside ionosphere, depletion of ionization is normally noticed in a dome-shaped region over the equator and at the low latitudes (e.g. Sato, 1966). Occasional deviations from these average patterns do also occur. For example, conspicuous decreases in NmF_2 with prominent increases in height of F-region are found in certain severe geomagnetic storms (e.g. Sastri, 1980), while enhancements of the strength of EIA are sometimes evidenced in the topside ionosphere (Raghava Rao and Sivaraman, 1973). Observations of such departures are instructive and interesting because they indicate that besides the electromagnetic drifts, other physical processes like neutral wind effects and neutral composition changes can also play a role in the storm-time behaviour of equatorial ionosphere. In fact, from a careful study of one particular ionospheric storm in the Indian region, Sastri (1980) concluded that the decreases in NmF_2 evidenced at locations near the dip equator during the recovery phase of the magnetic storm are due to localized changes in neutral atmospheric composition (increase $\frac{N_2}{O}$ and $\frac{O_2}{O}$ ratios). The AE-E satellite data analyzed by Gross (1985) showed that such changes in neutral composition and electron density in bottomside F-region do occur at equatorial latitudes during storm-time conditions. The very recent studies of the ionospheric effects of the magnetic storm of 13 March 1989 further strengthened the view that the composition of equatorial neutral atmosphere does gets altered during severe storms leading to 'negative' ionospheric storms (Batista et al., 1991; Walker and Wong, 1993). That the equatorial thermospheric temperature and density respond significantly to geomagnetic forcing has also been demonstrated by the very recent analyses of DE-2 and AE-E satellite data (Burns and Killeen, 1992; Burrage et al., 1992). Therefore simultaneous storm-time measurements of neutral temperature and winds, plasma drifts and plasma density distributions are needed to understand the varied facets of the equatorial ionospheric response to geomagnetic storms/substorms.

Keeping in view the necessity of simultaneous measurements of neutral and plasma

parameters, we have developed an optical interferometer (FPI) to measure neutral parameters. The chapter two presents a detailed description of the interferometer developed and commissioned at Kavalur (12.5°N, 78.5°E) during the year 1991. Simultaneous measurements of neutral and plasma parameters are achieved by simultaneous FPI operation at Kavalur and Ionosonde operation at Indian equatorial/lowlatitude stations respectively. The results from these measurements on specific days are presented in chapter 3.

1.6 Airglow

Many of the photochemical reactions within the upper atmosphere are accompanied by the emission of radiation in the visible, infrared or ultra-violet parts of the electromagnetic spectrum. These atmospheric emissions are termed as *airglow*. The name airglow was proposed by Elvey on the suggestion of Struve (see Chapman 1967). The airglow is different from *Aurora*. Aurora is a high latitude phenomena. Auroral emissions which are due to the excitation of atmospheric constituents by the charged particles of solar wind/magnetospheric origin show much structure in both space and time. Airglow in contrast is always present, covers all latitudes and is virtually unstructured. On a moon less night the airglow constitutes the major part of the light of the sky, exceeding starlight in total intensity though its presence is not generally appreciated because of its distribution over the entire sky.

An important application of airglow emission is to observe the Doppler width and shift of a known line so as to find temperature and velocity of emitting species. Since emitting species moves with the wind the velocity of the wind can be deduced. Spectroscopy of atomic oxygen line emission and its use in measuring the thermospheric temperature is presented in chapter 2.

1.7 Scope of the present work

Chapter 2 presents :

• A detailed description of Fabry-Perot interferometer (FPI) which is developed to measure neutral thermospheric parameters at Kavalur(12.5°N, 78.5°E), India close to

the geomagnetic/geographic equator.

• Details of data acquisition and data reduction technique.

Chapter 3 presents :

• Characteristics of night time neutral thermospheric temperature (measured with the FPI) over Kavalur and comparison of the same with MSIS-86 model predictions.

• Characteristics of the equatorial midnight temperature maximum (MTM) in Indian zone and comparison of the same with that of MTM characteristics observed at Jicamarca(12°S, dip 2°N) in the American sector.

• Case studies of MTM related meridional winds and their effects on low latitude F-region height and density through simultaneous measurements of neutral and plasma parameters in the Indian equatorial region in December 1992.

Chapter 4 presents the studies of response of equatorial ionosphere to the transit of the interplanetary magnetic cloud of January 13-15, 1967. Response of the equatorial ionosphere is presented in two sections and they are :

• Transient disturbance in the F-region over Kodaikanal which is an example of low latitude penetration of sub-storm associated high-latitude electric fields.

• Persistent disturbance in the F-region which is an example of disturbance in thermospheric circulation and attendant disturbance dynamo electric fields.

Chapter 5 presents :

• A case study of the global nature of the substorm related composite electric field disturbance in equatorial ionosphere based on ionosonde data.

Chapter 6 consists of the summary of the studies/results presented in the thesis and scope for future work.

******

Chapter 2

Instrumentation and data reduction

2.1 Introduction

Several experimental techniques are available to measure neutral atmospheric parameters like temperature, winds, and densities at F-region altitudes. The prominent and widely used techniques are :

- Chemical releases from rockets (e.g. Haerendal et al., 1967; Bedinger, 1970; Gupta et al., 1986).

- Satellite drag and in-situ density measurements (e.g. Spencer et al., 1979).

- Plasma measurements with the incoherent scatter radar (e.g. Harper, 1973; Amayenc, 1974).

- Measurements of intensity of OI 135.6nm and 630nm airglow emissions from satellites (e.g. Bittencourt et al., 1976).

- Line profile and Doppler shift measurements of OI 630 nm airglow emissions from ground and space platforms (e.g. Biondi and Feibelman 1968; Hays et al., 1969, 1979; Hays and Roble 1971; Hernandez and Roble, 1976; Thuillier et al., 1977; Sipler et al., 1983; Meriwether et al., 1986).

Out of these only a few enable direct determination of temperature and winds. They are chemical releases from rockets, the incoherent scatter radar and high-resolution spectroscopy of OI 630 nm airglow emissions.

Chemical releases, although resourceful, are not amenable to study the long-term or even the local time variations, owing to the large number of rockets that would become necessary for such purposes. Besides, the data can be acquired only at locations with rocket launching facilities. The incoherent scatter radar is a investment - intensive technique and is thus adopted by only a few affluent groups in the world. In

contrast, groundbased high-resolution spectroscopy of 630 nm night airglow emissions with FP instrumentation is a relatively inexpensive and highly cost-effective technique available for thermospheric research. In fact, eversince the first detection of thermospheric motion by an interferometer was reported by Hays and Roble (1971), the FP interferometer (FPI) technique has enjoyed tremendous success and emerged as a major tool for thermospheric studies. This is partly due to the fact that the 630 nm night airglow emission is weak ($\sim$ 100R) and emanate from an extended source and, among the spectroscopic devices, the FP interferometer is the most luminous tool available for a given resolving power ($\lambda/\Delta\lambda$) for studies of extended sources, i.e, those which overfill the entrance aperture of the spectrometer.

The OI 630 nm night airglow emission is a product of chemical reactions between the ionospheric plasma (0^+, e) and the neutral atmosphere (N_2, 0_2) in the lower F-region. The underlying chemical reactions are charge transfer from the dominant ionospheric ion to neutrals, and the dissociative recombination of the molecular ion so formed with electrons:

$$0^+ + 0_2 \rightarrow 0_2^+ + 0 \tag{1}$$

$$0_2^+ + e \rightarrow (0_2^*) \rightarrow 0^* + 0^* \tag{2}$$

where * denotes that the dissociation products may lie in the electronically excited states ^{1}D and ^{1}S. See the energy level diagram shown below.

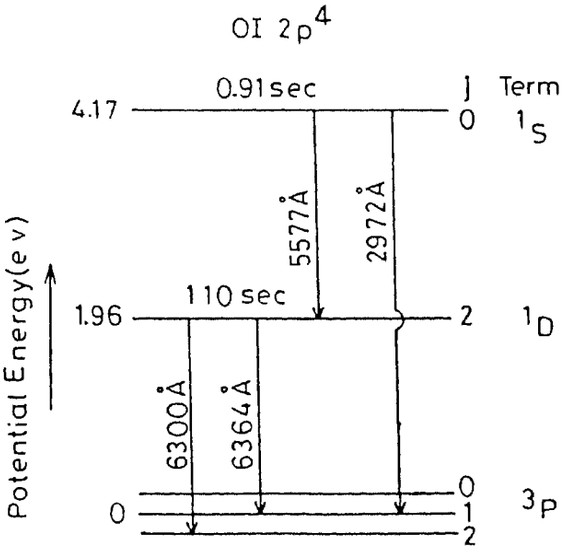

The rate of the process is controlled by the first reaction while the second reaction is responsible for the emission (Roach and Gordon, 1973). The 630 nm emission originates in the altitude range 250 - 350 km as shown in the figure 1.2 (chapter 1.) because the exponential decrease of 0_2 and N_2 densities with height reduces the production of molecular ions for recombination at high altitudes ($\geq$ 350 km), while quenching by N_2 and 0_2 of the long-lived ^{1}D state ($\tau_{rad} \sim 110$ sec) eliminates emission below about 250 km. The intensity of the emission is strongly dependent on the height of F-region peak as well as on the plasma content below the peak, and serves as a sensitive indicator of vertical plasma motions in the F-region (Barbier, 1959). It is precisely because of this property, the 630 nm emission has been extensively used to monitor large-scale ionospheric wave disturbances and plasma depletions (e.g. Sobral et al., 1980).

Limitations in using FPI :

As already mentioned, the neutral temperature and winds in the thermosphere are determined from the Doppler width and Doppler shift respectively of the 630 nm line emissions in the night sky (e. g. Hernandez and Roble, 1979 and references therein). Since the vertical temperature gradients of the atmosphere at F-region heights are small (e.g. Hernandez et al., 1975), the measurements of winds and temperature refer to a narrow height range centered about the peak of the emission in the night airglow. The FPI technique can not therefore provide information on the height variation of the wind (i.e. vertical shears) and this is one of the inherent limitations of the method. The other limitation is the restriction of the data coverage to only twilight and nighttime periods; only fifteen days in a month centered around new moon day. This however, can be overcome by the use of multiple etalon interferometry and interferometry with radial chopper and reports of successful observations of day glow with such systems already exist in the literature (e.g. Cocks et al., 1980; Narayanan et al., 1988).

Pressure-scanned FPI :

To achieve spectral scans we opted for the pressure-scanning (index-of-refraction change) method because it is less susceptible to the frequent loss of etalon alignment

as it does not involve any mechanical movement of spacers, and thus offers the distinct advantages of stability and simplicity. Pressure scanning, in fact, is being used by most of the airglow research groups round the world for thermospheric studies. It is to be borne in mind, however, that pressure-scanning is not a fast method of obtaining the line profiles, but this is not a major limitation because the type of the work which we have undertaken does not demand very high temporal resolution data on winds and temperatures.

2.2 Fabry-Perot Interferometer

We built the Fabry-Perot Interferometer (FPI) around an optically-contacted etalon of 100mm effective diameter procured from IC Optical Systems, U.K. The etalon is made-up of plates of $\lambda/100$ flatness with a reflectivity (R) of 0.85 at 630nm and spaced 10mm apart. The etalon plates have reflective coating of three layers of ZnS (μ=2.3) and two layers of MgF(μ=1.35). The reflective finesse of the etalon works out to be 19.3 from the formula $N_R = (\frac{\pi\sqrt{R}}{1-R})$. The etalon is housed in an air-tight chamber and the concentric-fringe pattern is imaged at the exit plane on an on-axis central aperture (dia 3mm, finesse 7) plate using a plano-convex lens (L_1) of 10cm diameter and 50cm focal length. A 50 mm diameter narrow-band (0.3nm) temperature-tuned interference filter (Andover Corporation, USA) is used to isolate the O(^{1}D) 630 nm line of the night airglow. An EMI photomultiplier (9863 A/350) housed in a thermoelectrically-cooled chamber (Model FACT 50 MK III) and operated in a photon counting mode is used as the detector. The schematic diagram of the FPI is shown in Fig.2.1 The wavelength scan is made by changing the air pressure inside the FP etalon chamber by a stepper-motor driven piston device. The chamber pressure is measured by a high-precision absolute pressure transducer (Datametrics, Barocel series 590). The scanning process as well as the data acquisition (simultaneous values of pressure and photon counts at each step of the scan) is controlled by a IBM compatible PC/AT through appropriate interface hardware and software (written in Turbo-Pascal) as shown in Fig.2.2 The sub-units of the interferometer housing the main optical elements and the detector, i.e, the

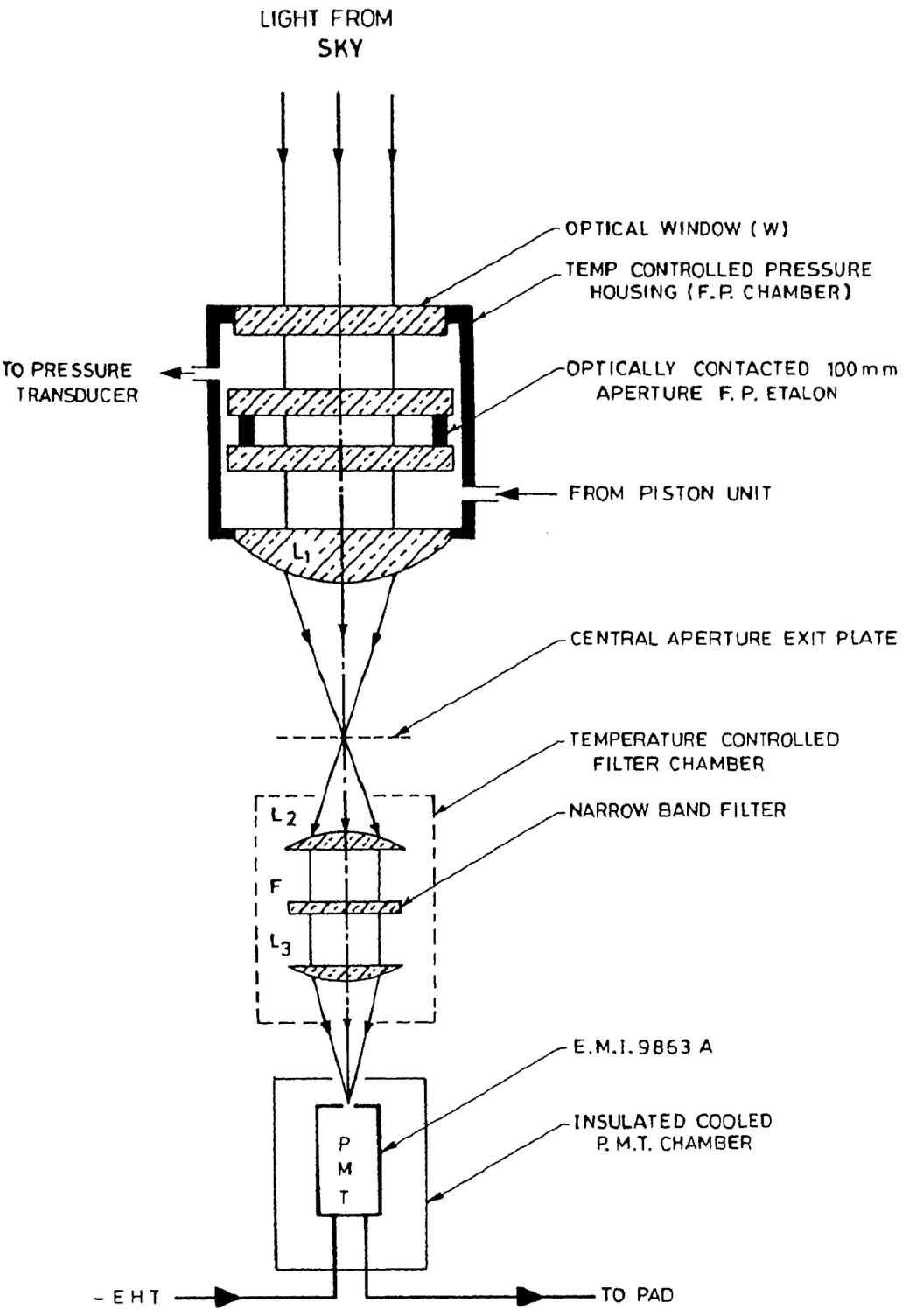

FIG 2.1 OPTICAL ARRANGEMENT OF FABRY-PEROT INTERFEROMETER

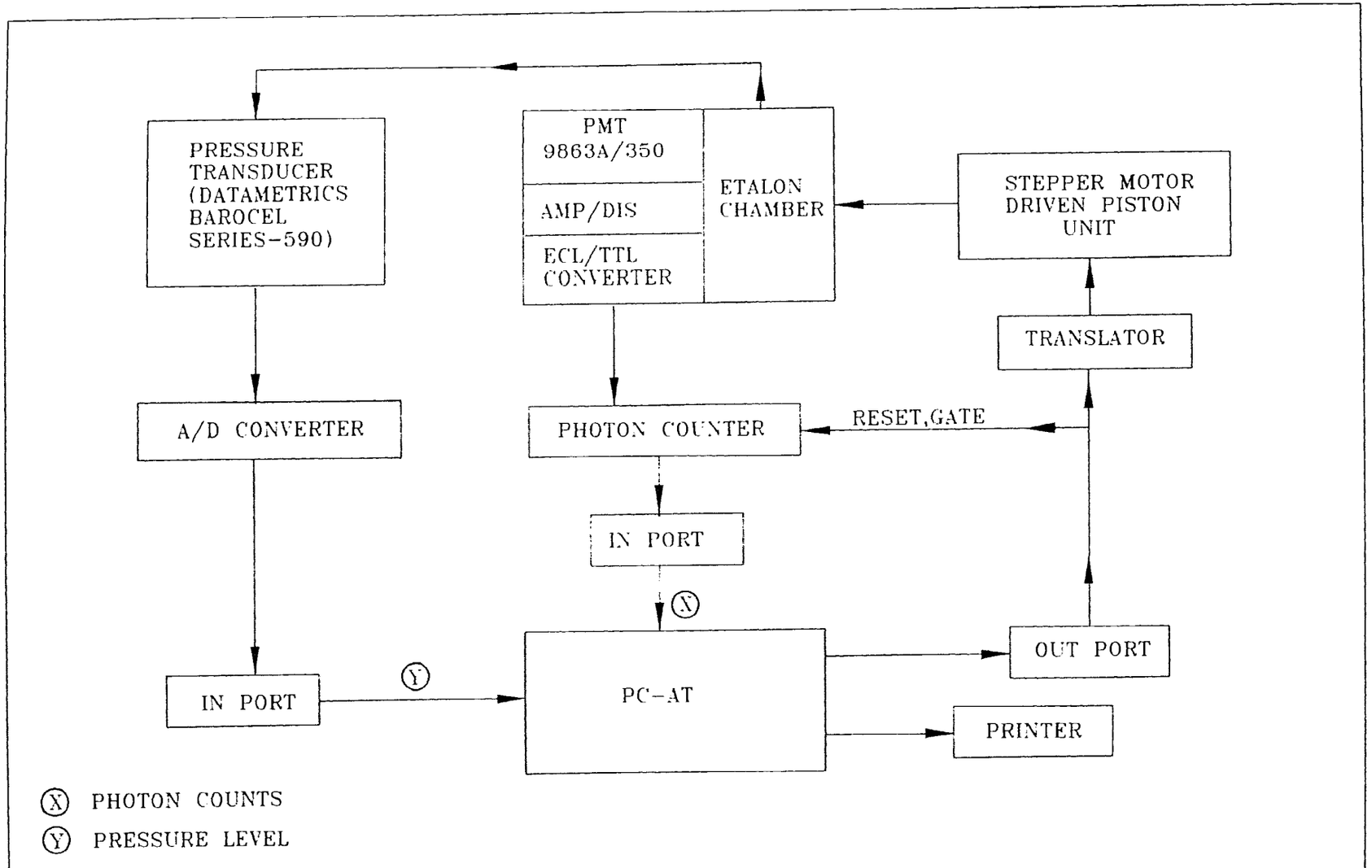

FIG 2.2
BLOCK DIAGRAM OF SCANNING ARRANGEMENT AND DIGITAL DATA AQUISITION WITH THE PRESSURE-SCANNED FABRY-PEROT INTERFEROMETER

etalon chamber, collimating tube, filter assembly with lens holders on eitherside and the PMT housing are integrated vertically in an iron-angle rack. The electronic circuitry, piston unit, EHT power supply for PMT, power supplies for electronic circuitry, etc. are housed in a standard 19″ rack. All the lenses used in the interferometer are anti-reflection coated. A laboratory $He-Ne$ laser (Melles-Griot) is used for laboratory evaluation of the FPI and for obtaining the 'instrumental' profile interspersed with the airglow observations. The specifications of the FPI are summarised in Table 2.1 The FPI set-up commissioned at Vainu Bappu Observatory (VBO), Kavalur is shown in Plate-II.

2.2.1. Opto-mechanical sub-units

The etalon chamber is made out of stainless steel with aluminium flanges on top and bottom. The etalon itself is housed in a brass cell at the center of the chamber. The optical glass window (w) and the condensing lens (L_1) are fixed to the etalon chamber at the top and bottom respectively with the help of rubber 'O' rings and aluminium flanges (see Fig. 2.1). The etalon chamber is gasketted on eitherside by silicone sealants to prevent air leakage. Screws are provided on the bottomside of the chamber at 90° apart for alignment of the interferometer. The chamber is provided with two nozzles for air 'inlet' and 'outlet' to alter and measure the air pressure in the chamber during the pressure-scanning process. A steel collimating tube is coupled to the etalon chamber. An aperture plate is mounted inside the tube at the focal plane of the objective lens (L_1) on a brass mount that can be moved vertically up and down (by $\sim$ 1cm) for fine adjustments of the definition of the concentric fringe pattern. A side-window with shutter is provided to view the fringe pattern. The collimating tube is coupled to the lens holder housing the plano-convex lens (L_2) of short focal length which collimates the light passing through the aperture on to the interference filter (see Fig.2.1). The lens holder is followed by the filter assembly unit and the two are coupled by steel flanges.

The filter assembly consists of a brass cell in which is housed the narrow-band interference filter with anti-reflection coated glass flats on eitherside for protection from

Table 2.1

Specifications of the Fabry-Perot Interferometer

at Vainu Bappu Observatory (VBO), Kavalur

1.	**Etalon plates**	
	Effective diameter	10cm
	Flatness	$\lambda/100$
	Reflective coatings	3 layers of ZnS and 2 layers of MgF
	Reflectivity (R)	0.85 at 630nm
	Reflective finesse (N_R)	19.3
	Spacing	1cm
2.	**Objective lens (L_1)**	
	Type	Circular, plano-convex
	Focal length	50 cm
	Diameter	10cm
3.	**Aperture**	
	Diameter	0.3cm
	Finesse	~ 7
4.	**Instrument field of view**	0.33°
5.	**Interference filter**	
	Diameter	5cm
	FWHM	0.291 nm
	Peak transmission	40.5%
	Peak wavelength	630.098 nm
6.	**Light detector**	PMT-EMI 9863A/350
		S-20 Cathode, 0.9cm size
7.	**Resolving power**	$\sim 6 \times 10^5$
8.	**Free-spectral range (FSR)**	0.01985nm ($0.5cm^{-1}$)
9.	**Scanning gas**	Air
10.	**Overall instrument finesse**	~ 5.3

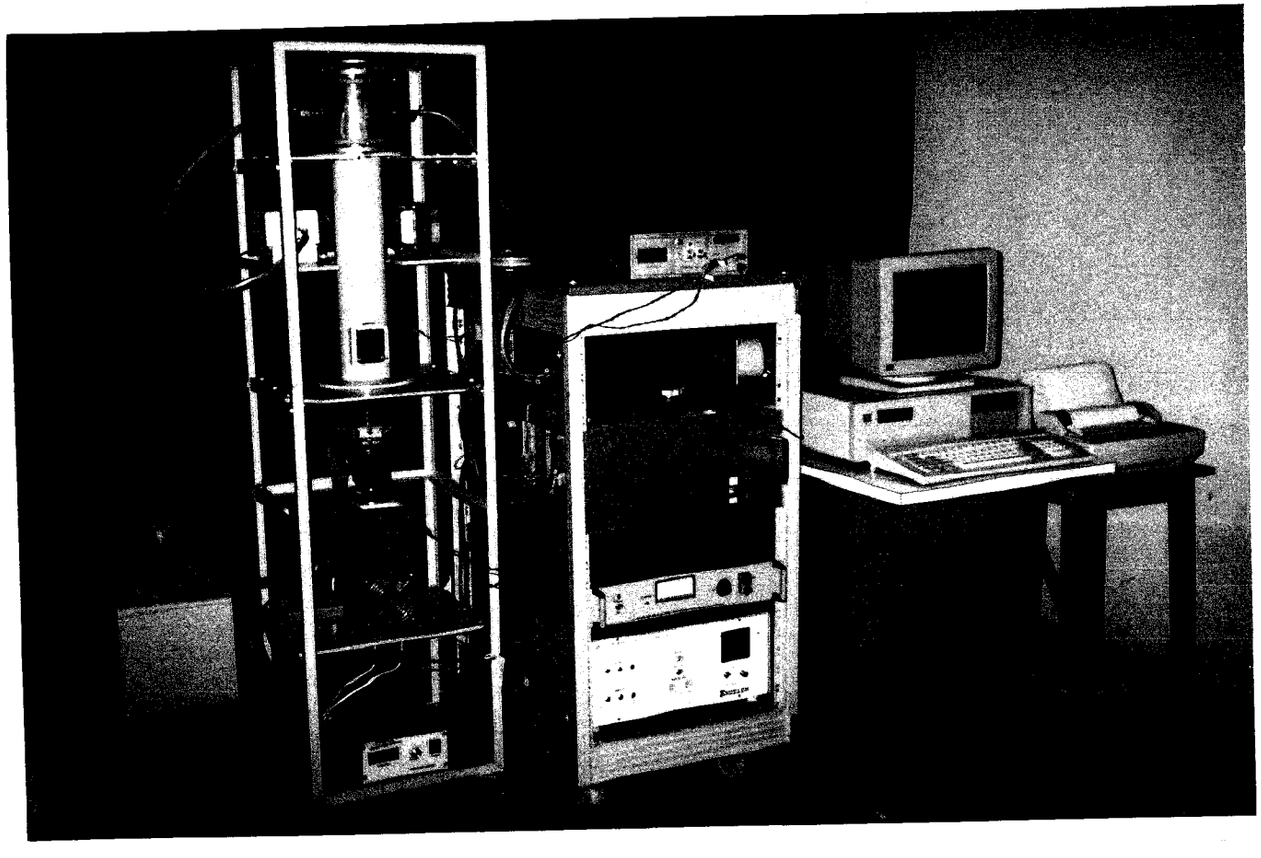

PRESSURE-SCANNED FABRY-PEROT INTERFEROMETER (FPI)

AT VAINU BAPPU OBSERVATORY (VBO), KAVALUR

PLATE-II

dust and moisture. Electrically heated nichrome coils are fixed just around these flats to arrest water condensation. The brass cell has four flat faces on its outerside. The cold junctions of the thermoelectric Peltier elements are kept in good thermal contact with these flat surfaces using heat sink compound. The hot junctions of the Peltier elements are sandwiched to four semi-hollow brass cubes through which water is circulated to remove heat from the hot junctions. A nylon cover surrounds the brass cell housing the interference filter for thermal insulation from the outside atmosphere. The engineering drawing which is the Fig.2.3 shows the schematic of water circulation for cooling the filter. The temperature of the brass cell and hence of the filter is monitored by an AD-590 sensor kept in contact with the cell, and is maintained (to within 0.1°C) with the help of a digital temperature controller (DTC - 2700 Servotronics, Ahmedabad) and the Peltier elements. The schematic diagram of the temperature control arrangement is shown in Fig.2.4. The four thermoelectric (Peltier) models are connected in series with the DTC-2700. The AD 590 sensor outputs current proportional to the temperature it senses on the filter holder to the DTC. This current is converted to a voltage signal with in the DTC and compared to the voltage corresponding to the set temperature. The DTC generates a current proportional to the difference of the two voltage signals and feeds it to the Peltier elements to maintain the temperature of the filter holder at the set value. The filter is temperature-tuned to the required wavelength and its pass-band characteristics (40.5% transmission at 630.098 nm at 23°C for normal incidence) are maintained by controlling the temperature. The transmission characteristics of the interference filter is shown in Fig.2.5.

The filter assembly unit is coupled to another lens holder which in turn is coupled to the PMT housing by steel flanges. A plano-convex lens of short focal length (L_3) is mounted in the lens holder to focus the light output from the filter onto the PMT cathode. The refractive-index or pressure-scanning is done with the piston unit which is connected to the etalon chamber with a nylon tube and nozzle-lock nut arrangement. The brass piston with a rubber 'O' ring is enclosed in a steel cylinder and is coupled to the shaft of the stepper-motor. A screw-rod-nut arrangement is used to achieve linear

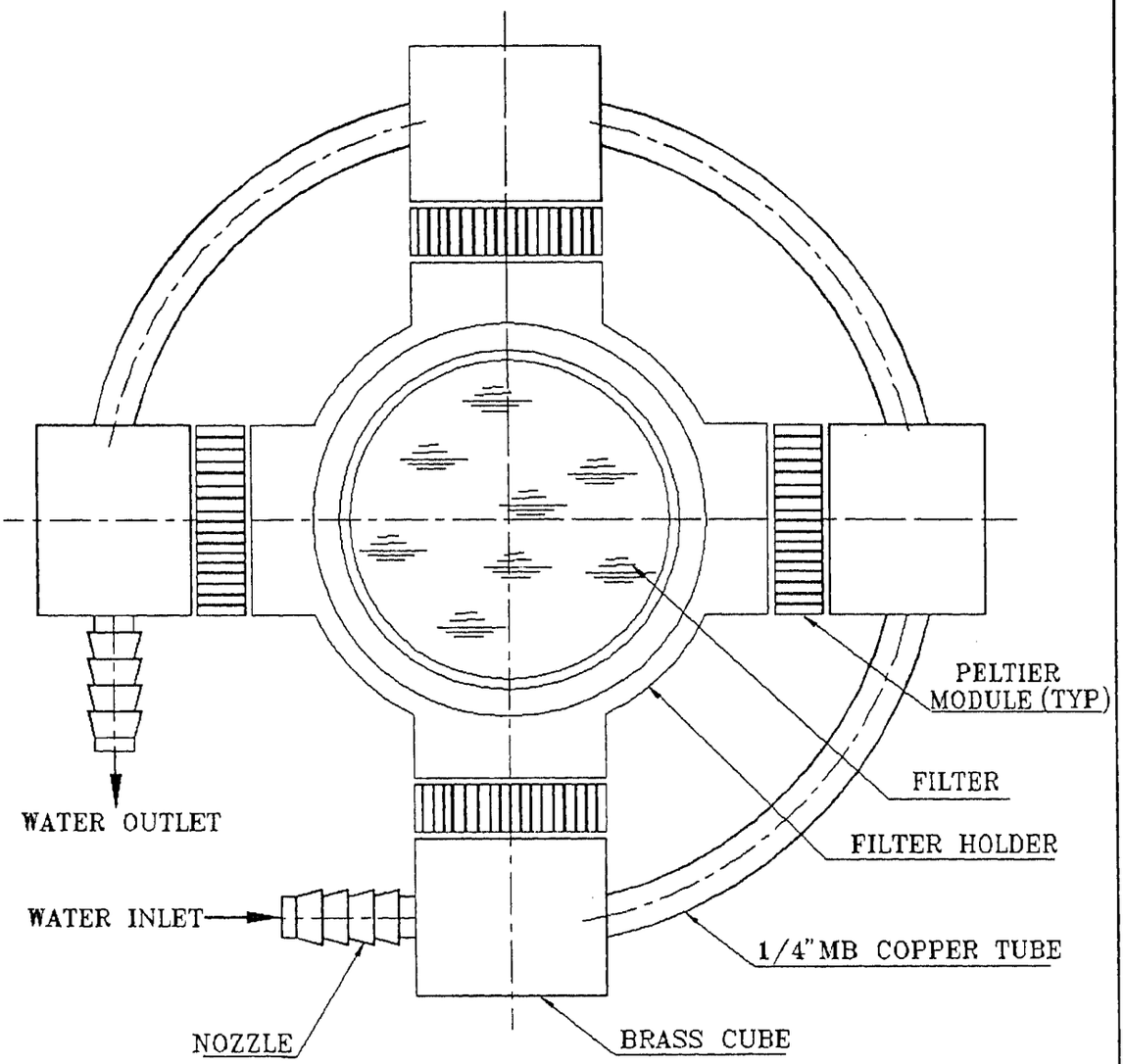

FIG 2.3
WATER CIRCULATION FOR COOLING THE FILTER
(SCHEMATIC DIAGRAM)

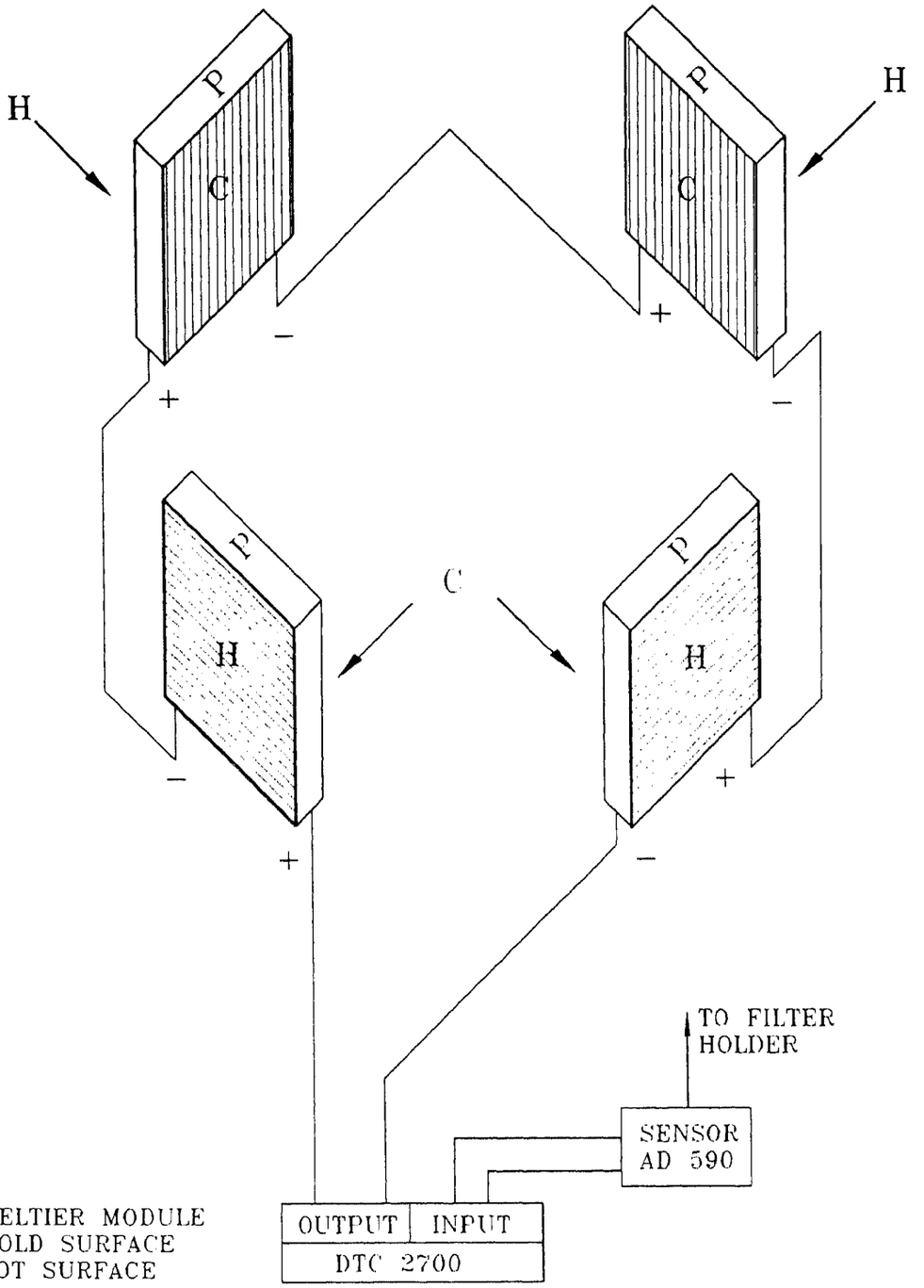

FIG 2.4
BLOCK DIAGRAM OF DIGITAL TEMPERATURE CONTROLLER (DTC) ARRANGEMENT FOR INTERFERENCE FILTER

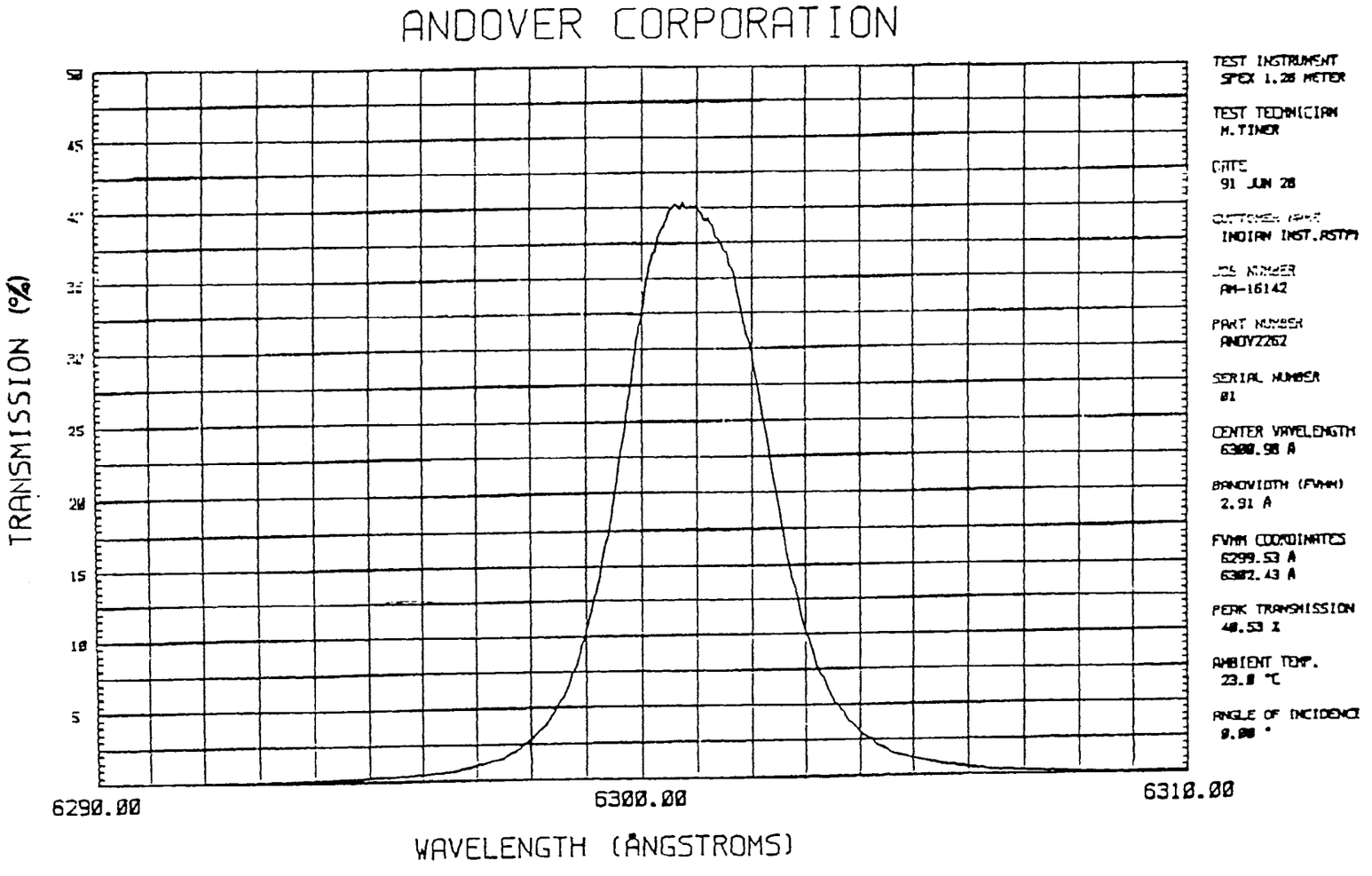
ANDOVER CORPORATION
TRANSMISSION (%)
45
25
20
15
10
5
6290.00
6300.00
6310.00
WAVELENGTH (ÅNGSTROMS)
TEST INSTRUMENT
SPEX 1.26 METER
TEST TECHNICIAN
M.TINER
DATE
91 JUN 28
INDIAN INST.ASTM
JOB NUMBER
AM-16142
PART NUMBER
ANDV2262
SERIAL NUMBER
01
CENTER WAVELENGTH
6300.98 A
BANDWIDTH (FWHM)
2.91 A
FWHM COORDINATES
6299.53 A
6302.43 A
PEAK TRANSMISSION
40.53 %
AMBIENT TEMP.
23.0 °C
ANGLE OF INCIDENCE
0.00 °

FIG 2.5

movement of the piston in steps under the control of the stepper-motor.

2.2.2 Electronics hardware

The output pulses from the PMT are fed to a preamplifier-discriminator, PAD (EMI Model C 604 A) where the pulse height is compared to a reference level (discrimination level). PAD generates standard ECL pulses whenever the amplitude of the incoming pulses reaches or exceeds the set discrimination level. The operating EHT voltage for the PMT and the discrimination level for PAD are fixed at minimum levels. The ECL pulses from the PAD are converted to TTL pulses to be compatible for feeding to the digital pulse counter. The details of the linkage between the PAD output and the pulse counter including the ECL to TTL conversion are shown in Fig. 2.6. The ECL pulses are fed to the chip 10125 and its TTL output is fed to the 74115 differential line driver. The output of 74115 is coupled to the pulse counter card through a twisted pair of wires and the line receiver 74116.

We have developed the hardware and software interfaces of an IBM compatible personal computer (PC) to the FPI for wavelength scanning and data acquisition. The approach constitutes a low-cost and effective solution for control and acquisition of data from the FPI, because the PC enables user-friendly dialogue for instrument-set up, provides flexibility in mode of operation (sequential versus random scans), on-line display of line profile build-up and storage of data as files in secondary storage media. The details of the PC hardware are as follows. A PC-XT (1024 KB RAM, 40 MB disk) is used for the control of the FPI and data acquisition with the help of three interface cards. They are: (1) a digital input/output card, (2) a gated pulse counter card with multiplexer and (3) a translator card for stepper-motor drive. The inter-connections between these cards and the other relevant sub-units of the FPI are shown in Fig.2.2.

The digital input/output (I/O) card supports up to 16 digital inputs and the same number of digital outputs. The digital inputs and outputs are each addressed as two bytes. The input port reads pulse counter information and the address assignment corresponds to locations 300 and 301 in Hexadecimal. The analogue voltage output of

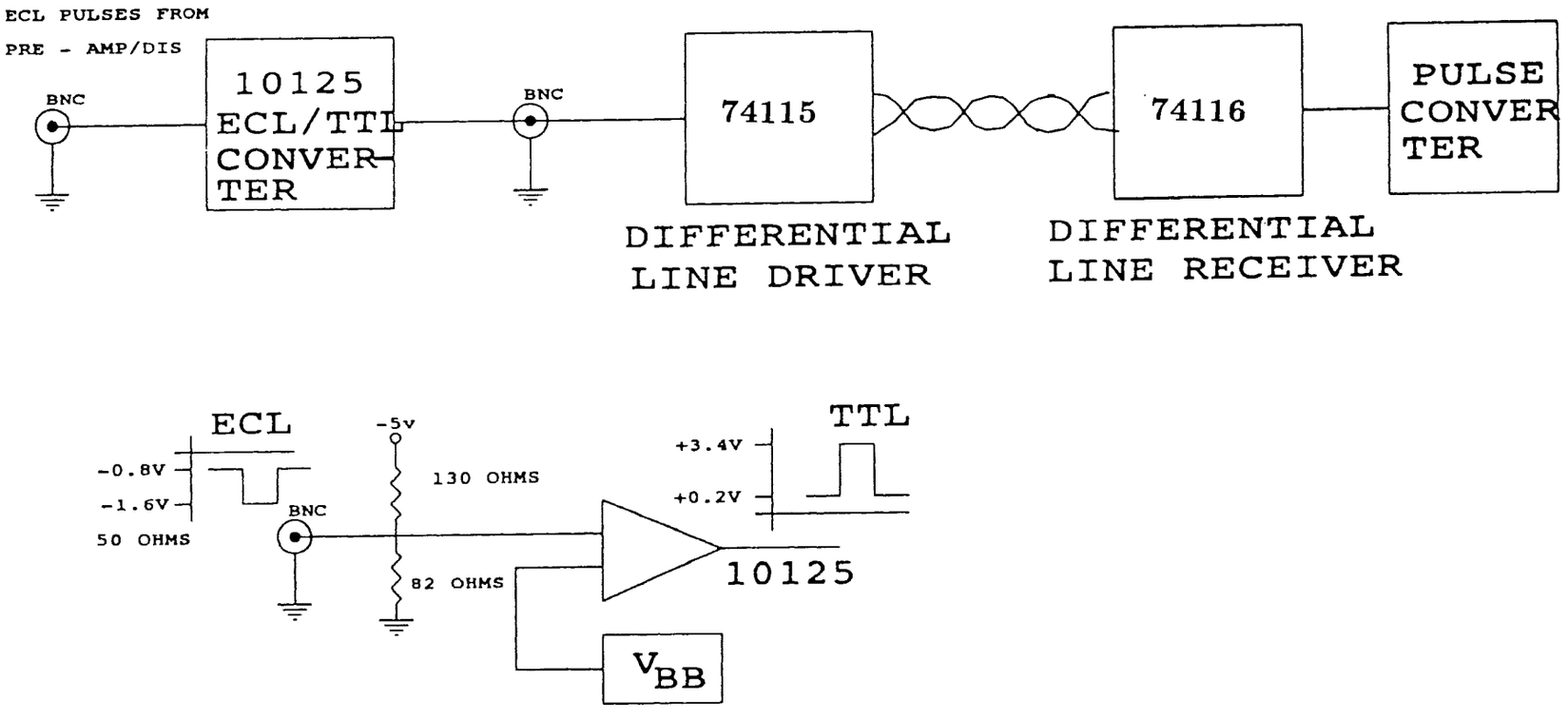

FIG 2.6

Indian Institute of Astrophysics. Koramangala Bangalore-34		
Title: ECL - TTL CONVERTOR WITH DIFF LN DRV/RCVR		
Size: A	Document Number	REV
Date: September 20, 1994	Sheet of	

the absolute pressure transducer (pressure level in the etalon chamber) is fed to the Digiana Card after A/D conversion. Digital data from the A/D converter is read as two bytes in which the byte at address 307 Hexadecimal gives 4 (LSB) bits as valid data and the next byte at the same address gives 8 (MSB) bits as valid data. The output port address resides at location 300 in Hexadecimal. The bit allocations are as follows. D_0 and D_1 provide the 'reset' and 'gate' signals to the pulse counter card respectively. D_2 forms the 'word select' signal to select the high/low (8/16 bit) word from the 24-bit pulse counter. D_3 and D_4 bits provide the direction control and the step pulses to the stepper-motor respectively. The pulse counter consists of six 4 bit synchronous binary counters (74 LS 193), cascaded to provide 24 bit counting. It can be reset to zero under program control and then gated for the desired integration time to count the pulses. The resulting count values are transferred to the computer using the programmed data transfer technique. Since the input instruction can only read a word of 16 bit at a time, a multiplexing arrangement is used to read the 24 bit counter value. The word select bit selects either the 'high word' or 'low byte' to read at a time. The schematic of the pulse counter is shown Fig. 2.7.

The computer provides pulses to the stepper- motor to move the piston which changes the pressure in the etalon chamber. The program specifies the number of steps to move and the direction. The translator card provides the necessary power level boosting through power transistors to drive the stepper-motor coils. The circuit diagrams of the translator card and its associated DC power supply are shown in Figs. 2.8 and 2.9 respectively. About two orders of fringe scanning is done by moving the piston in steps. Each step corresponds to 90°. The entire scanning operation is under the control of the computer program. The various parameters of the scan such as integration time and range of scan to be made are specified via the keyboard. Other pertinent data like type of scan (laser or airglow), date, start time and end time are also stored as a file in the computer. After every scan the line profile is displayed on the monitor screen for visual inspection.

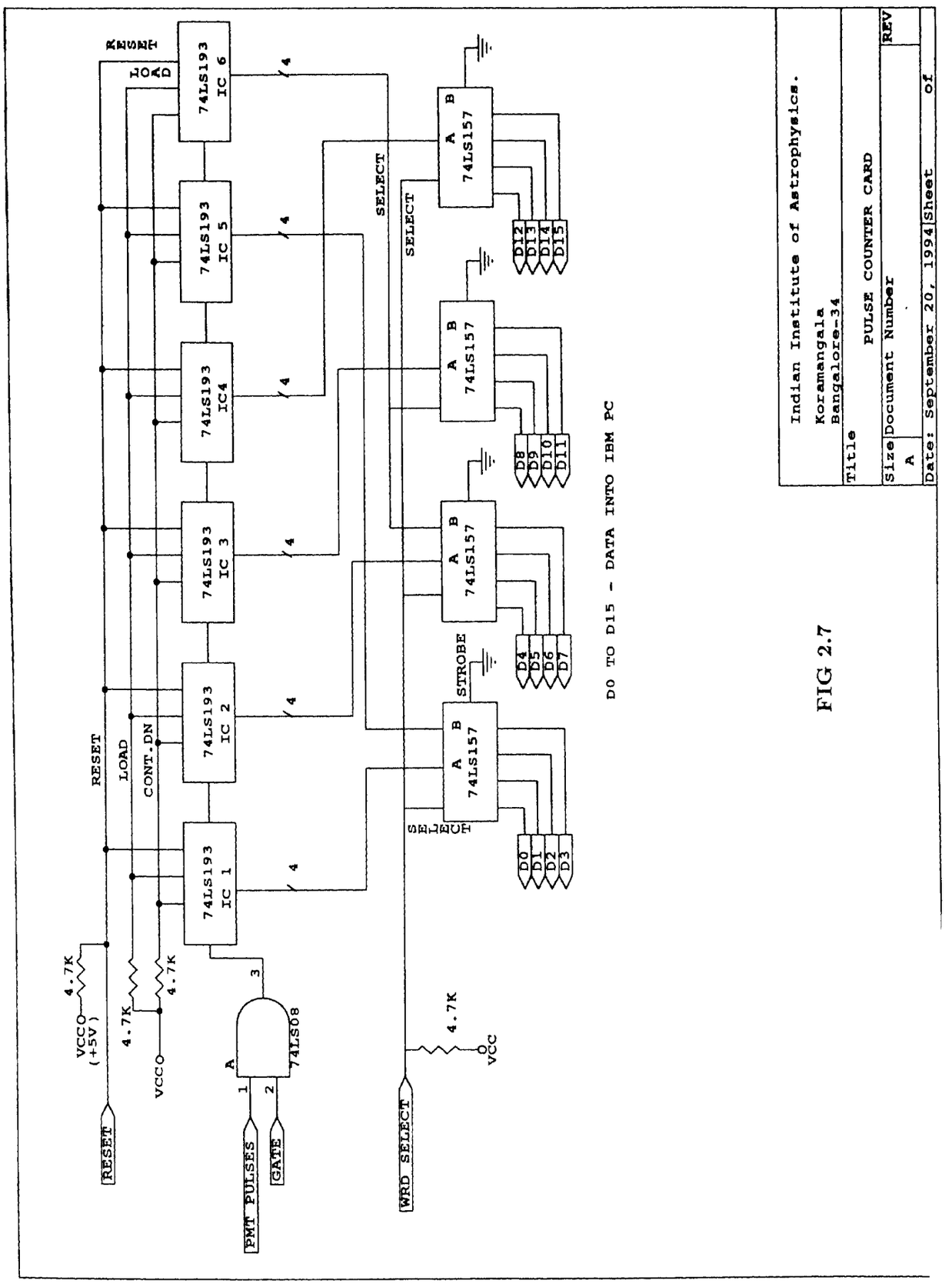
RESET
LOAD
CONT_DN
SELECT
STROBE
74LS193 IC 1
74LS193 IC 2
74LS193 IC 3
74LS193 IC4
74LS193 IC 5
74LS193 IC 6
74LS157
4.7K
VCCO (+5V)
74LS08
PMT PULSES
GATE
WRD SELECT
VCC
D0 TO D15 - DATA INTO IBM PC
Indian Institute of Astrophysics.
Koramangala
Bangalore-34
Title
PULSE COUNTER CARD
Size
Document Number
REV
Date: September 20, 1994
Sheet
of

FIG 2.7

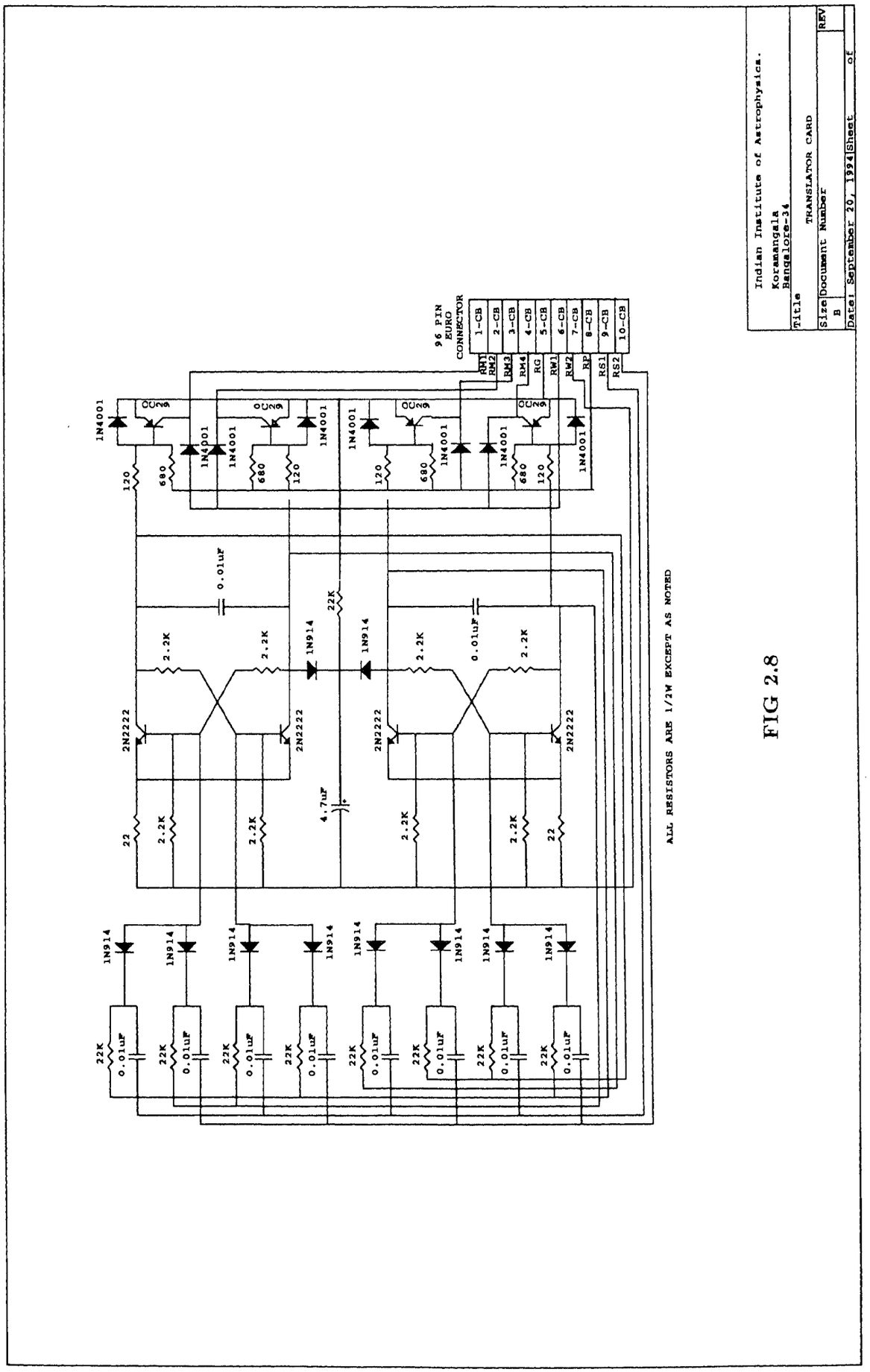
Indian Institute of Astrophysics.
Koramangala
Bangalore-34
Title
TRANSLATOR CARD
Size
B
Document Number
REV
Date: September 20, 1994
Sheet
of
96 PIN EURO CONNECTOR
1-CB
2-CB
3-CB
4-CB
5-CB
6-CB
7-CB
8-CB
9-CB
10-CB
RM1
RM2
RM3
RM4
RG
RW1
RW2
RP
RS1
RS2
1N4001
OC29
120
680
0.01uF
22K
2.2K
1N914
2N2222
4.7uF
22
ALL RESISTORS ARE 1/2W EXCEPT AS NOTED

FIG 2.8

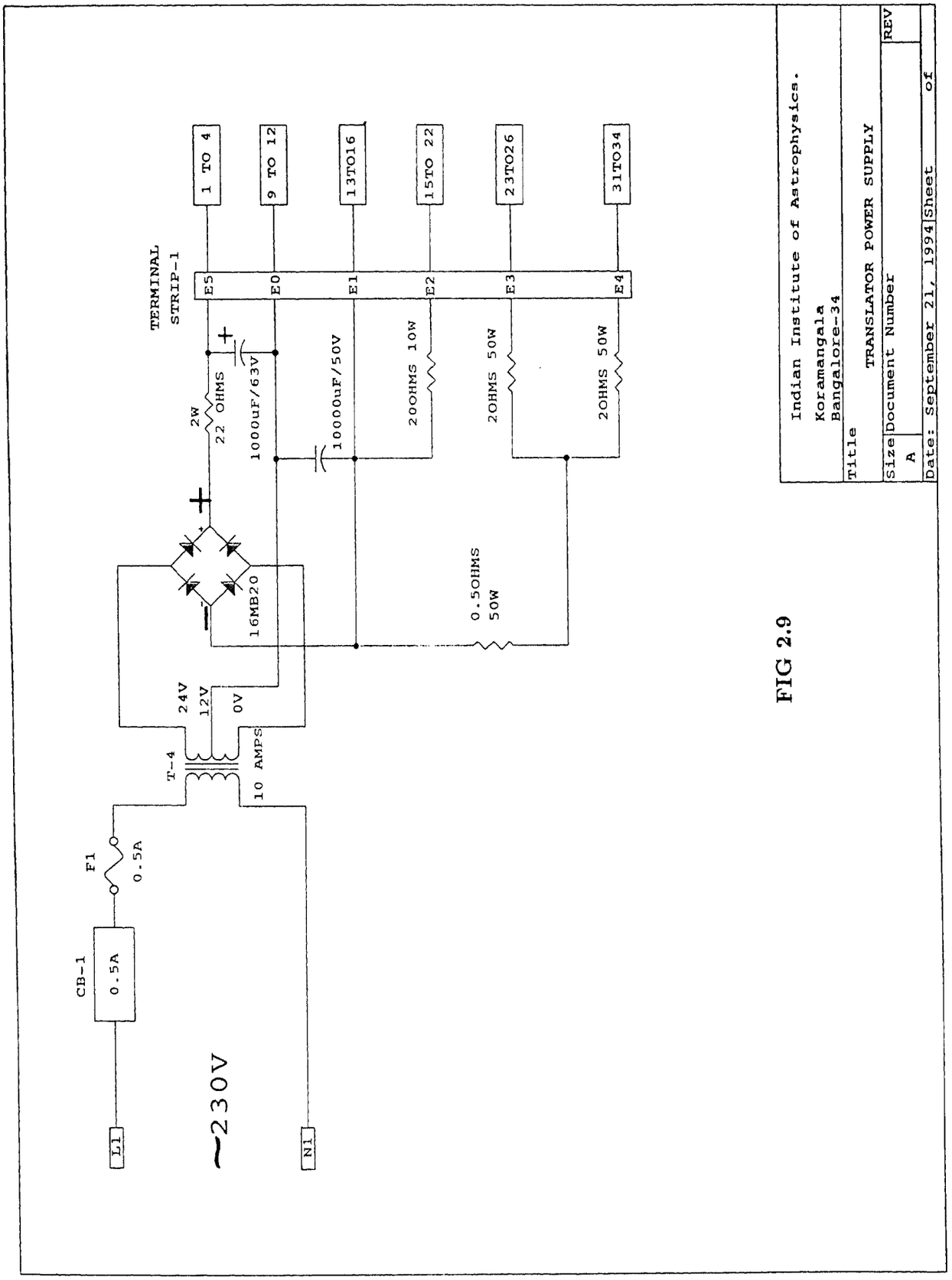
Indian Institute of Astrophysics.
Koramangala
Bangalore-34
Title
TRANSLATOR POWER SUPPLY
Size
A
Document Number
REV
Date: September 21, 1994
Sheet
of
~230V
L1
N1
CB-1
0.5A
F1
0.5A
T-4
10 AMPS
24V
12V
0V
16MB20
2W
22 OHMS
1000uF/63V
10000uF/50V
200HMS 10W
20HMS 50W
20HMS 50W
0.50HMS
50W
TERMINAL
STRIP-1
E5
E0
E1
E2
E3
E4
1 TO 4
9 TO 12
13TO16
15TO 22
23TO26
31TO34

FIG 2.9

2.2.3 Software

The software for the interferometer control and data acquisition is written in Turbo-Pascal. The various standard procedures and functions available in the language are utilised efficiently for the present purpose. The program is implemented using the following procedures: (1) Channel adjustment routine, (2) Gate generation routine, (3) Data acquisition routine, (4) Display routine, (5) Print routine and (6) Data storage routine. The scan covering about two orders of the interference pattern is divided into 120 channels. The initial adjustment of channel is made through user commands. The number of pulses routed to stepper-motor and the direction of movement is specified in the command. The PC generates the 'gate' pulse using a delay routine, the duration of which is specified by the user. The gating interval corresponds to the integration time for which the PMT pulses are counted. The 'channel-list' contains an array of up to 120 data giving channel addresses to be scanned. The scan program moves the piston through the stepper motor from the first channel position to the last channel by selecting the addresses from the 'channel-list' array. At each address a gate-signal corresponding to the integration time unit is generated, before moving the stepper-motor to the next address. A 'reset' signal is applied preceding the gate-signal to ensure that the pulse counters are initialized to zero values before any counting. A fixed delay of 3 sec is introduced at each step to make allowance for the pressure level to stabilise in the etalon chamber before any counting is done. At the end of the gate signal, the pulse counter values are read. The display routine presents the count values versus channel number (pressure) level to the graphic display. The flow-chart of the complete program is shown in Fig. 2.10, adopted from Srinivasan and Surendiranath (1991).

2.3 Observations with FPI

Night airglow observations are done for 15 nights in a month centered around newmoon. Cloudless sky preferably a photometric sky is a prerequisite for recording the weak airglow emissions. The climate at VBO, Kavalur usually permits optical observations only for six months from November through April. The observational

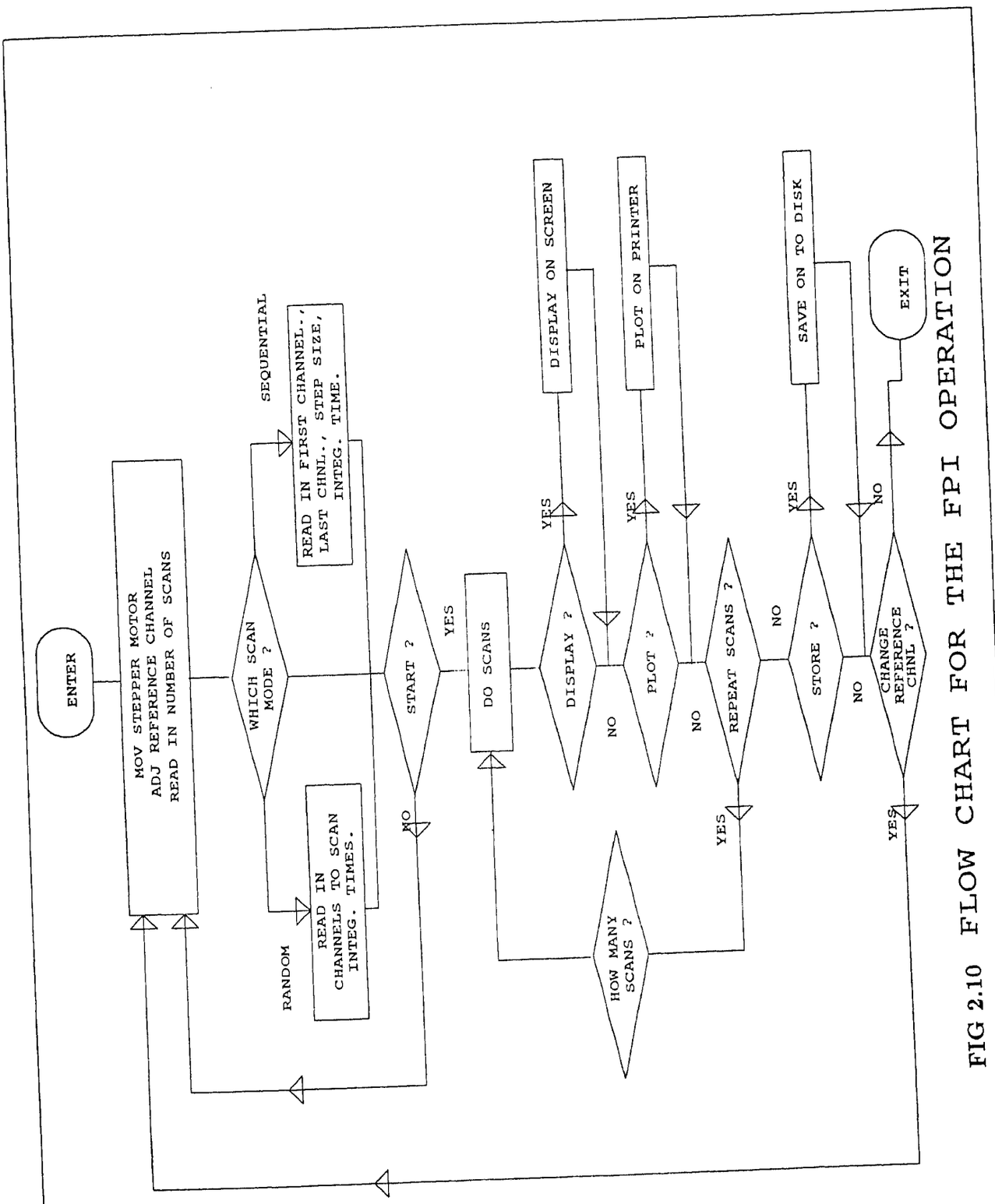

FIG 2.10 FLOW CHART FOR THE FPI OPERATION

(After Srinivasan and Surendranath, 1991)

procedure is as follows:

The light detector (PMT) is kept cooled to -20° C prior (by 6-8 hrs) to the start of airglow observations to reduce the dark count. The narrow-band interference filter is tuned for the wavelength of interest (630nm) using the digital temperature controller, DTC. The EHT voltage for the PMT and the discrimination level for PAD are set at optimised values. Since the voltage output from the absolute pressure transducer is very sensitive to temperature variations, the thermal base of the same is kept stabilised by powering the transducer prior to the start of the observational work. The etalon chamber and the piston chamber are constantly checked for air leakage. The observational run on each night starts with a laser scan. For this purpose the FP etalon is uniformly illuminated by a laboratory He-Ne laser source with the help of diffusers. The circular fringe pattern formed at the focal plane of the condensing lens L_1 (see Fig.2.1) is adjusted to be symmetric around the central aperture with the help of tilting screws on the bottomside of the etalon chamber. Care is taken to ensure that a uniform illumination of the different orders of the fringe pattern prevails on the aperture plane. Two orders of interference is scanned by changing the air pressure in the etalon chamber with the stepper-motor driven piston. The change of pressure is affected in discrete steps. The total number of steps over one free spectral range (FSR) varies in the range 70-80. The pressure change required to scan over one FSR is $\sim$ 0.1 atmospheres. The line profile obtained with the laser is known as the 'instrumental profile' from which the instrumental function is derived.

After the laser scan the FP etalon is exposed to the zenith sky. The temperature-tuned narrow-band interference filter helps to isolate the OI 630nm emission from the night sky. The 630nm airglow scans are done as with the laser source. Because the 630nm night airglow emission at equatorial latitudes is weak and variable, the light integration time is varied for individual scans in the range 4-16 sec. depending on the line intensity. The scan duration is around 30 min (the actual duration depends on the integration time). Laser scans are repeated during and at the end of the observational run on each night.

2.4 Data Reduction

The 630 nm line profile obtained with the FPI is a convolution of the source (airglow) line profile and the instrumental profile (which itself is a convolution of Airy function, plate defect function and the aperture function). The source line profile is therefore to be retrieved from the experimental profile by deconvolution methods. We have used the method of Sridharan et al., (1991) for the purpose. The key elements of the method are the use of the actual instrumental profile for deconvolution and the application of non-linear least-squares technique to the observed profile to arrive at the best set of parameters to describe the source profile. The temperature is determined from the derived source profile using the relation

$$\delta\lambda = 7.16 \times 10^{-7} \times \lambda \times (T_n/M)^{1/2} \tag{1}$$

where $\delta\lambda$ is the full width at half maximum (FWHM), λ is the wavelength of the airglow emission, Tn is the neutral temperature and M is the mass of the emitting species (oxygen) in a.m.u. Thermodynamic equilibrium between the emitting species and the dominant neutral species is implied in the usage of this relation for the determination of the neutral temperature.

The details of the data reduction procedure are as follows. The observed line profile data are first smoothed using cubic spline functions to minimise the random errors in the data. The observed airglow profile(O) is the convolution of the source(S) and the instrumental profile (I) and can be represented as

$$O(x_j; p_k) = \int I(x_j - x_i) S(x_i; p_k) dx_i \tag{2}$$

where x represents the ordinates of the data and p_k (k= 1,2,3) represent the parameters of the assumed Gaussian source profile, i.e. p_1 the peak intensity, p_2 full width at half maximum and p_3 wavelength corresponding to peak intensity. The integration is over one free spectral range. The convolved function is expanded by Taylor series about a well chosen set of initial values p_k with only first order terms retained. Application of

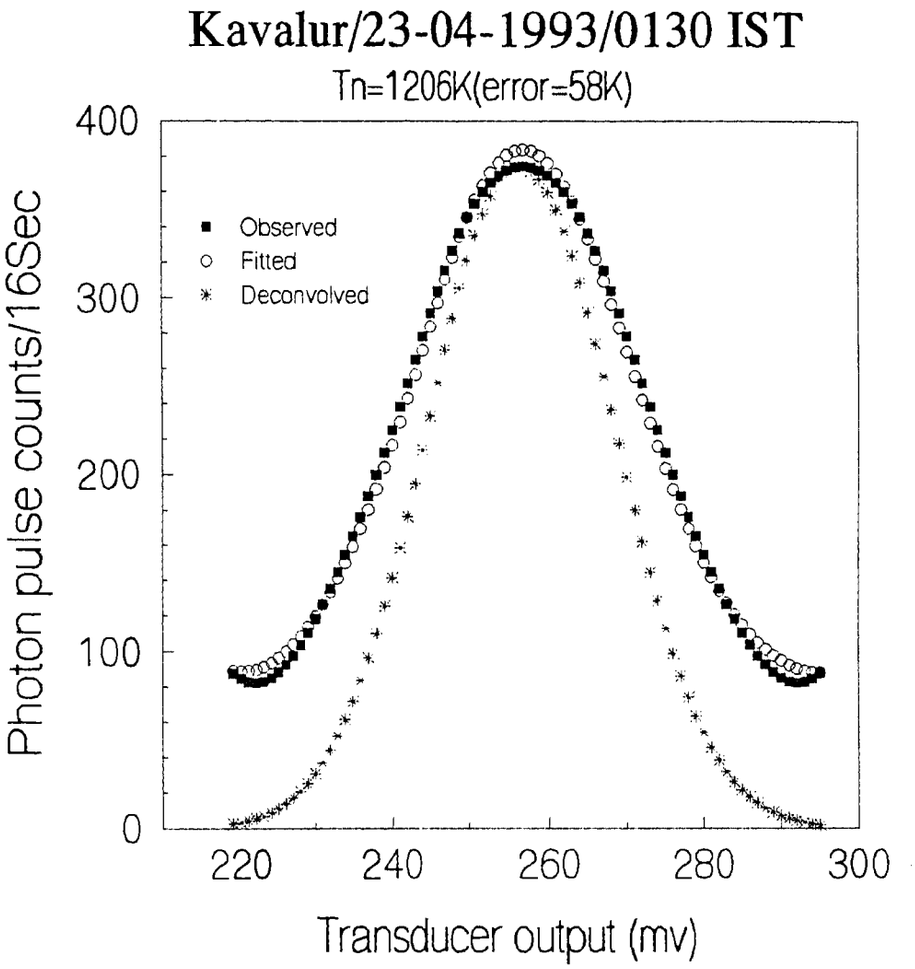

Fig 2.11 : Smoothed observed O (^{1}D) 630 nm line, Gaussian fitted and deconvolved source profile.

the least-squares method yields normal equations whose successive inversions determine the best set of values of p_k from which the Gaussian is deduced. While deducing the source profile proper evaluation and subtraction of the sky background is essential. For this purpose a zero background is initially assumed and the Doppler broadened profile is deduced. The transmission of etalon in response to this profile is evaluated by the method of Chabbal (1953). The actual contrast (C_{act}) of the profile is a function of the product of the instrumental contrast and the transmission of the etalon for the Doppler-broadened source. It is also defined as

$$C_{act} = \frac{I_{max} - BG}{I_{min} - BG} \tag{3}$$

where I_{max}, I_{min} and BG are the maximum and minimum intensities and the background level respectively. BG is calculated from (3) and subtracted from the experimental profile. The least-squares method is once again applied to the new profile to get a new set of p_k values and the whole procedure is repeated until the difference in the estimated temperatures between two successive profiles is less than 5K. The iteration is then terminated and the final temperature obtained. The uncertainty in the temperature thus derived is found to vary in the range $\pm$ 10-150K in the data analysed for the purpose of this thesis work. An example of the smoothed experimental profile along with the derived source profile is shown in Fig. 2.11(see previous page). The temperatures derived from FPI observations refer to the altitude range of the O(^{1}D) night airglow emission layer (250-300 km) and the mean temperature at the height of emission will be close to the exospheric temperature because of the small altitude gradient of the temperature ($\sim$0.2K/Km) at these altitudes (e.g. Hernandez et al., 1975).

* * * * * *

Chapter 3

Nighttime neutral thermospheric temperature over Kavalur (78.5°E, 12.5°N)

3.1 Introduction

Neutral thermospheric temperature is one of the important thermospheric parameters and whose measurement simultaneous with plasma parameters is very much necessary to understand the dynamics of thermosphere - ionosphere system. As mentioned earlier, groundbased measurement of the Doppler width of $O(^1D)$ 630 nm night airglow line emission constitutes one of the resourceful and established means of determining the thermospheric temperature. Such optical measurements have been extensively made over the past two decades at a number of locations ranging from low latitudes to the polar region using Fabry-Perot interferometers (e.g. Meriwether, 1983 and references therein; Burnside et al., 1983; Hernandez and Roble, 1984; Yagi and Dyson, 1985; Meriwether et al., 1988; Murty and Kim, 1988a, b; Hernandez et al., 1990; Batten and Rees, 1990). Unlike at midlatitudes, FPI measurements of thermospheric parameters at equatorial latitudes have been quite limited so far and confined to particular (usually campaign) periods at specific locations in the Indian, American and Pacific sectors: Mt. Abu, India (e.g. Rajaram et al., 1978; Sridharan et al., 1991); Arequipa, Peru (e.g. Meriwether et al., 1986; Biondi et al., 1990a, 1991); Kwajelein Atoll, Marshall Islands (e.g. Sipler et al., 1983); Sao Paulo, Brazil (e.g. Sahai et al., 1992) and Natal, Brazil (Biondi and Sipler, 1985). As mentioned earlier, we have initiated a long-term programme of measurement of thermospheric nighttime temperature over Kavalur (78.5°E, 12.5°N) using the pressure scanned FPI. Fig. 3.1 shows the geographic location of Kavalur.

The following sections describe the studies on general characteristics of night time thermospheric temperature over Kavalur, characteristics of the equatorial MTM in Indian sector and its effects on low latitude F - region height and density. *These studies*

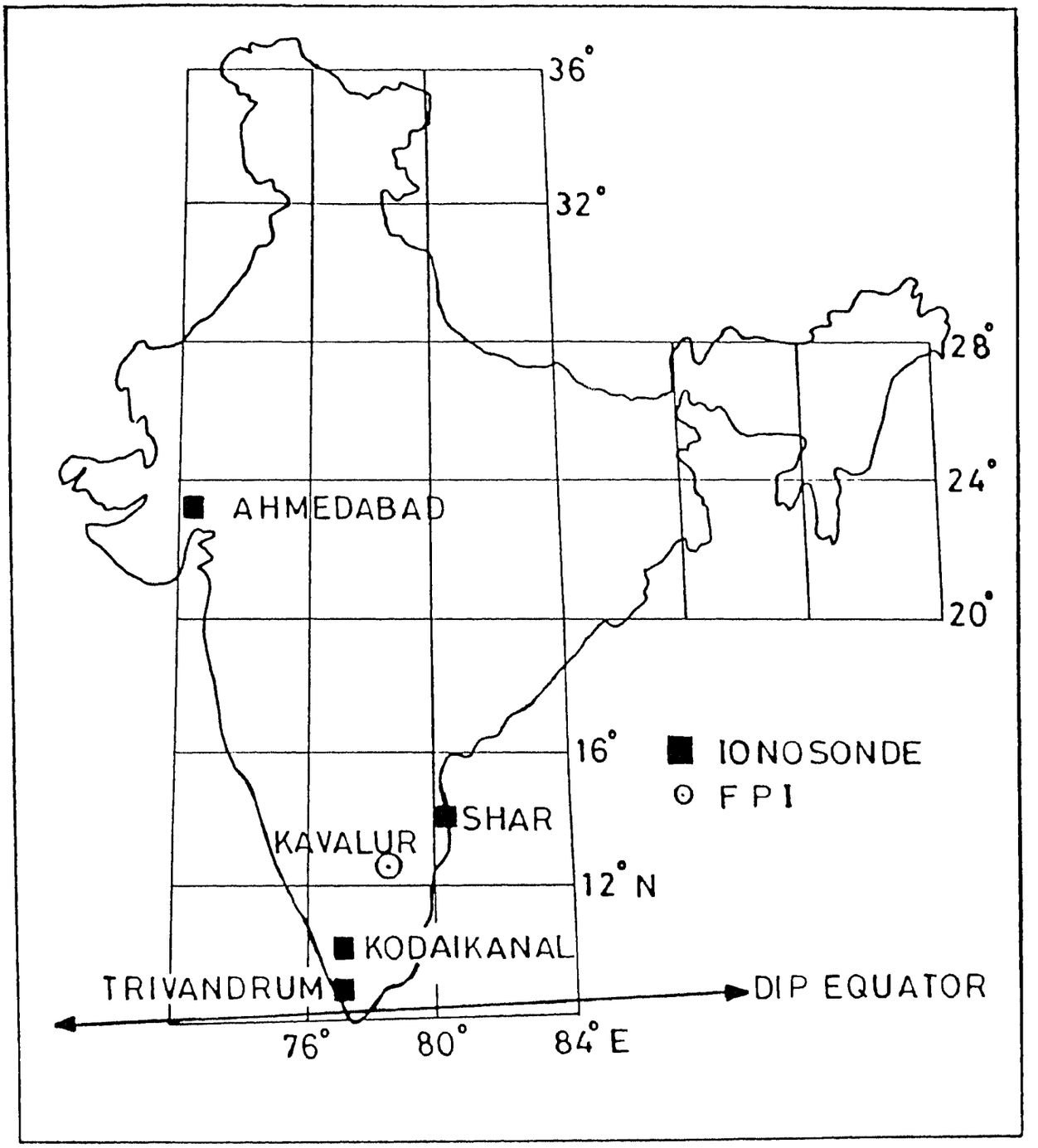

Fig 3.1 : Map showing the geographic locations of the FPI station at Kavalur and the ionosonde stations at Trivandrum, Kodaikanal, SHAR and Ahmedabad in India.

are first of their kind in the Indian zone.

3.2 Characteristics of nighttime neutral thermospheric temperatures over Kavalur.

Observations of the O(^{1}D) 630 nm night airglow line emission were made on 65 nights at Kavalur during March-April 1992 and November 1992 - April 1993. A total of about 500 individual line profiles covering the time interval 2030-0445 IST (IST = UT + 5.5 hrs) became available for study after rejection of many (34% of total) profiles with poor S/N ratio. The low intensity of the 630 nm emission in the post-sunset hours which is due to the vertical uplift of F region in the vicinity of dip equator (e.g. Bittencourt and Sahai, 1979) precluded measurements with our FPI where central aperture scanning is done. Shown in Figures 3.2 and 3.3 are the local time variation of the observed temperature (thick line) and MSIS-86 model predictions (dashed line) on a selected number of nights in our data base. It is clear from the plots that nighttime thermospheric neutral temperature over Kavalur exhibits considerable day-to-day variability in its magnitude and temporal variation . There is no significant temporal variability in observed temperatures on 8 March 1992 and 18 March 1993 as can be seen in FIg. 3.2. On 26 January 1993, there is a gradual reduction in temperature from post-sunset hours to midnight from 1300 K at 2000 IST to 850 K at 0030 IST. This is followed by gradual rise in temperature to early morning hours. The temperature behaviour on 26 December 1992 is an example of high variability which shows a large temperature reduction of about 500 K (during 0200 to 0330 hours IST) in about one and half an hour. Example of temperature variability shown in Fig 3.3 represent some sort of oscillations. The origin of this type of behaviour of nighttime thermosphere temperature need to be understood. One can also notice from the Figures 3.2 and 3.3 that MSIS-86 temperature predictions are much below the observed ones and the model does not predict the temporal variability unlike observed temperatures.

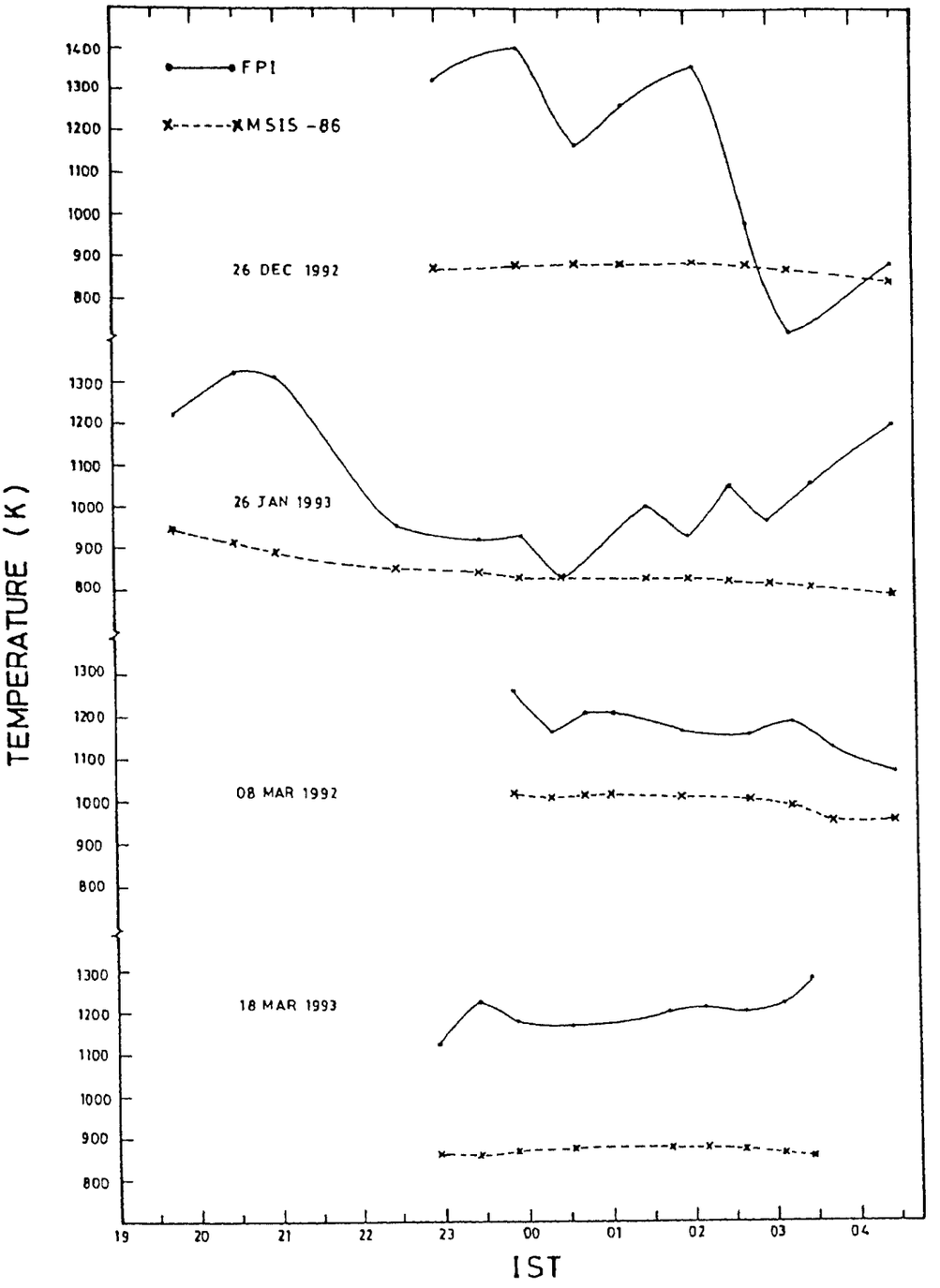

Fig 3.2 : Night-time neutral thermospheric temperature as a function of time for a selected number of nights to illustrate the day to day variability in nighttime temperature at Kavalur.

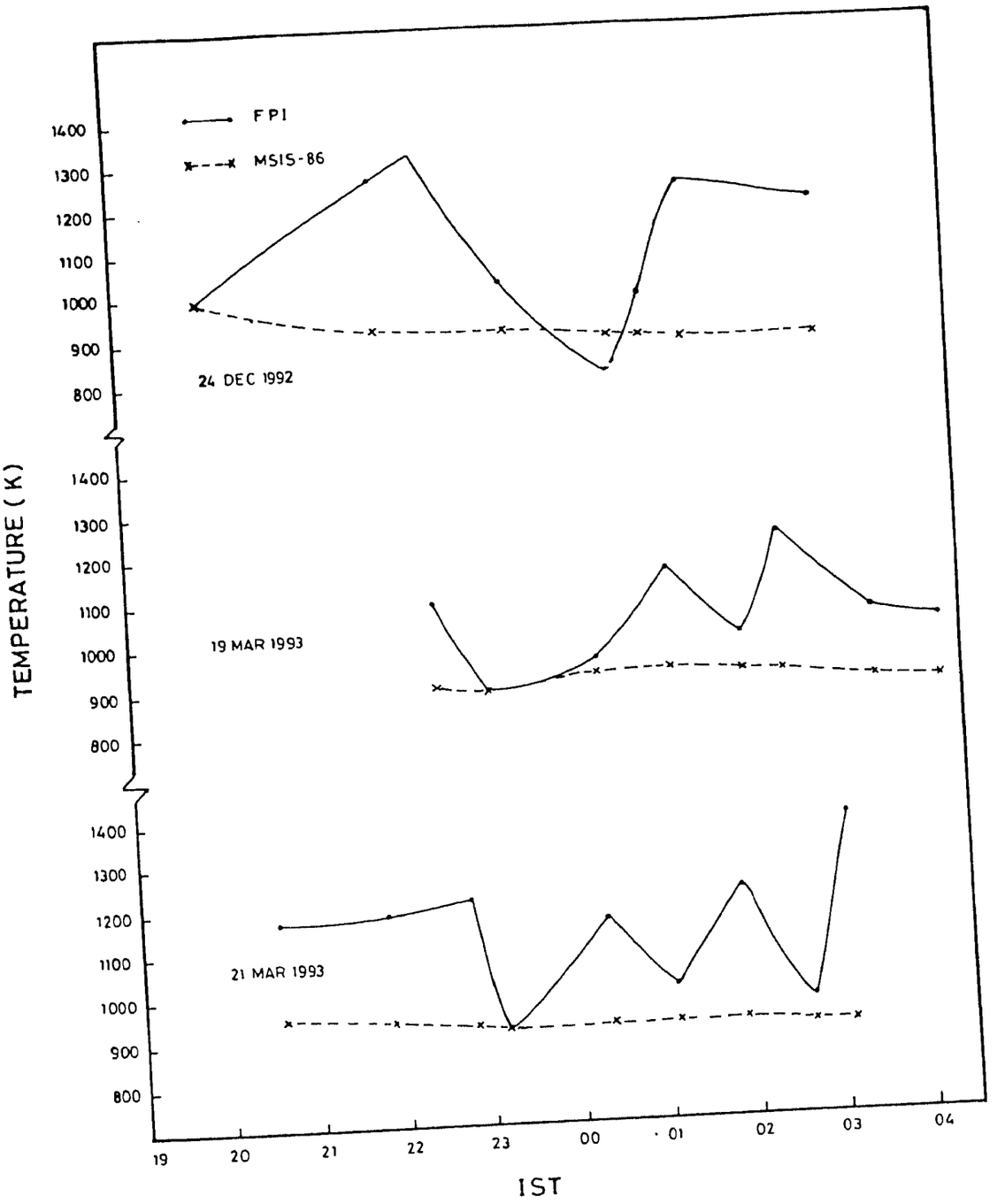

Fig 3.3 : Same as Fig 3.2

The FPI measurements reported here pertain to quiet and moderately disturbed geomagnetic conditions (see Table 3.1).

Table 3.1

Month	Monthly mean value of Solarflux	Number of nights	Mean A_p index for the days of observations	Number of days with $25 \leq A_p \leq 45$
Mar 1992	169.6	7	18.4	2
Apr 1992	159.7	8	14.6	1
Nov 1992	142.0	1	17.0	1
Dec 1992	134.6	8	08.8	0
Jan 1993	121.0	10	13.3	1
Feb 1993	142.6	11	13.3	3
Mar 1993	136.4	10	24.0	4
Apr 1993	116.7	10	14.4	1

A commonly used method of studying the temperature measurements is to average them over a suitable time interval and compare with values predicted by the various empirical thermospheric models (e.g Hernandez, 1982; Yagi and Dyson, 1985). In the present work the average of all measurements on individual nights is computed and compared with the average of MSIS-86 model (Hedin, 1987) values calculated for the same times as the observations. This approach is felt appropriate to derive general characteristics of night time thermospheric temperatures over Kavalur. The result is presented in Fig.3.4. From this presentation it is evident that: (a) *the mean nightly temperature exhibits considerable day-to-day variability* and (b) *the observed temperatures are consistently and significantly higher than the model values on all but three of the nights* (on two nights the observed temperatures closely match with the MSIS-86 values and on one night observed temperatures are below MSIS - 86 values.) The difference between the nightly values of the observed temperature and the model values varies in the range -16K to +585K with a mean value of 274K and a *S.E.(standard error)* of 145K. The average of all temperature determinations made is 1177K which is higher than the corresponding model value by 274K. These statistical details clearly show that the nighttime thermospheric temperature determined from FPI observations at Kavalur is significantly higher than the MSIS predictions. The earlier FPI observations at other

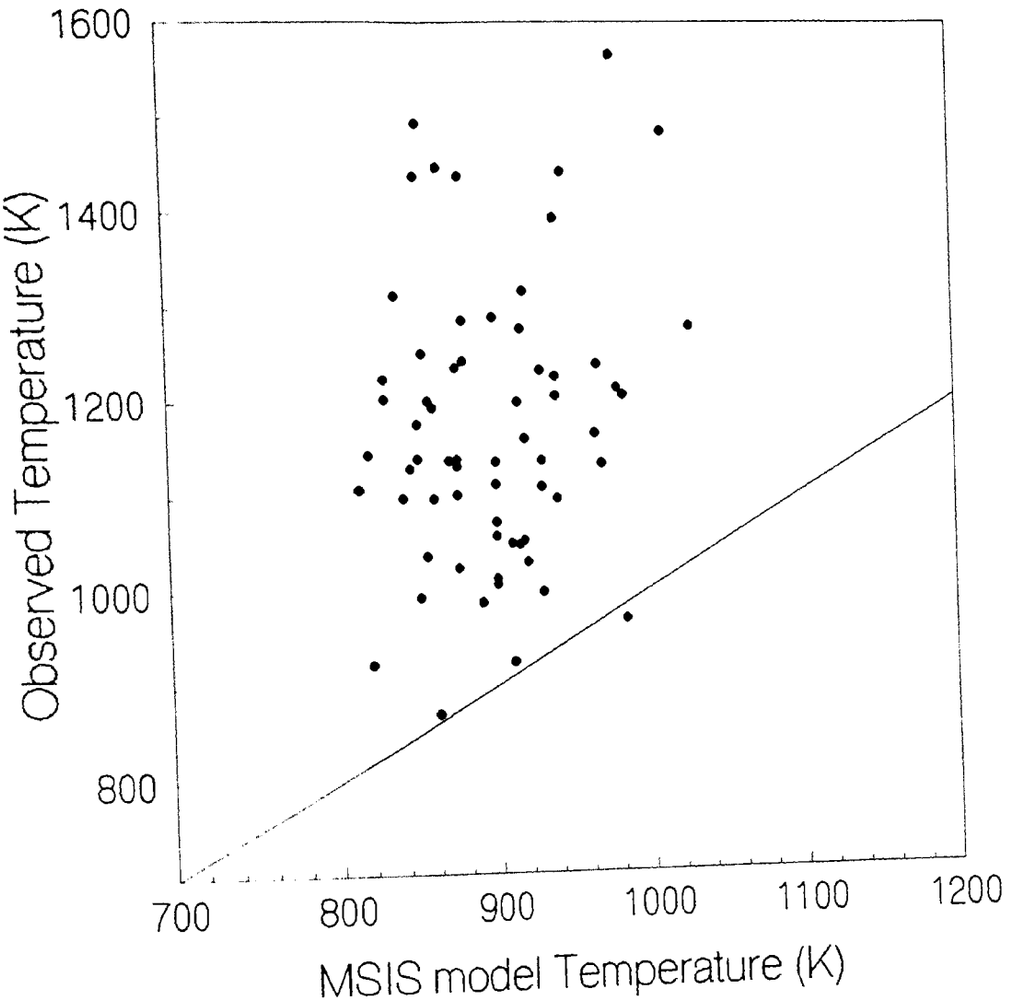

Fig 3.4 : Night time average (2030 – 0445 IST) thermospheric temperature at Kavalur vs MSIS–86 model predictions for 65 nights during March–April 1992 and November 1992–April 1993.

equatorial stations also showed the temperatures to exceed the model predictions, on the average, by 180-330K (Sipler et al., 1983; Biondi and Meriwether, 1985; Biondi et al., 1990a). The origin of this consistent difference between measurements of thermospheric temperature by optical techniques and model predictions merits evaluation and understanding as it manifests not only at equatorial latitudes but at midlatitudes as well (e.g Hernandez, 1982; Yagi and Dyson, 1985).

It is known that in the equatorial region ($\pm$ 20°), the thermospheric temperature does not always undergo a monotonic decrease throughout the night. A pronounced enhancement, typically around midnight, sometimes reaching or exceeding the daytime values (Spencer et al., 1979) is a frequent occurrence. This recurrent feature is referred to as the equatorial midnight temperature maximum (MTM) which is already introduced in Chapter 1 with an illustration. The characteristics of the MTM like shape, amplitude and time of occurrence are highly variable both on short-time (day-to-day) as well as long-time (season, year-to-year) scales (Spencer et al., 1979; Bamgboye and McClure, 1982; Herrero and Spencer, 1982). We hold the view that the marked day-to-day variability and the significantly higher values of the nightly temperatures at Kavalur over MSIS model values could, *in part*, be due to the variability in the manifestation of the MTM. This is particularly so because the time span (2030-0445 IST) of our FPI measurements is essentially the same as that of the peak of the MTM (21-04 LT). A detailed discussion on MTM characteristics in the Indian zone derived from Kavalur FPI data is presented in the following section.

3.3 Characteristics of MTM in the Indian Zone.

The current knowledge of the global characteristics of the equatorial MTM is extremely limited. The spatial (latitude-local time) distribution of MTM is synthesised from satellite data obtained for different locations and at different local times (Herrero and Spencer, 1982). Synoptic ground-based observations at a global network of stations are needed to comprehend the global/regional features of the equatorial MTM and its effects. This is because MTM is an energetically significant feature of the equatorial

thermosphere and exerts a direct influence on the dynamics of both the neutral thermosphere and the ionospheric plasma (Herrero et al., 1993). Synoptic information on MTM is, however, currently available only for Jicamarca (12°S, dip 2°N) in the American sector (Bomgboye and McClure, 1982). Against this background the characteristics of MTM for the Indian sector are presented in this section.

The present detailed study on MTM is based on FPI observations made on 65 nights during March-April 1992 and November 1992-April 1993. We found clear evidence of an enhancement in the nighttime temperature, i.e, the signature of the MTM on 19 nights. This frequency of occurrence of MTM over Kavalur (~30 percent of the nights) is compatible with that (~50 percent of the nights) seen at Jicamarca from ion temperature measurements with the Incoherent Scatter Radar(ISR)(Bamgboye and McClure, 1982). During the periods of our observations, the monthly mean value of the solar 10.7 cm flux varied in the range 117-170 units (one solar flux unit equals 10^{-22}J/m^2/Hz/Sec). The average value of geomagnetic A_p index for the days of our observations was 16 and moderately disturbed conditions ($A_p > 30$) were encountered on only 4 out of 19 nights. The MTM characteristics reported here thus correspond to quiet and moderately disturbed geomagnetic conditions at an epoch of moderate solar activity.

Figs. 3.5 and 3.6 illustrate the signatures of the MTM evidenced in our data during equinox and winter respectively. The pattern of the temperature variation on each of the days displayed shows the unambiguous presence of a night maximum. The temperature also exhibits one or more short duration secondary maxima on some of the nights, a behaviour also apparent in the Jicamarca radar data (Bamgboye and McClure, 1982). The MTM manifests in varied shapes ranging from a broad or flat-topped maximum (e.g. 16 April 1993) to a well-defined or sharp maximum (e.g. 18 Dec 1992). The duration of the MTM is 2 to 4 hrs. The local time of occurrence of MTM exhibits considerable variability and lies anywhere in the interval 2230-0230 hrs. These results on the shape, duration and local time of occurrence of the MTM over Kavalur are in broad agreement with those derived from in-situ satellite data (Spencer et al., 1979;

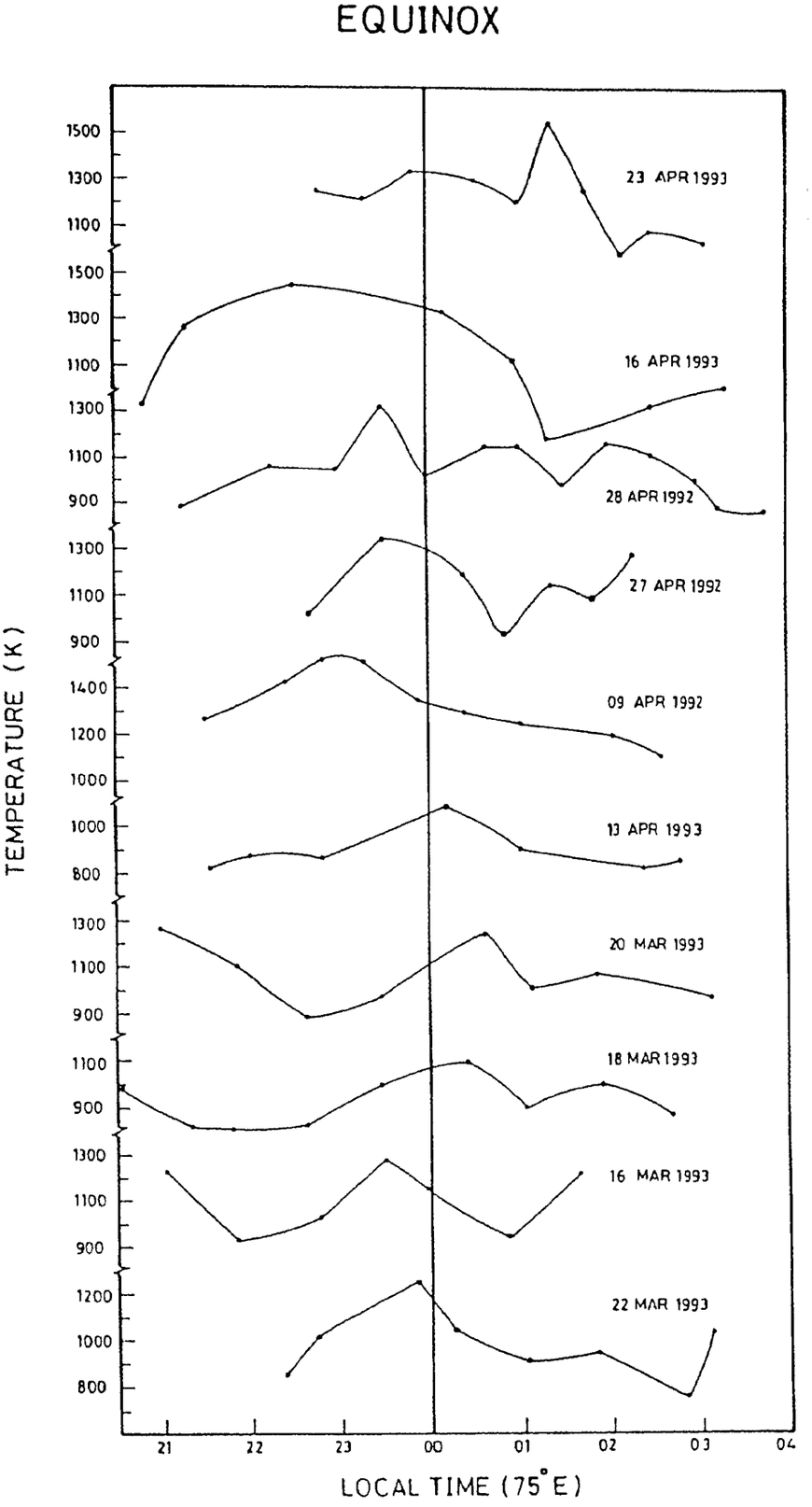

Fig 3.5 Signatures of MTM over Kavalur in equinox.

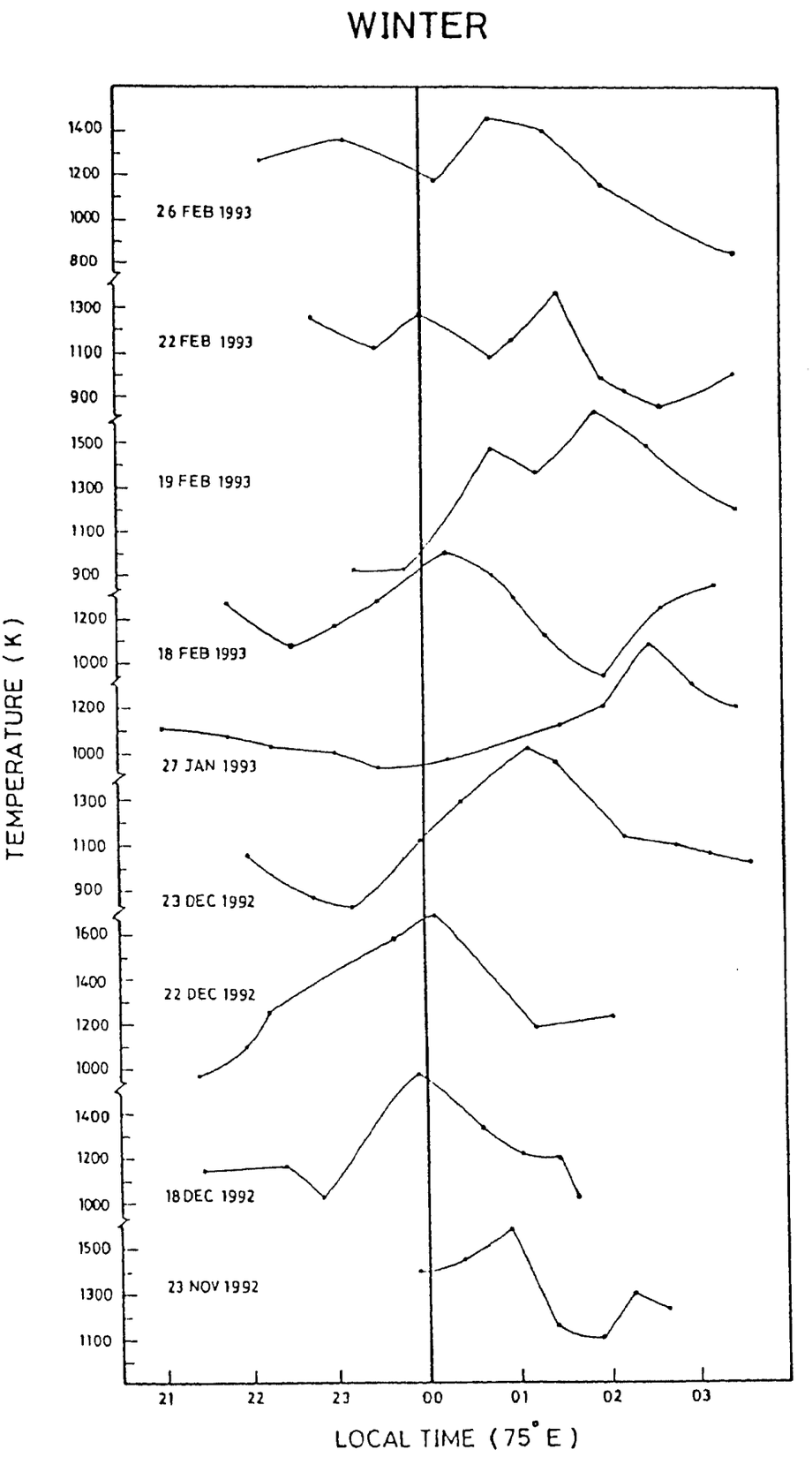

Fig 3.6 Signatures of MTM over Kavalur in local winter.

Herrero and Spencer, 1982), and also radar measurements at Jicamarca (Bamgboye and McClure, 1982).

The predominant occurrence of the temperature maximum around midnight at low latitudes evidenced in satellite measurements is, however, not seen in our FPI data. In fact, the temperature maximum occurred in the 1-hr window centred on local midnight is only ~47 percent of the data (9 out of 19 nights). What is seen instead is an unmistakable trend of a seasonal shift in the time of occurrence of MTM from local winter to vernal equinox. In winter MTM occurs predominantly in the interval 00-02 LT (in 8 out of 9 events), while in vernal equinox it does so in the interval 2230-0030 LT (in 9 out of 10 events). This seasonal pattern is brought out more clearly in Fig.3.7 wherein the time of MTM is plotted as a function of month. It is quite apparent that there is a transition in the time of occurrence of MTM from winter to March equinox through local midnight. The average time of occurrence of MTM (dashed line in Fig.3.7) is one hour after midnight in local winter and just before midnight (2345 LT) in vernal equinox. The preferential occurrence of MTM at and after local midnight in local winter at Kavalur is consistent with that at Jicamarca (Bomgboye and McClure, 1982) and also satellite data (Herrero and Spencer, 1982). See Fig 3.8 for a comparison of the time of occurrence of MTM at Kavalur and Jicamarca. We could not ascertain the presence of a changeover in the time of MTM from post-midnight to pre-midnight period between winter and summer as observed at Jicamarca, because the sky conditions over Kavalur are generally unfavourable for optical observations in local summer. The definite trend of a shift in the time of MTM from winter to vernal equinox noticed in our data is, nevertheless, a pointer for the prevalence of such a physical situation.

The mechanism for generation of the MTM may be understood in terms of tidal mode coupling (Mayer et al., 1979) as mentioned in the first chapter. A tidal analysis of 24 hr temperature maps of the AE-E data revealed significant variation of the tidal modes with season (Herrero et al., 1983). Analysis of Herrero et al (1983) also shows that the seasonal variations of the semidiurnal and terdiurnal modes were responsible for the observed variation in the MTM. The significant variation in semi diurnal component

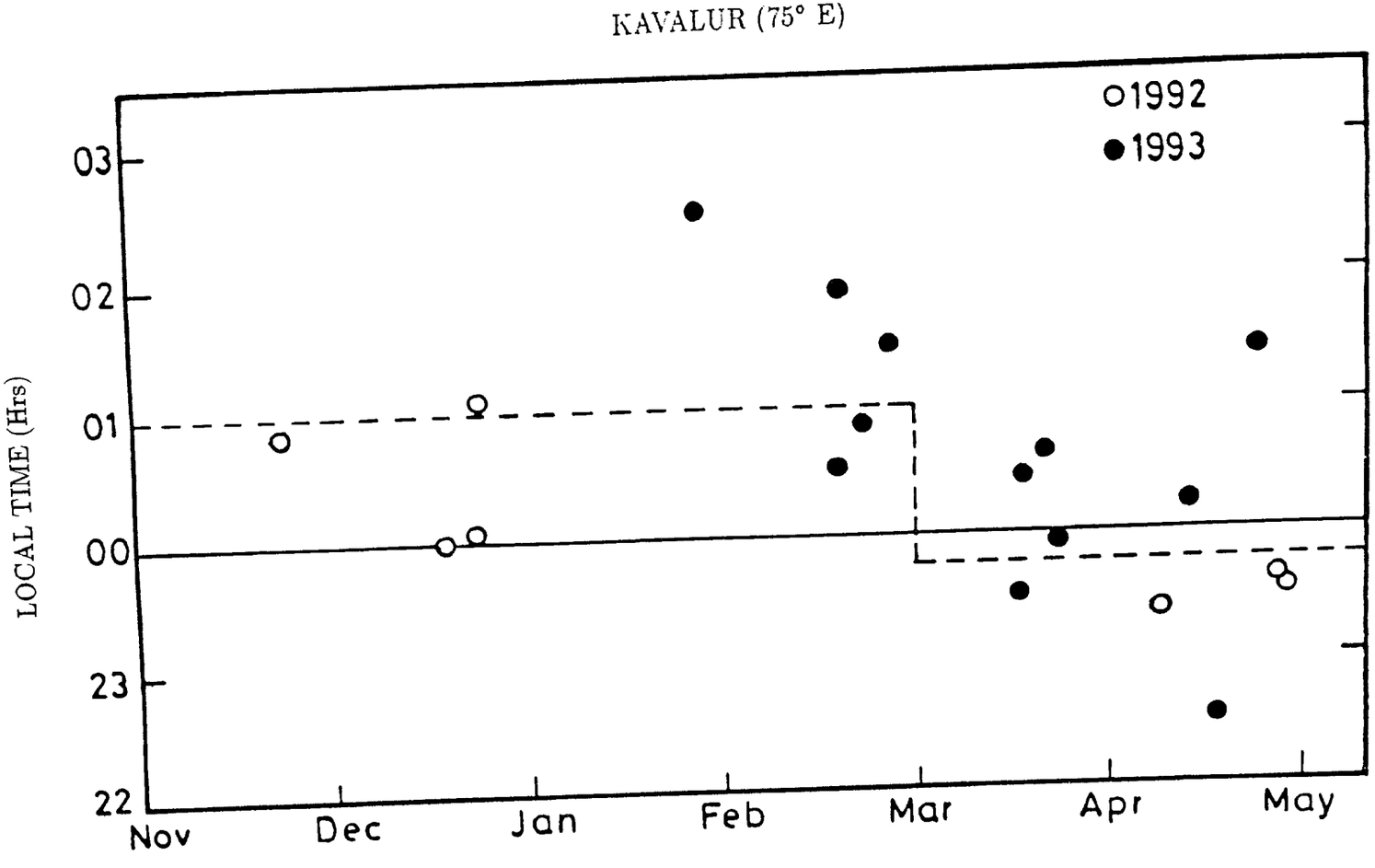

Fig 3.7 : Seasonal variation of the local time of occurrence of MTM in winter and March equinox. The dashed line represents the average time of occurrence for the two seasons.

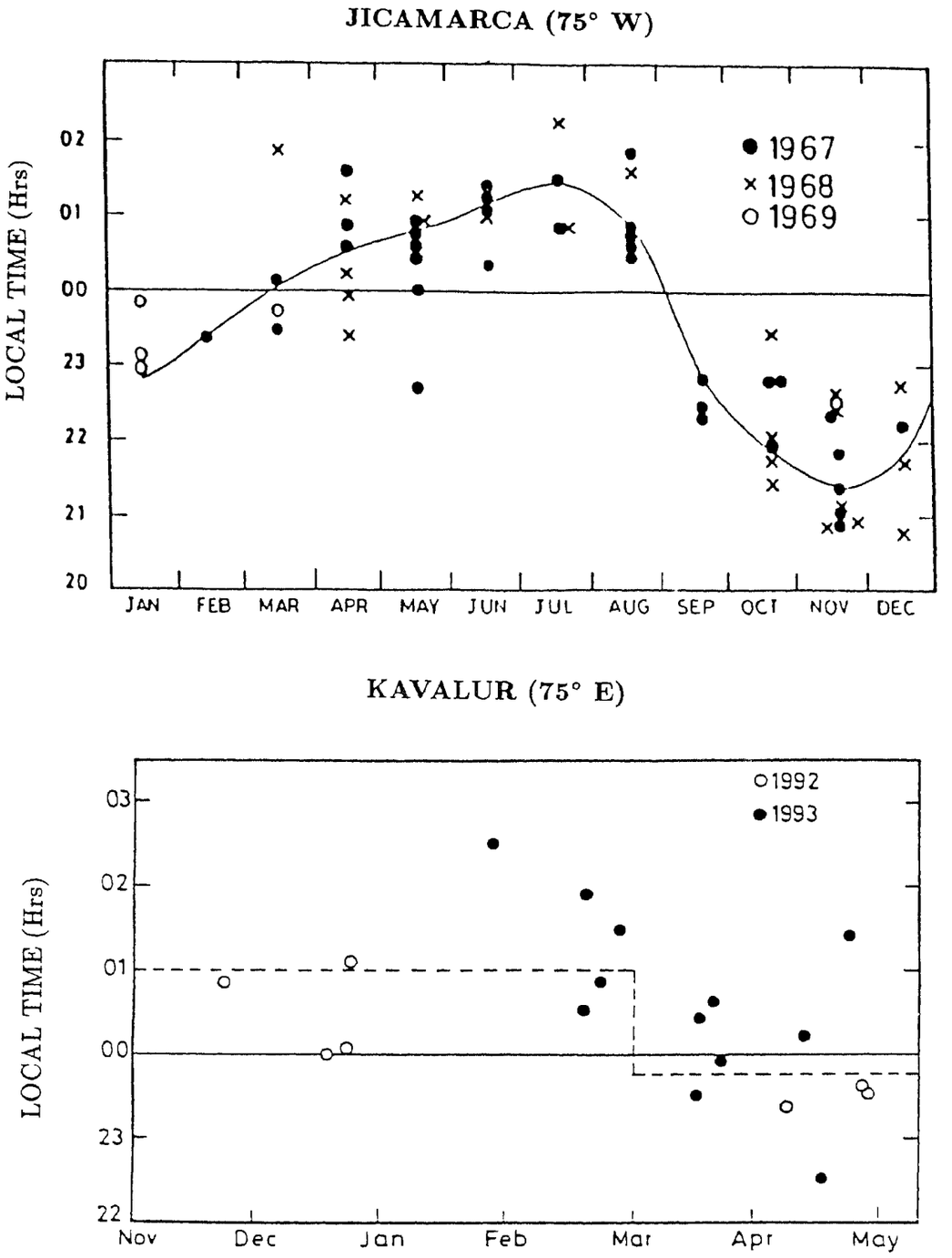

Fig 3.8 : Seasonal variation of the local time of occurrence of MTM for Jicamarca (top panel after Bamgboye and McClure, 1982) and Kavalur (bottom panel).

which is the dominant component in winter accounts for the winter MTM. In summer terdiurnal component is as strong as the semidiurnal and the superposition of the two reinforces the summer MTM.

Figure 3.9 taken from Spencer et al(1981) shows the diurnal variation of the meridional wind for summer to winter at three different altitudes and solar flux levels, as measured by the NATE instrument on the AE-E satellite. The most striking and reproduciable seasonal changes found in Fig. 3.9 is the pronounced nighttime maximum of the equatorward summer wind, which occurs at all three altitudes at almost the same time (between 2100 and 2200 LT). This is followed by significant abatement. The winter wind shows a significant nighttime abatement only at the lower altitude of 270 Km, and it occurs around 2300 LT, significantly later than in summer, consistent with the MTM and midnight pressure bulge seasonal variation.

The amplitude of MTM at Kavalur is found to be in general higher than that reported for Jicamarca. The amplitude of MTM is calculated as ΔT = (Maximum - e) − (Minimum + e) where 'e' is the estimated error in the Doppler temperature. The MTM minimum is taken as the beginning of the leading edge of the temperature increase. If the beginning of the leading edge is absent or is not recognisable then the ending of the trailing edge is taken as the minimum. For the MTM data presented in Figs 3.5 and 3.6, the amplitude ranges from 80K to 570K with an average value of 286K (the amplitude could not be estimated for the nights of 9 April 1992, 23 November 1992 and 22 March 1993 due to difficulty in identifying the minimum). In most cases (12 out of 16 events) the amplitude lies in the range 100-400K as can be seen from Fig.3.10. In contrast, the MTM amplitude at Jicamarca is smaller being in the range 40-200K (Bomgboye and McClure, 1982). A sizeable difference in the amplitude of MTM thus seems to be present between the Indian and the American equatorial regions. This important feature of the global manifestation of the equatorial MTM merits further investigation from coordinated FPI observations in the Indian and American sectors for specific periods, and confirmation from a large data base of Kavalur.

As detailed in chapter 1, the theoretical analysis of Mayr et al., (1979) showed that

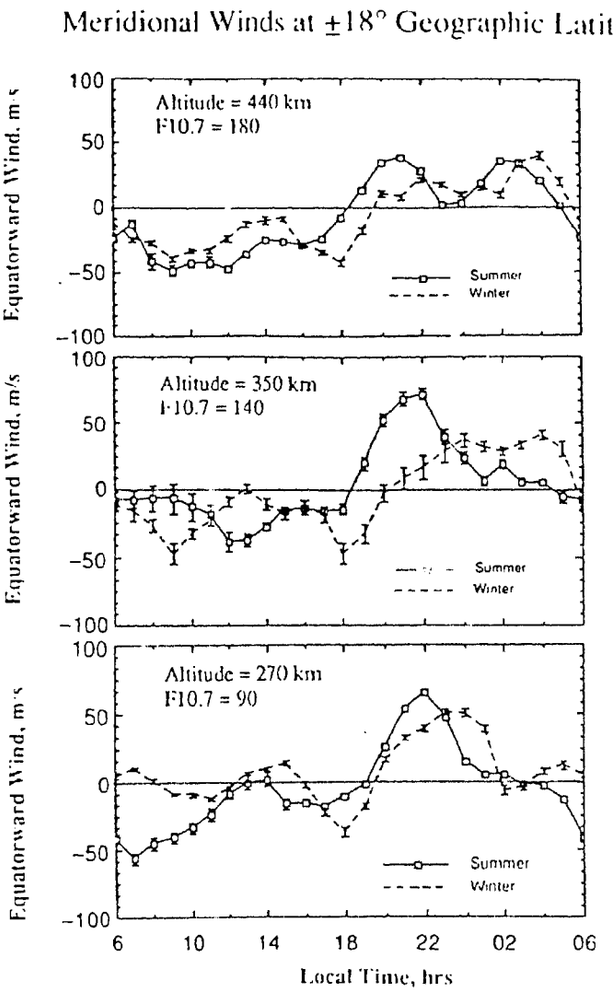

Fig 3.9 : Diurnal variation of the meridional wind for summer and winter at three different altitudes and solar flux levels, as measured by the NATE instrument on the AE-E satellite.
(After Spencer et al., 1981)

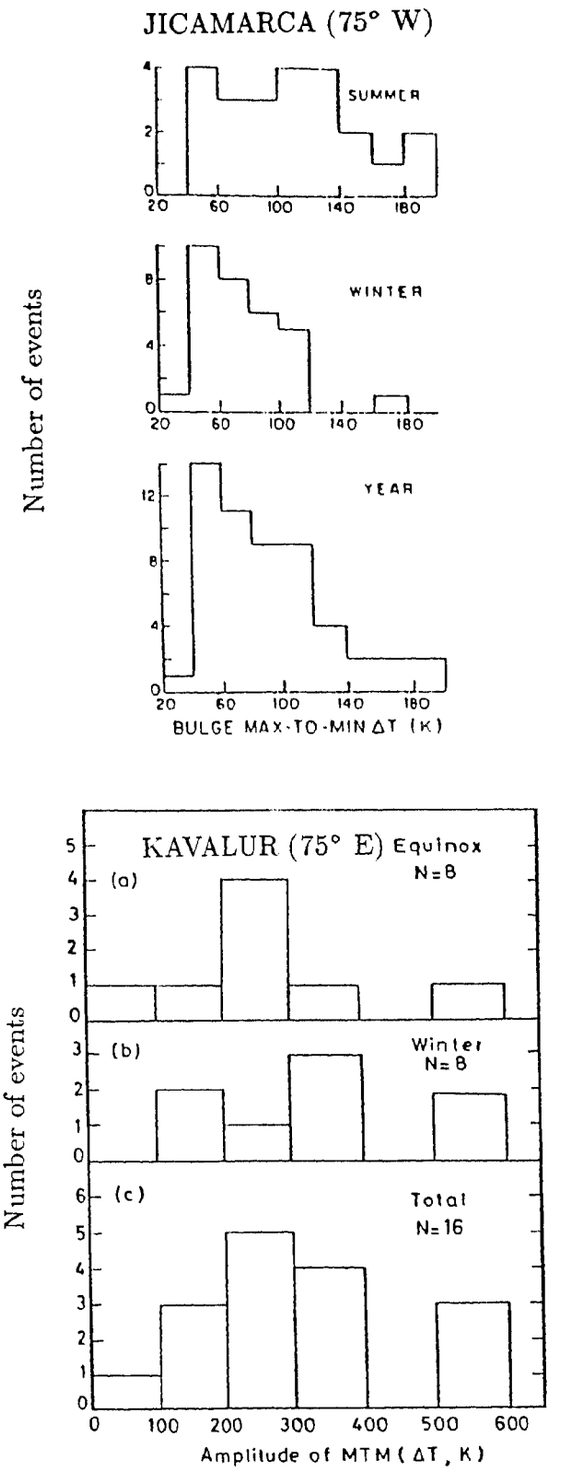

Fig 3.10 : Distribution of amplitude of MTM for Jicamarca (top histogram after Bamgboye and McClure, 1982) and Kavalur (bottom histogram).

the semidiurnal and higher order tidal modes responsible for the MTM originate from momentum coupling associated with the diurnal variation in ion drag and tidal waves propagating from the lower atmosphere. We hold the view that the noteworthy difference in the amplitude of MTM between the Indian and the American sectors brought to light by the present study could be due to the longitudinal difference in the in-situ neutral-ion drag interactions. It is known that the equatorial F-region electron density exhibits considerable longitudinal dependence on different time scales (e.g. Walker and Strickland, 1981), and is by itself quite sensitive to tide-generated dynamo electric fields through the fountain mechanism (Anderson, 1981). We do not discount the plausible role of upward propagating and *in-situ* tides but there is a glaring paucity of experimental data on upper atmospheric tides and their variability at equatorial latitudes. Coordinated measurements of the key parameters of the thermosphere and ionosphere at equatorial stations along the different meridians are needed for a better definition and understanding of the longitudinal dependence of the equatorial MTM.

3.4 MTM effects on low latitude F - region

3.4.1 MTM associated meridional wind effects on F-region height

The equatorial MTM is generally understood interms of a three-dimensional circulation in which the midnight sector of the equatorial thermosphere below 200 km is adiabatically heated by converging equatorward winds or by tides from below (Mayr et al., 1979; Fesen et al., 1986). Near the region of convergence, upward/downward neutral motions prevail by virtue of continuity. The upward motion carries heat and mass resulting in the MTM and the associated density enhancement above 200 km. The net result is the development of the midnight pressure bulge at F-region altitudes which, in turn, influences the thermospheric wind and F-region height and plasma density. This is because the pressure bulge represents a backpressure that counteracts the equatorward winds leading to an abatement or reversal of the meridional winds. Groundbased optical interferometer and incoherent scatter radar observations and 'in-situ' measurements provide convincing evidence for the abatement/reversal of the equatorward wind around

midnight in the equatorial region and also for the seasonal changes in the neutral wind pattern due to that in the causative MTM (e.g., Behnke and Harper, 1973; Burnside et al., 1981, 1983; Friedman and Herrero, 1982; Meriwether et al., 1986; Herrero et al., 1988). A consequence of the MTM-induced modification in the meridional wind is the 'midnight collapse' of the F-region.

The temperature enhancement seen at Kavalur on some nights and in the average pattern is therefore to be associated with perceptible changes in meridional wind pattern and F region height and plasma density. There are no neutral wind measurements at any location in the Indian zone simultaneous with the FPI observations presented here. But ionosonde data of Ahmedabad (23°N, 72°E, dip 34°N) are available but the coverage is only for the FPI data of April 1992, December 1992 and April 1993. In Figure 3.11 is shown the variation of the average values of h_pF_2 (i.e the height of F-region peak for parabolic distribution) at Ahmedabad for the days of our FPI observations (April 1992). It is quite evident that the enhancement evidenced at Kavalur in the average temperature around midnight in April is associated with a clearcut decrease in hpF_2 in the post-midnight hours at Ahmedabad. The change in hpF_2 amounts to a descent rate of ~6.5m/sec which is very close to the median value of about 8m/sec observed at Arecibo (Nelson and Cogger, 1971). It corresponds to a poleward wind of $\sim$ 14m/sec which is of the right order of magnitude of the winds seen around midnight in the equatorial region (e.g Meriwether et al., 1986; Krishnamurthy et al., 1990). It is interesting to note from Fig.3.11 that the temperature shows a tendency to undergo two enhancements in the night separated by a couple of hours particularly in the month of April. The physical significance of the secondary enhancements which are also evidenced in the Jicamarca incoherent scatter radar data (Bamgboye and McClure, 1982) is obscure at the moment and deserves further consideration.

Figures 3.12 and 3.13 represent for similar studies for December 1992 and April 1993 respectively. The height (hpF_2) descent rates for December 1992 and April 1993 are 12.9m/s and 6.1m/s respectively. These descent rates correspond to poleward winds of 27.8m/s and 13.1m/s respectively. These values are also comparable to the

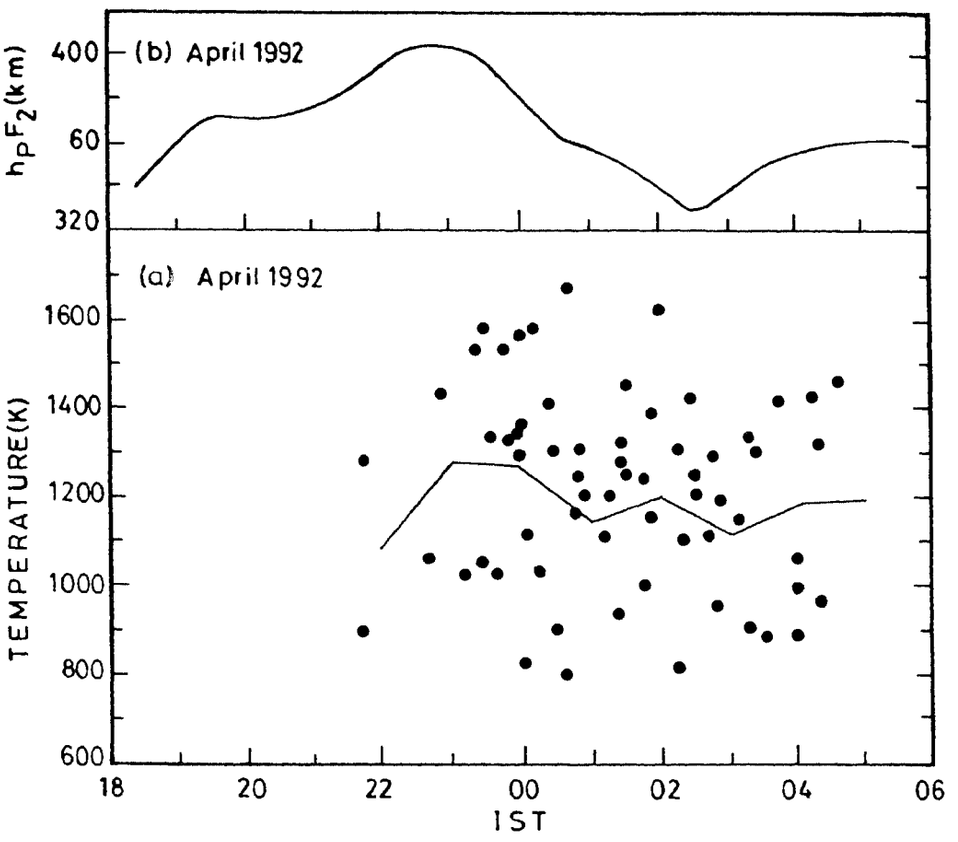

Fig 3.11 : Mass plots of the nighttime variation of thermospheric temperature over Kavalur in April 1992. The solid curve represents the average pattern of the temperature obtained by averaging the data in 1 hr bin centered on the full hour of IST. The top panel(b) shows the variation of mean hpF2 at Ahmedabad (23°N, 72°E) corresponding to the nights of FPI observations at Kavalur (12.5°N, 78.5°E)in April 1992.

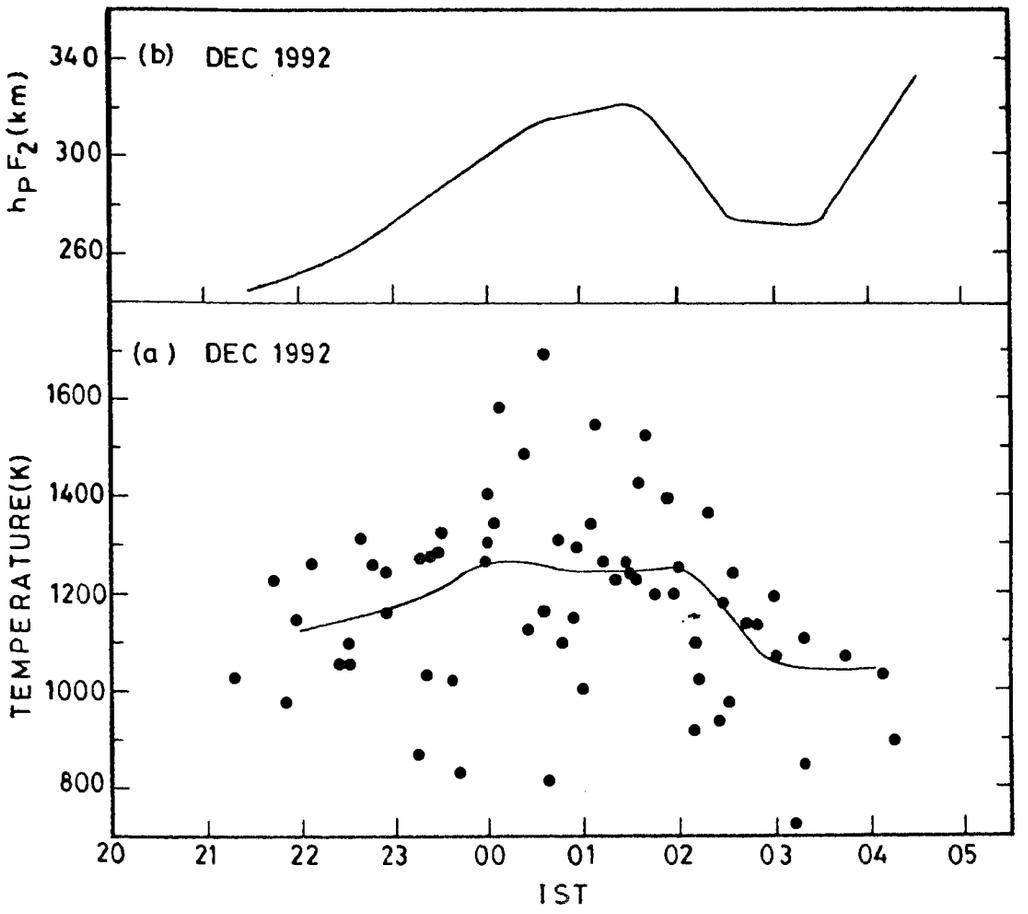

Fig 3.12 : Mass plots of the nighttime variation of thermospheric temperature over Kavalur in December 1992. The solid curve represents the average pattern of the temperature obtained by averaging the data in 1 hr bin centered on the full hour of IST. The top panel(b) shows the variation of mean hpF2 at Ahmedabad (23°N, 72°E) corresponding to the nights of FPI observations at Kavalur (12.5°N, 78.5°E)in December 1992.

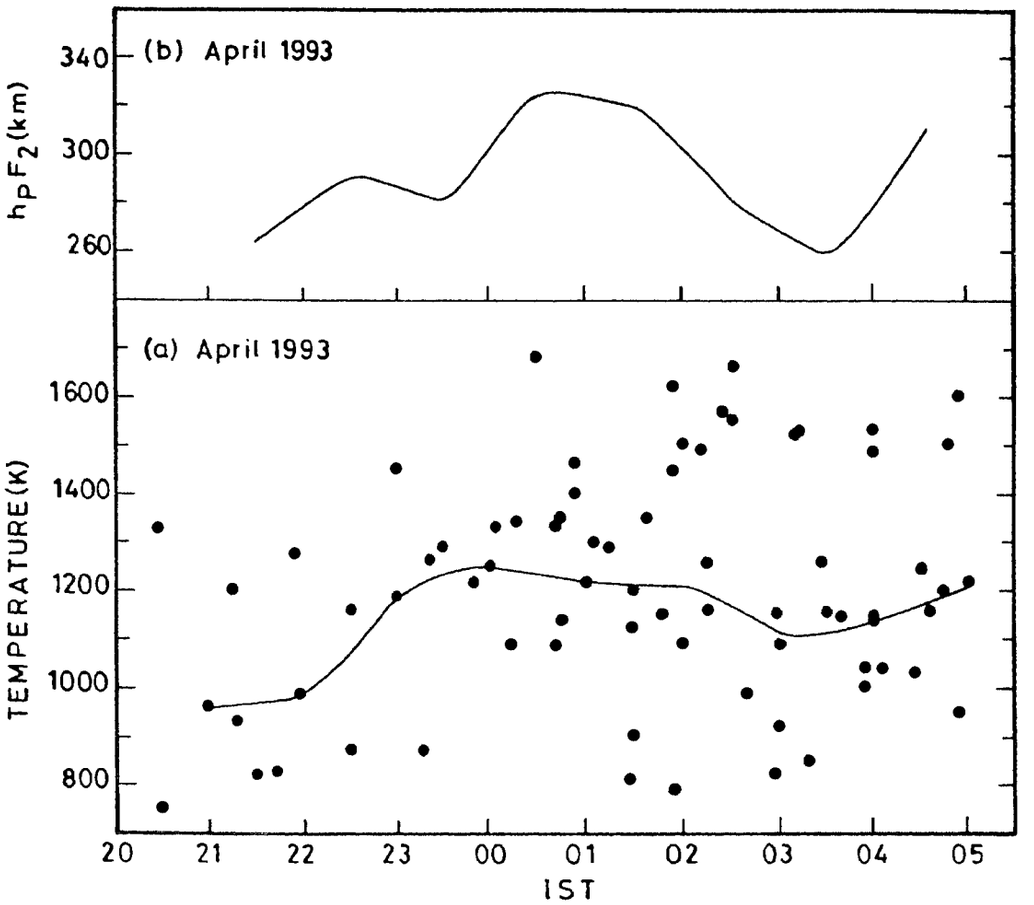

Fig 3.13 : Mass plots of the nighttime variation of thermospheric temperature over Kavalur in April 1993. The solid curve represents the average pattern of the temperature obtained by averaging the data in 1 hr bin centered on the full hour of IST. The top panel(b) shows the variation of mean hpF2 at Ahmedabad (23°N, 72°E) corresponding to the nights of FPI observations at Kavalur (12.5°N, 78.5°E)in April 1993.

magnitudes of winds seen around midnight in the equatorial region (see Fig. 3.14, after Krishnamurthy et al., 1990).

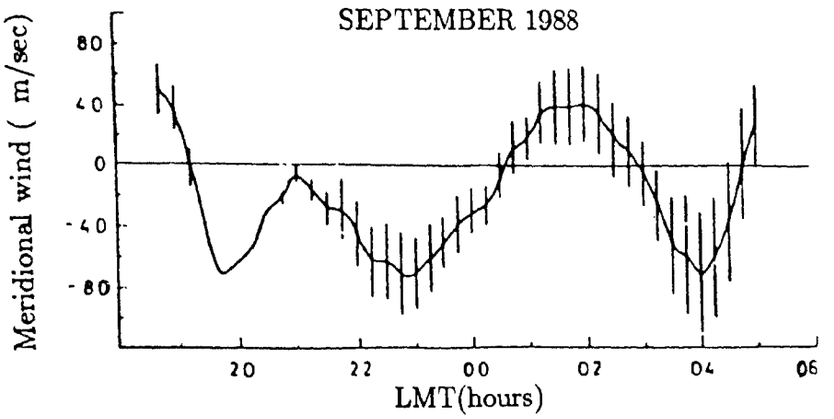

Fig 3.14 : Nocturnal variation of meridional wind (U) in September 1988
(average of seven nights)
(After Krishnamurthy et al., 1990)

3.4.2 Case studies on MTM effects on low latitude F-region height and density.

Case study (a)

Figure 3.15 illustrates a specific case of the association between the midnight temperature increase over Kavalur and the 'collapse' or descent of F-region over Ahmedabad evidenced in our data sample. The figure shows the time variations of the neutral temperature over Kavalur, hpF_2 and foF_2 at Ahmedabad and the ambient geomagnetic conditions (D_{st} and Kp indices) on the night of 9/10 April 1992. There was an unambiguous increase in neutral temperature peaking around 2330 IST on this night, with an amplitude of $\sim$ 250K (lack of measurements prior to 2130 IST rendered accurate evaluation of amplitude rather difficult). The peak temperature is $\approx$ 20% above the average temperature for the entire period of observation from 2130 to 0430 IST. The temperature enhancement was accompanied by a typical 'midnight collapse' of F-region over Ahmedabad with hpF_2 decreasing from 400 km at 0030 IST to 280 km at 0230

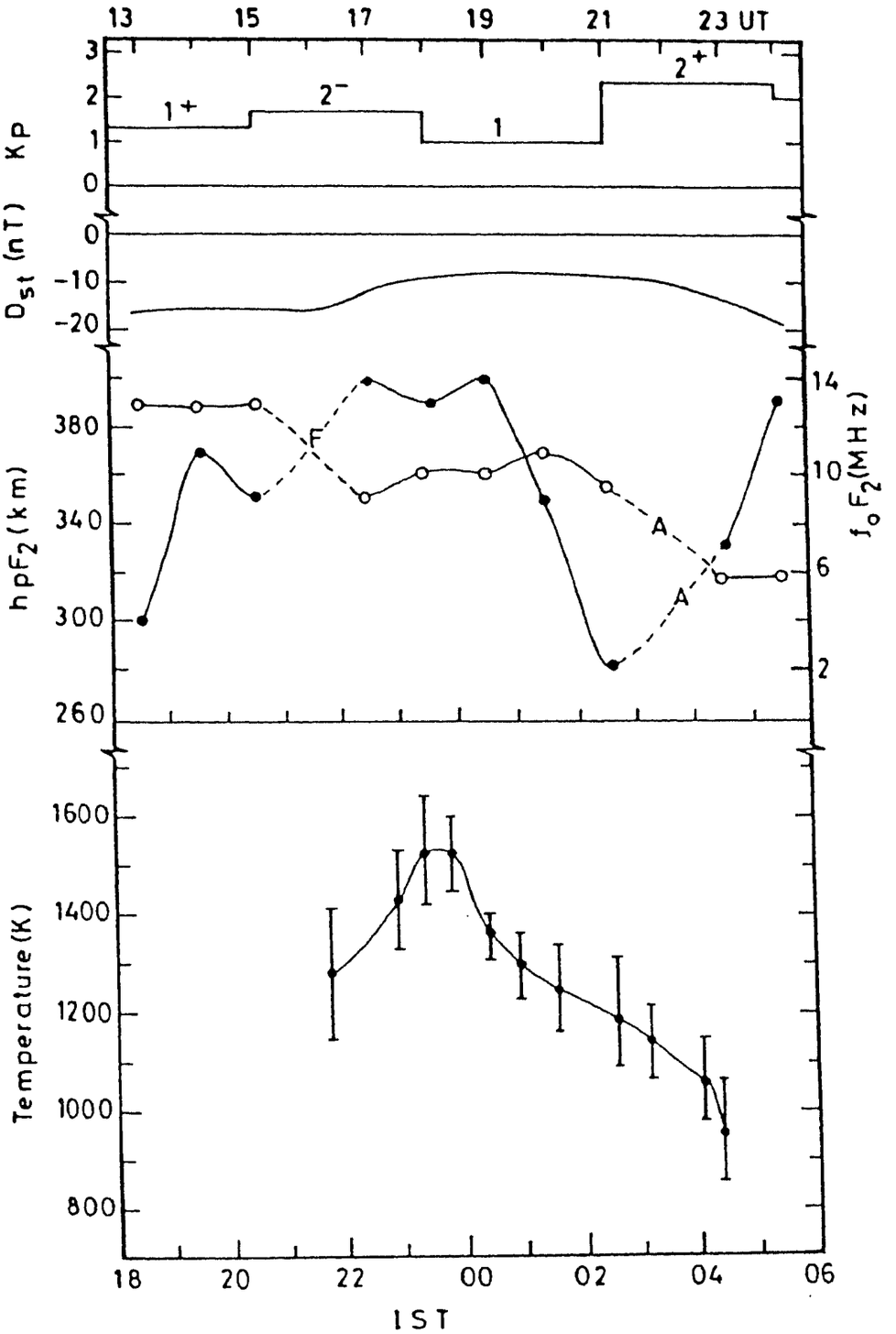

Fig. 3.15 : Temporal variation of the thermospheric gas temperature over Kavalur and the F region peak height (hpF2, • – •) and density (foF2, o – o) over Ahmedabad on the night of 9/10 April 1992 (Ap=6). The ambient geomagnetic conditions (Kp and Dst indices) are also shown (top panel). Note the temperature enhancement around midnight over Kavalur and the associated descent of F region over Ahmedabad in the same longitude zone.

IST, i.e. a decrease of 120 km in 2 hrs or a descent rate of $\sim$ 16m/sec. The prominent change in hpF_2 and the corresponding descent rate imply a poleward neutral wind of $\sim$ 42ms^{-1} for the location of Ahmedabad, of course, if attributed only to neutral wind effects. This is quite valid because of the ambient quiet geomagnetic conditions (Kp $\leq 2^+$). It is known that the F-region takes a certain time to respond to an imposed neutral wind field and this time constant for locations like Ahmedabad turns out to be $\sim$ 2 hr (Sridharan et al., 1991). We consider the time delay ($\sim$ 3 hrs) between the temperature maximum at Kavalur and the minimum height reached at Ahmedabad as representative of the response time of F region. This is not inconsistent with the expected keeping in view the time resolution (1 hr) of the ionosonde data used. We do not consider the time delay as indicative of the propagation time of the MTM and its related wind effects because the study of Herrero and Spencer (1982) based on AE-E satellite data showed that the two-dimensional (local time-latitude) distribution of thermospheric temperature at equinox is such that the MTM is symmetric about the equator with highest amplitude at the equator. The decrease in foF_2 in association with the descent of F-layer at Ahmedabad is to be expected because, in the absence of production, the downward motion of the layer leads to increased loss and hence reduction in plasma density. The initial small increase in foF_2 prior to the substantial decrease could be the outcome of a height-dependent downward drift which would lead to plasma pile up at and below F-region peak as observed by Basu et al., (1981). Experimental evidence for the relationship between the MTM and the consequent weakening or reversal of the normal equatorward winds and midnight collapse of F-region is limited hither to either to changes in temperature and winds (e.g. Spencer et al., 1979) or changes in winds and F-region height (e.g. Behnke and Harper, 1973; Burnside et al., 1983). The observations presented here constitute the first evidence of the (expected) relationship between temperature enhancement near the equator and F-region descent at a higher latitude station in the nocturnal equatorial region. Though the F-region height at low latitudes is known to be sensitive to temperature, we do not consider temperature change as responsible for the observed decrease in hpF_2 at Ahmedabad. This view is based on two considerations. They are :

(1) the temperature decrease required to account for the change in hpF_2 of 120km is $\sim$ 1100K [temperature dependence of F region height is $\sim$11 km/100K at Ahmedabad, (Sridharan et al., 1991) which is physically unreasonable and

(2) the temperature-related changes in F-region height are to occur on time-scales shorter than the response time ($\sim$ 2hr) to changes in meridional wind as shown by Sridharan et al., (1991), and there is no indication of such a behaviour on the night of 9/10 April (see Fig.3.15).

Case study (b)

Presented here is the first experimental evidence of the (expected) relationship between MTM and midnight descent or collapse of F-layer at a low latitude station, through thermospheric meridional neutral winds (derived by the method given by Krishnamurthy et al., 1990) associated with MTM. The relationship MTM $\rightarrow$ winds $\rightarrow$ F-layer collapse, is thus demonstrated in its totality.

Krishnamurthy et al(1990) introduced a method of deriving meridional neutral winds for the nighttime using h'F of the two equatorial stations, Trivandrum and Sriharikota (SHAR) in India. Their results showed a poleward reversal of the meridional winds in the postmidnight period both in winter and autumn equinox, which feature they attributed to the equatorial MTM. This interpretation remained unsubstantiated due to lack of simultaneous direct measurements of temperature near the equator and/or of winds at locations away from the equator. The availability of neutral temperature measurements at Kavalur provided opportunity to examine the validity of the derivation of meridional winds from $h'F$ data introduced by Krishnamurthy et al (1990). As a step in this direction coordinated measurements of $h'F$ at Trivandrum, Kodaikanal and Sriharikota(SHAR) and neutral temperature over Kavalur were undertaken on few nights in December 1992 and the details of the data-based case studies are as follows. See Fig. 3.1 for the geographic locations of the stations whose data is used in this study.

The nocturnal pattern of meridional winds is derived from the quarter-hourly h'F data of Trivandrum and SHAR following the method given by Krishnamurthy et

al.(1990). The method is based on the logical assumption that the F-region plasma vertical drift at Trivandrum very close to the magnetic equator is affected solely by zonal electric fields while that at SHAR is controlled by electric fields, meridional winds and plasma diffusion. The winds are calculated at 15-min intervals from the time derivatives of h'F at the two stations making allowance for chemical loss and plasma diffusion effects, and are smoothed for random fluctuations (if any) with a five-point running mean filter. The overall uncertainty in the estimated winds is $\pm$ 25 ms^{-1}. Figures 3.16 and 3.17 show the evidence obtained on two nights of coordinated measurements for the effect of neutral temperature variation near the equator on the neutral and plasma dynamics in the nocturnal equatorial F-region.

It is evident from Fig.3.16(b) that on the night of 18-19 December 1992, there is a distinct enhancement in the neutral temperature just after midnight (MTM) over Kavalur with an amplitude of about 280K. Such a feature is not predicted by empirical global thermospheric models such as MSIS-86 (Hedin, 1987) as can be seen from the MSIS model temperatures plotted in the figure. The peak temperature is 24% above the mean temperature for the entire period of observations from 2200 to 0230 IST on the night. Prominent changes in the F-region height at the dip equatorial stations accompanied the MTM over Kavalur. There is a distinct decrease in h'F at SHAR beginning at 0200 IST while both at Trivandrum and Kodaikanal h'F increased starting from 0130 IST. This feature indicates that while the F-region height at SHAR is under the influence of poleward winds, that at Trivandrum and Kodaikanal is under that of an eastward electric field. The electric field is, however, likely to be small because a part of the observed increase in h'F at Trivandrum and Kodaikanal is apparent due to layer decay as the layer is well below 300 km at the time (see Fig.3.16(c)). With a view to quantify the meridional wind effects on h'F at SHAR, the winds have been estimated from the ionosonde data of Trivandrum and SHAR adopting the procedure of Krishnamurthy et al (1990) detailed earlier. The result presented in Fig.3.16(e) substantiates the inferences drawn from the relative variations in h'F at the three stations: Trivandrum, Kodaikanal and SHAR. The wind is poleward and strong in the evening

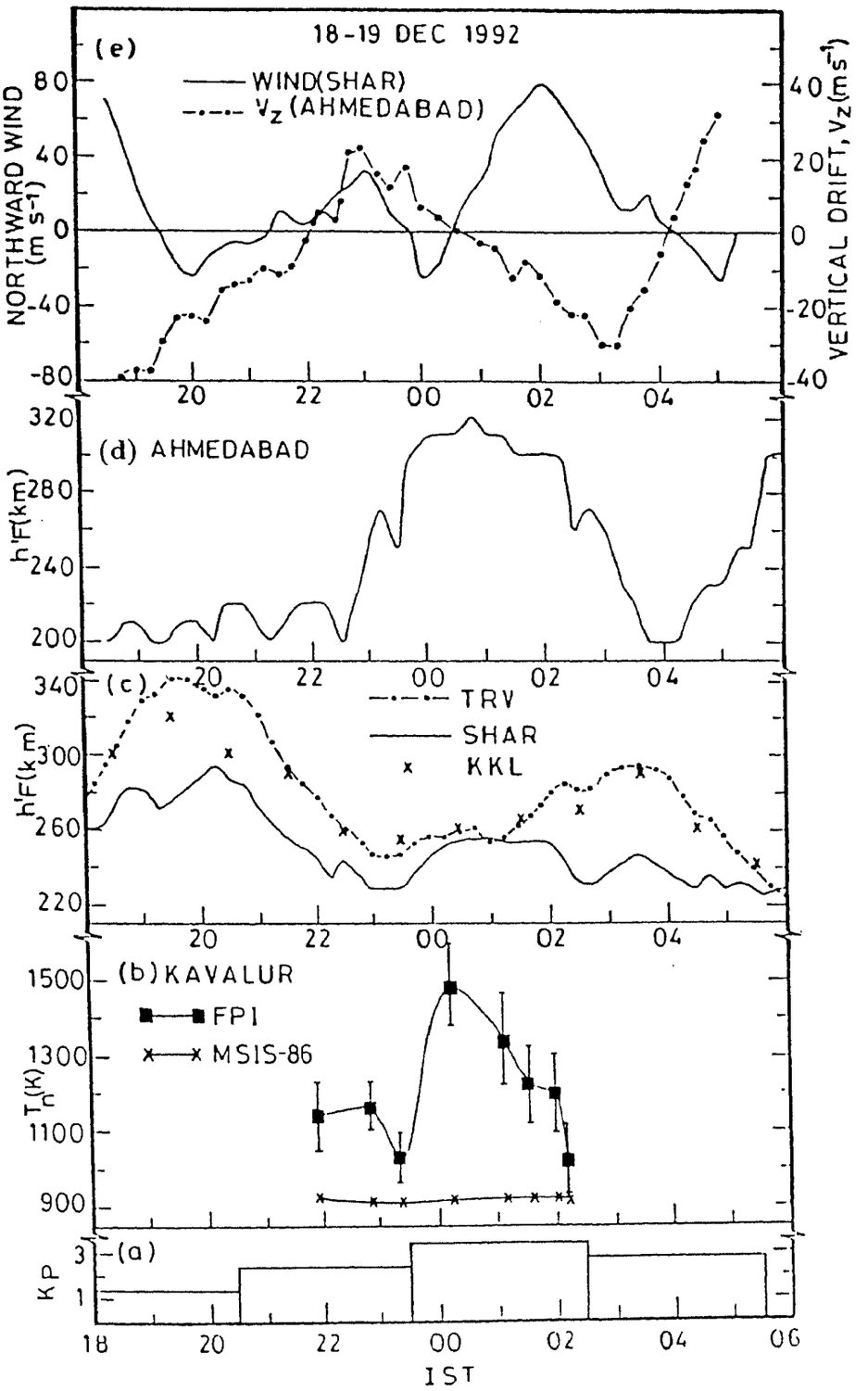

Fig 3.16 : Temporal variation of (a) the 3-hr geomagnetic Kp index, (b) thermospheric temperature at Kavalur and (c-d) h'F at Trivandrum (TRV), Kodaikanal (KKL), SHAR and Ahmedabad on the night of 18/19 December 1992 (Ap = 9). The topmost panel (e) shows the time histories of the meridional neutral winds derived from h'F data of Trivandrum and SHAR and the F-region vertical drift (Vz) at Ahmedabad derived from h'F data and corrected for chemical loss ,electric field and diffusion effects-see text for further details.

time and turned equatorward by 1930 IST and maintained that direction till 2115 IST. It became poleward there after attaining a maximum amplitude of 30 ms^{-1} at 2300 IST, and then turned equatorward for a short duration of 45 min around midnight. These short-term changes in wind direction and amplitude are not very significant (the exception is the strong poleward wind in evening hours) keeping in view the fact that the overall error in the estimated wind is $\pm$ 25ms^{-1}. In contrast the meridional wind turned poleward at 0030 IST and remained in that direction till 0400 IST attaining a peak value of $\approx$ 80ms^{-1} at 0200 IST. The magnitude of the poleward wind averaged over the period of its manifestation (0045-0345 IST) is 44.1 $\pm$ 23.4 ms $^{-1}$ which agrees well with the satellite measurements (Spencer et al., 1979). The data of Fig.3.16 thus demonstrate the unambiguous relationship of the inferred poleward winds after midnight derived from the ionosonde data of Trivandrum and SHAR with the MTM over Kavalur.

The presence of persistent poleward winds of large magnitude in the postmidnight period near the equator on the night of 18-19 December is to have a significant effect on F-region height at locations like Ahmedabad (dip 34° N). As can be seen from Fig.3.16(d), there is indeed a decrease in h'F at Ahmedabad over the period 0045-0345 IST. The layer descent is small to start with but became prominent from 0215 to 0345 IST when h'F decreased from 300 km to 200 km, i.e, a gross descent rate of 18.5ms^{-1}. The very fact that such a large layer descent prevailed in the altitude range 200-300 km where chemical loss effects could be important (Bittencourt and Abdu, 1981), indicates the presence of a significant downward drift of F-region plasma and hence sizeable poleward winds. With a view to ascertain this, the pattern of F-region V_z at Ahmedabad during the night is derived from the time derivates of h'F. To arrive at V_z solely due to meridional winds, the time derivatives of h'F are to be corrected for the effects of chemical loss, electric fields and plasma diffusion. The corrections due to chemical loss and diffusion are done following standard procedures the details of which are given in Krishnamurthy et al., (1990). The vertical drift at Trivandrum as corrected for layer decay is taken to represent purely the electrodynamic drift due to the electric fields and is scaled down to the latitude of Ahmedabad by the Cos (I) term where I is

the dip angle. The implicit assumption here is that the zonal electric field is spatially uniform in the equatorial region, which is reasonable particularly for the midnight-dawn period. Latitudinal gradients in equatorial electric fields are known to be present in evening twilight period (Raghava Rao et al., 1984; Aggson et al., 1987), but we are not aware of any reports of non-uniform electric fields for the postmidnight interval of specific interest here. The corrected values of the vertical drift, V_z are calculated at 15-min intervals and are smoothed with a 5-point running mean filter to smooth out random fluctuations if any (as in the case of the neutral winds).

The temporal pattern of V_z at Ahmedabad thus derived and graphed in Fig.3.16(e) is consistent with the meridional wind pattern derived from the ionosonde data of Trivandrum and SHAR. This is particularly so in the post-midnight period when a large downward V_z prevailed at the time of poleward winds associated with the MTM over Kavalur. The average value of downward V_z is 15.1 $\pm$ 9.4 ms^{-1} over the period 0045-0400 IST which corresponds to poleward winds of 32.7 $\pm$ 20.4 ms^{-1}. This is consistent with the average value of 44.1 $\pm$ 23.4 ms^{-1} for the poleward winds derived from the h'F data of Trivandrum and SHAR and attributed to the MTM over Kavalur. The F-region is known to take a certain time to respond to an imposed neutral wind field, and this time constant for Ahmedabad is about 2 hrs (Sridharan et al., 1991). We consider the time delay (about 3 hrs) between the temperature maximum at Kavalur and the minimum height reached at Ahmedabad in the postmidnight period as representative of the response time of F-region to the poleward winds set up by the MTM.

Case Study (c)

The gross features of the temporal variation of the thermospheric and ionospheric parameters on the night of 23/24 December are similar to those on the night of 18/19 December. There are distinct differences nevertheless in the details of the behaviour of the physical parameters between the two nights. As can be seen from Fig.3.17(b), the amplitude of the MTM over Kavalur on the night of 23/24 december is larger (about

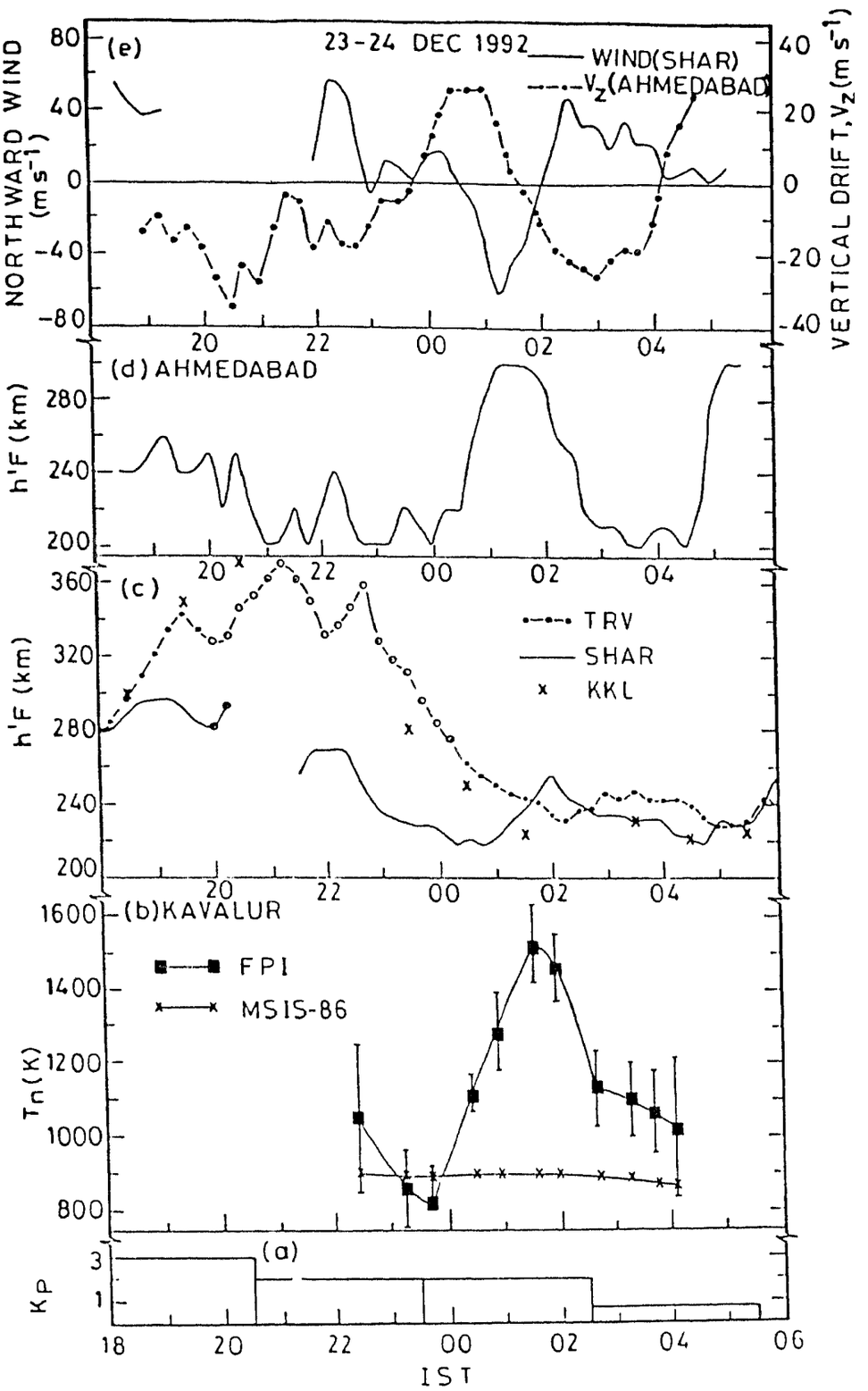

Fig 3.17 : same as in Fig 3.16 but for the night of 23-24 December 1992 (Ap = 8). Open circles on h'F plots of Trivandrum and SHAR indicate times when spread-F is present on ionograms.

450K), peaked later (around 0140 IST) and persisted longer than on the night of 18/19 December. The peak temperature is 34 % above the average temperature for the entire period of observations from 2230 to 0415 IST. The presence of spread-F conditions at SHAR and Trivandrum [see Fig.3.17(c)] did not permit unambiguous derivation of meridional neutral winds from h'F data for the premidnight period. For the same reason, V_z at Ahmedabad attributable to meridional winds (Fig.3.17(e)) is also to be treated with some caution for the premidnight period. Poleward winds (38-54 ms^{-1}) are, however, quite apparent during the period 1830-1915 IST (prior to the onset of spread-F) from the nature of the h'F variation at Trivandrum and SHAR and the wind pattern derived from the same as can be seen from Fig.3.17(c) and (e). Strong equatorward winds are seen for an hour and half beginning at 0030 IST with a maximum of 62 ms^{-1} at 0115 IST. Around the same time h'F at Ahmedabad experienced a significant increase and V_z (corrected for layer decay, electric field and diffusion effects) is upward with a peak value of 25.5 ms^{-1} [see Fig.3.17(c) and (e)]. But starting at 0200 IST, i.e. just after the temperature reached its maximum over Kavalur, h'F at SHAR underwent a decrease rather rapidly initially but slower afterwards, while h'F at Trivandrum showed an opposite trend till 0430 IST. This implies the presence of poleward winds during the period of subsidence of the MTM over Kavalur. Fig.3.17(e) shows that the strong equatorward winds indeed turned sharply poleward by 0200 IST and maintained that direction till 0445 IST. The average value of the poleward winds over the interval 0215-0400 IST is 28 $\pm$ 8.9 ms^{-1}. More or less in consonance with the poleward reversal of the meridional winds, the F-layer at Ahmedabad underwent a typical 'postmidnight descent' with h'F decreasing by 100 km over the period 0145-0330 IST. V_z at Ahmedabad is accordingly downward during this time with an average value of 17.6 $\pm$ 6.6 ms^{-1} for the period 0145-0400 IST, which corresponds to poleward winds of 38.0 $\pm$ 14.2 ms^{-1}. The mean magnitude of the poleward winds at Ahmedabad is in agreement with the value (28 $\pm$ 8.9 ms^{-1}) derived from h'F data of Trivandrum and SHAR.

It is to be noted that although the amplitude of the MTM is larger on the night of 23/24 December compared to that on 18/19 December, the magnitude of the poleward

wind is smaller at SHAR. This could be due to the difference in the latitudinal position and spatial structure of the midnight pressure bulge which determine the local wind pattern between the two nights.

These simultaneous multistation observations carried out in India on two nights in december 1992 with optical interferometer and ionosonde techniques confirm the prevailing view that the equatorial midnight temperature maximum (MTM) is responsible for the midnight poleward reversal of meridional winds there, which subsequently leads to the 'postmidnight collapse' of the F-layer at low latitude locations on the same meridian.

3.5 Summary

Successful measurements of nighttime neutral thermospheric temperatures over Kavalur using FPI provided an opportunity to understand some aspects of neutral-plasma coupling in the equatorial thermosphere - ionosphere system. The observed day-to-day variability in nighttime temperature over Kavalur and the inability of MSIS-86 model to predict the same is a pointer to the fact that the model needs improvement in the input parameters. Identification of MTM in Indian equatorial region is an important step in understanding the energetics of thermosphere - ionosphere system. Comparison of the characteristics of MTM in the Indian zone to that of American zone and finding the difference has generated interest to probe and ascertain the causes of the longitudinal dependence of the structure of the equatorial thermosphere-ionosphere system.

The demonstration of the relationship i.e., MTM $\rightarrow$ Winds $\rightarrow$ F layer collapse in its totality is accomplished though limited to two nights. This demonstration clearly supports the method introduced by Krishnamurthy et al (1990) to derive nighttime meridional wind pattern using h'F data from two equatorial stations (Trivandrum and SHAR) nearly on the same magnetic meridian. This is an important step in the process of obtaining indirect but reliable information on nighttime thermosphere winds for the Indian sector more or less on a routine basis from the ionosonde data.

******

Chapter 4

Equatorial Ionosphere and Interplanetary magnetic clouds

4.1 Introduction

Solar Coronal Mass Ejections (CMEs) :

Sudden expulsions of dense clouds of plasma from the outer atmosphere of the Sun are termed as 'coronal mass ejections' (CMEs) (Wagner, 1984). The coronal mass ejections are found to be associated with flares, eruptive prominences, soft X-ray event, radio bursts... etc. (Wilson and Hildner, 1986 and references therein). CMEs are a type of coronal transients. Figure 4.1 (taken from Hildner et al, 1989) is a schematic representation of a coronal transient event at different times of the event. In the figure the central core P is a remanant of the eruptive prominence and B is a narrow bright spike within the leg of CME. The major properties of CMEs i.e speed, mass and energy are given in Figure 4.2 (taken from Hildner et al, 1989). The speed and mass indicate that there should be interplanetary effects of CMEs. The association of interplanetary (Gosling et al., 1975) and coronal (Gosling et al., 1976) shocks with fast CMEs seemed to confirm this point of view. Gosling et al. (1977) suggested that non-compressive density enhancements (NCDE) observed in the solar wind are the interplanetary signatures of CMEs.

Magnetic clouds and their classification :

Klein and Burlaga (1982) have reported the observation of structures in the solar wind near Earth which may be manifestations of solar coronal mass ejections, and they called these structures *magnetic clouds*. These structures in the solar wind have typical radial lengths of $\approx$ 0.25AU (at 1AU) where the strength of the magnetic field is high, and the direction of magnetic field changes by means of rotation nearly parallel

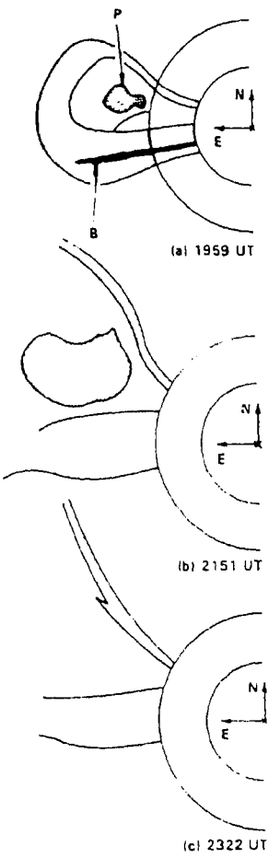

FIG. 4.1

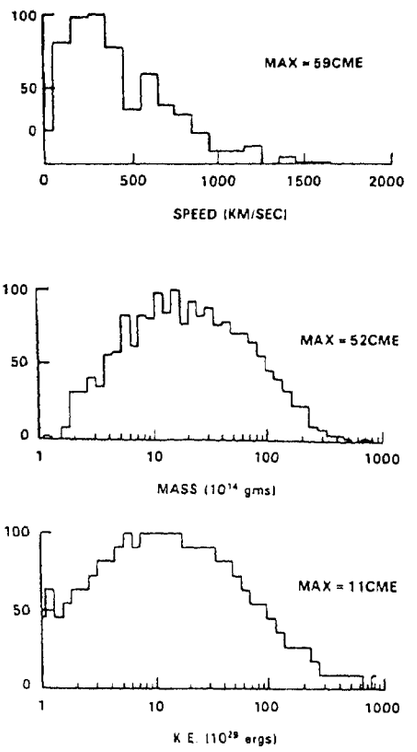

FIG. 4.2

Fig 4.1 : Schematic representation of the 5 August 1980 coronal transient at several times during the event. P is the remanant of an erupting prominence; B is a narrow, bright spike within the leg of the CME. (a) 1959 UT; (b) 2151 UT; (c) 2322 UT. (After Hildner et al., 1989)

Fig 4.2 : Properties of all CMEs during the interval surrounding the maximum of the solar cycle, 1979-1981. The distributions of speed, mass and kinetic energy are plotted as histograms. Each plot has been normalized to 100% of the maximum number of CMEs. The maximum values used in the normalizations are indicated on the plots. (After Hildner et al., 1989)

to a plane. Klein and Burlaga (1982) have identified 45 magnetic clouds and classified them in to three classes. They are : (1) Cloud preceeded by a shock, (2) Cloud associated with a stream interface and (3) Cloud associated with a CME.

Cloud preceded by a shock :

Shown in the Fig. 4.3 are magnetic field strength (F), magnetic field latitude (θ) and longitude (ϕ) in solar ecliptic coordinates, bulk speed (V), density (N), and proton temperature (T_p) versus time for the period February 9 to February 14, 1969. Between the lines marked B and D one can see a distinct structure with the following characteristics of the magnetic cloud of this categary : (a) the magnetic field direction changes slowly from a southward to northward orientation and the magnetic field strength is high (10nT for 36 hours), (b) the temperature is unusually low, (c) the speed is relatively high, especially near the front of the structure, (d) the density decreases monotonically from higher than average values to unusually low values. This magnetic cloud was preceeded by a shock indicated by the line A. The high resolution magnetic field data clearly show a shock at 2024 UT on February 10.

Cloud associated with a stream interface :

The Fig. 4.4 shows an example of a magnetic cloud associated with stream interface. The interface is identified with the simultaneous increase in T and V and a decrease in N at a time when F is maximum.

Cloud associated with a CME but not with an interface or shock :

A magnetic cloud associated with a CME but not with an interface or shock is illustrated in Fig. 4.5. The CME is identified as a region of low temperature and high field strength. The boundaries of the cloud are chosen on the basis of the temperature and field strength profiles.

These magnetic clouds have magnetic field strength $\approx$ 12nT, temperature $\approx 4 \times 10^4$K and density $\approx$ 10-14/cc. Wilson (1987) carried out a superposed epoch analysis of equatorial D_{st} index for 19 of the magnetic clouds listed by Klein and Burlaga (1982).

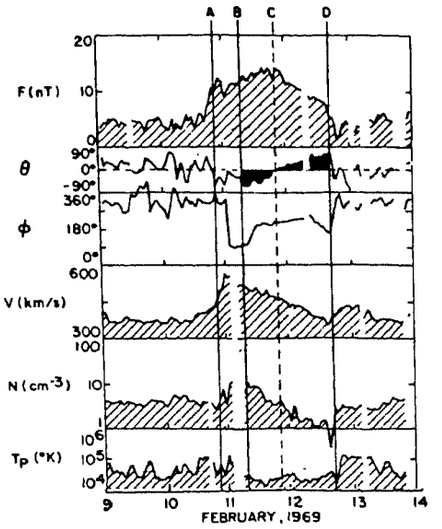

Fig 4.3 : Magnetic field and flow parameters associated with a magnetic cloud. The cloud is between B and D, where the latitude angle of B varies systematically from large negative values to large positive values. This cloud is cold and moves faster than the surrounding flows.

(After Klein and Burlaga, 1982)

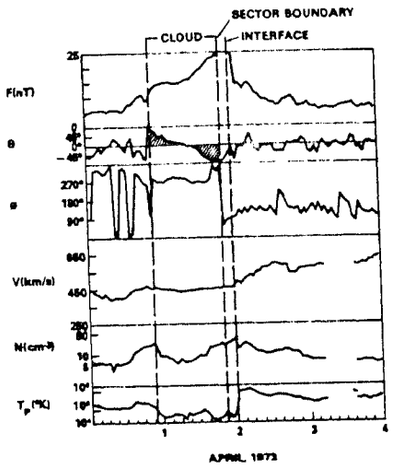

FIG. 4.4

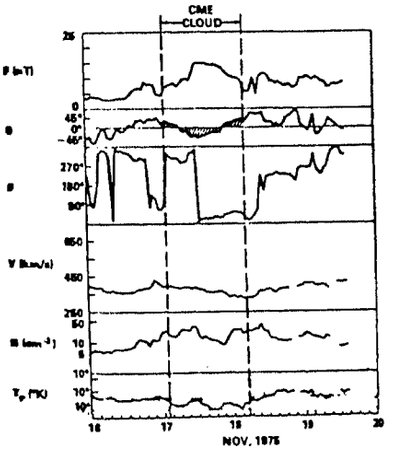

FIG. 4.5

Fig 4.4 : A magnetic cloud followed by a stream interface and sector boundary.

(After Klein and Burlaga, 1982)

Fig 4.5 : A magnetic cloud associated with a CME (a cold region in which the magnetic field strength is enhanced).

(After Klein and Burlaga, 1982)

He suggested that there exist a genuine association between passage of the clouds past the Earth and moderate geomagnetic disturbances and attributed this as a consequence of the presence of southward B_z in the initial portion of clouds. Zhang and Burlaga (1988) extended the previous catalogue with 19 additional clouds of 1978 to 1982 and classified them into two classes of negative and positive clouds. In the negative (positive) cloud, the B_z component of IMF swings smoothly from southward (northward) to northward (southward). See the middle panel of Fig 4.6 for examples of negative and positive clouds.

Significance of magnetic clouds :

Keeping in view the irrefutable link between the southward-oriented interplanetary magnetic field (IMF) and geomagnetic activity (Akasofu, 1981 and references therein), and the fact that magnetic clouds possess a large southward IMF over a part of their $\sim$1 day duration at Earth, Crooker (1983) argued for a plausible geomagnetic response to the passage of magnetic clouds at Earth. Recent studies demonstrated that magnetic clouds indeed produce geomagnetic disturbances with characteristics in conformity with the well known sensitivity of geomagnetic activity to the orientation of IMF and solar wind flow speed (Wilson, 1987; Zhang and Burlaga, 1988). The discovery of magnetic clouds by Burlaga et al.(1981) and the subsequent studies strongly linking the clouds with the forms of solar activity that are known to give rise to CMEs on the one hand, and with geomagnetic storms on the other, have revealed a new facet of solar-terrestrial relationships wherein a logical and transparent cause-and-effect sequence prevails. The response of the near-earth space environment to the passage of magnetic clouds at earth merits in-depth investigations in view of the clear perspective they provide of the coupling between solar/interplanetary and magnetospheric/ionospheric variabilities. It is to be recalled here that the solar sources and thermosphere-ionosphere system effects of geomagnetic storms are major topics of current research in solar- terrestrial physics (e.g. Rishbeth et al., 1987; Marubashi, 1989; Prolss et al., 1991).

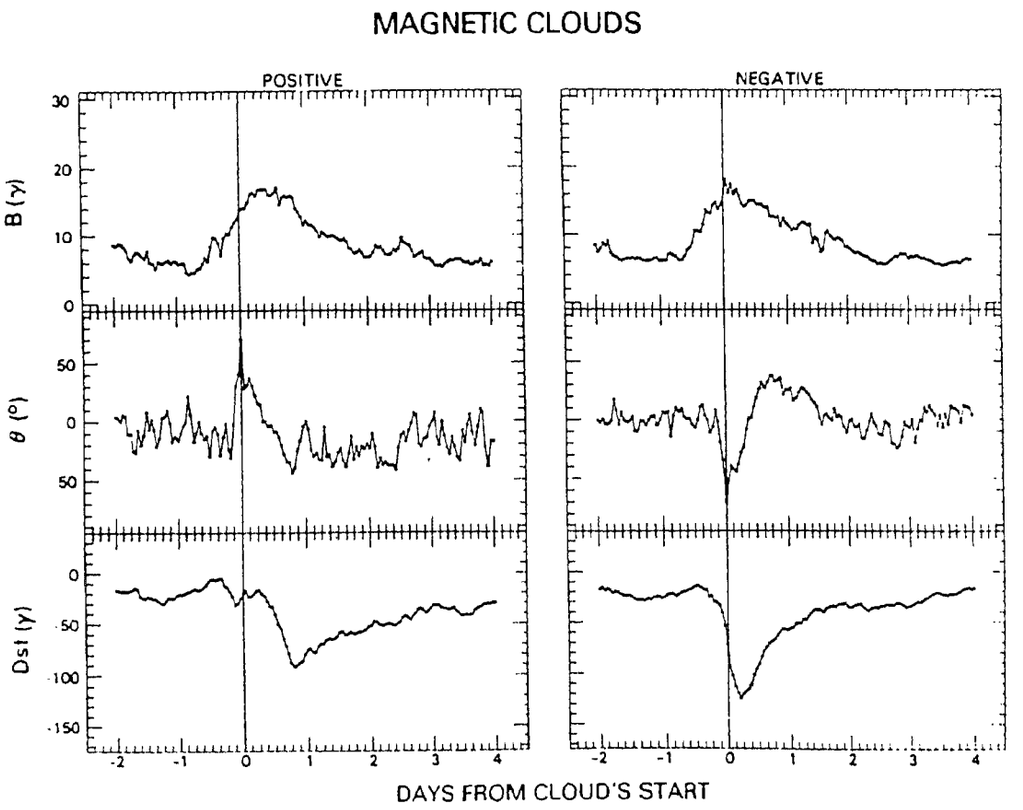

Fig 4.6 : Geomagentic disturbances associated with positive and negative magneitc clouds. (Left) Positive magnetic clouds, where the magnetic field is oriented northward at onset (Right) Negative magnetic clouds, where the magnetic field is oriented southward at onset. From the top to the bottom: the magnetic field strength B (in gammas), the elevation angle θ (in degress) and the Dst index (in gamma). The curves are plots based on superposed epoch analysis with zero epoch equal to the time of cloud onset. Positive clouds comprise 6 of 19 clouds, while negative clouds comprise 13 of 19 clouds. (After Zhang and Burlaga, 1988)

IMF induced geomagnetic storm/substorm :

Interplanetary magnetic field modulates the behaviour of the terrestrial magnetosphere - ionosphere system through regulation of the energy and momentum inputs to the magnetosphere as well as magnetospheric processes, primarily through its north-south (B_z) component (Akasofu, 1981; Baumjohann and Paschmann, 1987 and references there in). The geomagnetic substorm/storm, which is a classic example of IMF-induced disturbances in the near-earth space environment, has direct and dramatic effects on the polar thermosphere-ionosphere system through convection electric fields, particle precipitation, field aligned currents and heat flows (Schunk, 1987; Killen and Roble, 1988). The geomagnetic storm effects in the sub-auroral ionosphere on the other hand, are subtle and indirect and are generally considered to arise from electro dynamical and dynamical coupling of high-latitude and low-latitude ionospheres (e.g. Matuura, 1972; Testude et al., 1975; Behnke et al., 1985; Rishbeth et al., 1987; Berger and Barlier, 1988; Sastri, 1988b; Fesen et al., 1989; Reddy et al., 1990; Mazaudier and Venkateswaran, 1990; Prolss et al., 1991 and references therein). The main physical mechanisms underlying the storm-time behaviour of the F-region are changes in photochemical production, chemical - photochemical loss, plasma transport by electric fields, winds and waves, changes in neutral composition and in temperatures of neutral/ionized species. The geomagnetic storm effects in the F-region continue to fascinate researchers because of their complexity which, in large part, is due to the interactive nature of the processes responsible for the effects. At equatorial latitudes, as explained in chapter 1, electric fields of global E region dynamo origin that predominate during quiet geomagnetic conditions not only drive the intense ribbon-like equatorial electrojet (EEJ) current at E-region altitudes in the vicinity of the dip equator, but also effectively govern the structure and dynamics of the equatorial F-region through vertical plasma drift caused by the interaction of its East-West component with the horizontal North - South magnetic field there. It is now well established that the equatorial zonal electric field responds very sensitively to electrodynamic changes that occur in the magnetosphere-ionosphere system as a result of the highly variable solar wind-magnetosphere interac-

tions controlled by IMF B_z (Fejer, 1986; Reddy, 1989; Sastri, 1988b; Mazaudier and Venkateswaran, 1990; Fejer et al., 1990a,b). There is growing awareness now that the equatorial thermosphere-ionosphere system also responds quite significantly to neutral atmosphere disturbances (large scale perturbances in the neutral composition, wind and temperature fields that propagate from high latitudes to the equator) generated by the storm-time deposition of energy and momentum at high latitudes (e. g. Berger et al., 1988; Fesen et al., 1989).

In this chapter the results of the detailed study of the behaviour of equatorial ionosphere in the Indian sector in relation to the passage of an interplanetary magnetic cloud at Earth during January 13-15, 1967 are presented. This particular cloud was chosen because the changes in the solar wind magnetospheric coupling brought about by its transit, and their relationship to the features of the attendant geomagnetic storm (as evidenced in geomagnetic indices AE, D_{st}, etc.) have already been studied (Perrault and Akasofu, 1978; Akasofu, 1981). The studies and the results are presented in two sections based on the type of disturbance observed in the equatorial ionosphere due to the transit of magnetic cloud at Earth. They are : (1) transient disturbance that prevailed in the F-region near the dip equator (Kodaikanal) during the initial phase of the sudden commencement (SC) geomagnetic storm associated with the cloud's transit and (2) prominent and persistent ionospheric disturbances which prevailed in the main and recovery phases of the geomagnetic storm.

4.2 Response of equatorial ionosphere to the transit of interplanetary magnetic cloud of January 13-15 , 1967

4.2.1 Features of the magnetic cloud and associated geomagnetic storm

The magnetic cloud under discussion followed an interplanetary shock at 12:02 UT on 13 January 1967 at earth and its transit was assessed as from 21:00 UT of 13 January to 07:00 UT of 15 January 1967 from minimum variance analysis (Klein and Burlaga, 1982) (see Fig. 4.7). According to the latest classification scheme mentioned earlier, the cloud can be identified as class 1, i.e. a negative cloud with shock association. The

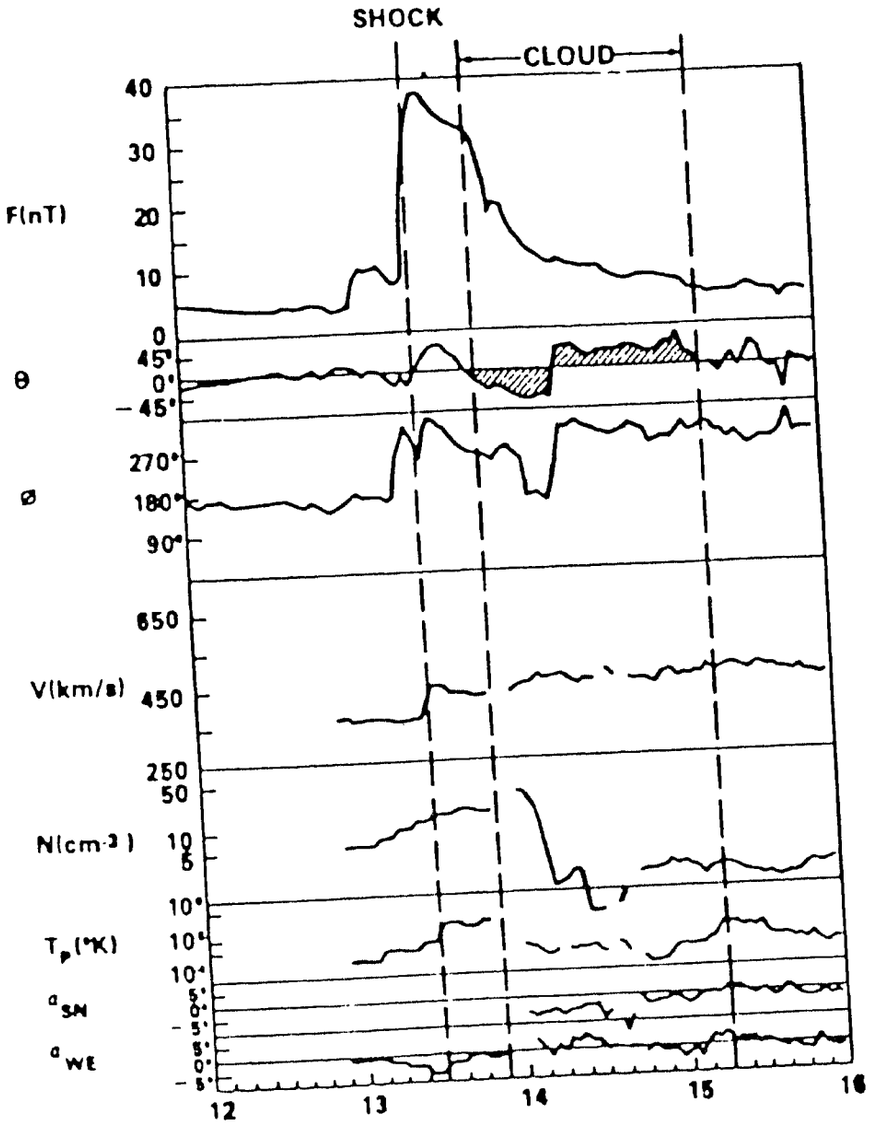

Fig 4.7 : Magnetic cloud (preceded by shock) of January 13-14, 1967.
(After Hildner et al., 1989)

IMF B_z turned southward around 20:00 UT on 13 January 1967 and maintained that direction for 13 h with a mean amplitude of -14.3 ± 5.1 nT. It swung northward around 10:00 UT on 14 January and stayed in that direction across the remaining part of the structure with a mean amplitude of 4.1 ± 2.3 nT. This large monotonic variation in IMF B_z and high values of $|B|$ characteristic of magnetic clouds can be seen from the time histories of IMF $|B|$ and B_z for the period 13–14 January 1967 presented in the top panels of Fig.4.8 taken from Perrault and Akasofu (1978).

The passage of the cloud did result in an intense geomagnetic storm ($|D_{st}|$ max, 176 nT) which began with a sudden commencement (SC) at 12:02 UT on 13 January (due to the interplanetary shock that preceded the cloud) and ended by 11:00 UT on 14 January. The main features of the morphology of the storm as seen in the auroral electrojet index (AE), the low-latitude asymmetry index (ASY), equatorial D_{st} index and the ring current injection rate (Ui) presented in Fig.4.8 are as follows:

(a) A substorm of moderate strength accompanied by development of asymmetric ring current started just around the onset of the geomagnetic storm, primarily due to large values of $|B|$ and strong southward B_z. A prominent northward swing of B_z some time between 13:00 and 14:00 UT (gap in data forbids definition of the time of transition, see Fig.4.8) triggered the decay of the substorm as well as the asymmetric ring current.

(b) The presence of a strong northward B_z from about 14:30 UT delayed the onset of the storm main phase till about 20:00 UT when it was seen accompanied by significant enhancement of substorm activity and of asymmetric ring current development. It is interesting to note that the beginning of the cloud proper and onset of the storm main phase are practically coincident. The recovery phase of the storm began around 03:00 UT on 14 January, but AE and ASY continued to be high for more than 5 h after its onset.

(c) A high-time resolution study of the ring current injection rate (Ui) showed it to be discontinuous with large positive and negative impulses in the first few hours of

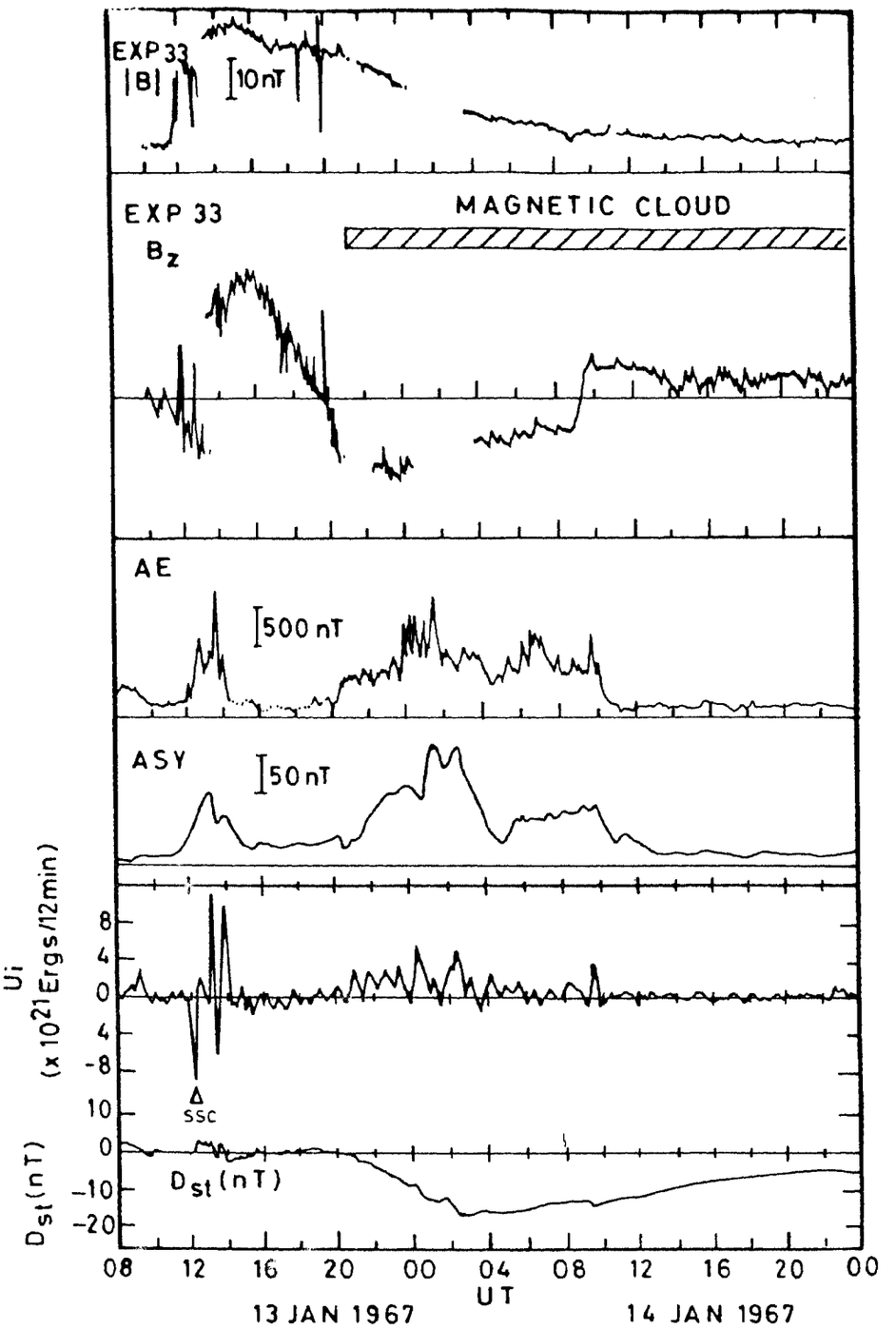

Fig 4.8 : Time histories of IMF $|B|$, Bz and geomagnetic indices AE, ASY (Low-latitude asymmetry index). Dst and ring current injection rate (Ui) over the period 08:00 UT 13 January 1967 to 00:00 UT 15 Jan 1967. The composite plot, adopted from Perrault and Akasofu (1978), illustrates the geomagnetic response to the transit of an interplanetary magnetic cloud (negative cloud with shock association) during the period. Note the occurrence of an isolated substorm accompanied by asymmetric ring current development just after the storm sudden commencement (SSC) at 12:02 UT. The duration of the cloud is indicated by the hatched rectangle.

the initial phase and three major injections during the development of the main phase (see bottom panels of Fig.4.8). It is worth noting here that in this storm, although substorm activity as a whole is grossly correlated with periods of southward B_z, the occurrence of individual substorms, especially in the storm main phase (i.e. during the transit of the front portion of the cloud), did not bear a direct relationship either to B_z or to ring current injections.

4.2.2 Transient disturbance in the F-region

Disturbance in F-region height and vertical drift near dip equator during initial phase of the geomagnetic storm :

Scrutiny of data scaled from quarter-hourly ionograms of Kodaikanal (10.2°N, 76.5°E, dip 3°N) revealed the occurrence of a prominent short-duration disturbance in F-region height just after the storm sudden commencement (SSC) at 12:02 UT (17:02 LT) i.e. in the early part of storm initial phase on January 13, 1967. The evidence for the F-region height disturbance is presented in Fig.4.9, which shows the variation of the minimum virtual height of F-region ($h'F$) at Kodaikanal for the interval 17:00-00:00 LT (12:00-19:00 UT) on 13 January, with the monthly median pattern (dashed curve) superposed for reference (median pattern of $h'F$ is based on 30 min interval data). Also shown in Fig.4.9 are the time histories (hourly values) of the equatorial D_{st} index, auroral electrojet indices (AU/AL), IMF B_z (GSM, geocentric solar magnetospheric coordinates) and B for the period 07:00-19:00 UT (12:00-00:00 LT) taken from various published data sources. These low-time resolution data show the basic characteristic of the storm initial phase (evident in the high-time resolution profiles of the parameters shown in Fig.4.8), namely, the development of an auroral substorm just around the time of SSC at 12:02 UT and its decay beginning some time between 13:00 and 14:00 UT (18:00-19:00 LT) triggered by the conspicuous northward transition of B_z. The extensive measurements of F-region plasma drifts at Jicamarca (dip 2° N) established that the F-region moves upward (downward) during day-time (night-time) with reversals in direction occurring around sunset and sunrise (Fejer, 1981). During

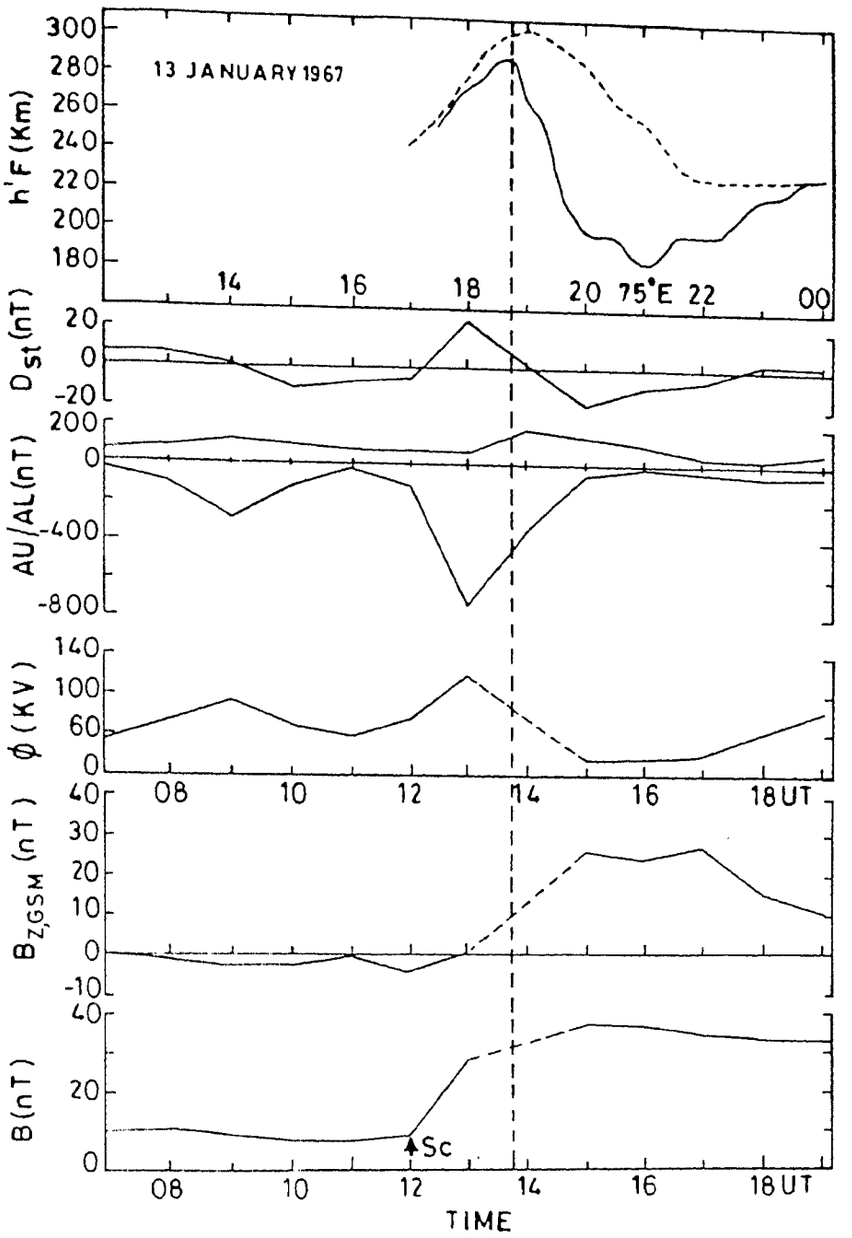

Fig 4.9 : Time variation of IMF B. Bz (GSM) AU/AL and Dst (hourly averaged values) on 13 Jan 1967 encompassing the initial phase of the sudden commencement geomagnetic storm associated with the transit of the interplanetary magnetic cloud. The variation of polar cap potential (ϕ) derived from IMF parameters is also shown. The top panel shows the variation of h'F at Kodaikanal (dip 3°N) on Jan 1967 with the monthly median pattern (dashed curve) superposed to serve as reference. The time resolution is 30 min for the median and 15 min for January 13. Note the anomalous and rapid decrease of h'F beginning at 18:45 LT (13:45 UT) in the recovery phase of substorm and its temporal association with the prominent northward swing of Bz and decrease in ϕ.

periods of moderate and high solar activity, the day-time upward V_z undergoes a short-lived enhancement after sunset before reversing to downward direction (Fejer et al., 1989 and references therein). The post-sunset enhancement in V_z is widely considered to be due to F-region dynamo electric fields, the generation of which depends on several factors such as F-region zonal wind, ratio of conductivity in E and F-regions, the separation of geographic and dip equators (Farley et al., 1986; Batista et al., 1986; Goel et al., 1990). This commonly noticeable feature in V_z manifest in ionosonde data as a conspicuous post-sunset increase in $h'F$ (the minimum virtual height of F-region that is widely taken to represent the height of bottomside F-region during night-time) in a narrow latitudinal belt around the dip equator (e.g. Rao, 1963a). The monthly median pattern of $h'F$ at Kodaikanal, in particular that of its time derivative $[d(h'F)/dt]$, which is proportional to V_z, shown in Figs.4.9 (top panel) and 4.10 respectively, reflect the typical behaviour of V_z for the prevailing level of solar activity (median value of 10.7 cm flux for January 1967 was 143 units) namely, an increase in upward drift during post-sunset hours and downward drift there after in the night. The time variation of $[d(h'F)/dt]$ displayed in Figure 4.10 shows that in general, maximum upward/downward V_z of $\sim 11\,ms^{-1}$ is reached in the intervals 17:45-18:45 LT and 20:15-21:15 LT respectively. It is to be stressed here that though $[d(h'F)/dt]$ near the dip equator provides valuable information on V_z, reliable data of V_z can be obtained only when $h'F \geq 300$ km because of the dominance of the chemical loss at lower altitudes in the F-region (Bittencourt and Abdu, 1981; Batista et al., 1986). The monthly median values of V_z taken as $[d(h'F)/dt]$ mentioned above, therefore, represent only apparent values because $h'F$ was $\leq$300 km for a substantial part of the pre-midnight period in January 1967.

After the sudden commencement of the geomagnetic storm at 12:02 UT on January 13, h'F at Kodaikanal more or less followed the median pattern of an increase till 18:45 LT (13:45 UT), indicating the prevalence of the usual upward V_z. (see Figs.4.9 and 4.10). But, starting at 18:45 LT, the F-region experienced an anomalous and sudden reduction in height such that $h'F$ decreased from 290 km at 18:45 LT to 200 km at 20:00 LT., i.e. a decrease of 90 km in 75 min or a gross apparent downward drift

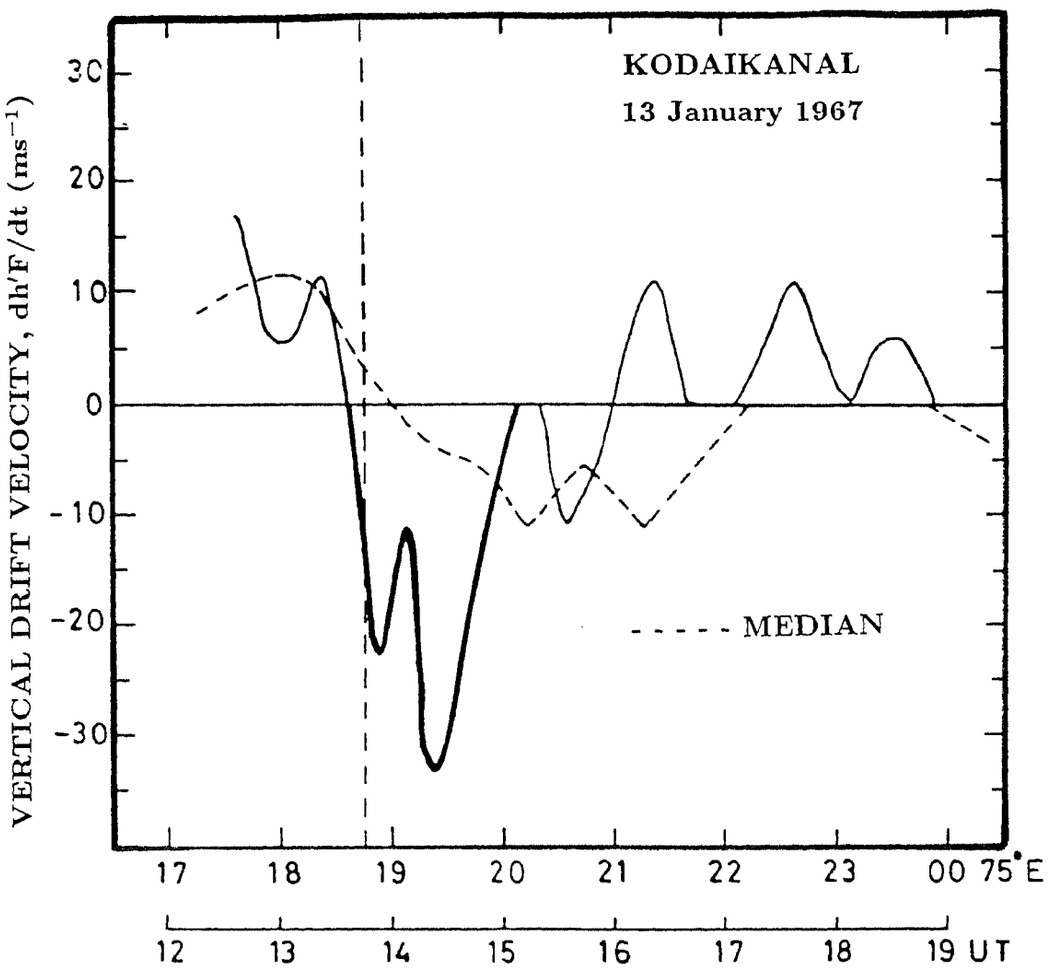

Fig 4.10 : Vertical plasma drift velocity derived from 15 min interval h'F data during the pre-midnight period on Jan 1967. The monthly median values (30 min interval) are also shown for reference. The vertical dashed line indicates the time of onset of the conspicuous reduction in h'F (Fig 4.9) and the heavy line represents the corresponding disturbance in vertical drift velocity.

velocity of 17.8 ms^{-1}. This behaviour is in sharp contrast to the general pattern of an increase in $h'F$ till 19:00 LT and relatively slower decrease there after with maximum apparent upward/downward drifts of ~11 ms^{-1} as mentioned earlier. The temporal profile of apparent V_z presented in Fig.4.10 in fact shows the presence of downward drifts of 11-33 ms^{-1} during the interval 18:45-19:45 LT, while the median values are $< 5ms^{-1}$. The height disturbance began to decay from about 21:00 LT with $h'F$ slowly recovering to the median values by local midnight. Profiles of the height distribution of electron density (N_e-h) derived from ionograms (discussed in detail later in this chapter) showed that the abnormal decrease in height prevailed not only on the bottomside but at all levels in the F-region up to the peak, and such in-phase changes throughout the F-region indicate a downward movement as a whole of the F-layer. These observations constitute unambiguous evidence for a transient disturbance in vertical plasma drift and hence in the East-West electric field that causes it (abnormal downward drift or westward electric fields) during the post-sunset period on January 13. This conclusion stems from the well-known facts and they are :

(1) Vertical plasma diffusion due to the plasma density gradient and the gravitational acceleration are very ineffective near the dip equator. During night-time at 250 km, for example, the velocity due to plasma pressure gradients is 4 cm s^{-1}, while the force of gravity (at 2° dip lat.) produces a diffusion velocity of 0.75 ms^{-1} (Anderson and Rusch, 1980)

(2) Vertical transport of plasma due to large-scale winds is also usually ineffective [the vertical component of plasma drift induced by North-South wind, U in the magnetic meridional plane, is $U\sin(I)\cos(I)$ where I is the dip angle (Rishbeth and Garriott, 1969)].

Vertical $E \times B$ drift induced by the zonal electric field is thus the most important plasma transport process in the vicinity of the geomagnetic equator. It is to be recalled that the values of downward V_z derived from the time rate of change of $h'F$ (Fig.4.10) represent underestimates because, for altitudes below 300 km, the height increase due to chemical loss (βN_e) counteracts the height decrease caused by the westward electric

field. The veracity of this physical situation has been established from theoretical studies (Bittencourt and Abdu, 1981) as well as from comparison of direct measurements of V_z with the incoherent scatter radar, with those estimated from ionosonde $h'F$ data (Batista et al., 1986). Moreover, the very fact that apparent downward V_z of 11-33 ms^{-1} prevailed when $h'F$ was in the range 200-275 km (during the interval 19:00-20:00 LT, see Figs.4.9 and 4.10) indicates the presence of strong westward electric fields. To arrive at the magnitude of the transient westward electric field perturbation, the estimates of downward V_z are corrected for chemical loss, $V_\beta = \beta L$, where β is the chemical loss rate coefficient and $L\left[= \left\{(dN/dz)/N\right\}^{-1}\right]$ is the electron density scale length. β is calculated from MSIS-86 thermospheric model (Hedin, 1987) derived values of neutral composition for the relevant geophysical conditions, local times, using the expression of Titheridge and Buonsanto (1983) which is valid for Tn in the range 750-1300K, as is found to be the case. The values of L for the relevant times are evaluated from the true height profiles of electron density ($N_e - h$) profiles derived from the ionograms. The corrected values of V_z, i.e. $[d(h'F)/dt - V_\beta]$ showed that the maximum amplitude of the westward electric field perturbation during 18:45-20:00 LT was ~1.9 mV m^{-1}.

Global nature of the substorm :

It is interesting to note that the onset at 18:45 LT (13:45 UT) of the perturbation in F-region height at Kodaikanal occurred during the decay of the auroral westward electrojet (AL index) as well as of the asymmetric ring current (ASY index). This feature can be seen from Fig.4.9 where the time of beginning of the rapid decrease in $h'F$ is indicated by the vertical dashed line. Magnetograms of several high-latitude stations have been examined to assess the spatial extent of the auroral substorm and to substantiate the temporal association of the height disturbance at Kodaikanal with its recovery phase. The magnetogram data showed the substorm signature (bay disturbance) at auroral latitude stations widely separated in longitude, implying the near-global nature of the substorm, that prevailed in the initial phase of the geomagnetic storm associated with the interplanetary magnetic cloud. This can be seen from the geomagnetic field (H-comp) variations observed at Thule (67° N, 291° E), College (64.9° N, 212° E), Cape

Chelyuskin (77.7° N, 104° E) and Heiss Island (80.6° N, 58° E) over the interval 10:00-16:00 UT on January 13, 1967 reproduced in Fig.4.11 to a common time scale. During 12:00-14:15 UT College in the early morning sector and Thule in the morning sector show in particular the presence of a bay disturbance with a well-defined start and end. It is quite evident from Fig.4.11 that the onset of the perturbation in F-region height (indicated by the vertical dashed line in Fig.4.11) corresponds to the recovery phase of the bay disturbance. The height disturbance also bears a temporal relationship to the prominent northward swing in B_z as well as a decrease (by 85 kV) in the polar cap potential drop ϕ, as may be seen from the middle panels of Fig.4.9. ϕ is determined from IMF data using the empirical formula of Reiff and Luhmann (1986).

F-region electron density distribution :

The quarter-hourly ionograms at Kodaikanal for January 13, 1967 are reduced using the POLAN program developed by Titheridge (1985) to obtain real height profiles of electron density (N_e-h) in the bottomside F-region. The (N_e-h) profile data not only confirmed the abnormal and sudden decrease in F-region height in the pre-midnight period, but also revealed the occurrence of marked changes in the electron density distribution associated with it. Figures 4.12-4.14 drawn to the same scales depict (N_e-h) profiles before the onset of the transient height disturbance at 18:45 LT (17:00-18:45 LT); during its development (18:45-20:30 LT) and in its decay phase (20:30-22:00 LT) respectively. Plots of isodensity contours in the height-time domain and profiles of electron density variations with time at specific heights, as derived from the data of Figs. 4.12-4.14, are displayed in Figs. 4.15 and 4.16 respectively. This is done to provide an overview of the changes in F-region height and electron density during the premidnight period on January 13, 1967, and to bring out clearly some of the characteristics of the transient disturbance.

(N_e-h) profile data presented in Fig.4.12 show that before the onset of the disturbance, the F-region over Kodaikanal exhibited the typical post-sunset behaviour, namely, a vertical uplift of the entire F-region due to an enhancement of the eastward electric field, accompanied by a reduction in electron density. During the interval

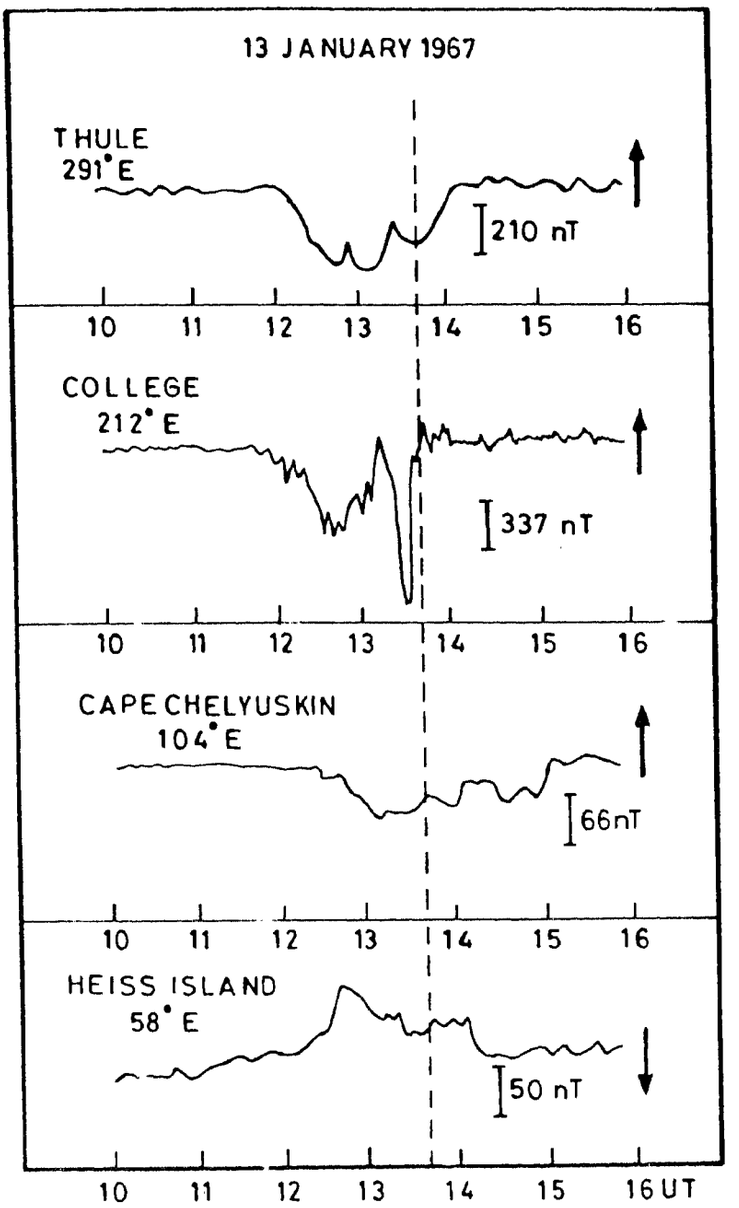

Fig 4.11 : Common scale magnetograms of high-latitude stations, Thule (77.5°N, 291°E), College (65°N, 212°E), Cape Chelyuskin (77.7°N, 104°E) and Heiss Island (80.6°N, 58°E) for the period 10:00-16:00 UT on January 13, 1967. The vertical dashed line indicates the time of onset of the disturbance in F region height and vertical drift velocity at Kodaikanal. Note the occurrence of the F region disturbance during the recovery phase of the auroral bay disturbance (substorm).

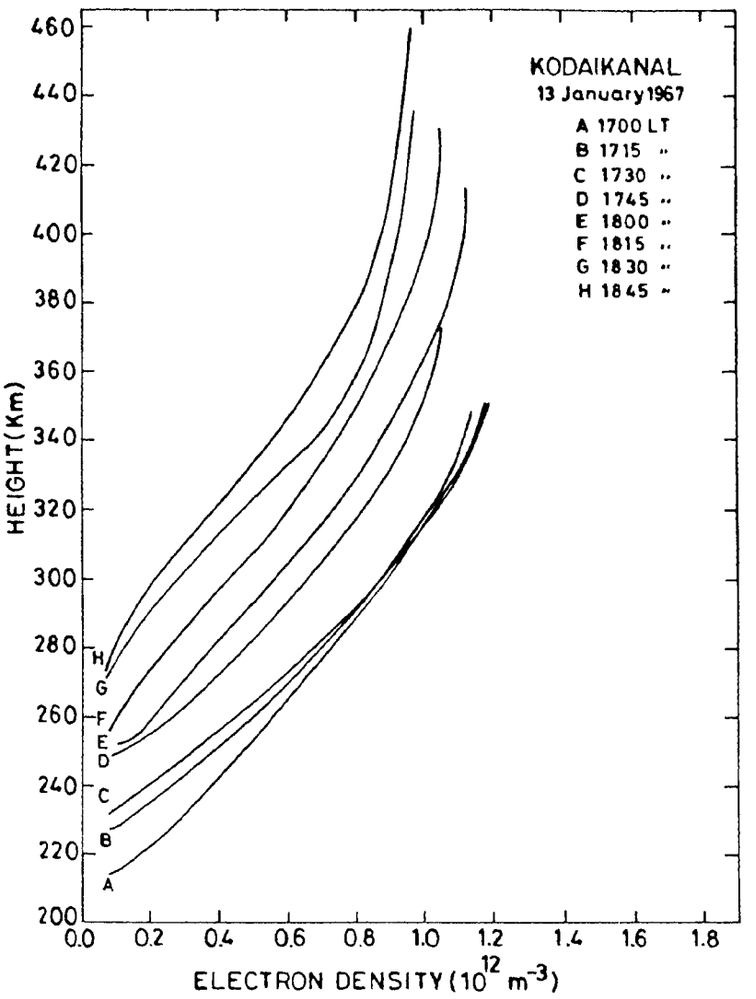

Fig 4.12 : Height profiles of electron density (Ne) in bottomside F region derived from ionograms of Kodaikanal (Dip 3°N) from 17:00 to 18:45 LT on Jan 13, 1967. LT is 75° E. Note the vertical uplift of the entire F region which is a commonly noticeable feature at locations near the dip Equator during post-sunset hours due to enhanced $(E \times B)/B^2$ drift. The cloud-associated geomagnetic storm started with a sudden commencement (SC) at 12:02 UT (17:02 LT).

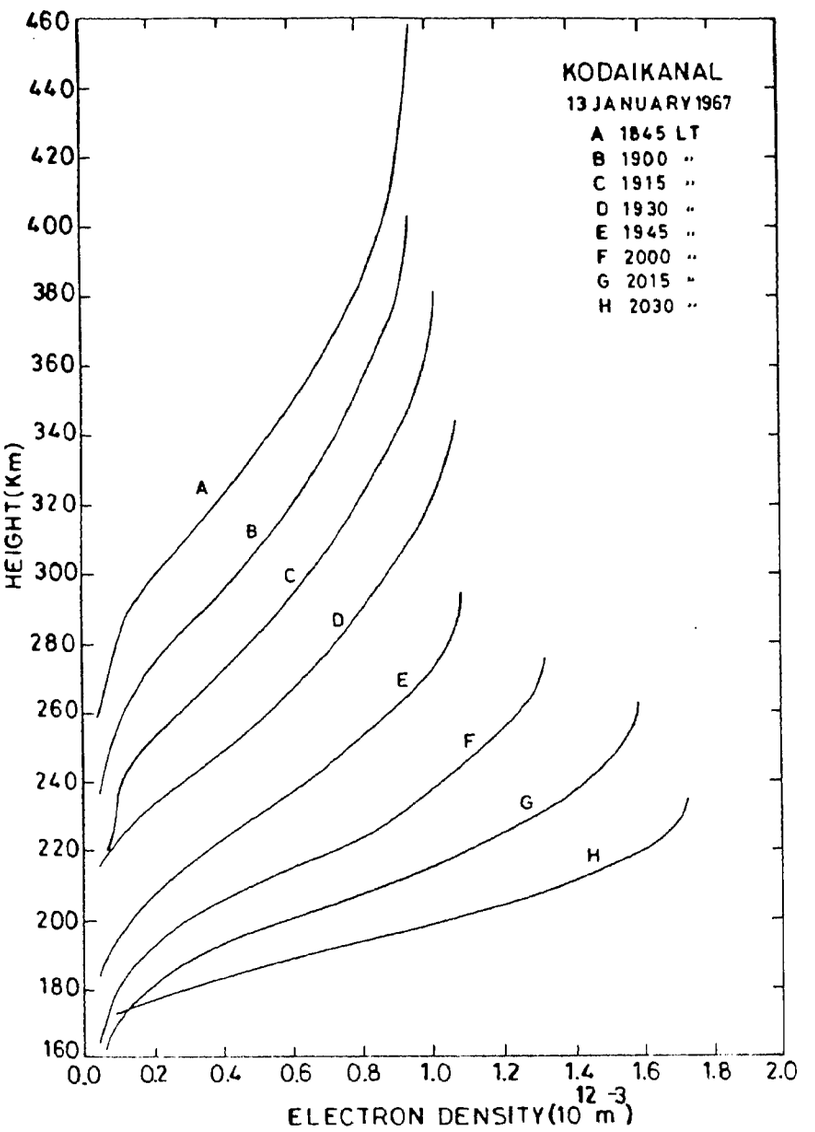

Fig 4.13 : Same as figure 4.12 but for the period 18:45-20:30 LT. Note the anomalous and rapid downward movement of the entire F-region, accompanied by enhancement of electron density.

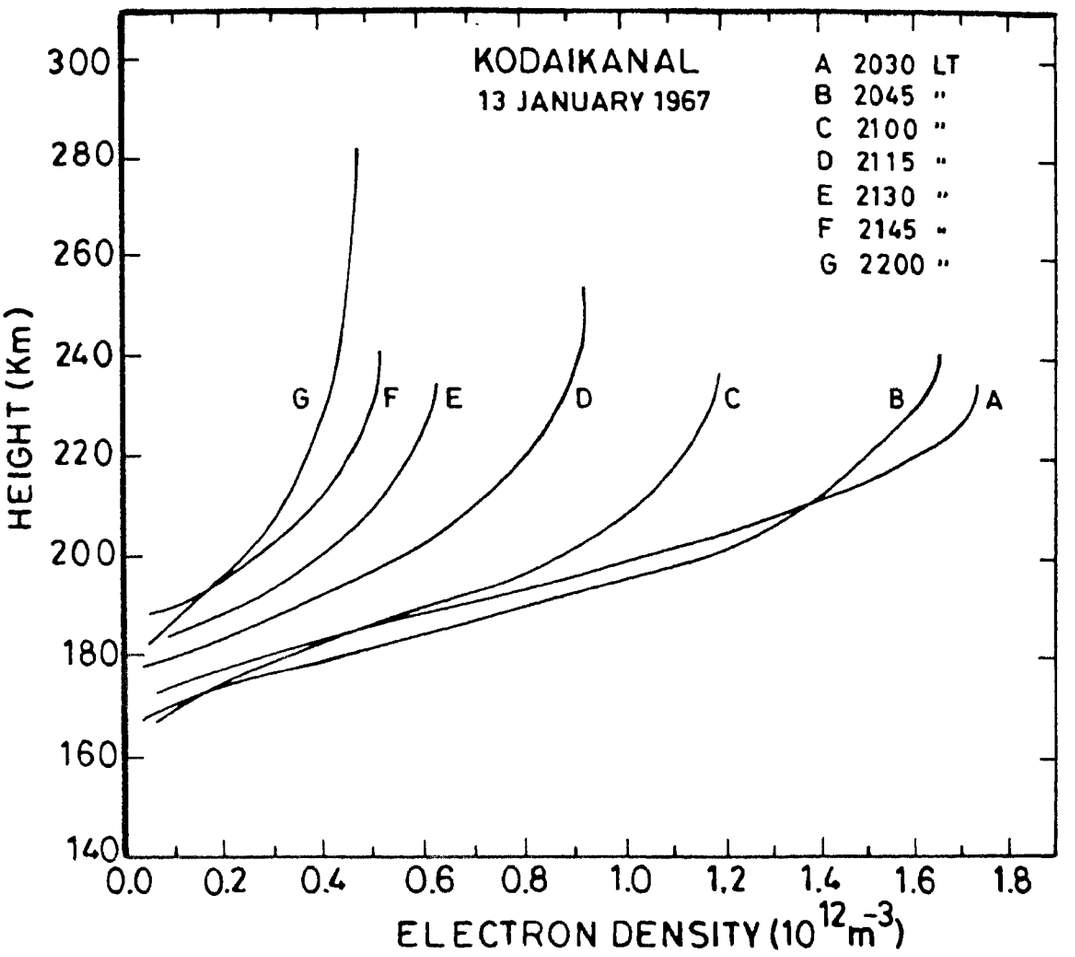

Fig 4.14 : Same as in Fig 4.12 but for the period 20:30-22:00 LT. Illustrating the decay of the F-layer when it reached altitudes <250 km.

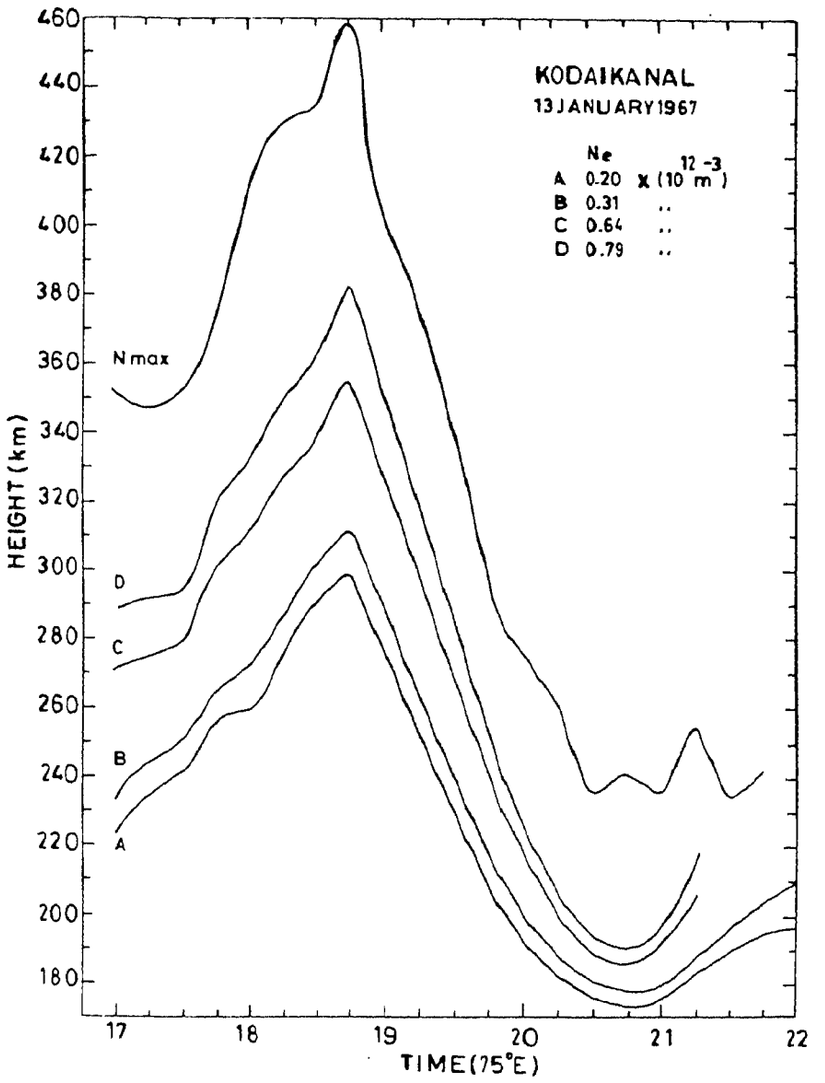

Fig 4.15 : Height versus time plots of some specified electron density values for the period 17:00-22:00 LT on January 13, 1967 as derived from (Ne-h) profiles shown in figures 4.12-4.14. Note the rapid drop in the height of isodensity contours between 18:45 and 20:30 LT.

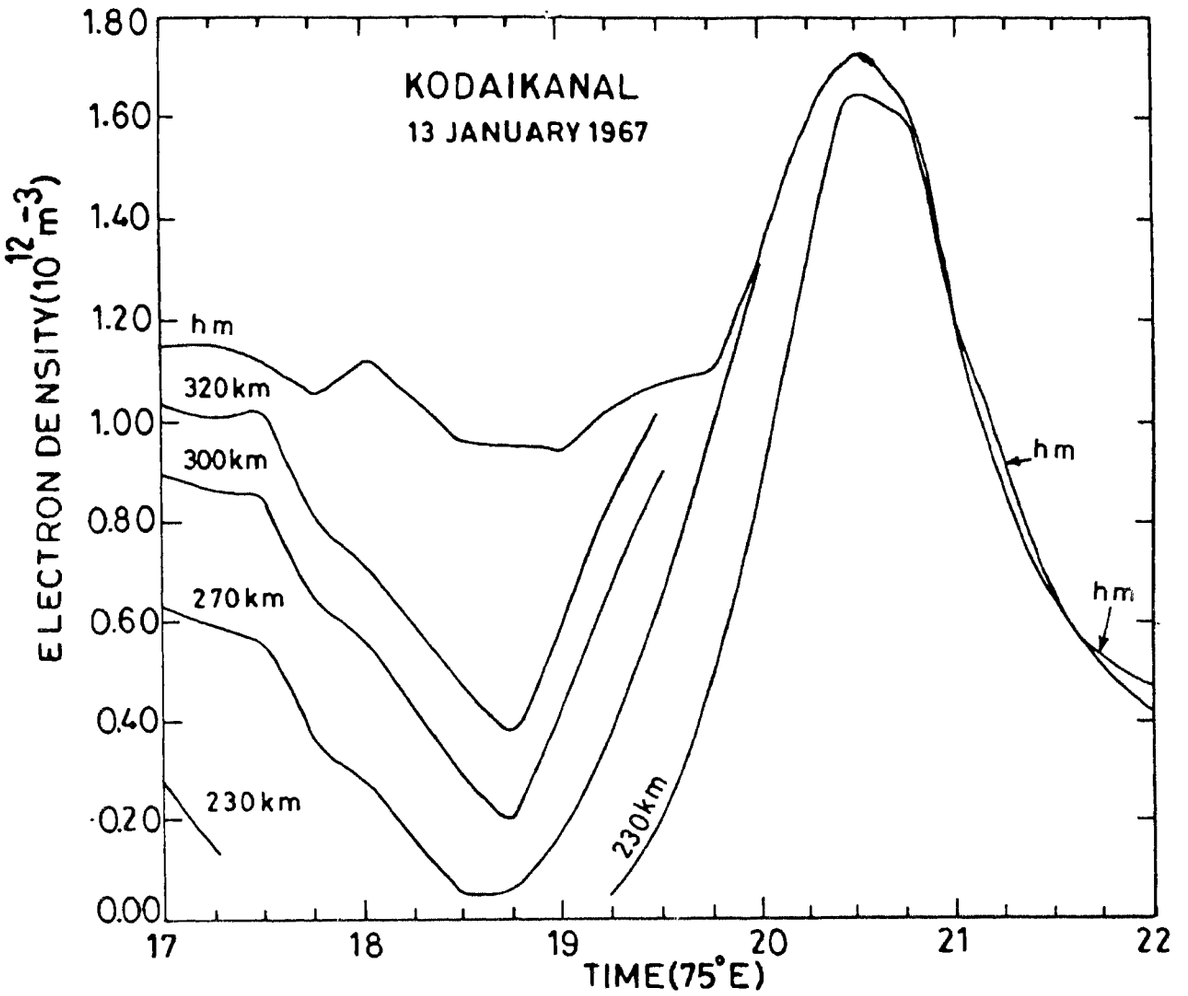

Fig 4.16 : Electron density versus time plots for some specified heights for the period 17-22 LT on Jan 13, 1967 as derived from (N-h) profile data shown in figures 4.12-4.14. Note the abnormal increase in electron density caused by the rapid downward movement of the F-region between 18:45 and 20:30 LT.

17:00-18:45 LT, the height of F-region peak (hm) increased from 351 to 458 km, while the peak electron density (Nm) decreased from $1.17 \times 10^{12} m^{-3}$ to $0.95 \times 10^{12} m^{-3}$. The change in hm corresponds to a gross apparent upward drift of 16.7 ms^{-1}. The vertical upward movement is, nevertheless, non-uniform as can be seen from the temporal profiles of $h'F$ and $[d(h'F)/dt]$ shown in Figs.4.9 and 4.10 respectively, as well as from (N_e-h) profiles shown in Fig.4.12. The decrease in Nm over Kodaikanal reflects the increased outflow of ionization from locations near the dip equator due to the enhanced electric field which, in turn, results in a post-sunset enhancement of the equatorial anomaly, a feature commonly noticed during epochs of moderate and high solar activity (e.g. Rao, 1963b; Sastri, 1982). With the onset of the disturbance at 18:45 LT, the entire F-region rapidly moved downward accompanied by enhancement of electron density at progressively lower altitudes as the perturbation developed. This conspicuous behaviour can clearly be seen in the (N_e-h) profile data displayed in Fig.4.13. In fact, hm decreased from 458 km at 18:45 LT to 235 km at 20:30 LT, i.e. a decrease of 223 km in 105 min, implying a gross apparent downward V_z of 35.4 ms^{-1}. At the same time, Nm increased approximately by a factor of 2 from $0.95 \times 10^{12} m^{-3}$ to $1.72 \times 10^{12} m^{-3}$. It is instructive to note here that although the entire F-region experienced an apparent downward movement, its magnitude displayed an obvious dependence on the electron density level. This feature can clearly be seen from the height-time plots of isodensity contours presented in Fig.4.15. During the interval 18:45-20:30 LT, while hm decreased by 223 km as mentioned earlier, the change in the height of electron density levels of 0.20, 0.31, 0.64 and $0.9 \times 10^{12} m^{-3}$ (represented by curves A-D respectively in Fig.4.15) are 123, 130, 165 and 88 km, respectively. The progressive reduction in the magnitude of height change with decreasing value of the electron density (i.e. at progressively lower altitudes in the F-region) amply demonstrates the importance of chemical loss effects at lower altitudes (<300 km). Due to the marked height variation of the chemical loss rate coefficient (β), the height increase induced by chemical loss will be small above 300 km, but will be substantial at lower altitudes, particularly in the range 200-250 km. For a given value of the westward electric field, the consequent apparent downward movement of F-layer will, therefore, decrease with decreasing altitude due to the increasing

counter-effect from chemical loss as observed.

Figure 4.16 displays the changes in electron density at selected altitudes including *hm* associated with the transient height (electric field) perturbation. Prior to the onset of the disturbance, electron density throughout the bottomside F-region showed a continuous decrease due to the normal post-sunset vertical uplift of the layer associated with the enhanced electric field. The decrease in electron density is, however, more prominent at altitudes below *hm*, due to the faster rate of recombination of ionization on the bottomside than at the layer peak. The sudden onset of the abnormally large downward drift of the F-layer characterising the electric field perturbation, caused a conspicuous increase in electron density at progressively lower altitudes as it evolved, as can be seen from the (N_e-h) profile data in Fig.4.13 and the (N_e-t) plots corresponding to fixed heights in Fig. 4.16. It is quite noteworthy that a significant increase in Nm occurred only when the F-layer peak moved below 300 km. At 230 km where the time evolution of the electron density changes due to the electric field perturbation can be seen for a major part of its manifestation, the electron density increased from $0.05 \times 10^{12} m^{-3}$ at 1915 to $1.65 \times 10^{12} m^{-3}$ at 20:30 LT, i.e. an increase by a factor of 30. In contrast Nm increased by approximately a factor of 2 as mentioned earlier. With the cessation of the height disturbance around 20:30 LT, the F-layer decayed due to the predominance of chemical loss in the altitude range 200-250 km (see Fig.4.14).

The above observations reveal a remarkable and unique response of the equatorial F-region plasma density distribution to the transient westward electric field disturbance that occurred in the pre-midnight period on January 13, 1967. The response is considered unique because the fate of the night-time F-layer near the dip equator is governed by chemical loss and plasma transport, and when the layer is below 300 km it has to decay as a rule due to enhanced chemical loss, while what is observed is exactly the opposite. This strongly suggests that the rate of ionization convergence brought about by the rapid and large downward drift of the plasma far exceeded the chemical loss (βN_e) rate at altitudes below 300 km, to produce the evident increase in electron density at and below the F-layer peak. A semi-quantitative treatment of this interesting

physical situation is given in the next section. The occurrence of the prominent westward electric field disturbance during the post-sunset period on January 13, 1967 may be expected to modify the behaviour of the equatorial anomaly because, the normal post-sunset increase of the eastward electric field leads to a corresponding enhancement of the anomaly through a renewal of the *fountain effect* (e.g. Sastri 1982). However, this anticipated response in the anomaly could not be assessed due to non-availability of 15 min interval ionosonde data from higher latitude stations in the Indian sector. Study of the published low-time resolution data (hourly values), nevertheless, indicated the presence of a trend of a change in the anomaly on the expected lines. The monthly median values of the depth of the anomaly, R (defined as the ratio of electron density at the crest of the anomaly to that at the trough), are 1.26, 1.07, 1.35 and 1.17 from 18:00 LT, through 21:00 LT, respectively. R is evaluated from foF_2 data of Ahmedabad (dip 34° N, around the crest) and Kodaikanal (dip 3° N, in the trough region). The median values of R indicate the post-sunset increase in general, of the anomaly depth due to strengthening of the *fountain effect* by the pre-reversal enhancement of eastward electric field around (the anomaly responds to changes in zonal electric field with a delay of ~2 h due to the time needed for ionization lifted upward at and around the dip equator to get meridionally transported to higher latitudes). The values of R at 18:00, 19:00 and 21:00 LT on January 13 were 1.11, 1.07 and 0.86 respectively (foF_2 values of Ahmedabad at 20:00 and 22:00 LT are not available). The decrease of R from 19:00 LT to 21:00 LT instead of the normal increase and the low value of R at 21:00 LT (lower by 26% than the median value) hint at a weakening of the anomaly, due to the westward electric field perturbation that set in at 18:45 LT.

4.2.2.1 Discussion

The present study shows that, during the initial phase of the sudden commencement geomagnetic storm associated with the passage of the interplanetary magnetic cloud of January 13-15, 1967, a prominent transient disturbance in zonal electric field prevailed near the dip equator in the dusk-midnight sector. The electric field distur-

bance manifested as a sudden and abnormal reduction in height of the entire bottomside F-region for a short duration (18:45-20:00 LT), in temporal coincidence with the decay phase of an auroral sub-storm and asymmetric ring current that developed at the onset of the geomagnetic storm. The decay of the substorm as well as the asymmetric ring current is apparently triggered by a conspicuous northward swing of IMF B_z and bears a close temporal association with a decrease in polar cap potential estimated from IMF parameters. The values of vertical drift velocities estimated from the time rate of change of $h'F$ and corrected for chemical loss effects $[d(h'F)dt - V_\beta]$ showed that the maximum amplitude of the electric field disturbance (westward) is $\sim 1.9 mVm^{-1}$. The perturbation in F-region height was accompanied by significant short-term changes in the height distribution of F-region electron density. The highlight of these changes was the increase in electron density at and below the F-layer peak when the layer moved below 300 km, at which altitudes the decay of the layer is the rule due to the predominance of chemical loss (βN). The entire sequence of a large downward movement of the layer accompanied by an increase in electron density manifested over a time span of just about 2 h (18:45-20:00 LT).

It is known that large enhancements of electric fields and conductivities in the auroral dynamo region originating in magnetospheric substorms, are responsible for the intensification of auroral electrojet currents that characterise the geomagnetic substorm or bay disturbance (Banks et al., 1973; Brekke et al., 1974; Kamide and Richmond, 1986). The substorm- related auroral electric fields, in turn, penetrate instantaneously to middle, low and equatorial latitudes through the earth- ionosphere wave guide (e.g., Kikuchi et al., 1978). The problem of prompt penetration of magnetospherically generated electric fields into the sub- auroral ionosphere has been extensively studied in recent times by several researchers (e.g. Nisbet et al., 1978; Nopper and Carovillano, 1978; Kamide and Matsushita, 1981; Senior and Blanc, 1984, 1987; Spiro et al., 1988; Zamay, 1989) with the convection model approach introduced by Vasyliunas (1970). The semi- analytical model of Senior and Blanc (1984) and the numerical model of Spiro et al. (1988) represent fairly realistic global convection models, as they treat the

process of electric field penetration in a comprehensive manner by considering magnetosphere- ionosphere as a coupled system, and paying attention to the various processes operative in it. The basic inputs to these models are the step- like changes in the polar cap potential drop (ϕ) representing those in the IMF B_z. These models predict essentially the same pattern for the plasmaspheric electric fields, and have been fairly successful in explaining the basic characteristics of transient electric field disturbances (diurnal pattern of polarity and amplitude, latitudinal variation, etc.) observed at sub-auroral latitudes in association with sudden changes in B_z and substorm activity (e.g. Fejer et al., 1990 a, b). The models predict that with a decrease in convection (decrease in polar cap potential drop, ϕ) transient westward electric fields occur at equatorial latitudes in the dusk- midnight section- relevant to the observations presented here (Senior and Blanc, 1984; Spiro et al., 1988: Fejer et al., 1990b). The unambiguous short-duration westward electric field perturbation observed at Kodaikanal in the post-sunset period (18:45-20:30 LT) on January 13, in the recovery phase of the auroral substorm and around the time of a conspicuous northward swing of B_z and decrease of polar cap potential (see Fig. 4.9) thus finds a logical interpretation in terms of low-latitude penetration of substorm-associated high- latitude electric fields. It is to be emphasized that the electric field disturbance dealt with here constitutes an important addition to the current empirical knowledge of penetration electric fields at equatorial latitudes, because the observations available to date indicate that transient equatorial electric field disturbances (eastward) manifest predominantly and with large amplitudes in the midnight-dawn sector in association with sudden decreases in magnetospheric convection (Fejer et al., 1991a, b). This pattern, which is an established feature of the daily variation of perturbation electric fields, is in fact well predicted by the models. But the models also indicate that transient westward electric fields ought to prevail at equatorial latitudes in the 18:00-21:00 LT sector in association with sudden decrease in magnetospheric convection. But explicit observational evidence has not been shown so far. The results of the present study, therefore, validate, the predictions of the global convection models as regards the polarity of the perturbations in equatorial zonal electric field due to decrease in magnetospheric convection for the dusk- midnight sector also.

The duration and amplitude of the disturbance electric fields observed on January 13 do not, however, seem to agree with the models. For example, the recent modeling results of Fejer et al.(1990b) show that the westward electric field perturbation at 15° latitude produced by a decrease in the polar cap potential(ϕ), by 70 kV completely decays in less than 80 min and its maximum amplitude is $\sim 0.2mVm^{-1}$. The electric field disturbance presented here is of much larger amplitude ($\sim 1.9mVm^{-1}$) and persisted for a longer time (105 min) though it is associated with a decrease in ϕ of the same order by $84kV$ (see Fig.4.9). That the current convection models cannot fully account for the persistence (typical duration, 2h) of the transient zonal electric field perturbations associated with decreases in magnetospheric convection is now well realized. The discrepancy in the details of the predicted and observed characteristics of the transient electric field disturbance reaffirms the prevailing view that though the process of low- latitude penetration of magnetospherically generated electric fields is understood, comprehension of physical processes that control the magnitude and duration of the perturbation is at a nascent stage (Fejer et al., 1990b). It is to be noted that thermospheric winds and waves cannot explain the abnormal descent of post- sunset F-region observed at Kodaikanal (dip 3° N) on January 13, 1967. Substorm generated wind and wave disturbances being equatorward will increase the height of F-layer in the northern hemisphere rather than decrease it. Currently available experimental data on meridional winds indicate that at equatorial latitudes and in local winter months, the day-time poleward winds, in general turn equatorward around 21:00 LT, reach maximum amplitude around 22:00 LT, followed by an abatement around midnight before finally becoming poleward in the early morning hours (see Fig. 3.14 in chapter 3). Since the meridional winds are poleward in the post- sunset hours and exhibit considerable day- to- day variability, the observed F-region descent at Kodaikanal could, in principle, be due to wind effects. This nevertheless is very unlikely because the wind velocities required to cause a downward movement of F-region peak by 15-55 ms^{-1} at Kodaikanal (see Table 4.1) are in the unrealistic range of 287-1052 ms^{-1}. The increase in electron density at and below the F-layer peak that accompanied the rapid and spectacular downward motion of the layer in the post-sunset hours at Kodaikanal on January 13, 1967 is a unique feature

Table 4.1

Vertical drift velocity of F-region peak required for an increase in Nm at Kodaikanal according to theory (Tan, 1982) and observed during the pre-midnight disturbance on Jan 13, 1967.

Time interval (LT)	hm (km)	Drift velocity required (ms^{-1})	Drift velocity observed (ms^{-1})
19:00 - 19:15	393	−00.6	−25.2
19:15 - 19:30	363	−01.3	−41.4
19:30 - 19:45	320	−03.6	−55.7
19:45 - 20:00	285	−09.6	−20.8
20:00 - 20:15	269	−14.6	−14.1
20:15 - 20:30	249	−26.4	−31.6

of the transient response of equatorial ionosphere to the geomagnetic storm associated with the interplanetary magnetic cloud. Reports of such fast and prominent changes in the height distribution of F-region plasma density are quite uncommon in the literature. In fact, there is only one event in the extensive published work on equatorial F-region morphology that is similar in nature to the one presented in the present study. The lone earlier observation refers to the increase in Nm on the night of February 2-3, 1965 at Jicamarca (dip 2°N) when the F-layer experienced significant downward movement over the period 23:25-03:23 LT. ($Ne-h$) profiles derived from the incoherent scatter technique indeed show a remarkable downward motion of the layer in the period 00:16-01:50 LT, when the height of F-layer peak (hm) dipped by 131 km implying an apparent downward velocity at the peak of $23.4ms^{-1}$. Nm increased in this interval from $\sim 1.1 \times 10^{11}m^{-3}$ to $1.3 \times 10^{11}m^{-3}$, i.e. by a factor of 1.18 without any appreciable change in the shape of the layer. This observation was analysed by Tan (1982) from the viewpoint of providing a theoretical explanation. From a study of the continuity equation of nocturnal F-region plasma density (0^+) at the dip equator, he found that an increase in Nm occurs in a limited altitude range above 250 km if a sufficiently large downward drift prevails such that the compression of the plasma induced by the drift overcomes the chemical loss rate (βNe). The condition derived by him for an increase in Nm to occur is $V_z < \frac{-\beta\gamma}{6}$ where V_z is the drift velocity, γ is the radial coordinate and β is the loss coefficient. The theoretical condition was found to apply well for the changes observed in $(Ne-h)$ profiles at Jicamarca during the post-midnight period of February 2-3, 1965 (Tan, 1982).

It is obvious from the above discussion that the basic characteristics of the transient F- region disturbance manifest at Kodaikanal during the initial phase of the geomagnetic storm are similar to those observed earlier at Jicamarca. There are, however, noteworthy differences between the two events. They are :

(1) The disturbance at Kodaikanal displayed a temporal association with the decay phase of a sub-storm as well as asymmetric ring current and also appropriate changes in B_z and polar cap potential drop ϕ. The disturbance is thus of geomagnetic

sub-storm origin as detailed earlier. The large downward motion of F-layer at Jicamarca on the night of February 2-3, 1965, on the other hand, occurred under very quiet geomagnetic conditions. *Ap* values for 2 and 3 February 1965 are 2 and 5, respectively, and the *AE* index varied in the range 16-56 nT on the night of February 2-3, 1965 at Jicamarca (18:06 LT/23:11 UT).

(2) The magnitudes of the apparent downward drift of F-layer peak and the increase in Nm were higher for the pre-midnight disturbance observed at Kodaikanal as compared to the post-midnight event at Jicamarca. The physical mechanism underlying the increase in Nm, nevertheless, ought to be the same for the two events. Therefore it is examined that the validity of the altitude-dependent condition derived by Tan (1982) by evaluating the relevant parameters (β and hence the drift velocity required for an increase in Nm according to the theoretical condition; drift velocity implied by the observed changes in hm when Nm increased in the interval 19:00-20:30 LT; see Fig.4.13). The results given in Table 4.1 clearly show that the theoretical condition holds good in the altitude range 250-395 km, confirming that the increase in Nm is due to the ionization convergence rate exceeding the βNe loss rate, when the layer as a whole experienced a large downward drift due to the penetration of substorm related electric fields into the equatorial ionosphere.

4.2.3 Persistent Disturbance in the F-Region

Studies of prominent and persistent disturbances in equatorial ionosphere which prevailed during the main and recovery phases of the geomagnetic storm associated with the cloud passage are presented in this section.

Data :

Published data from a number of ground based ionosonde and magnetometer stations in the Indian (75°E) and Japanese (135° E) sectors are used to derive and study the response pattern of the ionospheric characteristics to the cloud passage. The details of the stations are listed in Table 4.2. Out of the two magnetometer stations

Table 4.2

Ionosonde stations

Station(symbol)	Geographic Latitude	Geographic Longitude	Dip
Tomsk(TK)	56°28′N	84°56′E	75.4°N
Alma-Ata(AL)	45°15′N	76°55′E	69.9°N
Wakkanai(WK)	45°24′N	141°41′E	59.4°N
Delhi(DL)	28°38′N	77°13′E	42.4°N
Ahmedabad(AH)	23°01′N	72°37′E	34.0°N
Haringhata(HA)	22°58′N	88°34′E	32.0°N
Hyderabad(HD)	17°21′N	78°28′E	21.5°N
Tiruchirapalli(TI)	10°49′N	78°42′E	4.8°N
Kodaikanal(KD)	10°14′N	77°29′E	3.0°N
Trivandrum(TR)	8°29′N	76°57′E	0.6°S

Magnetometer stations

Station	Geographic Latitude	Geographic Longitude	Dip
Alibag	18°38′N	72°52′E	
Trivandrum	08°29′N	76°57′E	0.6°S

in the Indian sector, Trivandrum is located close to the axis of the equatorial electrojet, while Alibag lies well outside the electrojet influence. The simultaneous H-field data from these stations is well suited and widely used to estimate the strength of the equatorial electrojet (and hence inference of the electric field that drives it) for day time conditions when ionospheric conductivity and currents are high (e.g Bhargava et al., 1980; Sastri, 1989). The parameter ΔSdI calculated following the procedure introduced by Kane (1973) is taken to represent the equatorial electrojet strength. The choice of ΔSdI is appropriate because the behaviour of the electrojet can only be studied through this parameter for disturbed geomagnetic conditions when the ground based magnetic variations receive contributions not only from over head ionospheric currents but also from distant currents associated with magnetospheric sources (Kane, 1976). The diurnal profile of equatorial electric field is then inferred by coupling the data on electrojet strength with that of h'F/hpF$_2$ from a station close to the dip equator (Kodaikanal), as the later reflect the electric field pattern during night time because of their sensitivity to the vertical E$\times$B plasma drifts especially in the post-sunset hours (Bittencourt and Abdu, 1981; Sastri, 1984; Batista et al., 1986). This approach of analysing in combination the equatorial geomagnetic and ionospheric data from a network of stations helps in detecting large amplitude electric field disturbances as is demonstrated here, and is a useful substitute for the more direct information on electric fields from VHF incoherent/coherent scatter radar measurements. The ionosonde data from the meridional network of ionosondes in the Indian (75°E) and in the Japanese (135°E) sectors are used to derive the changes in the equatorial anomaly and F-region parameters from high-midlatitudes to the dip equator. It is to be mentioned that the emphasis in this work is on assessing the response pattern of the characteristics of the equatorial ionosphere (electric field, equatorial anomaly, etc.) to the passage of the magnetic cloud and attendant severe geomagnetic storm, and the ionospheric behaviour at higher latitudes are dealt with primarily to help understand the physical processes responsible for the changes seen in the equatorial region.

Disturbance in equatorial electric field :

Careful scrutiny of the reduced data of the electrojet strength (from H-field data) and nighttime h'F/hpF$_2$ near dip equator (from original ionograms at Kodaikanal) revealed the striking presence of a large-scale disturbance in the equatorial electric field in the Indian sector, in association with the magnetic cloud passage. The evidence for this inference can be seen in Fig.4.17 wherein the diurnal profiles of the electrojet strength (ΔSdI) and the nightime pattern of h'F/hpF$_2$ at Kodaikanal for the period 13-15 January 1967 are shown, together with the time histories of the geomagnetic indices D_{st}, ASY and AE as well as IMF parameters B and B_z. The quiet day average patterns of ΔSdI and h'F/hpF$_2$ are superimposed on the individual day's profiles (solid curves in the bottom two panels of Fig.4.17) to provide a reference for comparison and to assess the response to the cloud-induced geomagnetic storm. The quiet day profile of ΔSdI demonstrates the regular build-up and decay of the electrojet strength during day time primarily due to variations in the E-region plasma density with the zenith angle, while that of h'F displays the characteristic postsunset rise which is well established to be due to an enhancement of the day-time eastward electric field before reversing direction to westward (Rishbeth, 1977). As mentioned earlier, the transit of the magnetic cloud resulted in a severe geomagnetic storm with storm sudden commencement (SSC) at 1202UT on 13 January. On 14 January corresponding to the recovery phase of the storm, the electrojet strength underwent a conspicuous reduction practically throughout day-time, when compared to adjacent days as well as the quiet day average behaviour as can clearly be seen in Fig.4.17. The suppression of the electrojet strength is such that it even led to counter-electrojet conditions (ΔSdI below the nightime level accompanied by disappearance of E_{sq} on ionograms at Kodaikanal) during the afternoon hours. The average percentage of reduction in ΔSdI around local noon (9-14LT) when compared to the average quiet day values is about 75 which is remarkable because the day-to-day variability of the electrojet electric field (and hence electrojet strength) is rather small around local noon as compared to other local time sectors such as around sunrise/sunset and afternoon hours (Fejer, 1986; Viswanathan et al., 1987). The overall reduction

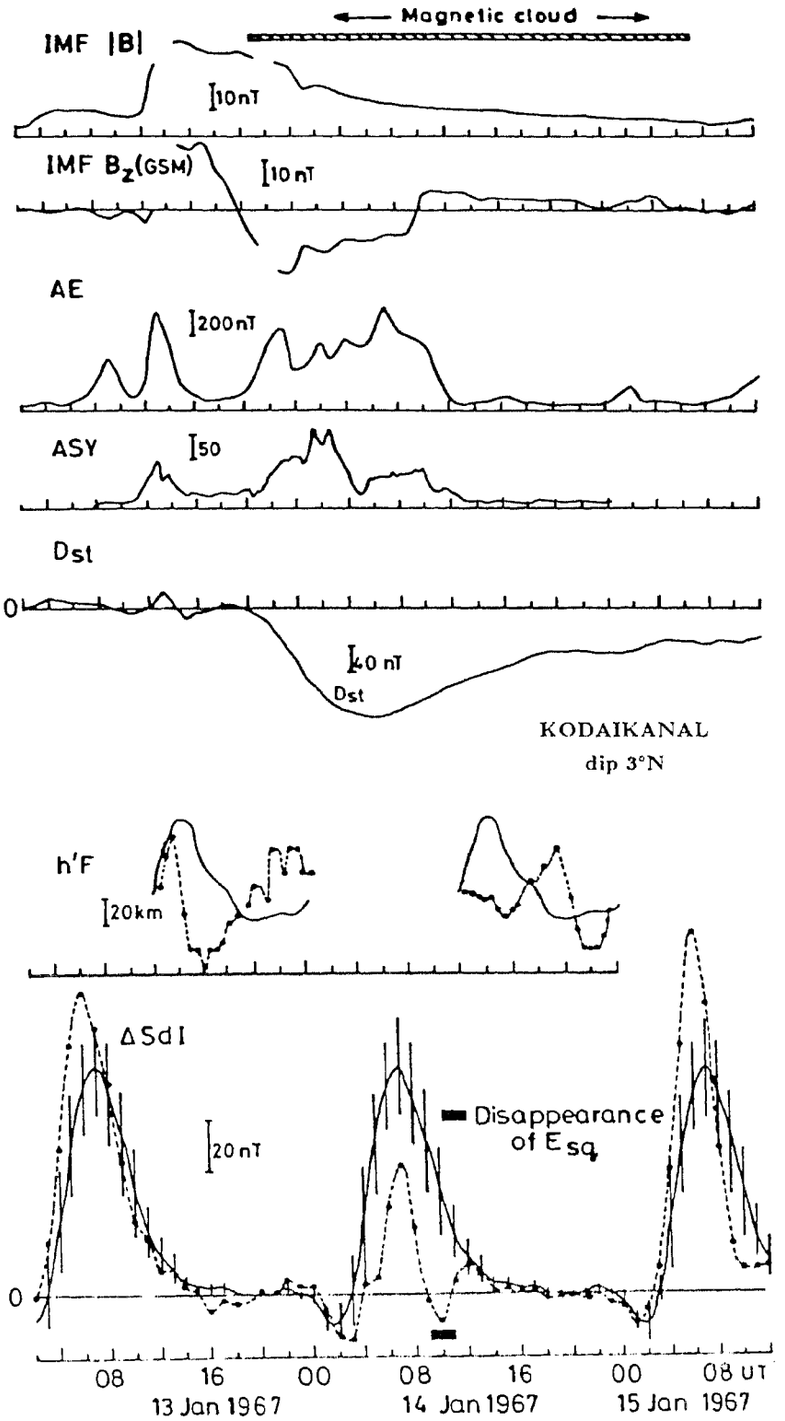

Fig. 4.17 : Temporal patterns of equatorial electrojet strength, ΔSdI (Computed from ground level H-field of Trivandrum and Alibag) and nighttime h'F/hpF$_2$ near dip equator (Kodaikanal) in the Indian (75°E) sector during the transit of a interplanetary 'negative' magnetic cloud at Earth from 13 to 15 January 1967. The solid curves in the plots of ΔSdI and h'F/hpF$_2$ represent the quiet day average patterns of the parameters. Time histories of the geomagnetic indices D_{st}, AE and the asymmetric component of ring current (ASY) as well as of IMF |B| and B_z are shown in the top panels. Note the prominent and sustained reduction in ΔSdI and the striking absence of the usual post-sunset rise in h'F/hpF$_2$ at Kodaikanal on 14 January corresponding to the recovery phase of the severe geomagnetic storm induced by the cloud passage.

in the electrojet strength during day-time on 14 January was followed by conspicuous inhibition of the normal post-sunset enhancement of h'F/hpF$_2$ at Kodaikanal and hence of the eastward electric field that drives the electrojet current during the day time. One can also observe in Fig 4.17 that in addition to the above mentioned response of equatorial ionospere, there was an unusual vertical uplift of F-layer in the pre-sunrise period (at the start of the cloud passage) and anomalous vertical uplift of F-layer for about 5 h around midnight on 14 January. While the pre-sunrise F-layer height rise and the day-time reduction in electrojet strength on 14 January manifested during the growth and decay of the ring current (D_{st}) with a significant asymmetric component, the later perturbations occurred when the ring current became symmetrical and was in the recovery phase (see Fig. 4.17). These unambigious features indicate the prevalence of a sustained disturbance in the equatorial electric field in phase opposition to the normal quite day dynamo field in the Indian sector during the disturbed conditions set up by the cloud passage.

Inhibition of equatorial Ionization Anomaly :

The equatorial ionization anomaly (EIA) which is a characteristic feature of the latitudinal distribution of F-region plasma density (foF$_2$) at equatorial latitudes, is primarily controlled by the electrojet electric field through the *fountain* mechanism as detailed in Chapter 1. A study is made on EIA behaviour on 14 January to ascertain the response of EIA to the electric field perturbations evidenced in ΔSdI and nighttime h'F/hpF$_2$. In Fig. 4.18 are shown the latitudinal profiles of foF$_2$ at different local times on 14 January in the Indian sector, with the quiet day average patterns superposed for reference. The quiet day profiles clearly show the normal day-time development of EIA beginning at 0900LT and its sustenance into the post-sunset hours with higher values of foF$_2$ around 34°dip (crest region) than near the dip equator (trough region). In contrast, the usual development of EIA was markedly inhibited during day time on 14 January. In fact, the latitudinal profile of foF$_2$ was reversed with lower values of foF$_2$ around the crest region than around the trough region as can be seen from Fig.4.18. The only exception to this behaviour is the apparent recovery of the EIA signature at

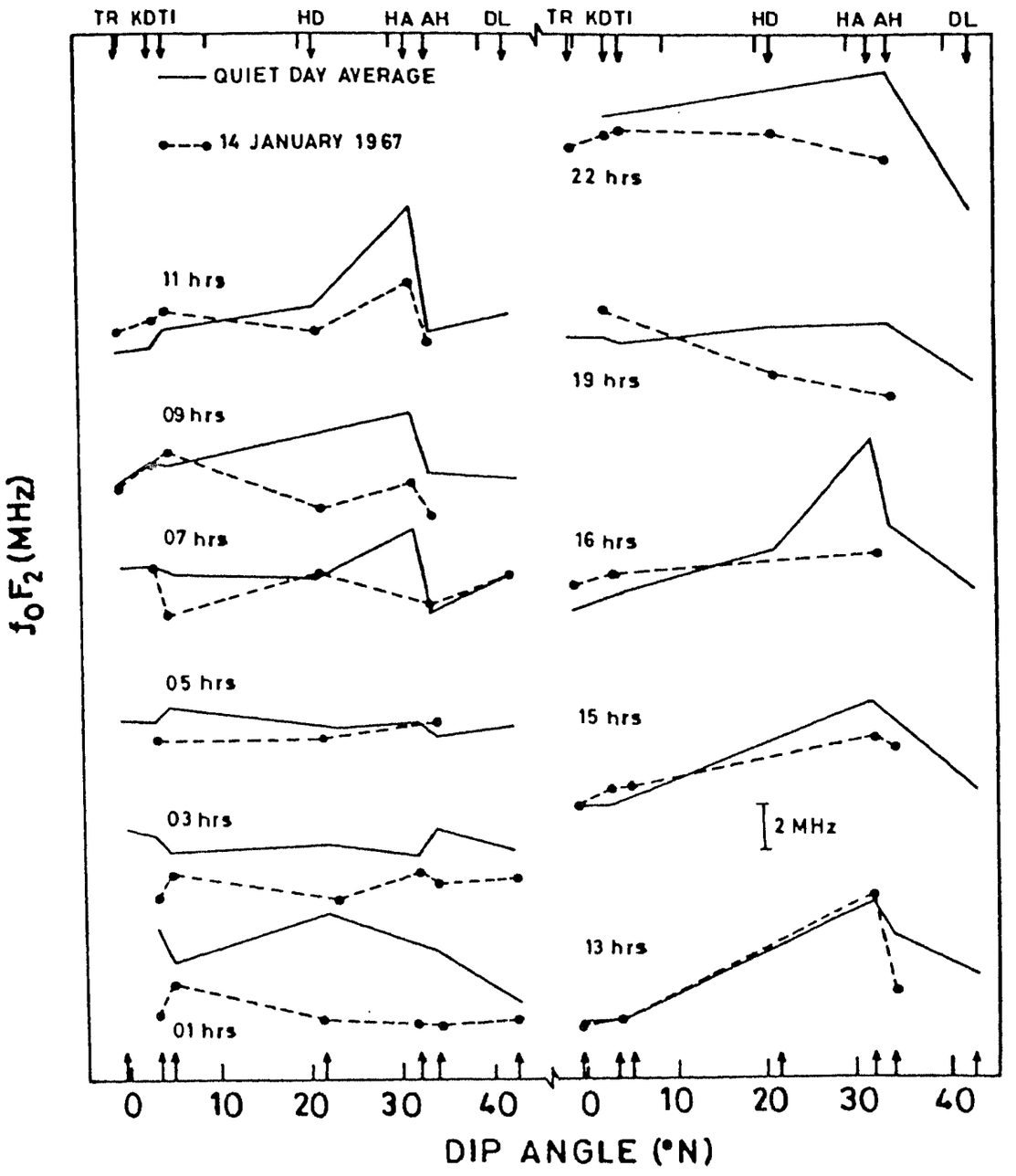

Fig. 4.18 : Plots showing the dip angle variation of foF_2 at specified local times on 14 January 1967 (dashed curves) in the Indian sector with reference to the quiet day average patterns (solid curves). Note the inhibition of the EIA and the occasional reversal of the latitudional profile of foF_2 during daytime (09, 19hrs LT) on 14 January when the electricfield experienced substantial reduction in strength.

15LT. The lack of development of EIA on 14 January further corroborates the reduction in the electrojet electric field inferred from the behaviour of ΔSdI and nighttime h'F near the dip equator. It is interesting to note, however, that the contribution of changes in foF_2 near the crest region were much larger than those around the trough region of EIA to the evidenced inhibition of EIA and reversal of the usual latitudinal profile of foF_2 (for example, while the reduction in foF_2 from the quiet day average at Ahmedabad was 18.8% and 34.8% at 15hrs and 19hrs respectively, the corresponding enhancement at Kodaikanal was only 1% and 15.3%).

Disturbance in thermospheric circulation :

In order to investigate the physical processes such as disturbance in thermospheric circulation and associated changes in thermospheric composition (which give rise to positive and negative ionospheric storm effects) responsible for the observed disturbances in equatorial ionosphere, the analysis of ionosonde data taken from highmid, mid and low latitude stations was carried out. The analysis revealed the presence of equatorward propagating disturbance winds, negative storm effects at highmid latitudes and positive storm effects at mid latitudes. The details of analysis are as given below.

Shown in the Fig.4.19 from the bottom are the temporal profiles during the intervals 13 to 15 Jan 1967, of the electrojet strength deviation from the average 'Sq' patterns of the month ($\Delta SdI - \overline{\Delta SdI}$) for Kodaikanal, deviation of diurnal foF_2, hmF_2 and $V_{effective}$ from quiet day averages (ΔfoF_2, ΔhmF_2 and $V_{effective}$ for Kodaikanal, Ahmedabad, Wakkanai, Alma Ata and Tomsk). The $V_{effective}$ which represents effective meridional winds (positive southward), inferred from hmF_2, was calculated by the method given by Forbes and Codrescu (1988). The method is as follows :

The height of the maximum electron concentration hmF_2, is derived using an empirical formula developed and evaluated by Bradley and Dudeney (1973) and Dudeney (1983) :

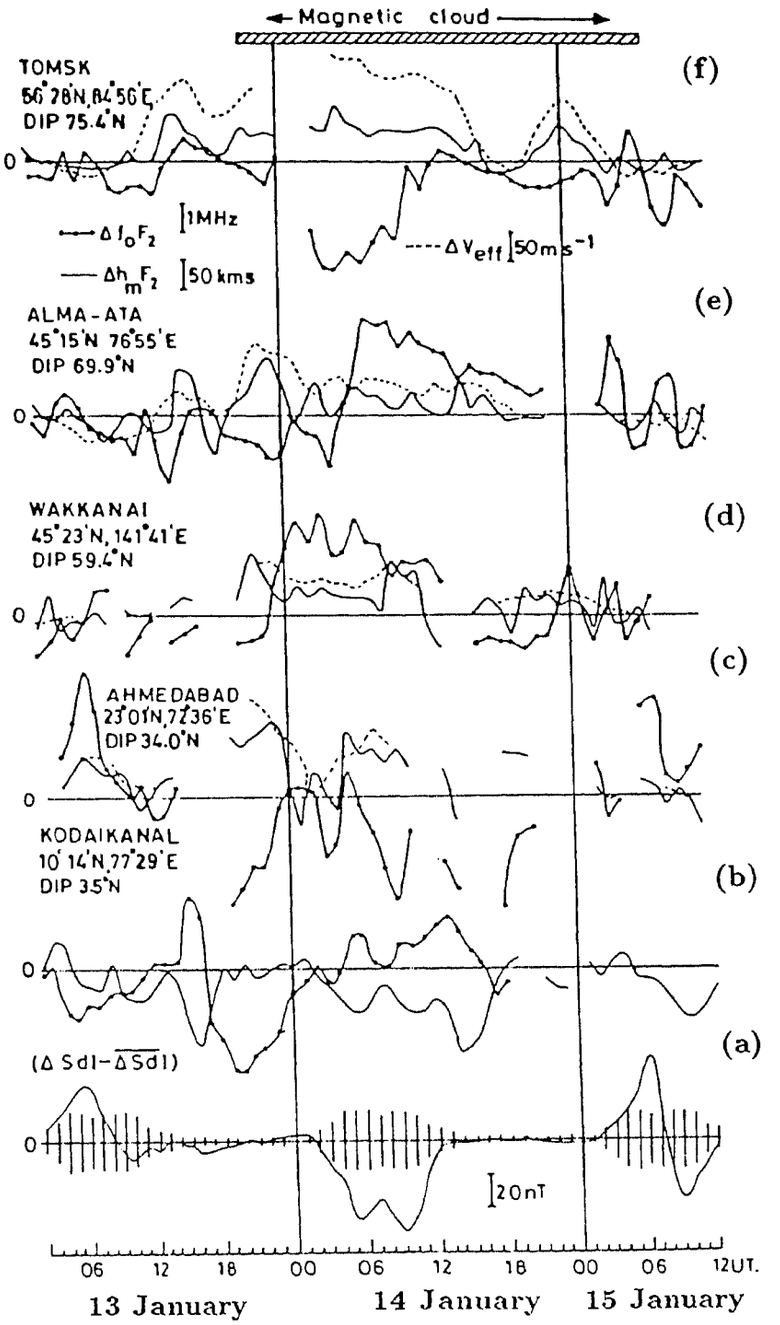

Fig. 4.19 : Composite plot showing the temporal variations of the deviations from the quiet day averages of the electrojet strength (ΔSdI - $\overline{\Delta SdI}$) and F-region parameters (ΔfoF$_2$ and ΔhmF$_2$) at latitudinal chain of stations in the Indian sector during 13-15 January 1967. The vertical bars on the plot of (ΔSdI - $\overline{\Delta SdI}$) represent the standard deviations of the quiet day averages of ΔSdI. The pattern of the effective meridional neutral wind, Δ $V_{effective}$ in ms^{-1} (positive equatorward, calculated from ΔhmF$_2$ -see text for details) is also shown for the mid and low latitude stations. Note (1) the presence of equatorward winds at Tomsk, Alma-Ata, Wakkanai and Ahmedabad and (2) the anti-phase relationship between ΔfoF$_2$ and ΔhmF$_2$ at Ahmedabad during daytime on 14 January, when ΔSdI experienced a prominent and sustained reduction in amplitude and the development of the equatorial anomaly was inhibited.

$$hmF_2 = \frac{1490}{M(3000)F_2 + \Delta M} - 176 \quad (km)$$

where

$$\Delta M = \frac{0.18}{X_E - 1.4} \quad X_E > 1.7$$

$$X_E = \frac{f0F_2}{f0E}$$

$M(3000)F_2$ = Maximum usable frequency

$f0F_2$ = Critical frequency in the F region

f0E = Critical frequency in the E region

For foF_2 and hmF_2 reference values are calculated for every station and every hour of local time using the quiet days of the month (January). The reference values are then subtracted from the data to be plotted to separate the storm effects and centered 5-hour running averages are performed. This averaging tends to remove short time scale electric field and wave effects and emphasizing large-scale circulation effects. An effective meridional wind ΔV_{eff} (positive southwards in ms^{-1}) representing storm-induced effects is then computed from ΔhmF_2 using the following relationship :

$$\Delta V_{eff} = \frac{\Delta hmF_2}{\alpha} \quad (m/s)$$

where

$$\alpha = 2 * [1 + 0.25Cos\frac{2\pi}{24}(t - 14)]Sin(I)Cos(I) \quad (kmm^{-1}s)$$

t is local time in hours and I is magnetic dip angle.

The disturbance in thermospheric wind circulation resulted in setting up equatorward propagating winds and weakening of normal poleward wind during morning hours of 14 January. The equatorward winds had time delays and reduction in their amplitudes (150m/s to 50m/s) as they propagated towards equator from high-mid latitudes.

The typical negative ionospheric storm (in foF_2) (e.g. Prolss 1980, 1987) is evident at Tomsk during morning hours of 14 January. This negative ionospheric storm is in phase opposition to the equatorward propagating meridional winds. Modification of thermospheric composition, typically characterized by an increase in the molecular to atomic ratio, produced by enhanced heat input into the high latitude thermosphere and its transport to lower latitudes by the disturbance thermospheric circulation, is thought to be an important source of modification of the midlatitude F-region (e.g Rishbeth, 1975; Prolss and Von Zahn, 1977; Prolss, 1982; Prolss et al., 1991). Electron density depletions are not expected under normal (quiet) conditions when the F-layer peak is situated at heights above 300km as chemical loss rate decreases exponentially with height. The F-layer peak is above 300km (during morning hours of 14 January) at Tomsk and hence negative storm effect seen could be the cause of composition changes brought about by storm time disturbance in thermospheric circulation. Further evidence for the disturbance in thermospheric circulation can be seen in Figs. 4.19 (d and c) in the form of positive storm effects at Alma-Ata and Wakkanai, separated in localtime by 5 hours. Positive storm effects can be caused due to the uplifting of F-layer by equatorward propagating winds during ionization production times. This happens primarily (but not exclusively) during day time conditions (Prolss et al., 1991). At Alma-Ata in fact at 05UT(10LT) on 14 January the F-layer has been lifted up in temporal coherence with meridional winds of about 60m/s velocity. This can be clearly seen in the Fig.4.19 where Δhmf2, $\Delta V_{effective}$ and Δ foF_2 are all inphase beginning at 10LT on 14 january. Similar behaviour is also evident at Wakkanai during early morning hours. The behaviour at two stations separated by $\sim$ 70 degrees in longitude indicate the disturbance in spatial extent.

4.2.3.1 Discussion

The observed large scale disturbance in the equatorial ionosphere to the transit of interplanetary magnetic cloud of 13-15 january 1967 can be identified as an *observational evidence* for a modification of EIA by equatorward propagating disturbances originating

from high latitude energy deposition processes (under storm time conditions) which produce disturbance thermospheric circulation involving disturbance winds, composition changes and disturbance electric fields, all having latitude dependent time delays (Rishbeth, 1975; Blanc and Richmond, 1980; Fejer et al., 1983; Sastri, 1988; Mazaudier and Venkateswaran 1990). The observed disturbance in equatorial electric field observed at Kodaikanal in the morning hours on January 14 in the main and recovery phases of the geomagnetic storm thus finds interpretation in terms of disturbance dynamo electric field effects. This interpretation is logical because of the following observations.

Prevalence of equatorward winds on 14th morning at midlatitudes which is a prerequisite for the establishment of disturbance dynamo electric field (Blanc and Richmond, 1980). The disturbance persisted about 12 hours in equatorial electric field in phase opposition to the normal quite day dynamo field in the Indian sector. The disturbance in electric field set up at the dip equator, had a time delay of about 8hrs from the onset of the magnetic cloud induced geomagnetic storm. This time delay is in good agreement with the time delay predicted by Blanc and Richmond (1980) for the onset of disturbance dynamo electric field effects. This time delay also coincides with the delay found by Bowman (1977) in his data sample . But this time delay does not match with the time delay of 16-24 hrs observed by Fejer et al., (1983) and 13-22 hrs observed by Sastri (1988) in their samples which showed disturbance dynamo electric field effects at the equatorial latitudes. The inhibition of EIA development is due to weakening of E×B plasma drift at the equator because of drastic reduction in usual day time eastward electric field and due to equatorward propagating meridional winds which oppose the E×B lifted plasma diffusion down the magnetic field lines to the crest location of the anomaly. The observed disturbance on 14 January in equatorial zonal electric field can not be due to the penetration electric fields not only because of the time scale of its manifestation, but also because there were no rapid and prominent swings in B_z during the time interval of the reduction in the electrojet strength as may be seen in Fig 4.17.

The interesting feature of the observed EIA response is that the contribution of changes in foF_2 near the crest region were much larger than those around the trough

region of EIA to the evidenced inhibition of EIA and reversal of the usual latitudinal profile of foF_2 (for example, while the reduction in foF_2 from the quiet day average at Ahmedabad was 18.8% and 34.8% at 15hrs and 19hrs respectively, the corresponding enhancement at Kodaikanal was only 1% and 15.3%). This could be due to the effect of disturbed thermospheric composition on the equatorial F-layer densities. Although disturbed thermospheric composition has been measured by satellites, its effects on the equatorial F-layer densities have not yet been confirmed from ionospheric observations. Some low latitude observations do seem to suggest the presence of such effects (Matuura, 1972; Batista et al., 1990, 1991; Walker and Wong, 1993). Lack of neutral composition data for the present study prevents us to look for such an effect.

******

Chapter 5

Substorm related electric field disturbances in Equatorial Ionosphere

5.1 Introduction

There are two main sources of electric fields in the ionosphere. They are: (a) ionospheric E-layer tide-induced dynamo electric field which is already mentioned in chapter 1 and (b) magnetospheric electric field due to solar wind - magnetosphere interaction. Mostly (a) dominates the electrical structure of ionosphere at low and midlatitudes and (b) dominates at higher latitudes (Mozer, 1973). However, considerable evidence now exists in the literature for the penetration of magnetospheric/high latitude electric fields to equatorial latitudes during magnetically active periods such as substorm activity (Kelley et al., 1979; Rastogi and Patel, 1975; Fejer, 1986; Gonzales et al., 1979; Fejer et al., 1990a, b). Enhanced solar wind - magnetosphere interactions associated with IMF polarity changes and the consequent development of polar cap potential drops, substorm onsets and recovery phases, and geomagnetic sudden commencements (SC) are the circumstances that produce magnetospheric/high latitude electric field penetration to equatorial latitudes (See Kikuchi, 1986; Fejer, 1986; Fejer et al., 1979, 1990a, b; Sastri et al., 1993 and references therein). In the dip equatorial region the IMF/Substorm related prompt penetration electric field is transient (typical duration $\sim$ 2hrs) and global in nature and invariably manifests in the zonal component. The polarity of the zonal electric field disturbances associated with swift northward B_z turning is westward (eastward) during day (night), i.e in phase opposition to the S_q field pattern and these tend to occur during the recovery phase of the auroral substorms triggered by the rapid northward turning of B_z. Transient disturbances in phase with the S_q field pattern (eastward by day and westward by night) are also some times observed in association with sudden southward swing in IMF B_z. The amplitude and frequency of

occurrence of the electric field disturbances are strongly dependent on local time. In the case of disturbances associated with northward IMF turnings and substorm recovery phase onsets the disturbances occur quite frequently at all local times with maximum amplitudes in the midnight-dawn sector. In the case of disturbances associated with southward IMF B_z turnings, the disturbances occur occasionally with a preference for the midnight-noon sector with largest amplitudes just before sunrise (Fejer, 1986 and references therein). The manifestation of disturbances in equatorial zonal electric field to changes in IMF B_z and substorm activity is thus quite asymmetric. Simultaneous electric field measurements with a meridional network of incoherent scatter radars clearly indicated that the trasient disturbances in the equatorial zonal electric field are asoociated with rapid changes in magnetospheric convection induced by IMF B_z and represent the effects of prompt penetration of high latitude electric fields into the equatorial ionosphere (see Fejer, 1986; Fejer et al. 1990a, b and references therein).

Several models of penetration electric fields in the sub-auroral ionosphere associated with sudden changes in magnetospheric convection are now available. (e. g. Nisbet et al. 1978; Kamide and Matsushita, 1981; Senior and Blanc, 1984; Spiro et al, 1988; Zamay, 1989). The models have been found very useful in understanding the various observational aspects of the equatorial transient electric field disturbances. The global convection models of Senior and Blanc (1984) and Spiro et al (1988) treat the problem of electric field penetration in a comprehensive manner by considering magnetosphere-ionosphere as a coupled system and paying due attention to the various physical processes operative in it such as radial motion of the magnetospheric energetic plasma, azimuthal drifts of particles, precipitation of particles, flow of field aligned currents, ionospheric conductivities in the auroral and sub-auroral ionosphere. The basic input to these two models are the step-like changes in the polar cap potential representing those in the large -scale magnetospheric convection controlled by IMF B_z. Both the models predict mostly the same pattern for the penetration electric fields at different latitudes but with some miner differences which may be due to the differences in the inputs to the models such as the ionospheric conductivities (Fejer, 1990b). These global

convection models have been successful in explaining the basic characteristics of the equatorial transient electric field disturbances associated with sudden changes in IMF B_z and substorm activity derived from experiment. They predict correctly the diurnal pattern of the amplitude and polarity of the penetration electric fields associated with decrease as well as increase in polar cap potential particularly the maximum amplitude of the zonal electrc field perturbations near the dip equator in the midnight-dawn sector associated with decrease in polar cap potential. The latitudional variations of penetration electric fields is also predicted reasonally well by these models (Fejer et al., 1990a, b).

Besides successful predictions of certain parameters of penetration electric fields by models as explained above, there are some differences too between theory and observations. (a) Reddy et al. (1990a, b) present details of the discrepancy in polarity of a large electric field disturbances observed at middle and low latitudes during a substorm with model predictions, (b) the models can not explain the highly asymmetric response of the equatorial zonal electric field to sudden changes in polar cap potential, i.e higher sensitivity to decrease in polar cap potential than to increase as mentioned earlier, (c) the infrequent observation of penetration electric fields near the magnetospheric convection (even in the predawn sector) is generally attributed to inadequate temporal resolution of the experimental data. The SUNDIAL-86 campaign results from the Jicamarca (dip 2°N) radar data (basic time resolution 1 min) do not however support this view (Fejer et al, 1990b). (d) the models can not fully account for the persistence (typical duration 2 hours) of the zonal electric field perturbations associated with decreases in magnetospheric convection (see Fejer, 1990b for conceptual details of plausible physical mechanisms).

An interesting experimental fact about the transient electric field is that they appear either with an increase in convection at the onset of the substorm (due to southward turning of B_z) or with a decrease in convection during the recovery phase of the substorm (due to northward turning of B_z) but not both (Fejer et al., 1979). In any substorm increase in convection will be followed by a decrease in the recovery phase and

in fact the calculations of Spiro et al. (1988) and Fejer et al.(1990b) simulate the effects of sharp increase in polar cap potential followed by a sharp decrease as in a substorm. Therefore one can expect evidence for the occurrence of a composite effect i. e. an increase and a subsequent decrease in convection in a single substorm and also their effect on equatorial electric fields. Gonzales et al (1983) have reported the evidence of composite electric field effects and the details of their observations in comparison with that of the case study presented here will be discussed in section 5.2.2.

Recently Sastri et al. (1992) found unambigious evidence for a transient composite disturbance in the equatorial zonal electric field in the midnight - dawn sector, in close association with an isolated auroral substorm of moderate strength. In this chapter are presented the results of a case study of a transient composite electric field disturbance that is simultaneously seen both in the night and day hemispheres near the dip equator in close association with an event of isolated auroral substorm activity.

5.2 Case Study of 20th August 1979 event

F-layer height data derived from the ionograms recorded at Kodaikanal (10.2°N, 76.5°E, dip 3°N) and Huancayo (12°S, 75.3°W, dip 2°N) have been used for the present study. h_pF_2 (the height of F-region peak for parabolic distribution) is utilized to ascertain the changes in the vertical plasma drift and hence in the zonal electric field in the dayside sector. Similarly $h'F$ (virtual height of the bottom side of the F-layer) data is used to get information on zonal electric fields for the night sector. At night, $h'F$ and its time derivative [d($h'F$)/dt] near dip equator provide reliable information on F-region vertical plasma drift, V_z (e.g. Bittencourt and Abdu, 1981). The inherent limitations in the usage of $hpF_2/h'F$ i.e under estimation in the vertical plasma drift due to recombination/ionization effects when the layer is below 300 Km, (Batista et al., 1991) do not vitiate the conclusions of the present study as the interest here is not in the absolute values of the vertical plasma drift but the short - term changes in it on substorm time scales.

5.2.1 Results

The substorm-related perturbation in F-region height was seen at Kodaikanal and Huancayo on 20 August 1979, a moderately disturbed day (Ap = 42). The time histories of the auroral electrojet indices (AU/AL/AE) over the period 04-24 UT on the day shown in Figure 5.1 indicate the occurrence of severe auroral substorm activity (Kp = 7°) starting around 1630 UT. The relatively quiet geomagnetic conditions that preceded the substorm activity testify to its rather isolated nature. The wide spatial extent of the substorm activity can be inferred from the AE index which was > 2000nT at its maximum. Figure 5.2 shows the variations of $h'F$ at Kodaikanal and of hpF_2 at Huancayo for the interval 13 UT of 20 August to 01 UT of 21 August together with the monthly median patterns (dashed curves). Also shown are the low-time resolution (hourly averages) data of the auroral electrojet indices (AU/AL), IMF B_z (hourly values) and the polar cap potential drop (ϕ), estimated from IMF data using the empirical formula of Reiff and Luhmann (1986).

(a) Transient electric field disturbance at Kodaikanal (76.5°E) :

On 20 August 1979, $h'F$ at Kodaikanal displayed the usual post-sunset enhancement although the maximum in $h'F$ is higher and the time of its occurrence earlier than the corresponding median values (Figure 5.2). This feature implies that though the upward V_z is higher than the normal, its post-sunset enhancement is shorter in duration on 20 August (see Figure 5.3). After reaching the maximum, $h'F$ rapidly decreased indicating the prevalence of larger than normal values of downward V_z till 20 LT (Figures 5.2 and 5.3). This sort of departure from the median pattern is not uncommon because V_z is well known to undergo considerable day-to-day variability even on quiet days in the post-sunset period. $h'F$ and V_z recovered to the median values by 21 LT, but beginning at 2130 LT(1630 UT) there was a sudden and anomalous reduction in $h'F$ from 340 km to 260 km at 2230 LT (i.e. 80 km in 1 hr). The time variation of [d($h'F$)/dt] shows that a downward vertical drift of about 22 ms^{-1} prevailed for an hour while the median pattern shows much smaller drift ($\leq 8.3 ms^{-1}$) at that time

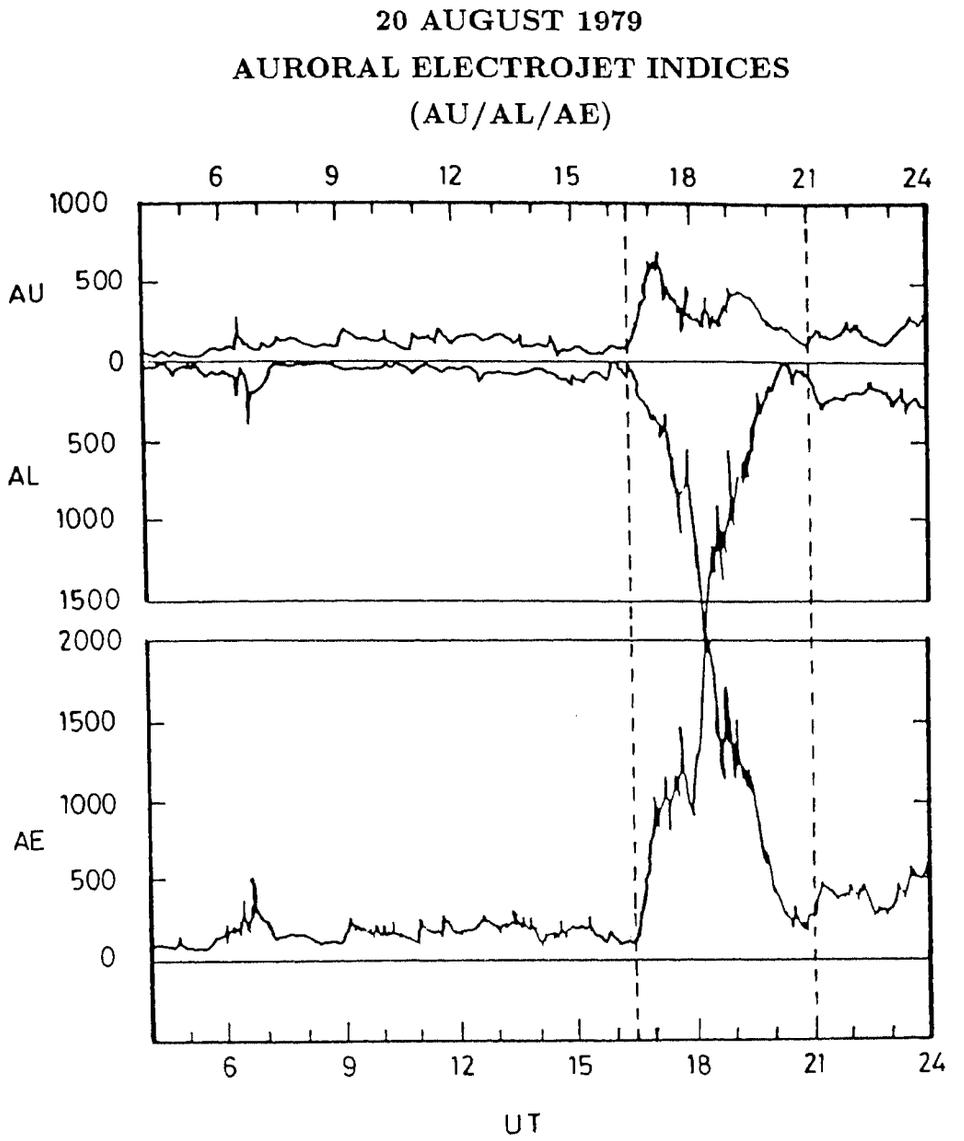

Fig 5.1 : Time histories of the auroral electrojet indices (AU/AL/AE) during the interval 04-24 UT on 20 August 1979 illustrating the onset of an isolated, severe substorm around 1630 UT. The vertical dashed lines indicate the period when a conspicuous perturbation in F-region height prevailed simultaneously at Kodaikanal (dip 3°N) and Huancayo (dip 2° N) separated by 10 hrs in local time.

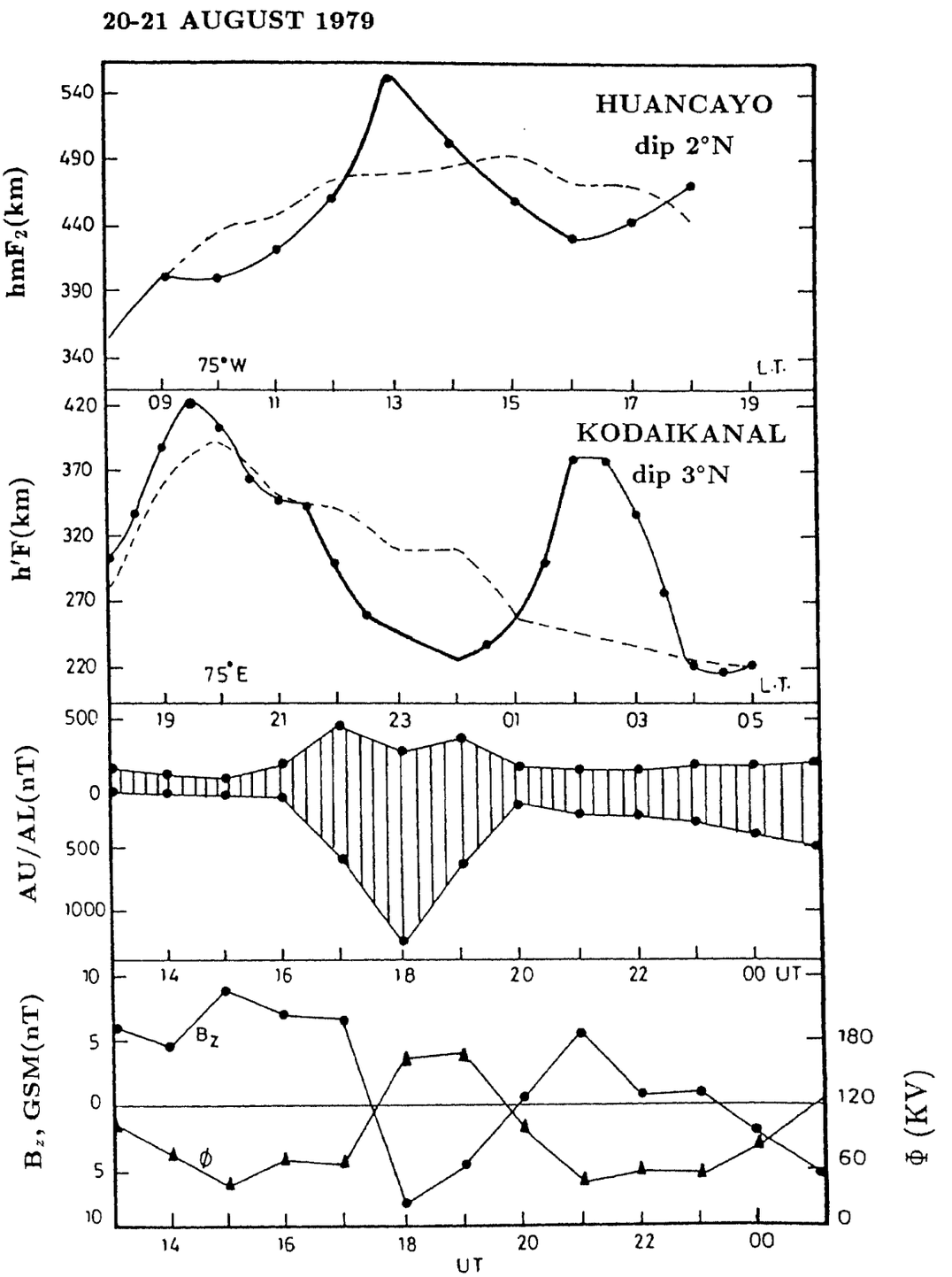

Fig 5.2 : Time variation (hourly values) of the north-south (Bz) component of IMF, auroral electrojet indices (AU/AL) from 13 UT of 20 Aug 1979 to 01 UT of 21 Aug 1979 (bottom and middle panels). The variations in the polar cap potential drop (ϕ) estimated from IMF parameters is also shown. The top panels show the variation of h'F at Kodaikanal (on the nightside), and of hpF2 at Huancayo (on the dayside) on 20 Aug 1979 with the monthly median patterns (dashed curves) superposed for reference.

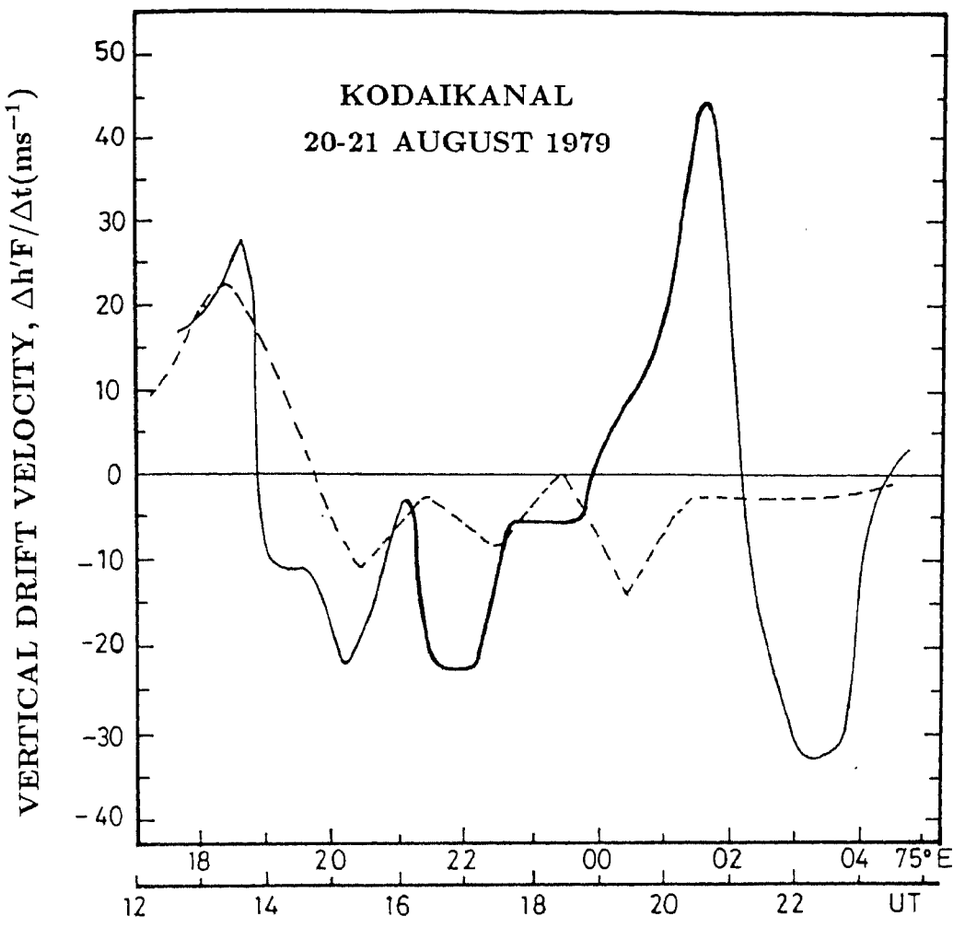

Fig 5.3 : F-region vertical drift velocity at Kodaikanal (derived from h'F data) on the night of 20-21 Aug 1979 along with the monthly median pattern (dashed curve). The transient disturbance in vertical drift associated with the substorm is indicated by the heavy line.

(Figure 5.3). The strong downward drift eased a bit by 2230 LT and moved closer to the median values. Subsequently the F-region height at Kodaikanal experienced another conspicuous perturbation in the form of an increase beginning at 00 LT (Figure 5.2). The increase was slow and small initially but was rapid and substantial later such that $h'F$ rose from 260 km at 01 LT (20 UT) to 380 km by 02 LT (21 UT) i.e. an increase of 120 km in 1 hour or a gross upward drift of 33.3 ms^{-1}.

(b) Transient electricfield disturbance at Huancayo (75.3°W) :

A similar perturbation in F-region peak height of mixed polarity prevailed at Huancayo on the dayside simultaneous to the one in $h'F$ Kodaikanal on the nightside, as can be seen from the behaviour of hpF_2 shown in Figure 5.2 (top panel). The polarity pattern of the disturbance in hpF_2 is exactly the opposite of that in $h'F$. At the time of the sudden and rapid decrease in $h'F$ at Kodaikanal (indicating the onset of strong downward drift) beginning at 2130 LT (1630 UT), hpF_2 at Huancayo experienced a rapid and significant rise from 458 km at 12 LT (17 UT) to 551 km at 13 LT (19 UT) i.e. an increase of 93 km in 1 hr. Thereafter the F-layer underwent a continuous and anomalous descent for 3hrs, so much so that hpF_2 decreased from 551 km at 13 LT (18 UT) to 432 km by 16 LT (21 UT). These rapid and significant change in hpF_2, which are in marked deviation to the general trend of a steady and slow increase (6 km/hr) around noon (see Figure 5.2), constitute signatures of a transient disturbance in F-region vertical plasma drift. In view of the known sensitivity of F-layer peak electron density near dip equator (trough region of the equatorial ionization anomaly) to the zonal electric field through the $E \times B$ plasma drift (basic ingredient of the 'fountain' process responsible for the anomaly), it has also been examined the day-time behaviour of foF_2 at Huancayo on 20 August 1979 for a plausible response. The data presented in Figure 5.4 clearly shows a prominent disturbance in foF_2 of the expected nature in association with that in hpF_2 namely, an initial decrease (by 2.4 MHz over the period 12 - 14 LT) and a subsequent increase (by 1.2 MHz over the period 14 - 16 LT). These changes in foF_2 indicate that the perturbation in hpF_2 is a manifestation of that in vertical plasma drift. This conclusion also draws support from the study of Batista

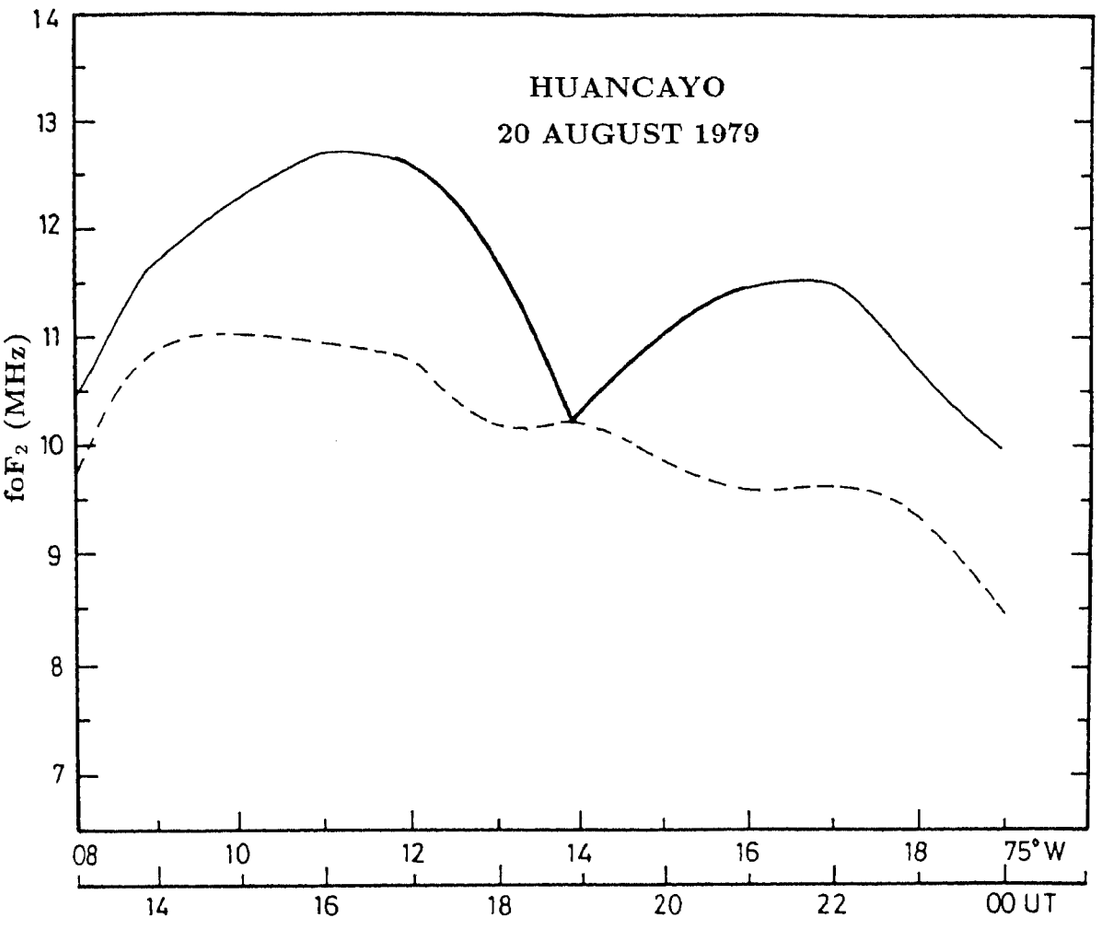

Fig 5.4 : Day time variation of foF2 at Huancayo on 20 Aug 1979 along with the monthly median pattern (dashed curve). The perturbation associated with that in hpF2 and the substorm is indicated by the heavy line.

et al., (1991) which showed that a downward drift (westward electric field) during daytime causes a lowering of F-region peak height and a sharp and rapid rise in peak electron density. Transient changes in foF_2 and hpF_2 of opposite polarity will prevail if an increase in the ambient upward drift (eastward electric field) were to occur.

5.2.2 Discussion

The geomagnetic, interplanetary and ionospheric data presented in Figures 5.1 and 5.2 demonstrate the excellent coincidence of the simultaneous disturbance in F-layer height of composite nature at Kodaikanal and Huancayo with the sub-storm activity and related changes in IMF $B_z$and polar cap potential drop (ϕ). The unambiguous temporal relationship strongly suggests the substorm origin of the disturbance in equatorial F-region height and hence in the zonal electric field. The contribution of substorm-related neutral winds and waves to the observed height changes can be discounted on several points : (a) the known insensitivity of F-region height near dip equator to horizontal neutral winds, (b) the wind and wave effects will manifest at equatorial latitudes with a delay from the onset of the substorm (a wave disturbance originating at 65° geomag. lat. for example, would reach Kodaikanal after ~2 hrs even if it propagates at 1000m/s) and (c) the substorm-generated winds being equatorward can only cause an increase in F-region height in the northern hemisphere but not the observed increase and decrease.

The theoretical work most relevant to the observations presented in this chapter are the semi-analytical/numerical models which simulate the perturbations in sub-auroral electric fields following rapid changes in high latitude convection (Senior and Blanc, 1984; Fejer et al., 1990a). These models based on the convection approach predict westward (eastward) electric fields at equatorial latitudes during night (day) for a sudden increase in polar cap potential (ϕ), and fields of opposite polarity for a sudden decrease. And this indeed is the polarity pattern observed at the dip equatorial stations during the substorm activity on 20 August studied here. The comparison of observations with theory can also be attempted with regards to the amplitude of the transient electric fields, because the estimated changes in ϕ during the substorm (Figure 5.2) are very

close to the values assumed in the model simulations available in literature i.e. an increase and decrease in ϕ of 45KV and 70KV respectively. The comparison is, however, done only for the night sector because of the availability of direct information of V_z from $h'F$ data at Kodaikanal. To estimate the magnitude of the substorm-related electric fields, the values of V_z derived from $h'F$ data at Kodaikanal are corrected for chemical loss effects. The correction procedure is as explained in the chapter 4. The corrected values of V_z showed the maximum amplitudes of the transient westward (around 22 LT) and eastward (at 02 LT) electric fields at Kodaikanal to be ~0.9 mV/m and ~1.7 mV/m respectively. The theoretical initial time response curves of the equatorial zonal electric field for $\Delta\phi$ = 45KV and $\Delta\phi = -70$KV show the amplitude of the westward and eastward perturbation fields for the relevant local times to be $\sim$ 0.1 mV/m and $\sim$ 0.8 mV/m respectively(see Fig. 5.5) (Fejer et al., 1990a, b). The observed amplitude of the transient electric fields especially the eastward field around 02 LT is higher than the model results. The occurrence of such large eastward electric fields (> 1.5 mV/m) in the midnight-dawn sector at equatorial and low latitudes in association with sudden northward swing of B_z/onset of substorm recovery phase is known from recent case studies (e.g. Fejer et al., 1990a; Sastri et al, 1992; Somayajulu et al, 1991).

The earlier study on composite electric field disturbances by Gonzales et al., (1983) is similar to the work presented here. The polarity pattern of the disturbance over the period 08-09 UT on 11 October 1980 reported by them is the same as that presented here, namely, eastward (westward) fields near dip equator on the nightside (dayside) with a decrease in convection (at 08 UT), and fields of opposite polarity with an increase in convection (at 09 UT). There are noteworthy differences, however, between the two electric field disturbances. They are :

(1) The electric field disturbance on 20 August 1979 discussed here occurred in close association with *isolated substorm activity* and with a natural sequence of convection changes, i.e, an increase followed by a decrease, and the comparison of its characteristics (on the nightside) with theoretical results is rather straightforward. The electric field disturbance on 11 October 1980 studied by Gonzales et al (1983), on the other

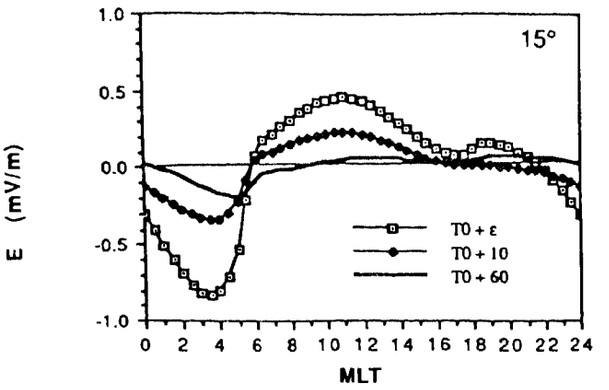

Fig 5.5(a) : Time variation of the eastward electric field at 15° latitude resulting from a sudden increase of 45KV in the polar cap potential drop. (After Fejer et al., 1990a)

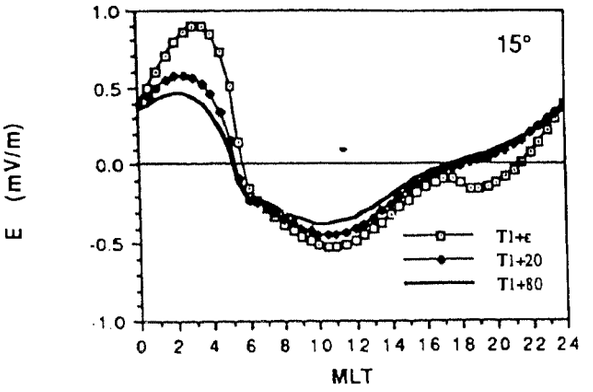

Fig 5.5(b) : Time variation of the eastward electric field at 15° latitude resulting from a sudden decrease of 70KV in the polar cap potential drop. (After Fejer et al., 1990a)

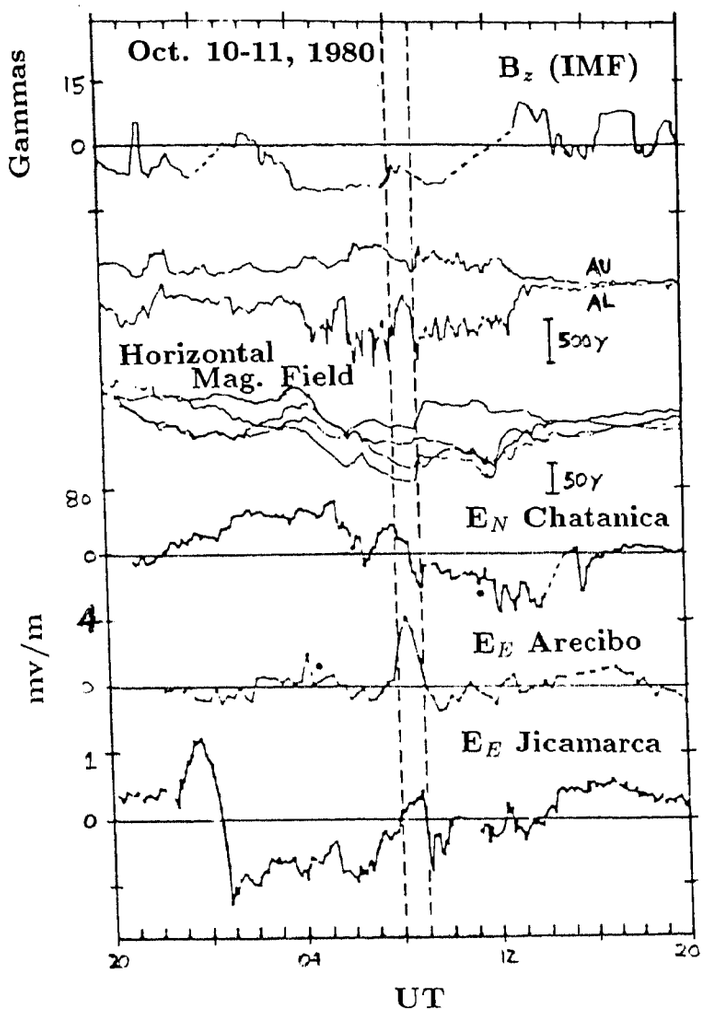

Fig 5.6 : Zonal electric field component at Jicamarca and Aricibo; the meridional E-field at Chatanica; midlatitude magnetometer data; AU-AL (auroral indices); IMF B_z; Dots indicate local magnetic midnight.
(After Gonzales et al., 1983)

hand, manifested during the course of prolonged substorm activity (moderate auroral activity also prevailed over the preceeding 12 hrs with AE index exceeding 500nT several time, and the electric field penetration is evidenced first with a decrease and then with an increase).

(2) Scrutiny of Figure 5.6 (see previous page)(Fig. 5 of Gonzales et al., 1983) shows that rapid decrease and increase in convection also occurred around 0540 UT and 0625 UT respectively as at 08 and 09 UT. But while the latter are accompanied by unmistakable worldwide perturbations in equatorial zonal electric field, there is no perceptible response to the former even on the nightside at Jicamarca (75°W). Instead, eastward fields are seen at Jicamarca at 0500 UT and 0710 UT when there are no changes in IMF B_z, AL index and high latitude electric fields. The lack of detectable perturbation electric fields due to the convection changes over the period 0540-0625 UT could be due to the strong local time dependence of penetration electric fields (the amplitude is smaller around midnight than in the predawn period) or enhanced attenuation of high latitude fields in penetrating to dip equator or both. The measurements of Gonzales et al.(1983) for the plasmaspheric electric field campaign of october 1980, stand testimony to the complexity of the physical situation that obtains during prolonged substorm activity, and the difficulties in understanding the electric field disturbances under such geophysical conditions.

* * * * **

Chapter 6

Summary and scope for further work

6.1 Summary of the results

6.1.1 Results based on measurements of neutral and plasma parameters

It is widely recognised now that the neutral atmosphere can significantly influence the structure and dynamics of the ionosphere at equatorial latitudes. Interactions between the plasma and the neutral constituents of the atmosphere are, infact, a normal feature at F-region altitudes due to the dominance of ion-drag effects. The importance of the plasma-neutral coupling is found in various phenomena of the equatorial thermosphere-ionosphere system such as the Post-sunset enhancement of EIA strength, Equatorial spread-F, Equatorial temperature and wind anomaly (ETWA) and Equatorial midnight temperature maximum (MTM). Simultaneous measurements of neutral and plasma parameters as a function of space and time are essential to improve our understanding of above phenomena. Since adequate diagnostic facilities for monitoring the ionospheric plasma medium such as ionosonde, HF Doppler radar, VHF Backscatter radar, VHF polarimeters are available at several locations in the country, it is imperative to establish a network of Fabry-Perot Interferometer(FPI) stations to undertake simultaneous measurements of the neutral and plasma parameters of the equatorial upper atmosphere. As a step in this direction we have developed a pressure-scanned Fabry-Perot Interferometer for operation at Vainu Bappu Observatory (VBO), Kavalur (12.5°N, 78.5°E, dip 9.5°N), close to the geographic/geomagnetic equator under the RESPOND PROJECT.

Based on simultaneous measurements of neutral and plasma parameters using the FPI at Kavalur and Ionosondes (at Indian equatorial and low latitude stations) respectively, the following results are obtained concerning the equatorial thermosphere-

ionosphere system in the Indian sector.

(a) Characteristics of nighttime neutral thermospheric temperature over Kavalur

Characteristics of the nighttime neutral thermospheric temperature at Kavalur are derived by analysing 65 days of temperature data obtained during March - April 1992 and November 1992 - April 1993. The temperature data are obtained by the measurement of Doppler width of O(^{1}D) 630nm night airglow line emission using the Fabry-Perot interferometer. A total of 500 individual line profiles covering the time interval 2030-0445 IST (IST = UT + 5.5hrs) are selected for analysis leaving about 260 line profiles with poor S/N ratio. Averaging the temperature measurements over a suitable time interval and comparing the same with values predicted by empirical models, is a common method to study the characteristics of temperature at a given location (Hernandez, 1982; Yagi and Dyson, 1985). In the present work the average of all measurements in a particular night is computed and compared with the average of MSIS-86 model values calculated for the same times as the observations. By this approach it is found that the mean nightly temperature exhibits considerable day-to-day variability and the observed temperatures are consistently and significantly higher than the model values on all but three of the nights (two nights match closely with MSIS-86 and one night below MSIS-86 values). The difference between the nightly values of the observed temperature and the model values varies in the range -16K to +585K with a mean value of 274K and a standard error of 145K. The average of all temperature determinations made is 1177K which is higher than the corresponding model value by 275K. These statistical details clearly show that: the nighttime thermospheric temperature determined from FPI observations at Kavalur is significantly higher than the MSIS predictions. The day-to-day variability and higher values of the nightly average temperature over MSIS could be due to the variability (amplitude, shape and duration) in the manifestation of the equatorial midnight temperature maximum.

(b) Characteristics of MTM in Indian Zone

It is known that in the equatorial region (± 20°), the thermospheric temperature does not always undergo a monotonic decrease throughout the night. A pronounced enhancement, typically around midnight, sometimes reaching or exceeding the daytime values, is a frequent occurrence. This recurrent feature is referred to as the equatorial midnight temperature maximum (MTM). The characteristics of the MTM like shape, amplitude and time of occurrence are highly variable both on short-time (day-to-day) as well as long-time (season, year-to-year) scales. Temperature measurements showed MTM on about 30% of nights (covering time interval 2030 - 0445 IST). The amplitude of MTM over Kavalur was found to be in general larger than that of Jicamarca (12°S, 75°W, dip 2°N) in American sector. The time of occurrence of MTM in two seasons, namely winter and vernal equinox is also studied. It is found that the MTM occurs, on the average, one hour after midnight in local winter and just before midnight in vernal equinox, a seasonal pattern that is in broad agreement with that at Jicamarca.

(c) MTM effects on low latitude F-region height and density

In order to understand the MTM effects on equatorial/lowlatitude F-region height and density, coordinated measurements were undertaken on few nights in April 1992, April 1993 and December 1992 of thermospheric temperature with FPI at Kavalur (dip$\sim$ 9.5° N) and of F-layer height and plasma density with ionosondes at Trivandrum (dip$\sim$ 0.6° S), Kodaikanal (dip 3°N), Sriharikota (dip$\sim$ 10.5° N) and Ahmedabad (dip 34°N) in India. These measurements revealed some important effects associated with MTM. They are : (1) the presence of MTM induced meridional winds and (2) the wind induced 'midnight collapse' and decrease of F-region density at low latitudes. The most important result of these simultaneous thermospheric and ionospheric observations is the first time demonstration of the relationship *in totality* between the equatorial midnight temperature maximum, poleward reversal of nighttime (inferred) meridional winds and 'postmidnight collapse' of F-layer at low latitudes.

6.1.2 Results from a case study on the response of equatorial ionosphere to the passage of interplanetary magnetic cloud at Earth

In addition to the results on equatorial thermosphere-ionosphere system based on neutral and plasma measurements, we have obtained new results based on ionosonde and magnetometer data analysis on (a) response of equatorial ionosphere to the transit of interplanetary magnetic cloud and (b) substorm related electric field disturbances in the equatorial ionosphere. The results are as follows.

Interplanetary magnetic clouds are currently considered as one of the interplanetary manifestations of solar coronal mass ejections (CMEs). Geomagnetic activity can be expected to respond to the passage of clouds because they possess a large southward IMF over a part of their $\sim$ 1 day duration at Earth. Recent studies demonstrated that clouds indeed produce geomagnetic disturbances. A detailed study was carried out to evaluate the behaviour of equatorial ionosphere in relation to the transit of a magnetic cloud at the Earth during January 13-15, 1967. The cloud caused an intense sudden commencement (SC) type geomagnetic storm. Analysis of quarter-hourly ionograms of Kodaikanal (10.2°N, 76.5°E, dip 3°N) revealed the occurrence of a prominent, short-lived, westward disturbance in the equatorial zonal electric field during the initial phase of the geomagnetic storm induced by the cloud's passage. The electric field disturbance manifested as a sudden and abnormal descent of the entire bottomside F-region for a short duration (1845-2030LT), in temporal coincidence with the decay phase of an auroral substorm and asymmetric ring current that developed at the onset of the geomagnetic storm. The evidenced electric field perturbation finds a logical interpretation in terms of prompt penetration of substorm-associated high latitude electric fields to the dip equator as its polarity is consistent with the model results. This is considered as an important addition to the current knowledge on penetration electric fields in the sub-auroral ionosphere. Another unique feature of the transient response of equatorial ionosphere to the cloud passage is the remarkable increase in electron density at and below the F layer peak over Kodaikanal, that accompanied the rapid and spectacular downward motion of the layer in the post-sunset hours mentioned above. The response

is considered unique because the fate of nighttime F layer near the dip equator is governed by chemical loss and plasma transport, and when the layer is below 300km it has to decay as a rule due to enhanced chemical loss, while what is observed is exactly the opposite. Reports of such fast and prominent increase in electron density are quite uncommon in the literature. An earlier theoretical study indicates that the peak electron density can increase in a limited altitude range above 250km, if a sufficiently large downward drift prevails such that the plasma compression induced by drift overcomes the chemical loss. Evaluation of the relevant parameters according to the theory showed that the theoretical condition holds good in the altitude range 250-395km. This confirms that the observed increase in peak electron density is due to the ionization convergence rate exceeding the chemical loss rate, when the layer as a whole experienced a large downward drift because of the penetration of substorm-related electric fields into the equatorial ionosphere.

Besides the transient disturbance in equatorial electric field there were prominent and persistent disturbances in the equatorial electric fields during the main and recovery phases of the magnetic cloud induced geomagnetic storm. The main results are :

(a) Striking presence of a large-scale disturbance in equatorial electric field in the Indian sector in association with the magnetic cloud passage.

(b) Disturbance in equatorial electric field manifested in inhibition of development of day time EIA due to the weakening of E×B plasma drifts and hence *fountain* process.

(c) Evidence of equatorward propagating disturbance neutral winds causing negative storm effects at high latitudes and positive storm effects at mid latitudes.

(d) Evidence of ionospheric disturbance dynamo electric fields at equatorial latitudes.

6.1.3 Results from a case study on substorm-related electricfield disturbances in the dip equatorial ionosphere.

It is very well evidenced in recent studies that electric fields of magnetospheric/high

latitude origin can instantaneously penetrate to low latitudes at times of sudden transitions in IMF Bz and attendant changes in polar cap potential drop, auroral substorm activity and asymmetric ring current. There is an interesting facet of the observational results regarding the manifestation of auroral substorm-related transient electric field disturbances in the equatorial ionosphere i.e.the perturbation electric field appear either with an increase in high latitude convection around the onset of a substorm which is due to southward turning of IMF Bz or with a decrease in convection during the substorm recovery phase which is due to northward turning of Bz but not both (Fejer et al, 1979). This mutually-exclusive nature of substorm-related electric field disturbances near the dip equator is not consistent with the current theoretical models. In a case study based on ionosonde data of Kodaikanal (77.2°E, dip 3°N) and Huancayo (75.3°W, dip 2°N), the simultaneous occurrence of a transient disturbance in F-region height of *composite polarity* in day and night sectors near the dip equator in association with isolated substorm activity on 20 August 1979 is demonstrated.

At Kodaikanal which is in the night hemisphere at the time of the substorm activity, the F-region height first underwent an abrupt and rapid decrease during 2130 to 2230 LT (80km in 1hr) followed by a much larger increase during 01-02 LT (120km in 1hr). Perturbation in F region height of exactly opposite polarity was simultaneously seen at Huancayo during 12 to 13 LT (increase in height of 93 km in 1 hr) and then during 13 LT to 16 LT (decrease in height of 119 km in 3 hrs) in the dayside hemisphere. The decrease in F region height at Kodaikanal (and increase at Huancayo) occurred in association with an increase in the polar cap potential drop, and the subsequent increase (decrease at Huancayo) with a decrease in the polar cap potential. The F-region height disturbance is interpreted as the manifestation of a global transient composite disturbance in the equatorial zonal electric field caused by the prompt penetration of substorm-related high latitude electric fields into the equatorial ionosphere. The polarity pattern of the electric field disturbance is consistent with the global convection models which predict westward (eastward) electric fields at night (by day) near the geomagnetic equator in response to an increase in the polar cap potential and fields of opposite polarity for a

decrease in the polar cap potential.

6.2 Scope for further work

The FPI which is developed and commissioned at VBO, Kavalur is utilized so far to measure the night time neutral thermospheric temperature in the zenith direction covering the time interval 2030-0445 IST. The FPI now needs to be upgraded to realise its full potential, *i.e* to be able to measure neutral wind field and temperature throughout the night right from local sunset. With the present set-up where central aperture scanning is done, it is not possible to obtain line profiles with good S/N prior to 2030 IST due to the low intensity of 630nm emission caused by the well known post-sunset vertical uplift of F-region in the vicinity of the dip equator.

6.2.1 Upgradation of FPI

(a) The line profile data are to be obtained with multi-zone aperture to enhance the throughput of FPI and to extend the local time coverage of the observations prior to 2030 IST.

(b) A pointing system (opto-mechanical unit) is to be designed, fabricated and installed to facilitate effective collection of light from different directions of the sky to the FPI for measurements of the wind components in the zonal and meridional directions.

(c) A well stabilized and perfectly horizontal platform is to be made for mounting the opto-mechanical sub-units of the FPI system to attempt measurements of the most important component of the wind vector, i.e. vertical wind. The magnitude of vertical winds in the equatorial thermosphere is generally believed to be small (10-15m/sec) and is therefore rather difficult to detect with groundbased techniques. A well-designed platform for the FPI is thus essential to minimise the contribution of the horizontal winds to the Doppler shift of the line profiles obtained in the zenith direction for vertical wind. It is worthwhile to mention in this context that our knowledge of vertical winds

in the equatorial thermosphere is limited to a few measurements scattered in time (e.g. Ananda Rao et al., 1978; Biondi and Sippler 1985; Raghava Rao et al., 1987). Vertical winds of significant and measurable magnitude (> 10m/sec) can however be expected to prevail in the nighttime equatorial thermosphere due to local heat sources like MTM and ETWA. Systematic measurements of the neutral wind vector including vertical winds are therefore essential to comprehend the origin and ionospheric effects of neutral wind systems in the equatorial region.

While the above mentioned upgradation of the FPI at VBO, Kavalur is the immediate requirement and task, there are also plans to develop an 'All Sky Imaging Fabry-Perot Spectrometer' to attempt two-dimensional mapping of the OI 630nm night airglow emission and thereby derive important information, for example, on the dynamics of the EIA. There is only one system of this type in operation in the country at Mt. Abu (24.5°N)(Sekar et al., 1993). One more unit is needed near the geomagnetic/geographic equator to advance our knowledge of the coupled dynamics of the neutral and ionized components of the equatorial upper atmosphere. Further the following studies based on measurements of night time thermospheric temperatures over Kavalur in Indian sector are planned for future from a large data base :

- Solar activity effects on night time neutral thermospheric temperature.
- Solar activity effects on amplitude of MTM.
- Seasonal variation of occurrence time and amplitude of MTM in Indian sector.

The operation of the FPI station at Kavalur has opened up the possibility of attempting concerted studies of the equatorial thermosphere structure and dynamics and related ionospheric effects by coordinating the FPI observations with those at Mt. Abu and also with the various ionospheric diagnostics (ionosondes, HF Doppler radar....etc) in the country. It is worthwhile to recall here most of the previous FPI observations in the equatorial region are from isolated stations and the much-needed multistation observations are just beginning to be made (Biondi et al, 1990). This approach will give us detailed information on the spatial/temporal structure of the MTM (which is hith-

erto derived from AE-E satellite data and the incoherent scatter radar measurements at Jicamarca), and the associated changes in the neutral and plasma dynamics.

6.2.2 Further studies on response of EIA under geomagnetically disturbed conditions

Our knowledge on the EIA response to magnetospheric disturbances seems still to be less than satisfactory. The main reason for this may be the investigations on this aspect are few in number. To understand response of EIA under geomagnetically disturbed conditions one need to have a detailed information on the disturbance behaviour of the forcing functions such as : (a) electric fields, (b) winds, (c) temperatures and (d) composition changes as a function of the different phases of the magnetospheric disturbances. Gaining comprehensive information on the above parameters is one ultimate task.

The following are some aspects of EIA response to disturbances for which our understanding needs improvement.

(a) The day time EIA enhancements are more frequently observed (e. g. Matsushita, 1976; Takahashi et al., 1987; Forbes, 1989) but mechanisms are not very clear and more observations are needed for study with reference to the AE indices and IMF B_z variations to understand the exact cause of such enhancements.

(b) Pre-midnight enhancement/inhibition of EIA has to be understood. The EIA inhibition could be due to (i) dusk-to-dawn disturbance electric field or (ii) disturbance dynamo electric fields or due to both (i) and (ii). More observations and studies are needed to distiguish between above two under different solar-geophysical conditions.

*****

References

Abdu, M.A., de Medeiros, R.T., Bittencourt, J.A and Batista, I.S 1983 *J. Geophys. Res.* **88**, 399.

Abdu et al. 1990 *Ann. Geophys.* **8**, 419.

Abdu, M.A., Sobral, J. H. A., De Paula, E.R and Batista, I.S 1991 *J. Atmos. Terr. Phys.* **53**, 757.

Abdu et al. 1993 *Ann. Geophys. Res.* **11**, 585.

Adeniyi, J.O. 1986 *J. Atmos. Terr. Phys.* **48**, 695.

Aggson, T.L., Maynard, L.C., Herrero, F.A., Mayr.H.G., Brace, L.H. and Liebrecht, M.S. 1987 *J. Geophys. Res.* **92**, 311.

Amayenc, P. 1974 *Radio Sci.* **9**, 281.

Akasofu, S.I. 1968 *Polar and Magnetosphere Substorms* Reidel. Pub. Com.

Akasofu, S.I. 1981 *Space Sci. Rev.* **28**, 121.

Akasofu, S.I., An, B.S., Kamide, Y., and Allen, J.H 1983 *J. Geophys. Res.* **88**, 5769.

Ananda Rao, B.G., Raghava Rao, R., Desai, J.N and Haerendel, G 1978 *J. Atmos. Terr. Phys.* **40**, 157.

Anderson, D.N. 1973a *Planet. Space Sci.***21**, 409.

Anderson, D.N. 1973b *Planet. Space Sci.* **21**, 421.

Anderson, D.N. 1981 *J. Atmos. Terr. Phys.* **43**, 753.

Anderson, D.N. and Klobuchar J.A. 1983 *J. Geophys. Res.* **88**, 8020.

Anderson, D.N. and Roble, R.G. 1981 *J. Atmos. Terr. Phys.* **43**, 835.

Anderson, D.N. and Rusch, D.W. 1980 *J. Geophys. Res.* **85**, 569.

Appleton, E.V. 1946 *Nature*, **157**, 691.

Avery, S.K. 1990 *Adva. Space Sci.* **10(10)**, 193.

Bamgboye, D.K., and McClure, J.P. 1982 *Geophys. Res. Lett.* **9**, 457.

Banks, P.M., Doupnik, J.R. and Akasofu, S.I. 1973 *J. Geophys. Res.* **78**, 6607.

Banks, P. M. 1977 *J. Atmos. Terr. Phys.* **39**, 179.

Barbier, D. 1959 *Ann. Geophys.* **15**, 179.

Basu Sunanda., Basu, S.,

Ganguly S. and Klobuchar J.A.	1981	*J. Geophys. Res.* **86**, 7607.
Batten, S.M. and Rees, D.	1990	*Planet. Space. Sci.* **38**, 675.
Batista, I.S., Abdu, M.A. and Bittencourt, J.A.	1986	*J. Geophys. Res.* **91**, 12055.
Batista, I.S., de Paula, E.R. Abdu, M.A. and Trivedi, N.B.	1991	*J. Geophys. Res.* **96**, 13943.
Baumjohann, W., and Paschmann, G.	1987	*Phys. Scripta* **18**, 61.
Bedinger, J.F.	1970	*J. Geophys. Res.* **75**, 683.
Behnke R.A. and Harper R.M.	1973	*J. Geophys. Res.* **78**, 8222.
Behnke, R.A., Kelley, M.C., Gonzales, C. A. and Larson, M.F.	1985	*J. Geophys. Res.* **90**, 4448.
Berger, C., Ill. M. and Barlier, F.	1988	*Ann. Geophys.* **6**, 541.
Bhargava. B.N., Sastri, N.S., Arora, B.R. and Rajaram, R.	1980	*Ann. Geophys.* **36**, 231.
Biondi, M.A. and Feibelman, W.A.	1968	*Planet. Space Sci.***16**, 431.
Biondi M.A. and Sipler D.P.	1985	*Planet.Space.Sci.* **33**, 817.
Biondi M.A. and Meriwether J.W.	1985	*Geophys.Res.Lett.* **12**, 267.
Biondi M.A., Meriwether J.W., Sahai, Y. and Takahashi H.	1990a	*Ann. Geophys.* **3**, 409 .
Biondi M.A., Meriwether J.W., Fejer B.G, Gonzales S.A.	1990b	*J.geophys.Res.* **95**, 12243.
Biondi M.A., Meriwether J.W., Fejer B.G, Gonzales S.A. and Hallenbeck D.C.	1991	*J.geophys.Res.* **96**, 15917.
Bittencourt J.A. and Sahai Y.	1979	*J. Atmos. Terr. Phys.* **41**, 1233.
Bittencourt, J.A. and Abdu, M.A.	1981	*J. Geophys. Res.* **86**, 2451.
Bittencourt et al.	1976	*J. Geophys. Res.* **81**, 3786.
Blanc, M. and Richmond, A.D.	1980	*J. Geophys. Res.* **85**, 1669.
Brace, L.H., Maier, E.J., Hoffman, J.H., Whitteker, J., Sepherd, G.G.	1982	*Geophys. Res. Lett.* **9**, 989.
Bowman, G.G.	1977	*J. Atmos. Terr. Phys.* **39**, 1169.
Bradley, A. and Dudeney, J. R	1973	*J. Atmos. Terr. Phys.* **35**, 2131.

Brekke, A., Dompnik, J.R. and Banks, P.M.	1974	*J. Geophys. Res.* **79**, 3773.
Burlaga, L.F., Silter, E., Mariani, F. and Schwenn, T.	1981	*J. Geophys. Res.* **86**, 6673.
Buonsanto, M.J	1994	*J. Geophys. Res.* **99**, 6437.
Burlaga, L.F., and Behannon	1982	*Sol. Phys.* **81**, 181.
Burlaga, L.F. et al.	1982	*Geophys. Res. Lett.* **9**, 1317.
Burns, A.G. and Killeen, T.L.	1992	*J. Geophys. Res. Lett.* **19** , 977.
Burns, A.G., Killeen, T.L., Crowley, G., Emery, B.A., Roble, R.G.	1989	*J.Geophys. Res.* **94**, 16961.
Burnside R.G., Herrero F.A., Meriwether J.W. and Walker J.C.G.	1981	*J. Geophys. Res.* **86**, 5532.
Burnside R.G., Behnke R.A. and Walker J.C.G.	1983	*J.geophys.Res.* **88**, 3181.
Burnside, R. G., R.G., Sulzer, M.P. and Walker, J.C.G.	1988	*J. Geophys. Res.* **93**, 8642.
Burnside, R. G. and Tepley, C. A.	1989	*J.Geophys. Res.* **94**, 2711.
Burrage, M.D., Fesen, C.G., and Abreu, V.J.	1990	*J.Geophys. Res.* **95**, 10357.
Burrage, M.D., Abreu, V.J., Orsini, N., Fesen, C.G., Roble, R.G.	1992	*J.Geophys. Res.* **97**, 4177.
Carignan, G.R., Dachev, T., Hedin, A.E., Reber, C.A. and Spencer, N.W.	1982	*Geophys. Res. Lett.* **9**, 949.
Carovillano, R. L and Forbes, J.M.	1983	*Solar Terrestrial physics* Astrophy. Space. Sci. Lib **104**, 1
Chandra, S.E., Fleming, E.L., Schoeberl, M.R and Barnett, J.J.	1990	*Adv. Space. Res.* **10(6)**, 3
Chapman, S.	1951	*Arch. Meteo. Geophys. Bioklimatal. Ser.* **A,4**, 368

Chapman, S.	1967	*Aurora and Airglow* Reinhold. Pub- USA p15.
Chabbal R.J.	1953	*J. Rech. Centre Nat. Rech. Sci. Lab., Bellevue*(Paris) **24**, 138.
Chauhan, N., Gurm, H.S., Janve, A.V.	1980	*J. Atmos. Terr. Phys.* **42**, 265.
Cocks, T.D., Creighton, D.F., Jacka, F.	1980	*J. Atmos. Terr. Phys.* **42**, 499.
Cole, K. D.	1971	*Planet. Space. Sci.* **19**, 59.
Cole, K. D.	1975	*J. Atmos. Terr. Phys.* **35**, 939.
Crain, D.J., Heelis, R.A Bailey, G.J	1993	*J. Geophys. Res.* **98**, 6033.
Crooker, N.V.	1983	*NASA Conf. Pub. 2280. JPL., Pasadena, California.*
Crowley, G.	1991	*Rev. Geophys. Supplement.* p1143.
Crowley, G., Emery, B.A., Roble, R.G., Carlson, H.C (Jr)., Knipp, D.J.	1989a	*J. Geophys. Res.* **94**, 16925.
Crowley et al.	1989b	*J. Geophys. Res.* **94**, 16945.
Dickinson, R.E., Roble, R.G., Bougher, S.W.	1987	*Adv. Space. Res.* **7(10)**, 5
Dudeney, J. R.	1983	*J. Atmos. Terr. Phys.* **45**, 629.
Crooker, N.V.	1983	*NASA Conf. Pub. 2280. JPL., Pasadena, California.*
Crowley, G.	1991	*Rev. Geophys. Supplement.* p1143.
Crowley, G., Emery, B.A., Roble, R.G., Carlson, H.C (Jr)., Knipp, D.J.	1989a	*J. Geophys. Res.* **94**, 16925.
Crowley et al.	1989b	*J. Geophys. Res.* **94**, 16945.
Dickinson, R.E., Roble, R.G., Bougher, S.W.	1987	*Adv. Space. Res.* **7(10)**, 5
Dudeney, J. R.	1983	*J. Atmos. Terr. Phys.* **45**, 629.

Egedal, J.	1947	*J. Geophys. Res.* **52**, 449.
Farley, D.T., Bonelli, E., Fejer, B.G. and Larson, M.F.	1986	*J. Geophys. Res.* **91**. 13723.
Fejer, B.G.	1981	*J. Atmos. Terr. Phys.* **43**, 377.
Fejer, B.G.	1986	*Solar Wind Magnetosphere Coupling* (Edited by Kamide, Y.and Slavin, J.A.) p519. Terra, Tokyo.
Fejer, B.G.	1991	*J. Atmos. Terr. Phys.* **53**, 677.
Fejer, B.G., Gonzales, C.A., Farely, D.T., Kelley, M.C. and Woodman, R.F.	1979	*J. Geophys. Res.* **84**, 5792.
Fejer, B.G and Kelley, M.C.	1980	*Rev. Geophys. Space. Phys.* **18**, 401.
Fejer, B.G., Larson, M.F. and Farley, D.T.	1983	*Geophys. Res. Lett.* **10**, 537.
Fejer, B.G., de Paula, E.R., Batista, I.S., Bonelli, E., and Woodman, F.R.	1989	*J. Geophys. Res.* **94**, 12049.
Fejer, B.G., Spiro, R.W., Wolf, R.A. and Foster, J.G.	1990a	*Ann. Geophys.* **8**, 441.
Fejer, B.G., Kelley, M.C., Senior, C., de la Beaujardiere, O., Holt, J.A., Tepley, C.A.,	1990b	*J. Geophys. Res.* **95**, 2367.
Fejer, B.G., de Paula, E.R., Gonzales, S.A. and Woodman, R.F.	1990c	*J. Geophys. Res.* **96**, 13901.
Feherm, V.G. M.	1991	*J. Atmos. Terr. Phys.* **53**, 677.
Fesen, C. G. and Abreu, V. J.	1987	*J. Geophys. Res.* **92**, 1231.
Fesen, C.G., Dickinson R.E. and Roble R.G	1986	*J. Geophys. Res.* **91**, 4471.
Fesen, C.G., Crowley, G. and Roble, R.G.	1989	*J. Geophys. Res.* **94**, 5405.
Forbes, J.M.	1981	*Rev. Geophys. Space Phys.* **19**, 469.
Forbes, J. M.	1982	*J. Geophys. Res.* **87**, 5228.

Forbes, J. M.	1987	*Phy. Scripta.* **T18**, 240.
Forbes, J. M. and Roble, R. G.	1990	*J. Geophys. Res.* **95**, 201.
Forbes, J.M., Codrescu, M., and Hall, T.J.	1988	*Geophys. Res. Lett.* **15**, 249.
Forbes, J.M.	1989	*J. Geophys. Res.* **94**, 16999.
Feldstein, Y.I and Starkov, G.V.	1968	*Planet. Space. Sci.* **16**, 129.
Friedman J.F. and Herrero F.A.	1982	*Geophys. Res. Lett.* **9**, 785.
Ganguly, S. Behnke, R.A. Emry, B.A.	1987	*J. Geophys. Res.* **92**, 1199.
Gerald, J. C. and Roble, R. G.	1988	*Planet. Space. Sci.* **36**, 271.
Goel, M.K, Singh, S.S. and Rao, B.C.N	1990	*J. Geophys. Res.* **95**, 6237.
Gonzales, C.A., Kelley, M.C., Vickrey, J.F., and Woodman, R.F.	1979	*J. Geophys. Res.* **84**, 5803.
Gonzales, C.A., Kelley, M.C., Behnke, R.A., Vickrey J.F., Wand, R. and Holt, J.,	1983	*J. Geophys. Res.* **88**, 9135.
Gosling et al.	1975	*Solar phys.* **40**, 439
Gosling et al.	1976	*Solar phys.* **48**, 389
Gosling, J.T., Hildner, E., Asbridge, J.R., Bame, S.J., Feldman, W.C.	1977	*J. Geophys. Res.* **82**, 5005.
Groves, G. V. and Forbes, J. M	1985	*Planet. Space. Sci.* **33**, 283.
Greenspan, J.A	1966	*J. Atmos. Terr. Phys.* **28**, 739.
Gross, S.H.	1985	*J. Atmos. Terr. Phys.* **47**, 941.
Guptha, R., Desai, J.N., Raghava Rao, R., Sekar, R., Sridharan, R and Narayanan, R.	1986	*Geophys. Res. Lett.* **13**, 1055.
Haerendal, G., Lust, R., Reiger, E.	1967	*Planet. Space. Sci.* **15**, 1.
Hagan, M.E. and Salah, J.E.	1988	*J. Geophys. Res.* **93**, 9927.
Hanson, W.B. and Moffett, R.J.	1966	*J. Atmos. Terr. Phys.* **71**, 5559.
Hardy, D., Gussenhoven, M.S.,		

and Holemen, E.	1985	*J. Geophys. Res.* **90**, 4229.
Hargreaves, J.K.	1992	*The Solar Terrestrial Environment*, Cambridge University Press.
Harper, R.M.	1973	*J. Atmos. Terr. Phys.* **35**, 2023.
Hays, P.B., Nagy, A.F. and Roble, R.G.	1969	*J. Geophys. Res.* **74**, 4162.
Hays, P.B. and Roble, R.G.	1971	*J. Geophys. Res.* **76**, 5316.
Hays, P.B., Meriwether, J.W., and Roble, R.G.	1979	*J. Geophys. Res.* **84**, 1905.
Hedin, A.E.	1983	*J. Geophys. Res.* **88**, 10170.
Hedin, A.E.	1987	*J. Geophys. Res.* **92**, 4849.
Hedin, A.E.	1988	*Adva. Space. Res.* **8**, 9.
Hedin, A.E. and Mayr, H.G.	1973	*J. Geophys. Res.* **78**, 1688.
Hedin, A.E. and Mayr, H.G.	1987a	*J. Geophys. Res.* **92**, 11159.
Hedin, A.E. and Mayr, H.G.	1987b	*J. Geophys. Res.* **92D**, 869.
Hedin, A.E., Spencer, N.W., and Killeen, T.L..	1988	*J. Geophys. Res.* **93**, 9959.
Hedin et al.	1991	*J. Geophys. Res.* **96**, 7657.
Heelis, R.A., Kendall, D.C., Moffet, R.J., Windle, D.W., Rishbeth, H.	1974	*Planet. Space. Sci.* **22**, 743.
Hernandez G.	1982	*J.geophys.Res.* **87**, 1623.
Hernandez G., Van Zandt T.E., Peterson V.L. and Turtle J.P.	1975	*J. geophys. Res.* **80**, 3271.
Hernandez, G., and Roble, R.G.	1979	*Appl. Opp.* **18**, 3376.
Hernandez, G., and Roble, R.G.	1976	*J. Geophys. Res.* **81**, 2065.
Hernandez G. and Roble R.G.	1984	*J.geophys.Res.* **89**, 327.
Hernandez G., Smith R.W., Roble R.G., Gress J. and Clark K.C.	1990	*Geophys. Res. Lett.* **17**, 1255.
Herrero F.A., Mayr H.G. and Spencer N.W.	1988	*J.atmos.Terr.Phys.* **50**,1001.

Herrero, F.A., and Spencer N.W.	1982	*Geophys. Res. Lett.* **9**, 1179.
Herrero, F.A., Mayr, H.G., Spencer, N.W	1983	*J.geophys.Res.* **88**, 7225.
Herrero, F.A., Spencer N.W., and Mayr, H.G.	1993	*Adv. Space Res.* **13**, 201.
Hines, C. O.	1960	*Can. J. phys.***42**, 1441
Hines, C. O.	1965	*J.geophys.Res.* **70**, 177.
Hinteregger, H.E.	1976	*J.atmos.Terr.Phys.* **38**,791.
Hildner et al.	1989	*Astrophys. and Space. Sci. lib* **153**, 497.
Hoffman, R.A.	1988	*Rev. Geophys.* **26**, 209.
Johnson, R.M., Wickwar, V.B., Roble, R.G. and Luhman, J.G.	1987	*Ann. Geophys.* **5A**, 383.
Kamide, Y and Akasofu, S. I.	1983	*Rev. Geophys. Space. Phys* **21**, 1647.
Kamide, Y. and Matsushita, S.	1981	*J. Atmos. Terr. Phys.* **43**, 441.
Kamide, Y. and Richmond, A.D.	1986	*J. Geomag. Geoelectr.* **38**, 653.
Kane, R.P.	1973	*J.atmos.Terr.Phys.* **35**,1565.
Kane, R.P.	1976	*Space. Sci. Rev.* **18**, 413.
Kato, S.	1980	*Dynamics of the upper atmosphere, Reidel pub. company, Japan.*
Kelley, M.C.	1985	*J. Atmos. Terr. Phys.* **47**, 745.
Kelley, M.C.	1989	*The Earth's Ionosphere* Academic Press, INC.
Kelley, M.C., Fejer, B.G., and Gonzales, C.A.	1979	*Geophys. Res. Lett.* **6**, 301.
Kelley, M.C., Larsen, M.F., La Hoz, C.A and McClure, J.P.	1981	*J. Geophys. Res.* **86**, 9087.
Kikuchi, T.	1986	*J. Geophys. Res.* **91**,3101.
Kikuchi, T., Araki, T., Maeda, H. and Maekawa, K.	1978	*Nature* **273**, 650.
Killeen, T. L.	1987	*Rev. Geophys.* **25**), 433.
Killeen, T.L. and Roble, R.G.	1986	*J. Geophys. Res.* **91**, 11291.

Killeen, T.L. and Roble, R.G.	1988	*Rev. Geophys.* **26**, 329.
Klein, L.W. and Burlaga, L.F.	1982	*J. Geophys. Res.* **87**, 613.
Krishnamurthy, B.V., Hari, S. and Somayajulu, V.V.	1990	*J. Geophys. Res.* **95**, 4307.
Lockwood, G.E.K. and Nelmes, G.L.	1964	*J. Atmos. Terr. Phys.* **26**, 564.
Lyon, A.J. and Thomas, L.	1963	*J. Atmos. Terr. Phys.* **25**, 373.
MacQueen, R.M.	1980	*Phil. Trans. R. Soc. Lond.* **297**, 605.
Martyn, D.F.	1947	*Proc. Roy. Sci. (Lond)* **A 219**, 214.
Marubashi, K.	1986	*Adv. Space Res.* **6**, 335.
Marubashi, K.	1989	*Space Sci. Rev.* **51**, 197.
Matsushita, S.	1962	*J. Geophys. Res.* **67**, 3753.
Matsushita, S.	1969	*Radio. Sci.* **4**, 771.
Matsushita, S.	1976	*Space Sci. Rev.* **19**, 713.
Matsushita, S.	1977	*J. Atmos. Terr. Phys.* **38**, 1207.
Matsushita, S. and Balsley, B.	1972	*Planet. Space. Sci.* **20**, 1259.
Matuura, N.	1972	*Space Sci. Rev.* **13**, 124.
Mayr, H.G. and Volland, H	1972	*Planet. Space. Sci.* **20**, 379.
Mayr, H.G., Harris, I., Spencer, N.W., Hedin A.E., and Wharton, L.E.	1979	*Geophys. Res. Lett.* **6**, 447.
Mayr, H.G., Harris, I., Varosi, F and Herrero, F.A.	1984a	*J. Geophys. Res.* **89**, 10929.
Mayr, H.G., Harris, I., Varosi, F and Herrero, F.A.	1984b	*J. Geophys. Res.* **89**, 10961.
Mayr, H.G., Harris, I., Varosi, F and Herrero, F.A.	1987	*J. Geophys. Res.* **92**, 7657.
Mayr, H.G., Harris, I., and Herrero, F.A.	1990a	*Planet. Space. Sci.* **38**, 301.
Mayr, H.G., Harris, I., Dube, M.	1990b	*J. Atmos. Terr. Phys.* **52**, 103.
Mayr, H.G., Harris I., Herrero F.A., Spencer N.W.,		

Varosi, F and Pesnell, W.D.	1990c	*Space Sci. Rev.***54**, 297.
Mazaudier, C. and Venkateswaran, S.V.	1990	*Ann. Geophys.* **8**, 511.
Meriwether, J.W.	1983	*Radio Sci.* **18**, 1035.
Meriwether, J.W., Moody J.W., Biondi M.A. and Roble R.G.	1986	*J. Geophys. Res.* **91**, 5557.
Meriwether, J.W (Jr.), Killeen T.L., McCormac F.G., Burns A.C. and Roble R.G.	1988	*J. Geophys. Res.* **93**, 7478.
Miller, K.L., Hedin, A.E., Wilkinson, P.J., Torr, DG., Richards, P.G	1990	*Adva. Space. Res.* **10(8)**, 99.
Miller, K.L., Richards., P.G, Wu, H.Y.	1993	Ann. Geophysicae. **11**, 572.
Moffett, R.J.	1979	*Fundamentals of Cos. Phy.* **4**, 313.
Mozer, F.S.	1973	*Rev. Geophys. Space Phys.* **11**, 755.
Murty, G.S.N. and Kim, J.S.	1988a	*Planet Space Sci.* **36**, 197.
Murty, G.S.N. and Kim, J.S.	1988b	*Planet Space Sci.* **36**, 677.
Narayanan, R., Desai, J.N., Modi, N.K., Raghava Rao, R., Sridharan, R.	1988	*Applied Optics* **28**, 2138
Nelson, G.L. and Cogger, L.L.	1971	*J. Atmos. Terr. Phys.* **33,**, 1711.
Nisbet, J.S., Miller, M.J. and Carpenter, L.A.	1978	*J. Geophys. Res.* **83**, 2647.
Nishida, A.	1968	*J. Geophys. Res.* **73**, 1795.
Nishida, A.	1971	*Planet Space Sci.* **19**, 205.
Nishida, A and Kokuban, S	1971	*Rev. Geophys. Space.Phys.* **9**, 417.
Nopper, K.W. and Carovillano, R.L.	1978	*Geophys. Res. Lett.* **5**, 699.
Oliver, W. L. and Salah, J. E	1988	*J. Geophys. Res.* **93**, 4039.
Oliver et al.	1990	*J. Geophys. Res.* **95**, 7603.
Ossakow, S.L., Zalesak, S.T., McDonanld, B.E., and Chaturvedi, P.K.	1979	*J. Geophys. Res.* **84**, 17.
Onwumechilli, C.A.	1967	*Phys. of Geomagnetic Phenomena*

		(ed. S.Matsushita and W.H.Campbell), p.425, Academic Press, NY.
Patel, V. L.	1978	*J. Geophys. Res.* **83**, 2137.
Perrault, P. and Akasofu, S.I.	1978	*Geophys. J. R. Astr. Soc.* **54**, 547.
Prolss, G.W.	1980	*Rev. Geophys.* **18**, 183.
Prolss, G.W.	1982	*J. Geophys. Res.* **87**, 5260.
Prolss, G.W.	1987	*Planet. Space. Sci.* **35**, 807.
Prolss, G.W.	1993	*J. Geophys. Res.* **98**, 5981.
Prolss, G.W. and Von Zahn, U.	1977	*Space Sci. Res.* **17**, 313.
Prolss, G.W., Brace, L.H., Mayr, H.G., Carignan, G.R., Killeen, T.L., and Klobuchar, J.A.	1991	*J. Geophys. Res.* **96**, 1275.
Raghava Rao R., and Sivaraman, M.R.	1973	*J. Atmos.Terr. Phys.* **35**, 2091.
Raghava Rao R., and Sivaraman, M.R.	1975	*Space Res.* **XV**, 385.
Raghava Rao R., Sharma, P. Sivaraman M.R.	1978	*Space Res.* **XVII**, 277.
Raghava Rao, R., Desai, J.N. Narayanan, R., Sekar, R., Gupta, R., Babu, V.V., Sudhakar, V.	1984	*J. Atmos.Terr. Phys.* **46**, 355.
Raghava Rao et al.	1987	*J. Atmos. Terr. Phys.* **49**, 485.
Raghava Rao, R., Wharton, L.E., Spencer, N.W., Mayr, H.G. and Brace, L.H.	1991	*Geophys. Res. Lett.* **18**, 1193.
Rajaram, G.	1977	*J. Atmos. Terr.Phys.* **39** , 1125.
Rajaram, T.N., Desai J.N., Degaonkar S.S. and Cole K.D.	1978	*Nature* **272**, 516.
Rao, B.C.N.	1963a	*J. Geophys. Res.* **68**, 2541.
Rao, B.C.N.	1963b	*J. Geophys. Res.* **68**, 2551.
Rastogi, R.G.	1959	*J. Geophys. Res.* **64**, 727.
Rastogi, R.G. and Patel, V.L.	1975	*Proc. Indian Acad. Sci.* **82**, 121.
Reddy, C.A.	1989	*PAGEOPH* **131**, 485.

Reddy, C.A.	1981	*J. Atmos. Terr. Phys.* **43**, 557.
Reddy et al.	1990	*Geophys. Res. Let.* **17**, 2333.
Reddy et al.	1991	*J. Geophys. Res.* **95**, 21077.
Rees et al.	1985	*Planet. Space. Sci.* **33**, 617.
Reiff, P.H. and Luhmann, J.G.	1986	*Solar Wind Magnetosphere coupling* (Edited by Kamide, Y. and Slavin, J.A.), p.453, Terra Scientific, Tokyo.
Rice et al.	1988	*Radio. Sci* **23**, 919
Richmond, A.D. and Matsushita, S.	1975	*J. Geophys. Res.* **80**, 2839.
Richmond, A.D., Matsushita, S., and Tarpley, J.D.	1976	*J. Geophys. Res.* **81**, 547.
Richmond, A.D., Ridley, E.C., Roble, R.G.	1992	*Geophys. Res. Lett.* **19**, 601.
Rishbeth, H.	1971a	*Planet. Space. Sci.* **19**, 263.
Rishbeth, H.	1971b	*Planet. Space. Sci.* **19**, 357.
Rishbeth, H.	1975	*J. Atmos. Terr. Phys.* **37**, 1055.
Rishbeth, H.	1977	*J. Atmos. Terr. Phys.* **39**, 1159.
Rishbeth, H.	1979	*J. Atmos. Terr. Phys.* **41**, 885.
Rishbeth, H.	1981	*J. Atmos. Terr. Phys.* **43**, 389.
Rishbeth, H. and Garriott, K.	1969	*Introduction to Ionospheric Physics.* Academic Press, New York.
Rishbeth, H., Fuller-Rowell, T.J. and Rodger, A.S.	1987	*Phys. Scripta* **36**, 327.
Roach, F.E. and Gordan, J.L.	1973	*The light of the Night Sky* *D. Reidel*, p.66.
Roble, R. G.	1987	*The Solar Wind and the Earth* **p245** (Terra. Pub, Tokyo.)
Roble, R.G., Dickinson, R.E.	1973	*J. Geophys. Res.* **78**, 249.
Roble, R. G and Emery, B. A.	1983	*Planet. Space. Sci.* **31**, 597.
Roble, R.G., Dickinson, R.E. Ridley, E.L.	1982	*J. Geophys. Res.* **87**, 1599.
Roble, R. G. and Ridley, E. C.	1987	*Ann. Geophys.* **5A**, 369

Roble et al.	1983	*Planet. Space. Sci.* **31**, 1479.
Roble, R.G., Forbes, J.M., and Marcos, F.A.	1987a	*J. Geophys. Res.* **92**, 6045.
Roble, R.G., Ridley, E.C., and Dickinson, R.E.	1987b	*J. Geophys. Res.* **92**, 8745.
Roble et al.	1988a	*J. Geophys. Res.* **93**, 209.
Roble, R.G., Ridley, E.C., Richmond, A.D. and Dickinson, R.E	1988b	*J. Geophys. Res.* **15**, 1325.
Rottger, J. and Meyer, W	1987	*J. Atmos. Terr. Phys.* **49**, 689.
Rottger, J.	1977	*J. Atmos. Terr. Phys.* **39**, 987.
Sahai Y., Takahashi H., Gafundes P.R., Clemesha B.R., Teixeira N.R and Bittencourt J.A.	1992	*Planet. Space. Sci.* **40**, 767.
Sastri, J.H.	1980	*Ind. J. Radio Space Phys.* **9**, 209.
Sastri, J.H.	1982	*Indian J. Rad. Space Phys.* **11**, 33.
Sastri, J.H.	1984	Ann. Geophysicae. **2**, 353.
Sastri, J.H.	1985	*Adv. Space Res.* **5**, 199.
Sastri, J.H.	1988a	*Planet. Space. Sci.* **36**, 785.
Sastri, J.H.	1988b	*Annales, Geophys.* **6**, 635.
Sastri, J.H.	1989	*Planet. Space. Sci.* **37**, 1403.
Sastri, J.H.	1990	*Ind. J. Radio Space Phys.* **19**, 225.
Sastri, J.H., Ramesh, K.B. and Karunakaran, D.	1992	*Planet. Space Sci.* **40**, 95.
Sastri, J.H., Rao, J.V.S.V., Ramesh. K.B.	1993	*J. Geophys. Res.* **98**, 17517.
Sato, T.	1966	*Rep. Ionos. Space Res. Japan* **20**, 150.
Schunk, R.W.	1987	*Phys. Scripta* **18**, 256.
Schieldge, J.P., Venkateswaran, S.V. Richmond, A.D.	1973	*J. Atmos. Terr. Phys.* **35**, 1045.
Sekar, R., Gurubaran, S., and Sridharan, R.	1993	*Indian. J. Radio. Space. Phys.* **22**, 197.

Senior, C. and Blanc, M.	1984	*J. Geophys. Res.* **89**, 261.
Senior, C. and Blanc, M.	1987	*Ann. Geophys.* **5**, 405.
Sipler, D.P., Luokkala, B.B., Biondi, M.A	1982	*Planet. Space. Sci.* **30**, 1025.
Sipler D.P., Biondi M.A., and Roble R.G.	1983	*Planet. Space. Sci.* **31**, 53.
Sobral, J.H.A., Abdu, M.A., Batista, I.S.	1980	*Ann Geophys.* **36**, 199.
Somayajulu, Y.V.	1964	*J. Geophys. Res.* **69**, 561.
Somayajulu, V.V.	1963	*J. Geophys. Res.* **68**, 189.
Somayajulu, V.V., Devasia, C.V., Reddy, C.A. and Viswanathan, K.S.	1987	*Geophys. Res. Lett.* **14**, 876.
Somayajulu. V.V., Krishnamurthy, B.V., Subbarao, K.S.V.	1991	*J. Atmos. Terr. Phys.* **53**, 965.
Spencer, N.W., Carignan, G.R., Mayr, H.G., Niemann, H.B., Theis, R.F., and Wharton, L.E.	1979	*Geophys. Res. Lett.* **6**, 444.
Spencer, N.W., Wharton, L.E., Nieman, H.B., Hedin, A.E., Canignan, G.R.	1981	*Space. Sci. inst.* **5**, 417.
Spiro, R.W., Reiff, P.H., Maher (Jr), L.J.	1982	*J. Geophys. Res.* **87**, 8215.
Spiro, R.W., Wolf, R.A. and Fejer, B.G.	1988	*Ann. Geophys.* **6**, 39.
Sridharan, R., Gurubaran, S., Raghava Rao, R., and Suhasini, R.	1991	*J. Atmos. Terr. Phys.* **53**, 515.
Srinivasan, R. and Surendiranath, R.	1991	*Ind. J. Pure. Appl. Phys.* **29**, 267.
Sterling, D.L., Hanson, W.B., Moffett, R.J. and Baxter, R.G.	1969	*Radio Sci.* **4**, 1005.
Stewart, B.	1883	*Terrestrial magnetism , Encyclopedia Britanica* **16**, 159.
Sugiura, M. and Poros, D.J.	1969	*J. Geophys. Res.* **74**, 4025.

Takahashi, T., Oya, H., and Watanabe, S.	1987	*J. Geomag. Geoelec.* **39**, 187.
Tan, A.	1982	*J. Atmos. Terr. Phys.* **44**, 377.
Tanaka, T.	1979	*J. Atmos. Terr. Phys.* **48**, 695.
Tanaka, T.	1981	*J. Geophys. Res.* **86**, 11335.
Tanaka, T.	1986	*Geophys. Res. Lett.* **13**, 1399.
Thuillier, G., Falin, J.L., Watchtel, C.	1977	*J. Atmos. Terr. Phys.* **39**, 399.
Tinsley, B. A.	1981	*J. Atmos. Terr. Phys.* **43**, 617.
Titheridge, J.E., and Buonsanto, M.J.	1983	*J. Atmos. Terr. Phys.* **45**, 863.
Titheridge, J.E., and Buonsanto, M.J.	1988	*J. Atmos. Terr. Phys.* **50**, 763.
Tsunomura, S. and Araki, T.	1984	*Planet. Space Sci.* **32**, 599.
Untiedt, J.	1967	*J. Atmos. Terr. Phys.* **55**, 995.
Vasyliunas, V. M.	1970	*Particles and Fields in Magnetosphere p 60*, D. Reidel . Pub, Massachusetts.
Vial, F	1989	*J. Atmos. Terr. Phys.* **51**, 3.
Vial, F. and Forbes, J. M.	1989	*J. Atmos. Terr. Phys.* **51**, 663.
Vestine, E. H.	1960	*Physics of the Earth's Upper Atmosphere*, Aca. Press.
Viswanathan, K.S., Vikrama Kumar, B.T., and Reddy, C.A.	1987	*J. Atmos. Terr. Phys.* **49**, 193.
Wagner, W.J.	1984	*Rev. Astron. Astrophys.* **22**, 267.
Waldock, J. A and Jones, T.B	1987	*J. Atmos. Terr. Phys.* **49**, 105.
Walker, G.O., and Ma, J.H.K.	1972	*J. Atmos. Terr. Phys.* **34**, 6249.
Walker, G.O.	1973	*J. Atmos. Terr. Phys.* **41**, 103.
Walker, G.O. and Strickland, A.E.	1981	*J. Atmos. Terr. Phys.* **43**, 589.
Walker, G.O. and Wong, Y.W.	1993	*J. Atmos. Terr. Phys.* **55**, 995.
Wilson, R.M. and Hildner, E.	1984	*Solar Phys.* **91**, 169.
Wilson, R.M. and Hildner, E.	1986	*J. Geophys. Res.* **91**, 5867.
Wilson R.M.	1987	*Planet. Space Sci.* **35**, 329.
Williams, D.J., Roelof, E.C.,		

Mitchell, D.G.	1992	*Rev. Geophys.* **30**, 183.
Woodman, R.F. and Calderon, C.	1979	*J. Geophys. Res.* **95**, 2367.
Woodman, R.F., Sterling, D.L. and Hanson, W.B.	1972	*Radio Sci.* **7**, 739.
Wright, J.W.	1971	*Planet. Space Sci.*, **19**, 1327.
Yagi T. and Dyson P.L.	1985	*Planet. Space. Sci.* **83**, 203.
Zamay, S. S.	1989	*Geomag. Aeron.* **29**, 104.
Zhang, G. and Burlaga, L.F.	1988	*J. Geophys. Res.* **93**, 2511.